Characterising the Role of *Vibrio vulnificus* Type 6 Secretion Systems 1 and 2 in an *in vivo* Oyster Model

Submitted by Cameron Lawrence Hubert to the University of Exeter as a thesis for the degree of Doctor of Philosophy in Biological Sciences in April 2020

I certify that all material in this thesis which is not my own work has been identified and that no material has been previously submitted and approved for the award of a degree by this or any other University.

Signature: ……

Abstract

Vibrio vulnificus is a significant human pathogen commonly isolated from temperate marine environments, where it is particularly abundant within filter-feeding shellfish. *V. vulnificus* is currently increasing in prevalence, theorised to be due to climate change facilitating *V. vulnificus* growth in previously inhospitable environments. Infection of susceptible individuals with *V. vulnificus* typically results in either primary septicaemia or necrotic wound infection, depending upon the route of entry, and frequently results in death if not treated rapidly.

Two type 6 secretion systems (T6SS) have been identified in *V. vulnificus*, termed the T6SS1 and the T6SS2. The T6SS is a molecular syringe utilised to inject cytotoxic effector proteins into neighbouring cells. Whilst the T6SS2 is present in all sequenced *V. vulnificus* strains, only a subset possesses the T6SS1. Previous bacterial co-culture killing assays between T6SS1$^+$ and T6SS1$^-$ *V. vulnificus* strains demonstrated thermoregulated T6SS1-mediated killing of T6SS1$^-$ strains. This study further characterised the role of both the T6SS1 and the T6SS2 *in vitro. In vitro* co-culture assays demonstrated that both the T6SS1 and the T6SS2 have antibacterial killing activity at the environmentally representative temperature of 21 °C. This is the first characterised role for the T6SS2 of *V. vulnificus.* No anti-eukaryotic activity was observed following co-culture with the phagocytic amoeba, *Dictyostelium discoideum*, suggesting that T6SS activity is purely antibacterial.

In vitro bacterial co-culture assays were replicated *in vivo* using an oyster model. To facilitate high-level uptake of bacterial strains of interest by oysters, an artificial marine snow model was developed where bacteria were incorporated into easily ingested phytoplankton aggregates. Uptake of bacteria from artificial marine snow was extremely successful, resulting in bacterial loads within oysters significantly greater than achieved by any study to date. Using this model, this study was able to demonstrate that *V. vulnificus* utilises both the T6SS1 and the T6SS2 to target and kill neighbouring bacteria, in both an intra and inter-species manner. This data suggests that the T6SSs of *V. vulnificus* play a key role in *V. vulnificus* ecology and the dynamics between bacterial populations *in vivo*.

Acknowledgements

I would like to extend my thanks to my supervisors, Dr Steve Michell and Dr Steve Porter, for all their support over the past four years. Your supervision and help have been vital throughout my studies. These thanks are also offered to Dr Craig Baker-Austin from CEFAS, who was kind enough to provide essential training in marine snow generation, oyster husbandry, and qPCR.

My thanks also go to NERC for providing the funding for my project, and to all the facility staff and technicians who have helped me with my research and provided such a positive work environment. This includes the free Exeter minibus for saving me from having to climb the hill to work every day, for which my legs are grateful.

A big thank you goes out to all members of the coffee club, with particular thanks to Georgie, Jack, and Josh, of the Brain Trust, who helped keep me sane and provided much needed support and entertainment. Furthermore, I would like to thank all past and present members of the 4th floor throughout my time at Exeter, who were always ready to offer encouragement and advice.

A special thanks goes to Kirsty, for always believing in me and encouraging me to push myself, for the many lifts to work or to Dawlish to collect samples, and for listening to all my frustrations. Without you this would have been far more difficult, for which I am ever grateful.

My final thanks go to my parents and family, without who none of this would have been possible. You have been forever supportive of me and I can never express my appreciation enough for everything you have done for me.

Contents

Chapter Five - Development of an artificial marine snow model for bacterial incorporation

Chapter Six - *V. vulnificus* T6SS1 and T6SS2 have antibacterial activity in an *in vivo* oyster model

List of Tables

Chapter One

Chapter Two

List of Figures

Chapter One

Chapter Two

Chapter Three

Chapter Four

Chapter Five

Chapter Six

List of Equations

List of Appendices

List of Abbreviations

AHL	Acylated homoserine lactones
AIDS	Acquired immune deficiency syndrome
Amp	Ampicillin
AMS	Artificial marine snow
ANOVA	Analysis of variance
ASW	Artificial Seawater
ATP	Adenosine triphosphate
bp	Base pairs
CDC	Centre for Disease Control and Prevention
cDNA	Complementary DNA
CFU	Colony forming units
Cm	Chloramphenicol
cm	Centimetre
COVIS	Cholera and Other Vibrio Illness Surveillance System
CPS	Capsular polysaccharide
Ct	Cycle threshold
DNA	Deoxyribonucleic acid
dATP	Deoxyadenosine triphosphate
dNTP	Deoxynucleotide triphosphate
EPS	Exopolymeric substances
g	Gram
gDNA	Genomic DNA

GlcNAc	*N*-acetylglucosamine
Hcp	Haemolysin co-regulated protein
HGT	Horizontal gene transfer
HIV	Human immunodeficiency virus
Kan	Kanamycin
kb	Kilobase
L	Litres
LB	Luria-Bertani
LD_{50}	Lethal $Dose_{50}$
LDL	Low-density lipoprotein
LPB	Lactose/Peptone buffered
LPS	Lipopolysaccharide
M	Moles per Litre
m	Metres
MDa	Megadaltons
mg	Milligram
ml	Millilitre
MLST	Multilocus sequence typing
mm	Millimetre
MnSOD	Manganese-containing superoxide dismutase
MPN	Most probable number
mRNA	Messenger RNA
MW	Molecular weight
NEB	New England BioLabs
NMS	Natural marine snow

OE-PCR	Overlap extension polymerase chain reaction
OMV	Outer membrane vesicle
ORF	Open reading frame
PAAR	Proline-alanine-alanine-arginine repeat
PBS	Phosphate buffered saline
PCR	Polymerase chain reaction
PoNe	Polymorphic nuclease effector
PoNi	Polymorphic nuclease immunity
PorSS	Por secretion system
ppt	Parts per thousand
RAPD-PCR	Randomly amplified polymorphic DNA PCR
Rhs	Rearrangement hot spot
RNA	Ribonucleic acid
RP	Reef-Phytoplankton
rpm	Revolutions per minute
rRNA	Ribosomal ribonucleic acid
RT-PCR	Reverse transcription polymerase chain reaction
RTS	Repeats in toxin
SEM	Scanning electron microscopy
SI	Super-integron
SPI	*Salmonella* pathogenicity island
SST	Sea-surface temperature
T1SS	Type 1 secretion system
T2SS	Type 2 secretion system
T3SS	Type 3 secretion system
T4SS	Type 4 secretion system

T5SS	Type 5 secretion system
T6SS	Type 6 secretion system
T7SS	Type 7 secretion system
Tae	Type 6 secretion system amidase effector
Tai	Type 6 secretion system amidase immunity
TCBS	Thiosulfate-citrate-bile salts-sucrose agar
TEP	Transparent extracellular polysaccharide
Tge	Type 6 secretion system glycoside effectors
Tle	Type 6 secretion system lipase effector
Tli	Type 6 secretion system lipase immunity
Tmp	Trimethoprim
Tse	Type 6 secretion system effector
Tsi	Type 6 secretion system immunity
TPP	Threonine phosphorylation pathway
UV	Ultraviolet
V	Volts
VAS	Virulence-associated secretion
VBNC	Viable but non-culturable
vcg	Virulence correlated gene
VgrG	Valine-glycine repeat protein G
v/v	Volume per volume
WGS	Whole genome sequencing
WT	Wild type
w/v	Weight per volume
μg	Microgram
μl	Microlitre

μm	Micrometre

Chapter One

Introduction

1.1. *Vibrios* and *Vibrio vulnificus*

Vibrios are ubiquitous aquatic microorganisms typically found in association with organisms such as molluscs, fish, phytoplankton and corals [1–4]. *Vibrios* were first discovered in 1854, following the identification of *Vibrio cholerae* by Italian anatomist, Filippo Pacini [5]. *Vibrios* have since been divided into four families, *Vibrionaceae, Enterovibrionaceae, Salinivibrionaceae* and *Photobacteriaceae* [6]. To date, ~ 140 *Vibrionaceae* family members have been identified, including established species such as *Vibrio vulnificus, Vibrio parahaemolyticus*, *V. cholerae* and more recently discovered species such as *Vibrio crassostreae, Vibrio punensis* and *Vibrio celticus* [7–10]. *V. vulnificus* was originally isolated in 1976 by the Centre for Disease Control and Prevention (CDC) upon receipt of 38 cultures of an unnamed halophilic bacterium[11]. *V. vulnificus* is a Gram-negative, comma shaped bacterium measuring 1.4 – 2.6 μm in length and 0.5 – 0.8 μm in width [12]. Described as having a lower salt tolerance than *V. parahaemolyticus* and as being a lactose positive *Vibrio,* their isolation primarily from blood samples inspired further study by clinical microbiologists [13]. Initially typed as a new pathogenic species of genus *Beneckea*, this was adapted to *V. vulnificus* in 1979 following comparisons with other *Vibrio* species [14,15].

1.2. Genetic diversity

V. vulnificus is frequently notes as being a highly genetically diverse organism [4,16,17]. Numerous strains have been genome sequenced and assembled in full, including CMCP6, FORC_017 and the reference strain YJ016, with the species having a common two-chromosome organisation [16,18–20]. Chen *et al*., (2003) performed a chromosome-by-chromosome analysis of the sequences from *V. vulnificus* YJ016, *V.*

cholerae El Tor N16961 and *V. parahaemolyticus* RIMD 2210633 [16]. Results showed that overall *V. vulnificus* YJ016 displayed greater propensity towards conservation of gene organisation than *V. cholerae* and *V. parahaemolyticus*. Despite *Vibrio* genome evolution consisting of numerous intra and inter-chromosomal rearrangements, the overall topography of the larger chromosome was generally conserved. Further investigation into the functionalities contained within each chromosome revealed that the larger chromosome tends to contain housekeeping genes, such as those involved with growth whereas the smaller chromosome typically contains genes geared towards bacterial adaption [21,22].

1.3. Typing

Initially, *V. vulnificus* strains were subdivided by biotyping, the classification of a species based on a combination of serological, phenotypic and host range characteristics [12]. Based on this, three *V. vulnificus* biotypes were proposed, named biotype 1 – 3. Identified in 1980, biotype 1 strains are predominantly associated with human infection [23]. Biotype 2 strains were identified in 1982 and originally classified as eel pathogens [24]. However, subsequent studies showed that not only were biotype 2 strains capable of causing infection in humans, but when tested in a mouse model of infection they were more virulent (LD_{50} - 10^5 – 10^6 CFU) than biotype 1 strains (LD_{50} - 10^8 CFU) [25–28]. Biotype 3 strains were isolated following an outbreak of *V. vulnificus* wound infections in Israel, 1999 [29]. A 1996 – 1999 marketing policy enabling the sale of pond-raised tilapia and carp, combined with the hottest summers on record for 40 years, resulted in outbreak of a novel *V. vulnificus* clonal variant [30,31]. Patients suffered wound infections similar to those caused by biotype 1 strains, with 10 % mortality [31].

Interestingly, biotype 3 strains are geographically restricted, found exclusively within Israel and in the Sea of Galilee where they have caused ~ 200 infections between 1996 – 2008 [30]. An exploratory study into the genome of the biotype 3 *V. vulnificus* strain, VVyb1, revealed 90 % sequence similarity to clinical biotype 1 strains [32]. The authors also found that 29 of the 'unique' *V. vulnificus* VVyb1 genes had *Shewanella* homologues, a bacterium commonly co-isolated from Israeli aquaculture ponds. This suggests that biotype 3 strains may have evolved from a biotype 1 strain following acquisition of genes from *Shewanella* species.

Whilst biotyping can help us subdivide *V. vulnificus*, there is an overlap between the three biotypes in terms of biochemical properties, host range, genotypes and phenotypes. Therefore, researchers have attempted to identify biomarkers for division of *V. vulnificus* into pathogenic and non-pathogenic strains. This would allow rapid identification of strains significant to human health in fields such as aquaculture and clinical microbiology. Currently, four genetic markers have been identified, polymorphisms in 16S ribosomal RNA (rRNA), the virulence correlated gene (*vcg*), *pilF* polymorphisms and variation in the capsular polysaccharide (CPS) operon [33–37]. Perhaps the least well explored typing method, CPS composition has yet to be significantly correlated with pathogenicity [38,39].

However, multilocus sequence typing (MLST) analysis of the genetic diversity of *V. vulnificus* enabled division of *V. vulnificus* populations based on variance in the *pilF* gene [34]. 20 environmental and clinical strains were sequenced, and a multiplex PCR developed to identify *V. vulnificus* species dangerous to human health. Nearly all pathogenic strains were correctly identified, except for the type strain, CECT 529^T. However, the relevancy of this *pilF* typing method is obscured by the fact that CECT 529^T, supposedly a pathogenic blood isolate, was unable to cause infection in an iron-

overloaded mouse model and has been identified as an environmental isolate by other typing methods. More recently, Baker-Austin *et al*., (2012) have developed a real-time PCR assay for more rapid and efficient identification of pathogenic *V. vulnificus* strains based on a polymorphism in the *pilF* gene [40]. This method enabled 97.9 % detection of pathogenic isolates (n = 47).

16S rRNA-based subdivision of *V. vulnificus* into separate genotypes has been reported by Aznar *et al*., (1994) [36]. The authors hybridised oligonucleotide probes to the 16S rRNA of 13 *V. vulnificus* strains, dividing the strains into two groups, termed rRNA types A and B. This was based on a 17-nucleotide difference out of 1,536 bases in the 16S rRNA variable region. Nilsson *et al*., (2003) determined that rRNA type A strains are typically non-pathogenic (31 of 33), whereas rRNA type B strains are significantly correlated with disease in humans (26 of 34) [41].

The most commonly referenced method of *V. vulnificus* genotyping is based on presence or absence of the virulence-correlated gene (*vcg*) [42]. Randomly Amplified Polymorphic DNA PCR (RAPD-PCR) identified a 200 bp DNA fragment in all clinical *V. vulnificus* samples but only occasionally present in environmental isolates [42]. 90 % of isolates from human infection cases were found to harbour the *vcgC* sequence and 93 % of environmental strains the *vcgE* variant [43]. Interestingly, *vcgC* has not yet been found to code for any protein despite its ability to differentiate the two genotypes. Four 16S rRNA type B strains were characterised as C-type by *vcg* genotyping, while four other type A strains were classified as E-type. This serves to further support both methods as viable techniques for *V. vulnificus* genotyping to distinguish between clinical and environmental isolates.

The drawback to these typing methods is that the extensive genetic heterogeneity of *V. vulnificus* prevents 100 % prediction of pathogenicity. Even the development of multiplex PCR assays which combine biotype, CPS, *vcg* and 16S rRNA data are unable to provide a definitive classification [38,44]. The examination of multiplex PCR assays in comparison to MLST data has resulted in the division of *V. vulnificus* into two distinct lineages, LI and LII [44]. While LII was primarily comprised of clinical isolates, there were still environmental isolates found within this lineage. Therefore, the results are not a guarantee or indicator of virulence, but instead appear to suggest a strain's potential to cause disease.

1.4. Epidemiology

1.4.1. Environmental habitat

V. vulnificus is a halophilic bacterium, primarily isolated from brackish, temperate waters in tropical or sub-tropical climates. *V. vulnificus* is frequently found around the United States and the Gulf of Mexico where water commonly exceeds 18 °C and ranges between 15 - 25 ppt salinity. Due to its requirement for sodium ions to retain cell membrane integrity, *V. vulnificus* is unable to grow in freshwater [39]. Other *Vibrio* species such as *V. cholerae, V. anguillarum* and *V. mimicus* do not share this constraint, only utilising sodium ions for starvation survival, not growth [45]. Whilst most cases reported come from coastal waters surrounding Gulf Coast states, *V. vulnificus* has also been isolated from Japan, Malaysia, the Netherlands, Israel, Sweden, Brazil, Denmark, India, Thailand, Australia, Belgium, Italy, Korea, Germany, Turkey, Spain and Taiwan [46–55]. Isolation of *V. vulnificus* from water bodies has been shown to be temperature-dependent, with seasonal fluctuations [56,57]. Abundance is greatest in the summer when oceanic temperatures exceed 20 °C, viable cell counts fall to

undetectable levels when temperatures drop below 10 °C [57,58]. This is likely due to adaption into a viable but non-culturable (VBNC) state in which the cells retain enzymatic and respiratory activity but lack the ability to grow under standard laboratory conditions [59]. In this state cellular metabolism is restricted, enabling survival, but not proliferation, of the bacterium [60]. As ambient temperatures increase leading into spring, VBNC *V. vulnificus* gradually resuscitate, resulting in resumed detection in coastal waters and in association with other aquatic organisms [59].

V. vulnificus populations are commonly found concentrated in the digestive glands of filter feeding shellfish such as oysters, mussels and clams [11]. In oysters *V. vulnificus* concentrations can reach up to 10^6 CFU/g tissue [11,61]. This is due to the frequent association of *V. vulnificus* with marine biological flora such as diatoms, zooplankton, phytoplankton and algae upon which filter-feeding shellfish feed [62,63]. Greenfield *et al*., (2017) demonstrated a link between harmful algal blooms and an increase in pathogenic *V. vulnificus* population when temperatures > 10 °C [63]. Thickman *et al*., (2017) also presented similar findings for *V. parahaemolyticus* [64]. *V. vulnificus'* association with these aquatic organisms results in uptake and retention by shellfish. Consequently, consumption of raw or undercooked shellfish is the leading route of *V. vulnificus* infection [65]. There are other major *V. vulnificus* reservoirs that have been identified, such as the intestines of fish which can hold bacteria at levels 10,000-fold greater than in water samples [66]. However, as these food sources are typically cooked prior to consumption they are less likely to facilitate the infection of a human host through ingestion.

1.4.2. Consequences of climate change on *V. vulnificus* distribution and clinical incidence

In the past decade, the focus on *V. vulnificus* ecology has expanded in response to the impact of climate change on the prevalence of pathogenic bacteria [56,67–70]. Climate change has been linked to increased occurrences of *V. parahaemolyticus*, *V. cholerae*, *V. alginolyticus* and *V. mimicus* [68,71–73]. Increases in oceanic temperature and salinity gradients caused by global warming is expanding the available geographic range for *V. vulnificus* proliferation [69]. New regions are exposed to these bacteria, causing increasing *V. vulnificus* infections in zones where the pathogen had been previously undetectable. Baker-Austin *et al*., (2012) investigated the emergence of *Vibrios* at high latitudes in response to warming of the Baltic Sea [67]. Analysis of sea-surface temperatures (SST) showed a shift in temperature of up to 1 °C per decade, exceeding seven times the global rate. SST increases in conjunction with the low salinity (< 25 ppt NaCl) has also been shown to promote *V. vulnificus* growth and proliferation in the Baltic sea. Herrfurth *et al*., (2013) were able to isolate *V. vulnificus* from Baltic Sea blue mussels at concentrations of up to 2.2×10^7 CFU/g tissue [74]. Not only does the increase in SST result in greater proliferation of *Vibrios,* but it also has the effect of more people coming into contact with *V. vulnificus*, either through swimming in contaminated water or handling of contaminated seafood.

Climate change has other impacts aside from increases in SST. One of which is the increased variance in precipitation and extreme weather patterns, resulting in already wet areas experiencing increased rainfall, and dry areas becoming more arid [75]. Excessive rainfall can reduce the salinity of select marine ecosystems, indirectly creating the ideal environment for *Vibrio* growth. Esteves *et al*., (2015) monitored *V. vulnificus*, *V. parahaemolyticus* and *V. cholerae* populations in French Mediterranean

coastal lagoons following periods of heavy rainfall and freshwater flooding. The freshwater influx resulted in salinity reduction from 314 – 361 ppt to 22 – 164 ppt over 15 days [76]. *V. vulnificus* concentrations measured 0.7 – 2.1 × 10^3 most probable number (MPN)/L before salinity decrease. Once salinity dropped to ~150 ppt, this increased to 4.6 × 10^4 MPN/L. Extreme storms also have the potential to cause storm surges, where regions are flooded with seawater as a result of high wind speeds and changes in atmospheric pressure causing tsunami-like rising water [77]. This has the effect of bringing in *V. vulnificus*-containing seawater inland where it encounters other water bodies, floodwater and human populations. The environmental disturbance caused by Hurricane Katrina in 2005 resulted in widespread exposure of people to *Vibrio* contaminated water [78]. Over the following weeks, 22 *Vibrio* infections were reported, 82 % of which were *V. vulnificus*. Of these, all were wound infections, with only *V. cholerae* causing non-wound associated illness [79].

1.5. *V. vulnificus* infection

1.5.1. Clinical presentation

V. vulnificus infection can be contracted either via ingestion or wound exposure. Ingestion of raw or undercooked seafood, such as oysters, contaminated with virulent *V. vulnificus* is a major route for *V. vulnificus* transmission to humans [80]. It is believed that 10^6 bacilli are required to initiate *V. vulnificus* infection via ingestion of contaminated food, however this number may drop to as low as one bacterium in hosts suffering liver disease [81,82]. Following consumption gastroenteritis symptoms typically appear within 7 days, however it is not unknown for 14 days to pass before the infection presents itself [83,84]. Patients initially present with diarrhoea, nausea, vomiting,

abdominal cramps, headaches, chills and fever [85]. Although unpleasant, death is rare, with studies postulating that deaths from gastroenteritis were actually a consequence of undiagnosed septicaemia [86–88]. Progression of the infection to primary septicaemia results in development of more medically significant symptoms, including secondary lesions on the extremities and severe hypotension. In this case ~ 50 % of patients die within 48 hours of hospital admission [85].

The secondary route of infection is through exposure of an open wound. This can be as a result of either submersion in contaminated waters or following contact with infected seafood. Cases of *V. vulnificus* wound infection have been reported following seafood handling, submersion of a fresh tattoo in seawater and even acupuncture on a fish hatchery worker [89–91]. Within four hours to four days patients will present with erythema, haemorrhagic bullae, cellulitis and intense pain [92]. Failing immediate treatment, the infected lesions frequently turn necrotic. Whilst being visually more aggressive than primary septicaemia, wound infections carry a much lower mortality rate of ~ 25 % [85]. Interestingly, despite the relatively recent identification and classification of *V. vulnificus,* medical historians have identified several historical clinical cases which appear highly indicative of *V. vulnificus* wound infection. The oldest dates to the fifth century B.C. where Hippocrates observed the infection and rapid death of a patient whose foot became swollen, erythematous and developed black blisters following a wound in his toe [93]. Although other potential causative pathogens have been suggested, such as virulent *Streptococcus*, the rapid nature with which the disease killed the patient and the development of black blisters reminiscent of haemorrhagic bullae suggest a *V. vulnificus* infection.

1.5.2. Risk factors

Like many human pathogens, *V. vulnificus* infection severity is largely determined by the pre-existing health of the host. This includes patients with HIV/AIDS, liver disease, kidney disease, haematological disorders, cancers and the immunosuppressed [83,89,94]. Menon *et al*., (2015) analysed all Cholera and Other Vibrio Illness Surveillance System (COVIS)-reported cases of *V. vulnificus* infection from 1988 – 2006 to determine the importance of pre-existing medical conditions in establishment of *V. vulnificus* infection (n = 1,212) [94]. The authors reported that 80 % of patients already had at least one pre-existing medical condition, either liver disease (40 %), heart disease (23 %), diabetes (20 %), renal complications (10 %) or other conditions (< 10 %). This is likely due to the importance of iron in *V. vulnificus* establishment and proliferation in a human host. Most patients presenting with *V. vulnificus* infection have elevated serum- iron levels, either as a result of a haematological disorder or chronic liver disease causing high serum saturation of transferrin and ferritin [84,85,95–98]. Therefore, it is 80 times more likely that the immunosuppressed, or sufferers of chronic liver disease, will develop primary septicaemia compared to healthy individuals [83]. The importance of iron for sustaining *V. vulnificus* infection is so vital that researchers have been assessing the potential of a novel iron-chelator, deferiprone, to hinder *in vivo* growth [99,100]. Interestingly, studies have demonstrated that certain pre-existing conditions rendered patients more susceptible to either *V. vulnificus* septicaemia or wound infection. Patients with liver disease were more likely to develop primary septicaemia following ingestion of the pathogen, whereas those with renal complications or malignancy were more susceptible to infection through wound exposure [94].

Males are at a greater risk of infection from *V. vulnificus* than females. Of the 1,212 cases reported between 1988 and 2006 by COVIS, 86 % were male [101]. The only

current potential explanation for this disparity is the inhibitive effects of oestrogen on the impact of LPS-mediated endotoxic shock. Using a rat model, Merkel *et al*., (2001) were able to increase mortality in female rats following gonadectomy and decrease mortality in male rats via oestrogen supplementation [102]. However, to date no further studies have examined further the impact of oestrogen on inhibiting endotoxic shock and the benefits it may provide.

1.5.3. Diagnosis and treatment

Due to the fulminating nature of *V. vulnificus* infection it is critical that infection is diagnosed and treated as quickly as possible. Initial examination of patients will indicate a severe bacterial infection, with a marked shift in white blood cell count [89]. Patients fitting this description along with the previously discussed symptoms of fever, erythema, swelling, diarrhoea, nausea, vomiting and a change in mental status should be questioned to determine whether they have had any contact with seafood within the past week. This is especially relevant if they have a history of liver disease, immunodeficiency or renal complications. Radiography studies can be employed on affected tissues to identify changes in soft tissue and locate pockets of fluid, which can be used to exclude other possible conditions and advise attempts of surgery. In previous case studies where the species of pathogen was not already known, *V. vulnificus* was identified as an 'encapsulated, aerobic, Gram-negative bacillus' [97]. If *V. vulnificus* is suspected, it can be confirmed via culture on *Vibrio* selective thiosulfate-citrate-bile-salts-sucrose (TCBS) agar. TCBS utilises an alkaline pH, bile salts and a sucrose carbon source to inhibit growth of non-*Vibrio* species.

There is no defined cure for *V. vulnificus* infection, with the consensus being surgical debridement in combination with a variety of antibiotics [89,103]. Due to the speed with which the infection progresses it is crucial that surgery and administration of drugs is performed immediately. Patients who undergo surgical debridement are likely to require amputation of the infected limb to prevent further disease dissemination. A delay in treatment of greater than 24 hours prompts a rise in mortality rates, from 33 % to 53 %. If left untreated for 72 hours, mortality increases from 50 % to 100 % [103]. The CDC recommends 2 g ceftazidime intravenously/intramuscularly every 8 hours in combination with 100 mg doxycycline intravenously/peroral twice daily for up to two weeks. Some recent studies state that monotherapy with glycylcyclines, namely tigecycline, may present a better therapeutic option [104]. Nevertheless, case studies demonstrate the effectiveness of an extensive range of effective treatments, including the use of cefotaxime, gentamicin, minocycline and ciprofloxacin [83,89,104].

Worryingly, a study of Japanese emergency physicians by Osaka *et al*., (2004) reported that only 15.7 % (n = 235) had a basic understanding of *V. vulnificus* infection and the required treatment [46]. Due to the temperate climate, seafood intake, consumption of raw seafood and prevalence of chronic liver disease, Japan presents ideal conditions for *V. vulnificus* outbreak. For this reason, individuals at risk and the medical community should be familiar with the disease and how to treat it effectively and rapidly. Patients with liver disease, haematological conditions or cancer should be advised against the exposure of wounds to seawater. All patients should be seriously advised against the consumption of raw seafood.

1.5.4. Low global *V. vulnificus* clinical incidence

The CDC has reported a 115 % increase in *V. vulnificus* infections between 1996 and 2010 [105]. The ubiquity of the organism, in conjunction with increased prevalence due to climate change suggests that a greater number of infections would be reported annually, particularly in areas that are extremely conducive for *V. vulnificus* growth and proliferation such as the Gulf of Mexico, Japan and the USA. However, the number of reported cases is surprisingly low. The CDC estimates that *V. vulnificus* infects ~ 100 – 200 people annually in the USA, despite reporting ~ 80,000 infections caused by *Vibrio* species. Despite the severity of *V. vulnificus* infections, they are significantly rarer than less virulent but more prevalent *Vibrios*, such as *V. parahaemolyticus,* estimated to be responsible for ~ 45,000 infections annually in the USA [106,107].

One cause may be the underreporting of *V. vulnificus* cases due to infection misdiagnosis. *V. vulnificus* infections in the Gulf Coast have been monitored by the CDC since 1988, with the pathogen becoming a nationally notifiable disease in 2007. Disease caused by *Vibrio* species is reported through COVIS [108]. Healthy individuals typically only experience gastroenteritis, resulting in common food-borne illnesses such as *Salmonella*, *Campylobacter* or *Listeria* infections being implicated. Diagnosis is further hindered by clinical laboratories in Gulf Coast states not routinely testing for *V. vulnificus*. A survey of 201 clinical laboratories determined that of the 82 % that checked stool samples, only 20 % tested specifically for *V. vulnificus* [109]. To further complicate the diagnosis, when these tests are run, they may be affected by previous patient treatment regimens due to *V. vulnificus'* sensitivity to a range of antibiotics. Therefore, clinicians need to be aware of the unintended impact that recent antibiotic administration may have on diagnostic reliability. Lee *et al*., (2017) performed blood culture analysis on eight patients confirmed to have *V. vulnificus* infection but who had

been previously been administered antibiotics that had unintentional activity against *V. vulnificus* [104]. The study found no positive indication of *V. vulnificus* infection suggesting that *V. vulnificus* may not necessarily be ruled out even if not detected through culture. Other studies have demonstrated the efficacy of real-time PCR for detecting *V. vulnificus* from blood sample analysis, even if culturable *V. vulnificus* have been eliminated by antibiotic treatment. DNA copies in host tissues are far less affected by antibiotics than viable bacterial cells, as a result, molecular methods for identification of *V. vulnificus* present a far more reliable, rapid and accurate method of *V. vulnificus* diagnosis [110].

1.6. Virulence mechanisms of *V. vulnificus*

1.6.1. Adaption to low pH

As one of the two routes of infection for *V. vulnificus* is through ingestion it is vital that the bacterium can neutralise the acids of the digestive system. Exposure to gastric fluids and oxidative stress in the upper gastrointestinal tract following ingestion is partly counteracted via production of lysine decarboxylase, CadA [111]. Located within the *cadBA* operon, *cadA* expression is regulated by CadC, whose own expression is upregulated under low pH conditions [112]. CadA catalyses the decarboxylation of lysine into cadaverine and CO_2, which are exported out of the cell via CadB to counteract external acidification [113]. A *cadA V. vulnificus* mutant demonstrated significantly reduced tolerance to acidic stress relative to the wild-type strain [114]. CadA has also been shown to play a role in the acid responses of a number of other human pathogens, including *Salmonella enterica* and *Escherichia coli* [115].

Kim *et al*., (2005) also demonstrated that induction of manganese-containing superoxide dismutase (MnSOD) is essential for *V. vulnificus* acid tolerance [116]. MnSOD is involved in both acid neutralisation and superoxide reduction in a number of bacteria and has the beneficial effect of being a superoxide radical scavenger [116–119]. Repression of MnSOD resulted in significantly reduced tolerance to low pH, whereas a mutant de-repressing MnSOD demonstrated greater tolerance than the wild-type [116]. As would be expected from enzymes that neutralise low pH and reduce superoxide, both proteins are upregulated at low pH. However, this has been linked to the accumulation of intracellular superoxide as opposed to low pH itself.

1.6.2. Motility and adhesion

V. vulnificus employs several virulence factors involved in motility and adhesion to facilitate permeation of the intestinal wall and entrance to the bloodstream. Like many pathogens, *V. vulnificus* is highly motile, possessing a single polar flagellum which has been implied to have a role in adhesion, cytotoxicity, biofilm formation and lethality to mice [120]. Kim *et al*., (2014) performed mutagenesis studies on *V. vulnificus* to elucidate the role of the flagellin genes, *flaA-F* [121]. The authors found that motility was only fully suppressed when all six *fla* genes were deleted, whereas single mutants demonstrated varied levels of motility reduction and cytotoxicity. Interestingly, the *flaB/flaD* mutant demonstrated a 23 and 91-fold increase in LD_{50s}, highlighting the importance of the flagella and motility in *V. vulnificus* infection. Deletion of *V. vulnificus* structural pili genes, *pilA* and *pilD*, has been shown to have similar detrimental effects on adherence to host cells [122]. Paranjpye *et al*., (2005) showed that *pilA* deletion reduced the ability of *V. vulnificus* to form biofilms, to adhere to HEp-2 cells and significantly

reduced virulence in iron-dextran treated mice [122]. Inactivation of *pilD* resulted in reduced adherence to HEp-2 cells, decreased virulence and inhibition of Type 2 Secretion System (T2SS) exoenzymes. Inactivation of *V. vulnificus* pili results in reduced virulence, this is likely due the requirement for cell-cell contact for *V. vulnificus* cytotoxicity [123].

1.6.3. Surface proteins

Once *V. vulnificus* penetrates the epithelial lining and enters the bloodstream it is exposed to the host immune system, including the effects of opsonisation by complement and phagocytosis by host macrophages. A primary defence presented by the bacterium against opsonisation is the generation of a capsular layer, referred to as capsular polysaccharide (CPS), comprised of long-chain polysaccharides with repeat-unit structures [124]. CPS has been identified in a wide range of both Gram- negative and Gram-positive bacteria, including *Escherichia coli*, *Klebsiella pneumoniae*, *Staphylococcus aureus* and *Streptococcus pneumoniae* [124–128]. CPS is one of the few essential *V. vulnificus* virulence factors due to its role in evading opsonisation, masking immunogenic structures and resisting bactericidal serum [3,83,129]. Not all strains express CPS, however capsulated strains show significantly greater virulence compared to acapsular strains [129]. Expression of CPS on the cell surface facilitates slower systemic clearance and increased invasive activity towards subcutaneous tissues [3]. Wright *et al*., (1990) also demonstrated that when injected into an iron-overloaded mouse model, capsulated strains resulted in significantly greater mortality than acapsular strains [130].

V. vulnificus also produces lipopolysaccharide (LPS) which it incorporates into its outer membrane, responsible for causing endotoxic shock characteristic of severe *V. vulnificus* infection [39]. LPS is a known pyrogen and has been linked to neurodegeneration, neuronal injury through disruption of the blood-brain barrier, release of inflammatory mediators and release of reactive oxygen species [131]. Intraperitoneal injection of *V. vulnificus* LPS into mice resulted in significant drops in arterial pressure within 10 minutes resulting in death in as short as 30 minutes [132]. Interestingly, both oestrogen and low-density lipoprotein (LDL) cholesterol have been shown to have protective activity against the effects of LPS [102,133]. This serves to help explain the sexually dimorphic patient demographic for *V. vulnificus* infection. However, no further studies have managed to elucidate the mechanisms behind this protection.

1.6.4. Iron acquisition

Vibrios, amongst a multitude of other bacterial species, require iron for growth and proliferation as iron is essential for enzyme activity [134]. It is for this reason that *V. vulnificus* is commonly isolated from coastal and estuarine waters, where dissolved iron levels are far higher than in the open ocean due to terrestrial runoff [135]. Virulence assays in iron-overloaded mice demonstrate a direct correlation between *V. vulnificus* infectious dose and iron concentration showing that iron availability and the ability of *V. vulnificus* to acquire iron is a major virulence factor [82]. Studies show that C-type *V. vulnificus,* associated with causing infections in humans are far more capable of surviving in human serum than E-type strains [136]. In humans, 99 % of iron is sequestered in haemoglobin, myoglobin or ferritin-hemosiderin, whereas extracellular iron is associated with iron-binding molecules such as transferrin [99,137]. This results in

extremely low iron availability. However, patients suffering severe *V. vulnificus* infection frequently present with pre-existing medical conditions such as haemochromatosis or liver disease which result in increased serum iron levels [98,134].

The sequestration of iron for uptake by *V. vulnificus in vivo* is mediated by high affinity siderophores which bind iron for uptake by the bacterial cell [85]. These mechanisms are regulated by the ferric uptake regulator, Fur, and are expressed under low-iron conditions [138,139]. *V. vulnificus* has been shown to produce both catechol and hydroxymate siderophores which form ferrisiderophore complexes when associated with iron [134,140]. Uptake of siderophores is mediated by the TonB transport system and associated proteins, ExbB and ExbD [141,142]. Interestingly, *V. vulnificus* encodes three TonB systems, TonB1 – 3, as opposed to the two systems more commonly found in other pathogenic *Vibrios* [143]. All TonB systems within *V. vulnificus* mediate the uptake of iron-associated siderophore complexes, however these three membrane transporters recognise different receptors and vary in the conditions under which they are active [134] TonB systems have even been shown to have the ability to take up siderophores produced by foreign bacteria, enhancing their ability to compete with other bacteria for iron [144].

1.6.5. Effectors

V. vulnificus has been shown to secrete several fulminating and destructive cytotoxic effectors. The three most significant being; cytolytic haemolysin (VvhA), elastolytic protease (VvpE) and repeats in toxin exoprotein (RtxA1) [145–147]. VvhA and VvpE have a range of virulence attributes, including causing partial paralysis, fluid accumulation, vascular permeability, neutrophil recruitment, epithelial cell apoptosis, nitric oxide production,

tissue necrosis, cutaneous lesions, type IV collagen degradation and induction of inducible nitric oxide synthase activity [146,148–155]. Interestingly, despite these extensive induced conditions, inactivation of *vvhA* and *vvpE* both individually and together did not result in impaired virulence in a mouse model of infection [101,156]. Further exploration of the *V. vulnificus* genome led to the discovery of a gene encoding a repeats-in-toxin (RTX) exoprotein essential for virulence in mice and tissue cultures, termed RtxA1 [157]. RTX toxins have been identified in a wide range of Gram-negative bacteria, including *V. cholerae* [158,159]. Translocated in a contact-dependent manner via the type 1 secretion system (T1SS), these proteins consist of N- and C-terminal repeats believed to form pores in target cell plasma membranes, enabling translocation of the effector-containing central portion of the toxin [160]. Eukaryotic cells exposed to the wild-type protein demonstrated cytoskeletal rearrangements, blebbing and necrotic cell death [161]. Inactivation of RtxA1 resulted in significantly decreased cytotoxicity and reduced cell lysis, demonstrating that this is one of the key virulence factors in causing *V. vulnificus* infection.

1.7. The Type 6 Secretion System (T6SS)

Bacterial secretion systems demonstrate highly diverse structure, function and regulation. To date, nine secretion systems have been identified, termed T1SS – T9SS (Fig. 1.1) [162]. Whilst well characterised systems such as the T3SS have been identified and studied in a range of different microorganisms since their discovery, novel secretion systems are still being discovered and characterised [163–165]. The latest of which being the T9SS, identified in 2010 and labelled the Por secretion system

(PorSS), before being renamed to fit current secretion system naming nomenclature in diderm bacteria [166,167].

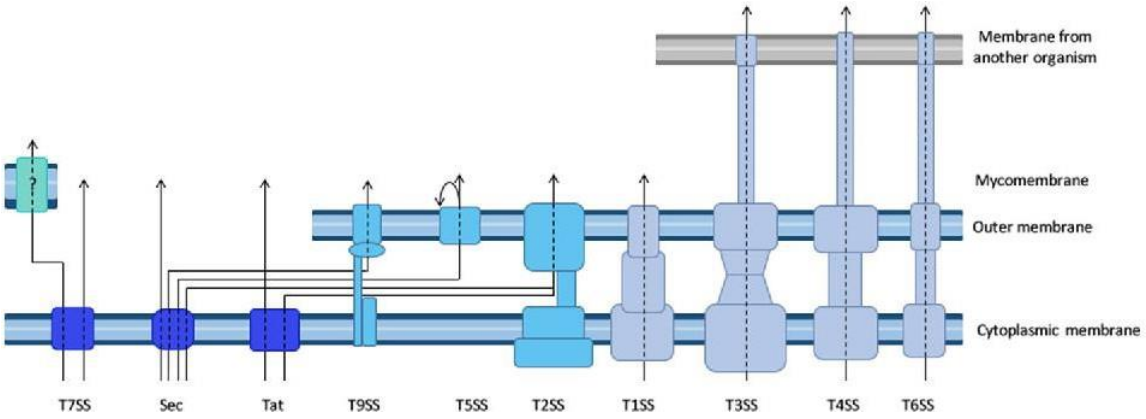

Figure 1.1: Bacterial secretion systems schematic. Secretion in monoderm bacteria (left) is largely mediated by the Sec and Tat transport pathways, or the T7SS. In diderm bacteria (middle and right), proteins are either secreted in a one-step process directly into the surrounding environment/target cell (T1SS, T3SS, T4SS, and T6SS), or they are first secreted into the periplasm by the Sec system (T2SS, T5SS, and T9SS) or the Tat system (T2SS). Figure taken from Maffei *et al*., (2017) [168].

The T6SS was identified by Pukatzki *et al*., (2006) following the observation that *V. cholerae* was able to target and kill the phagocytic amoeba, *Dictyostelium discoideum* [169]. This was linked to extracellular translocation of virulence-associated secretion (VAS) proteins. Further exploration demonstrated that VAS proteins were translocated in a contact-dependent manner. The study was also able to demonstrate similar cytotoxicity against mammalian J774 macrophages, suggesting an anti-eukaryotic role for the T6SS. Since its initial identification in *V. cholerae*, the T6SS has been discovered in > 25 % of proteobacterial genomes, and in 30 % of these genomes there are multiple copies of almost complete loci, encoding different T6SS variants [170]. Further genetic analysis confirms that these are not simply the result of duplication

events but have been conserved through evolution. This implies that these T6SS variations play a defined role, whether this be in competition, nutrient acquisition, quorum sensing, or other activities [170]. *Burkholderia pseudomallei*, for example, contains six T6SSs (T6SS1 – T6SS6), which have a range of roles including the formation of giant, multi-nucleated cells for bacterial propagation by the T6SS5 and the acquisition of metal ions by the T6SS4 in the surrogate organism, *Burkholderia thailandensis* [171]. Church *et al*., (2016) was the first study to identify the T6SS in *V. vulnificus* and to identify two T6SSs, named the T6SS1 and the T6SS2 (Fig. 1.2) [172]. Despite all sequenced *V. vulnificus* strains possessed the T6SS2, only a subset possessed the T6SS1. Furthermore, whilst the T6SS1 was demonstrated to have anti-bacterial activity at 30 °C *in vitro,* the T6SS2 demonstrated no anti-prokaryotic or anti-eukaryotic activity.

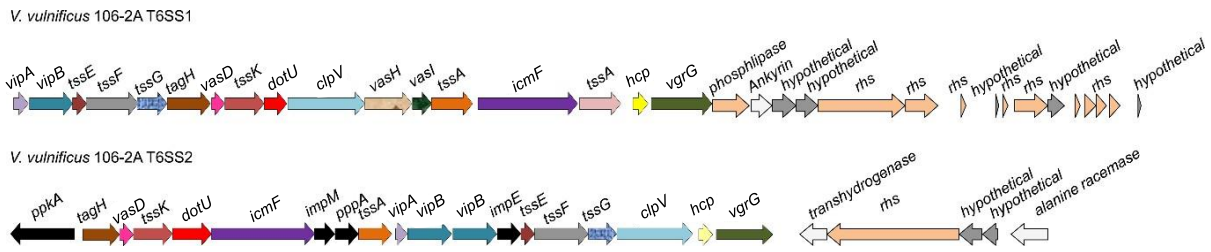

Figure 1.2: *V. vulnificus* T6SS1 and T6SS2 operons. This schematic shows the genetic organisation of the T6SS1 and T6SS2 operons from *V. vulnificus*. Genes have been colour matched to highlight matching genes. Figure taken from Church *et al.,* (2016) [172].

The anti-bacterial activity of the T6SS plays an important role in the interactions between microorganisms within a niche. Contrary to the environments in which *in vitro* studies are performed, *in vivo* conditions are far less nutrient rich, resulting in the need for a means to compete with other present microorganisms. Speare *et al*., (2018)

utilised a *Euprymna scolopes* squid model to demonstrate that attacker strains of *Vibrio fischeri* were able to target and kill prey strains *in vivo* in a T6SS-dependent manner [173]. The ability for the T6SS to target and kill neighbouring microorganisms can also be important in the context of causing disease. Recent studies have shown that *V. cholerae* kills host commensal microbiota *in vivo* in a T6SS-dependent manner, enhancing gut colonisation by the pathogen [174]. Furthermore, clearance of host microbiota was shown to increase Cholera-associated diarrhoea, suggesting that T6SS-antagonism of host commensals by *V. cholerae* can increase potential for transmission. These are just a selection of T6SS activities which have subsequently been identified in a range of human pathogens, such as *Serratia marcescens, P. aeruginosa* and *Acinetobacter baumannii* [175–177].

1.7.1. T6SS regulation

The T6SS is activated in response to a range of conditions, including temperature, salinity, iron-starvation, biofilms, stress response, and osmolarity [178–186]. The regulation of T6SS activity at both a transcriptional and translational level is theorised to be due to the high energetic requirements of assembly, firing and disassembly. There are a diverse range of transcriptional regulators involved in T6SS transcriptional regulation. These include proteins such as VasH, a bacterial enhancer binding protein that serves to activate σ^{54}, an alternative sigma factor [186]. Interestingly, in *V. cholerae, vasH* is encoded within the primary T6SS operon but has only been shown to activate transcription of two auxiliary clusters in the genome encoding *hcp* and *vgrG* variants. As *V. vulnificus* does not contain these auxiliary clusters it is yet unknown as to the target of VasH in T6SS transcription activation. Furthermore, *vasH*

is only found within the T6SS1 operon of *V. vulnificus*, T6SS1$^-$ strains possess no *vasH* gene that has yet been identified, perhaps suggesting that VasH in *V. vulnificus* is only required for T6SS1 regulation.

Bacteria also demonstrate post-translational control of T6SS activity. An example of this that has been identified in *P. aeruginosa* is the threonine phosphorylation pathway (TPP) [187,188]. Upon detecting a T6SS-mediated attack by neighbouring cells, a serine-threonine kinase (PpkA) phosphorylates a forkhead- associated protein (Fha), promoting assembly of a T6SS at the site of attack. A serine- threonine phosphatase (PppA) inhibits this interaction. The TPP has been shown to compete with the negative regulation of TagF to delay T6SS re-assembly post-firing to allow for spatial reorganisation and re-targeting of prey strains [188]. Interestingly, the T6SS2 of *V. vulnificus* encodes *pppA and ppkA ,* but the T6SS1 encodes neither of these, suggesting that the T6SS2 of *V. vulnificus* may be similarly regulated to the T6SSs of *P. aeruginosa* [172].

1.7.2. T6SS structure

The T6SS is a molecular syringe through which cytotoxic effectors are injected into target cells. The T6SS is typically composed of 13 core genes (listed in Table 1.1) required for secretion system assembly and mobilisation. The T6SS can be divided into the tail, trans-membrane and baseplate complexes. A schematic of the T6SS can be seen in Fig. 1.3. The tail complex is named after its remarkable similarity to the contractile tail of T4 bacteriophage [189]. When T4 bacteriophage make contact with

Protein	Function	Source
TssA	Involved in T6SS biogenesis through baseplate complex recruitment and TssB/C/D polymerisation.	Zoued *et al.,* (2016) [190]
TssB (VipA)	Forms a contractile sheath surrounding the Hcp needle in conjunction with TssC.	Brackmann *et al*., (2018) [191]
TssC (VipB)	Forms a contractile sheath surrounding the Hcp needle in conjunction with TssB.	Brackmann *et al*., (2018) [191]
TssD (Hcp)	Hcp subunits form a hollow tube for effector translocation. Involved in TssB/C recruitment.	Brunet *et al*., (2014) [192]
TssE	Baseplate complex protein also required for proper assemble of the Hcp tube.	Brunet *et al*., (2015) [193]
TssF	Baseplate complex protein, TssF and TssG stabilise one another for proper assembly of the Hcp tube.	Brunet *et al*., (2015) [193]
TssG	Baseplate complex protein, TssF and TssG stabilise one another for proper assembly of the Hcp tube.	Brunet *et al*., (2015) [193]
TssH (ClpV)	AAA+ ATPase, controls disassembly and recycling of the T6SS.	Basler *et al*., (2012) [189]
TssI (VgrG)	Forms a trimeric spike complex at the tip of the Hcp needle in association with PAAR proteins.	Hachani *et al*., (2014) [194]
TssJ (VasD)	Trans-membrane complex lipoprotein that anchors to the outer membrane in association with TssL/M.	Durand *et al*., (2015) [195]
TssK	Hypothesised to interact with TssD/L/C to link the TssB/C/D complex to the trans-membrane complex.	Zoued *et al*., (2014) [87]
TssL (DotU)	Trans-membrane complex lipoprotein, interacts with TssM/J to anchor the T6SS to the cell membrane.	Durand *et al*., (2012) [196]
TssM (IcmF)	Trans-membrane complex lipoprotein that anchors to the outer membrane in association with TssL/J.	Durand *et al*., (2015) [195]

Table 1.1: A list of the 13 proteins essential for T6SS assembly and function. All proteins have been labelled according to the type six secretion (Tss) nomenclature. More commonly utilised names for particular proteins have been identified in brackets.

target bacterial cells they inject genetic material through a contractile tail to which the T6SS bears remarkable similarity with the exception that the T6SS is translocating cytotoxic effectors as opposed to genetic material [197]. The needle of the bacterial T6SS is composed of stacked haemolysin co-regulated protein (Hcp) hexamers which share homology with the gp19 tube protein of T4 phage [198]. Protein crystallisation studies showed that Hcp forms a hollow tube with a 40 Å internal diameter, similar to that of T4 phage [199,200]. To facilitate penetration of target cell membranes, the Hcp needle is

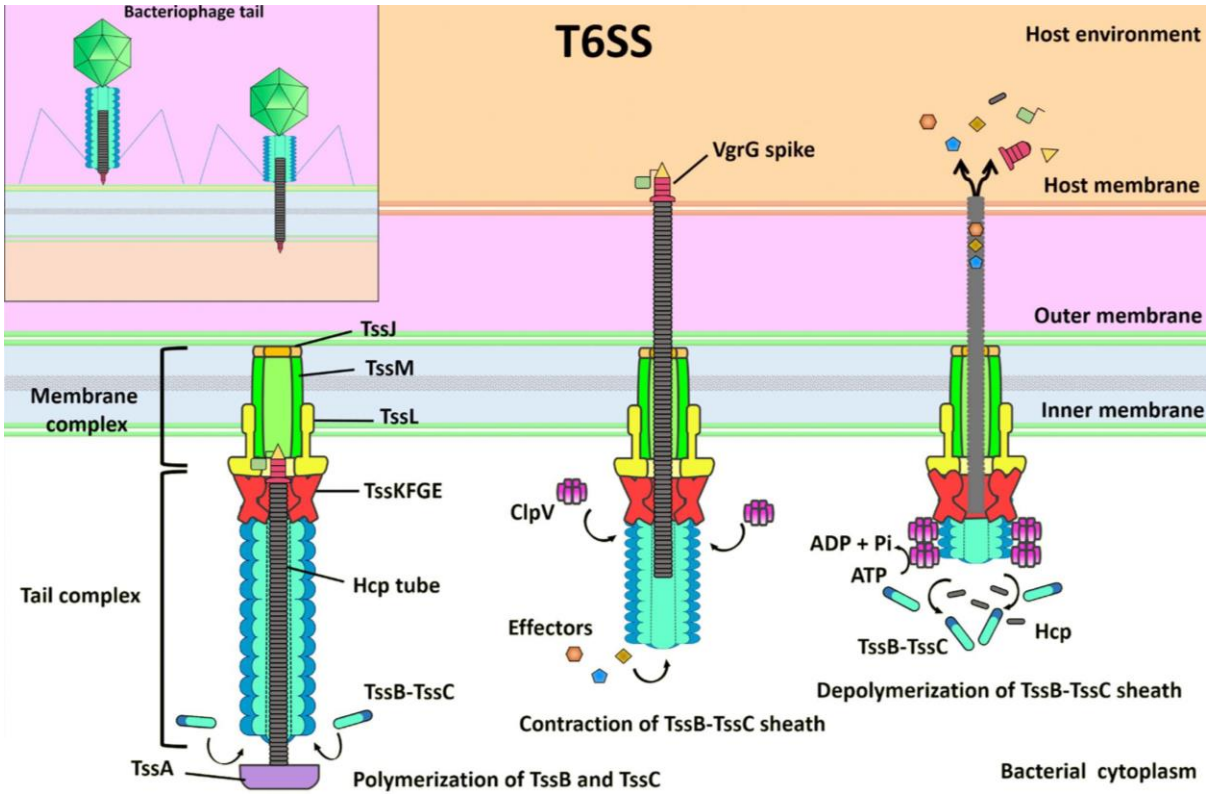

Figure 1.3: The structure of the T6SS. The host cell assembles the T6SS in the extended state. Here the Hcp needle is contained within a contractile TssB/C sheath anchored to a membrane complex consisting of TssM, TssJ and TssL and a baseplate complex consisting of TssE, TssF, TssG, and TssK. TssA serves to aid in baseplate recruitment and priming, coordination of tail/sheath extension, and maintenance of the sheath in its extended position. Contraction of TssB/C drives the Hcp/VgrG/PAAR complex into the neighbouring cell. Effector delivery into the target cell is followed by disassembly of the T6SS by the AAA+ ATPase, ClpV. A bacteriophage tail schematic has been included to highlight the similarities between the T6SS and the contractile phage tail. Figure taken from Navarro-Garcia et al., (2019) [201].

topped with a trimeric valine-glycine repeat G (VgrG) complex in association with proteins from the proline-alanine-alanine-arginine (PAAR) repeat superfamily [202]. This complex serves to 'sharpen' the tip of the needle and aid T6SS penetration of the target cell. Finally, the needle and tip complex are encased in a tubular cog-like sheath of VipA and VipB proteins, comparable to the gp15/gp18 contractile sheath of T4 phage [197]. Named after their interactions with the AAA+ ATPase, ClpV, VipA/VipB (ClpV–interacting proteins) are essential for T6SS functionality through their contraction to drive needle propulsion [203,204]. Once contracted, the VipA/VipB sheath is recognised and disassembled by ClpV.

The tail complex of Hcp, VgrG-PAAR and contractile VipA/B is bound to the host membrane through interactions with a baseplate complex consisting of interactions between six proteins, TssA, TssE, TssF, TssG, TssK, and VgrG [205]. In T4 phage the nucleus for tail assembly is the baseplate, this is comparably observed in bacterial T6SSs, with VgrG acting as the nucleus for tail formation [206,207]. Baseplate proteins are recruited to the inner-membrane where they interact with the trans-membrane complex consisting of two inner-membrane components, TssL and TssM, a lipoprotein associated with the outer membrane, TssJ, and an accessory protein, TagL (only present in a few bacterial T6SS baseplate complexes) [167]. Assembly of these two complexes is mediated by the baseplate proteins, TssL/K and TssL/M binding due to cytoplasmic loop interactions [190]. Once established, the baseplate and trans-membrane complexes are maintained through interactions between TssK/L, TssK/M, TssL/E, and TssM/G [190,193,208]. The trans-membrane complex allows for passage of the tail-complex and serves to maintain cell integrity during secretion.

1.7.3. T6SS effector and immunity proteins

Since the discovery of the T6SS, new effector and immunity proteins have been routinely discovered and characterised. Antibacterial effectors can be broadly divided into three separate classes: cell wall targeting effectors, membrane targeting effectors and nucleic acid targeting effectors [209]. Recently, T6SS effectors whose activity is not covered by these three categories have been identified in *P. aeruginosa* and *Yersinia pseudotuberculosis* suggesting that there is a potentially diverse array of T6SS associated effectors which have yet to be characterised [210,211]. Whilst more effectors have been identified than can be reasonably discussed in this work, the primary groups have been identified and discussed below.

1.7.3.1. Cell wall targeting effectors

T6SS effector-mediated degradation of peptidoglycan was first identified in *P. aeruginosa* in which two effector proteins, Tse1 and Tse3, were shown to hydrolyse peptidoglycan following delivery to the periplasm [212]. *P. aeruginosa* was shown to protect itself from the hydrolytic activity of Tse1/Tse3 through the possession of cognate immunity proteins, Tsi1 and Tsi3, which bind the cognate effectors. Characterisation of Tse1/Tse3 showed that these proteins have amidase and glycoside hydrolase activity respectively, interaction with peptidoglycan results in the cleaving of peptide cross-links between glycan strands by Tse1 and cleaving of the glycan backbone by Tse3, resulting in cell wall degradation and loss of integrity. Since their discovery in *P. aeruginosa,* further research has demonstrated that there is a versatile superfamily of T6SS peptidoglycan-degrading effectors which can be organised into four groups of different amidase specificities termed T6SS amidase effector 1 – 4 (Tae1 – 4) [212]. Similar effectors have been identified in *V. cholerae*.

Specifically, VgrG3, which is part of the VgrG trimeric complex forming the tip of the needle has been shown to have peptidoglycan degrading activity and TseH, which carries a hydrolase domain and results in *E. coli* death when expressed in the periplasm [213,214].

1.7.3.2. Membrane targeting effectors

The plasma membrane is vital for maintaining cell integrity in both prokaryotic and eukaryotic cells. As such, there are a range of T6SS effectors that have evolved to target this component as a means of inducing cell death. Russell *et al*., (2013) reported the discovery of a superfamily of bacterial phospholipase enzymes who were demonstrated to have roles as T6SS effector proteins [215]. These effectors were labelled type VI lipase effectors (Tle). Tle cognate immunity proteins are labelled type VI secretion lipase immunity (Tli) proteins and are believed to localise to the periplasm where they protect the host cell from the membrane targeting activity of Tle effectors. Tle phospholipase effectors have been identified in a range of bacteria, including *P. aeruginosa* PldB (Tle5b), *V. cholerae* TseL (Tle2) and *Burkholderia thailandensis* Tle1 [216–218]. Another type of membrane targeting effectors are pore-forming toxins. T6SS pore-forming toxins integrate into the membrane, where the pore in the inner membrane facilitates loss of membrane potential through a voltage-dependent ion channel, halting cellular respiration [219]. T6SS pore-forming toxins have been identified in a range of organisms, including *P. aeruginosa, S. marcescens,* and *B. thailandensis* [219].

Whilst more widely characterised, membrane-targeting effectors are not solely geared towards antibacterial activity. *S. marcescens,* was recently shown to possess antifungal activity mediated by T6SS-dependent secretion of two effectors, Tfe1 and

Tfe2 [218]. This is the first example of antifungal activity mediated by a T6SS. Characterisation of Tfe1 and Tfe2 identified Tfe1 as a membrane targeting effector, which stimulates depolarisation of the fungal cell membrane [220]. Furthermore, not all T6SS membrane-targeting effectors have membrane degradation functionality. VgrG-5, secreted in association with the T6SS5 of *B. thailandensis,* plays a role in the fusion of mammalian host membranes which results in the formation of multinucleated giant cell formation [221].

1.7.3.3. Nucleic acid targeting effectors

A subset of T6SS effector proteins have been demonstrated to target nucleic acids in prey cells for degradation resulting in cell death. Rearrangement hot spot (Rhs) proteins are large toxins with highly variable C-terminal domains. Rhs proteins in *Dickeya dadantii* were shown to inhibit cell growth in *E. coli* through contact-dependent degradation of host DNA [222]. Similarly to plasma membrane and cell wall targeting effectors, nucleic acid targeting effectors are expressed in association with their respective cognate immunity proteins (RhsI) [222]. In *S. marcescens* Db10, two of the primary determinants of antibacterial killing were shown to be Rhs effectors, termed Rhs1 and Rhs2 [223]. Of these effector proteins, Rhs2 was demonstrated to inhibit prey cell growth through DNase activity and degradation of target cell DNA.

Recently, Jana *et al*., (2019) identified a novel DNase toxin domain named PoNe (polymorphic nuclease effector) associated with the T5SS, T6SS and T7SS [224]. The PoNe toxin family was identified as a member of the PD-(D/E)xK superfamily of phosphodiesterases and was identified across a diverse range of bacterial species. As previously described, the respective PoNe immunity proteins were labelled PoNi and were typically identified downstream of cognate PoNe proteins. Whilst this study

has yet to characterise the precise method of activity of the PoNe family, they were able to confirm DNase activity by observing induction of a fluorescent SOS response in *E. coli* responding to DNA damage [224].

1.7.3.4. Micronutrient acquisition

All the previously discussed effector proteins function from within target cells following injection by the T6SS, however there have also been identified a range of T6SS effectors which demonstrate extracellular functionality. Lin *et al*., (2017) observed that a *P. aeruginosa* strain deficient in iron acquisition possessed the ability to grow in sequestered-iron media [225]. Further investigation showed that the T6SS H3 (H3-T6SS) secreted TseF for incorporation into outer membrane vesicles (OMVs). TseF acts as an activator of the Fe(III)-pyochelin receptor, FptA and OprF porin. TseF interaction with FptA and OprF facilitated the uptake of OMV-associated iron which is essential for growth and virulence of *P. aeruginosa* [143]. Similar micronutrient scavenging activity associated with the T6SS has been demonstrated in *B. thailandensis*. Manganese is vital for *B. thailandensis* response to oxidative stress as well as cellular processes such as transcriptional regulation [226,227]. The T6SS has been recently demonstrated to secrete a manganese-binding effector termed TseM which mediates the transfer of bound manganese across the cell membrane through interaction with MnoT, an outer membrane transport protein [228]. *B. thailandensis* has also demonstrated T6SS secretion of the zinc-binding protein, TseZ [210,229]. Similarly to TseM, TseZ binds to an outer membrane transporter, HmuR, to stimulate uptake of extracellular zinc following exposure to oxidative stress. TseZ secretion, zinc-binding and interaction with HmuR facilitates a sensitive response to perceived oxidative stresses.

1.7.3.5. T6SS effector delivery

T6SS effectors are classified into one of two categories according to their mode of delivery, these being either specialised or cargo effectors [230]. Cargo effectors are the more well characterised of two, consisting of an effector that non-covalently interacts with a structural component, such as VgrG or Hcp, for 'á la carte' delivery [194]. These effectors often require the assistance or one or more chaperone proteins to aid in their loading onto the lumen of the Hcp tube or VgrG spike [231]. Recently however, research has identified an alternative method of effector delivery, termed 'specialised' or 'evolved' effectors [231]. Specialised effectors contain C-terminal extension domains which facilitate fusion to the C-terminus of T6SS structure proteins, such as VgrG [230,231]. Interestingly, specialised effectors commonly possess enzymatic abilities, which in themselves facilitate host cell subversion, enabling bacterial uptake, as demonstrated by the VgrG-3 protein from *V. cholerae* [232]. The details of this covalent transport system have yet to be properly understood. It has been demonstrated that the C-terminal effector extension is not required for VgrG delivery [232], however there has been little research yet to characterise whether any extension domain can be delivered or if there is a limit to size and type of cargo. One study has demonstrated that various passenger domains, such as β-lactamase and Hcp-dependent T6SS toxin Tse2, could be fused to the C-terminus of a canonical VgrG (no C-terminus extension) and be successfully secreted into the extracellular milieu [230]. Whilst they identified no current limit to passenger type, they noted that efficacy varied greatly between passenger proteins.

1.8. Models and methodologies investigating bacterial interactions in oysters

1.8.1. Oyster microflora

Aquaculture of oysters typically involves growth in marine environments where the shellfish feed on phytoplankton present in the surrounding water column. However, as a side-effect of this practice, oysters also ingest local microorganisms, some of which may be pathogenic towards humans. Therefore, before consumption, oysters are required to meet 'category A' quality as determined by the Food Standards Agency's guidance on live bivalve molluscs in England, Wales, and Northern Ireland (2016) [233]. Category A oysters contain < 230 *E. coli*/100 g shellfish tissue and are suitable for immediate sale and raw consumption. Category B shellfish (230 – 4,600 *E. coli*/100 g tissue) require depuration or relaying to reduce bacterial loads. Category C (> 4,600 *E. coli*/100 g tissue) require relaying for a minimum two-month period. Oyster relaying involves transferring oysters to clean environments where contaminating microorganisms are purged by the oyster. Depuration involves immersing oysters in tanks through which UV-treated saltwater is circulated to stimulate further expulsion of contaminating microorganisms and pollutants [234]. It should be noted that whilst depuration can result in substantial bacterial clearance, studies have shown that total depuration of bacteria from oysters is difficult to achieve [235].

Consumption of contaminated oysters is widely recognised as the leading source of *V. vulnificus* infection [35,58,236]. A study on oysters taken from two individual estuaries in India identified *V. vulnificus* in 85 % of samples following enrichment [237]. A separate study isolated *V. vulnificus* from 67 % of raw oysters in Louisiana, USA, and more worryingly, from 25 % of cooked oysters sampled [238]l. Oysters commonly inhabit environments such as estuaries due to salinity, temperature, sediment content and pH conditions, where they perform a pivotal role in nutrient cycling and particle mediation of the water column [239–242]. As filter-feeders, oysters are exposed to a diverse range

of marine microorganisms which they ingest and retain within their digestive glands. Not all microorganisms are capable of surviving within oysters, due to resource availability and bacterial competition. This results in establishment of drastically different oyster microflora relative to the water column. Analysis of the bacterial flora of the Pacific oyster, *Crassostrea gigas*, collected from Hong Kong , showed that these shellfish were predominantly colonised by heterotrophic bacteria, including anaerobes and spore-forming bacteria, included in which were *Pseudomonas, Vibrio, Acinetobacter,* and *Aeromonas* species [243]. Conversely, the surrounding seawater consisted primarily of coliform and cornyeform bacteria. Interestingly, over 90 % of isolated heterotrophic microorganisms isolated from bivalve shellfish were associated with the digestive tract and stomach, indicating that ingested microorganisms primarily impacted the microflora of the digestive system. These findings were similar to studies performed using *C. gigas* collected from commercial oyster farms in Oregon (USA) in which the most frequently encountered microorganisms were *Vibrio, Pseudomonas, Acinetobacter, Flavobacterium* and Gram-positive *Bacillus* species [244].

1.8.2. Currently employed oyster models

Whilst there have been studies exploring *V. vulnificus* growth in homogenised oyster tissues, the majority of *V. vulnificus* studies in oysters have utilised a live oyster *in vivo* model [245,246]. However, these typically suffer from low-level uptake due to the size-based filter-feeding mechanism of oysters. Particles within a specific size range are preferentially retained and ingested whereas particles that fall outside the optimum range see drastically reduced uptake efficiencies. Riisgård, (1988) explored the efficiency of particle retention and filtration in six bivalve species, including the Eastern oyster, *Crassostrea virginica* and the blue mussel, *Mytilus edulis* [247]. Microscopic particles and phytoplankton were used to gauge the retention efficiency of particles of

varying sizes. Riisgård determined that larger particles were more effectively retained with only certain species being able to effectively filter and ingest smaller (< 7 μm) particles. *C. virginica,* has an optimum range of 5 – 7 μm, resulting in 90 % retention efficiency [248]. When particle size approximates to ~ 1.8 μm this drops to 50 % [249]. Other species of oyster display similar uptake efficiencies, with *C. gigas* having an optimal range of 4 - 6 μm and only retaining 17 % of particles ≤ 2 μm in size [250,251]. *V. vulnificus* measures 1.4 – 2.6 μm in length and 0.5 – 0.8 μm in width, falling below the ideal size for retention in filter-feeding bivalves. In *C. virginica*, *V. vulnificus* retention has been shown to be as low as 16 % [249].

Current methods for facilitating uptake of bacteria by oysters consist of inoculating oyster tanks with bacteria for filtration. Srivastava *et al.,* (2009) added 10^6 CFU/mL *V. vulnificus* to oyster tanks (4.5×10^9 CFU total). After 24 hours, *V. vulnificus* was isolated from oysters at 10^4 CFU/g tissue [252]. Froelich *et al*., (2013) inoculated oyster tanks with 7.5×10^5 CFU/mL *V. vulnificus* (3.75×10^8 CFU total) and recovered *V. vulnificus* from oysters at 10^4 CFU/g tissue [253]. Similar results were obtained by Pu *et al*., (2018) and Froelich *et al*., (2010) [254,255]. In every case, despite the total inoculating culture being > 10^8 CFU total, isolated *V. vulnificus* concentrations never rose above 10^5 CFU/g tissue. Similar studies performed with *Salmonella enterica* serovar Newport also managed to demonstrate ingestion to levels of 10^2 – 10^4 CFU/g tissue [256,257]. This shows that ingestion and retention of planktonic bacteria by oysters is highly inefficient when cultures are simply added to oyster tanks.

1.8.3. Marine snow as a vehicle for bacterial uptake by oysters

Marine microorganisms such as *V. vulnificus* are often naturally incorporated into aggregates in the environment commonly referred to as ‘marine snow’ [258]. These are

microcosms composed of diatoms, faecal matter, microorganisms, protists, inorganic dust, debris and other miscellaneous elements [259–261]. Free-floating microscopic particles are brought together at random by Brownian motion, where collision and adhesion results in formation of larger aggregates (Fig. 1.4). The rate at which aggregates form is dependent upon reaching a critical particle concentration and the 'stickiness' of these components [259]. Release of exopolymeric substances (EPS) by incorporated microorganisms promotes aggregation with neighbouring particles. EPS can vary in structure from a loose mucus layer to compact capsules and play many roles across the biological spectrum [262]. Notable examples include formation of protective capsules in human pathogens, attachment of nitrogen-fixing bacteria to plant roots and establishment of biofilms [263–266]. During aggregation, EPS coalesce into transparent extracellular polysaccharides (TEPs) which form a mucus web that functions to maintain the structure of the aggregate and aid in attachment of other particulate matter [260].

Marine snow plays a vital role in the transport of organic materials in the ocean, particularly vertically [267]. This has the side-effect of presenting a unique environment for bacterial colonisation and survival [261,268]. Aggregation offers a multitude of advantages to *V. vulnificus* and other organisms. Perhaps most key is the formation of the detritosphere, a microenvironment of enriched nutrients which incorporated organisms can exploit for growth and survival [269,270]. Aside from the concentrated presence of key nutrients, integration enables production and exchange of acylated homoserine lactones (AHLs) involved in quorum sensing, enhanced exchange of genetic material and increased nutrient uptake as a result of the increased availability of organic material at surfaces of transfer [271–273]. However, importantly for this study, incorporation of bacteria into marine snow facilitates more effective uptake by oysters as the larger microcosm is more effectively filtered and ingested.

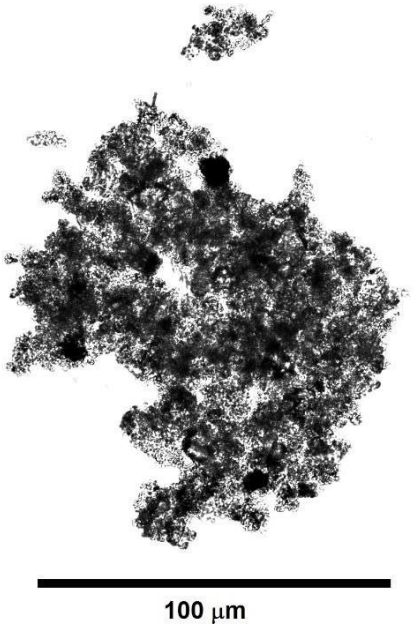

Figure 1.4: Micrograph of marine snow generated by this study. Seawater collected from Dawlish was utilised as a substrate to generate marine snow. Seawater (1 L) was supplemented with hyaluronic acid and incubated at 21 °C, 12 rpm for 24 hours to promote aggregation of particulate matter. The aggregate therefore consists of all the particulate matter present in the seawater substrate, such as sand, dust, algae, microorganisms and other miscellaneous components. Magnification × 400.

1.8.4. Incorporation of *V. vulnificus* into marine snow

The generation of marine snow for *V. vulnificus* incorporation and uptake by oysters has been explored by Froelich *et al.,* (2013) [249]. In their study the authors generated marine snow using seawater, into which they incorporated both E-type and C-type *V. vulnificus*. Enumeration of *V. vulnificus* from marine snow demonstrated successful integration, with the E-type strain recovered at 10^5 CFU/mL and the C-type strain recovered at < 10^5 CFU/mL (note that whilst the unit should be CFU/g marine snow, the authors in this study utilised CFU/mL marine snow as they would enumerate bacterial incorporation by extracting 1 mL of seawater containing marine snow for processing, not by establishing the weight of the aggregates). Whilst both strains

showed successful incorporation, E-type *V. vulnificus* strains showed significantly greater incorporation into marine snow than C- type [249]. These findings help explain the results put forwards by Warner and Oliver, (2008) who highlighted the elevated presence of E-type *V. vulnificus* in oysters relative to C-type [33]. Despite being present at similar concentrations in the surrounding water (E-type – 46.9 %, C-type – 53.1 %), E-type *V. vulnificus* outnumbered their counterparts 84.4 % to 15.6 % in oyster tissues. This inherent advantage presented by E-type strains not only offers an explanation for the disparity between E- and C- type presence in oysters, but also a potential explanation for the low clinical occurrence observed despite the organism's ubiquity. If C-type *V. vulnificus* strains capable of causing significant disease in humans demonstrate less efficient incorporation into marine snow and uptake by oysters this will reduce human exposure to pathogenic strains.

A possible reason for the disparity in marine snow incorporation is the difference in chitin-binding ability between E- and C-type *V. vulnificus*. Chitin is the second most abundant polysaccharide on earth behind cellulose and is composed of β-(1→4)-linked *N*-acetylglucosamine (GlcNAc) polymers [274,275]. Chitin is recognised as a major constituent of marine snow and studies have linked the ability of bacteria to bind chitin as a direct influence on cell counts recovered from aggregates [276,277]. E-type *V. vulnificus* were significantly more efficient at binding chitin than C-type strains. Williams *et al*., (2013) explored the role of surface proteins in chitin attachment, notably the type 4 pilus of *V. vulnificus* [276]. Two *V. vulnificus* type 4 pilus mutants, Δ*pilA* and Δ*pilD*, displayed significantly reduced attachment to chitin coated beads versus wild-type strains. To determine whether this was a genotype-specific occurrence, E- and C-type strains were incubated with chitin and relative gene expression monitored. Results demonstrated that E-type strains express 23-fold more PilA and 9-fold more

PilD than C-type strains. This supports the hypothesis that greater E-type aggregation is a result of heightened chitin binding.

However, expression levels of type 4 pilus genes are not the sole contributing factor. Parallel attachment assays at 30 °C and 37 °C showed an increase in C-type binding at 37 °C in conjunction with a decrease in E-type binding under the same conditions [278]. This suggests that the chitin binding potential of C-type strains may be predominantly geared towards human infection as opposed to ecological proliferation and survival. This hypothesis is further supported by the elevated expression of *gpbA* in C-type strains [276]. GbpA is an *N*-acetylglucosamine binding protein that is expressed at levels 46-fold greater in C-type strains. Initially this suggests a mechanism for enhanced binding of C-type strains to chitin-containing aggregates. However, Wong *et al*., (2012) drew a link between *V. cholerae* GbpA and host colonisation. The GbpA of *V. cholerae* has been shown to play a role in binding both chitin and mucins that contain GlcNAc [279]. Consequently, *V. cholerae* is capable of binding both marine chitin and mammalian intestinal mucins, suggesting that increased expression of *gbpA* in C-type *V. vulnificus* may be primarily utilised in host colonisation.

1.8.5. Marine snow uptake and bacterial retention by oysters

Oysters feed using a selective mucociliary clearance mechanism. Surrounding water is pumped through a set of filamentous gills (Fig. 1.5). Cilia covering these gills trap passing particles and encase them in mucus for transport to the labial palps, mouth and stomach where they are digested [280]. Filtration of suspended particles by bivalves is an active process and as a result there is some degree of selection as to what material is ingested. The primary factor is particle size. Preferential uptake and digestion of a microphytobenthos assemblage by the Pacific oyster, *C. gigas,* was

performed in which two diatom species out of sixteen showed greater propensity for uptake and digestion due to variations in size and mass [281]. Experiments geared towards quantifying bacterial uptake and depuration in bivalves, notably in oysters and mussels, involved the seeding of oyster holding tanks with pre-determined concentrations of bacterial culture [253,255,282]. However, this produced inherently unreliable results due to the size-based selection of particles by bivalves. While the morphology of the filter-feeding apparatus has been shown to have an impact on particle-retention**,** the principle factor is the size of the particle [252,254,264].

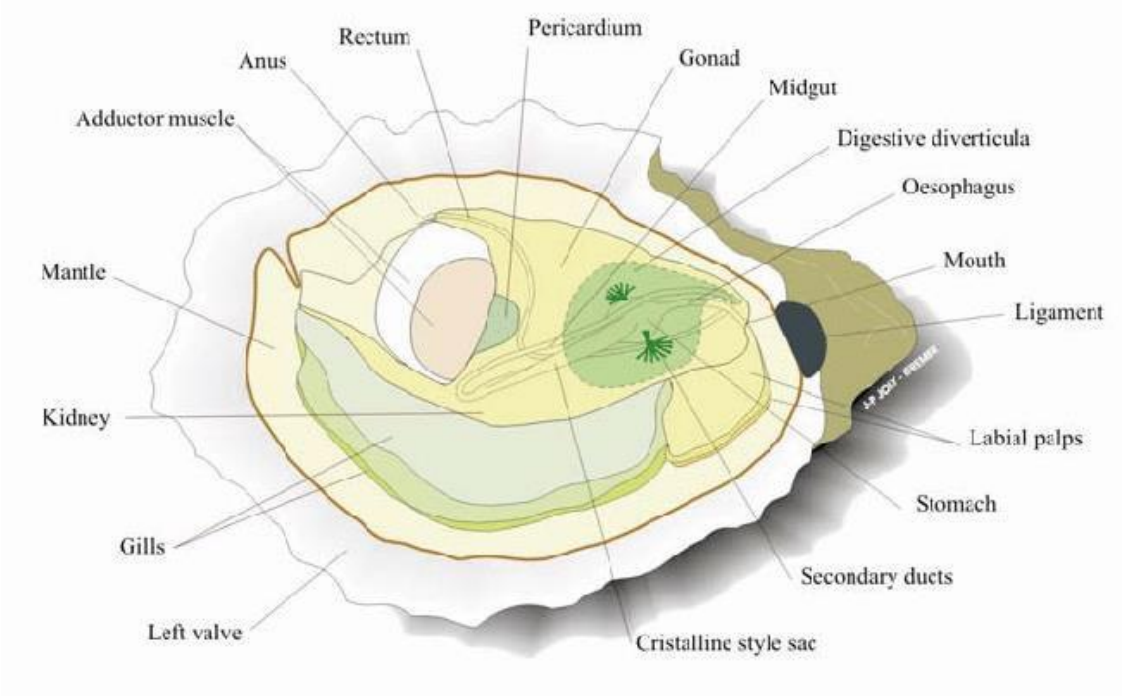

Figure 1.5: Anatomy of the Pacific oyster, *Crassostrea gigas*. Seawater is moved over the gills by the beating of cilia. Suspended particle matter, such as plankton and algae, are trapped in mucus for transport to the mouth and oesophagus where they are eaten and moved to the stomach for digestion. All indigestible material is released as faeces. Figure taken from Laurence *et al.,* (2009) [283].

Froelich *et al.,* (2013) exposed oysters to marine snow inoculated with *V. vulnificus* at concentrations of 10^5 CFU/mL [249]. The authors were able to demonstrate recovery of *V. vulnificus* from oyster tissues at concentrations of 10^2 – 10^3 CFU/g tissue. This is not particularly high, especially as marine snow demonstrated incorporation of *V. vulnificus* at 10^5 CFU/ml. The aim of using marine snow as a model for uptake is that it would facilitate greater uptake of *V. vulnificus* than previous tank-spiking practices. However, there are numerous studies that have achieved 10^3 – 10^5 CFU/g tissue without the use of marine snow as previously discussed in section 1.8.2. It is therefore apparent that this method would likely require substantial optimisation to develop a substantial model for promoting relevant uptake of *V. vulnificus* by oysters.

1.9. Research aims

V. vulnificus is a significant human pathogen, commonly found in high concentrations within filter-feeding shellfish such as oysters. Previous studies have shown that *V. vulnificus* possess two T6SSs, termed the T6SS1 and T6SS2. Of these two systems, the T6SS1 has been demonstrated to possess antibacterial at 30 °C *in* vitro. Therefore, this study seeks to elucidate T6SS activity *in vitro* at more environmentally representative conditions and the impact this may have on *V. vulnificus* ecology. To confirm that these results are representative of genuine *in vivo* interactions this study will also aim to develop an oyster model for *in vivo* bacterial co-culture killing assays. This will involve the development and optimisation of a marine snow model for facilitating high-level uptake of bacteria by oysters for *in vivo* competition.

Chapter Two

Materials and Methods

2.1. Culture conditions

All bacteria, phytoplankton and amoeba species and strains used in this study can be seen in Table 2.1.

2.1.1. Bacterial culture conditions

Bacterial strains were cultured in Luria-Bertani (LB) broth and on LB agar plates at either 30 °C or 37 °C. *Vibrio* species were cultured on Thiosulfate-Citrate-Bile Salts-Sucrose (TCBS) agar (Oxoid). *Salmonella* species were cultured on *Salmonella* ChromoSelect agar (Sigma) at 37 °C. Antibiotics were added to media where necessary at the following concentrations: ampicillin (100 μg/mL;), kanamycin (50 μg/mL), trimethoprim (50 μg/mL) and chloramphenicol (35 μg/mL for *Escherichia coli*, 10 μg/mL for *Vibrio*).

2.1.2. Diatom culture conditions

Thalassiosira pseudonana CCMP 1335 and *Phaeodactylum tricornutum* UTEX 646 were cultured in 20 ppt salinity water supplemented with 20 mL/L Guillard's F/2 media + Si (Sigma). Cultures were inoculated at 10^4 cells/mL in 50 mL of media and maintained at 20 °C, 70 rpm, on an orbital shaker under cool fluorescent light set to a 12:12 light:dark cycle. Total cell counts were performed daily using a haemocytometer. Cultures were regularly checked for bacterial contamination by plating on LB agar and incubating plates at 37 °C. Once diatom growth reached stationary phase, cultures were split for scaling up growth and maintaining reserve stocks. Once cultures reached 10^5 – 10^6 cells/mL in 2 L Erlenmeyer flasks cultures were removed from incubation for experimental use.

2.1.3. *Dictyostelium discoideum* culture conditions

D. discoideum AX3 (DictyBase accession number: DBS0235542) was ordered via DictyBase and received growing on a lawn of *E. coli* B/r [284]. An inoculating loop of *D. discoideum* fruiting bodies was resuspended in 250 μL of *E. coli* MG1655 culture and spread onto pre-dried LPB agar (0.1 % lactose, 0.1 % bacteriological peptone, 19 mM $Na_2HPO_4 \cdot 7H_2O$, 30 mM KH_2PO_4). Plates were incubated at 21 °C for 2 – 3 days to facilitate *D. discoideum* growth. *D. discoideum* cultures were routinely sub-cultured once *D. discoideum* had cleared the lawn of *E. coli* but before formation of fruiting bodies.

Axenic *D. discoideum* AX3 cultures were generated by inoculating 30 mL of HL5 media (Formedium™) supplemented with ampicillin (100 μg/mL) and streptomycin (300 μg/mL) with an inoculating loop of *D. discoideum* fruiting bodies. Cultures were incubated at 21 °C, 180 rpm for 2 – 3 days. Before cultures exceeded 10^6 cells/mL, 1 mL of culture was used to inoculate 30 mL of antibiotic-free HL5. Cultures were incubated at 21 °C, 180 rpm for 2 – 3 days and routinely checked for bacterial contamination.

2.2. Antibiotic stock solutions

Antibiotic stock solutions were made up as follows: ampicillin, 50 mg/mL in ddH_2O; streptomycin, 100 mg/mL in ddH_2O; chloramphenicol, 35 mg/mL in 70 % ethanol; trimethoprim, 10 mg/mL in DMSO; kanamycin, 50 mg/mL in ddH_2O. All antibiotic stocks were stored at -20 °C.

Table 2.1: List of strains and species used in this study.

Strain	Description	Source
V. vulnificus		
106-2A	Environmental isolate, T6SS1+ T6SS2+, C-genotype	Lab stock
ΔT6SS1	106-2A with a *hcp1* in-frame deletion, T6SS1- T6SS2+, C-genotype	This study
ΔT6SS2	106-2A with a *hcp2* in-frame deletion, T6SS1+ T6SS2-, C-genotype	This study
ΔT6SS1/2	106-2A with in-frame deletions of *hcp1* and *hcp2*, T6SS1- T6SS2-, C-genotype	This study
99-743	Environmental isolate, T6SS1- T6SS2+, E-genotype	Lab stock
106-2A pVv3-kan	106-2A containing pVv3-kan, (Kan^r)	This study
ΔT6SS1 pVv3-kan	106-2A ΔT6SS1 containing pVv3-kan, (Kan^r)	This study
ΔT6SS2 pVv3-kan	106-2A ΔT6SS1 containing pVv3-kan, (Kan^r)	This study
ΔT6SS1/2 pVv3-kan	106-2A ΔT6SS1/2 containing pVv3-kan, (Kan^r)	This study
99-743 pVv3-tmp	99-743 containing pVv3-tmp, (Tmp^r)	This study
***S.* Enteritidis**		
CC012	Wild-type *Salmonella enterica* serovar Enteritidis CC012	Lab stock
V. cholerae		
V52	O37 serogroup strain, (Sm^r)	Lab stock
E. coli		
S17-1 λ *pir*	Routine cloning strain and donor for triparental conjugation	Lab stock
HB101 pRK2013	Helper strain for triparental conjugation containing pRK2013, Kan	Lab stock
Dh5α	Routine cloning strain	Lab stock
JM109	Routine cloning strain	Lab stock
T. pseudonana		
CCMP 1335	Cosmopolitan centric diatom, 3 - 5 μm diameter	Samuel Barton
P. tricornutum		
UTEX 646	Pennate diatom, 10 - 20 μm in length	Dr Mike Allen
D. discoideum		
AX3	Peter Devreotes lab strain, axenic, Dictybase strain ID - DBS0235542	Dictybase

2.3. Molecular genetics

2.3.1. Genomic DNA extraction

gDNA was extracted from overnight bacterial cultures using the Wizard® genomic DNA purification kit (Promega) according to the manufacturers' instructions. Quality of purified gDNA was checked using 1 % agarose gel electrophoresis and quantified using a NanoDrop™ 1000 (ThermoFisher). gDNA was diluted 1 in 20 for use in downstream PCR reactions. gDNA samples were stored at -20 °C.

2.3.2. Polymerase chain reaction (PCR)

Oligonucleotides for PCR were designed and analysed using the Clone Manager software and synthesised by Eurofins MWG Operon. A list of the primers used in this study can be seen in Table 2.2. PCR products amplified with Phusion® High-Fidelity DNA polymerase were mixed with 4 μL 5× Phusion HF buffer, 0.4 μL dNTPs (10 mM), 1 μL forward primer (10 μM), 1 μL reverse primer (10 μM), 0.2 μL Phusion DNA polymerase, ~ 100 ng template DNA and ddH_2O up to 20 μL (all reagents NEB). Once mixed, reactions were placed in a PCR thermocycler and run at the following conditions. Initial denaturation – 98 °C for 30 seconds. 35 cycles of denaturation at 98 °C for 10 seconds, annealing at 50 °C for 20 seconds and extension at 72 °C for 20 seconds/kb. A final extension was ran at 72 °C for 10 minutes before holding at 4 °C.

PCR products amplified with HotStarTaq® DNA polymerase were mixed with 2.5 μL 10× PCR buffer, 0.5 μL dNTPs (10 mM), 0.5 μL forward primer (10 μM), 0.5 μL reverse primer (10 μM), ~ 100 ng template DNA, 0.2 μL DNA polymerase and 2 ddH_2O up to 25 μL (all reagents Qiagen). Once mixed, reactions were placed in a PCR thermocycler (Biometra TRIO 48, Analytik Jena) and run at the following conditions.

Table 2.2: List of primers used in this study.

Primers	Description	Sequence (5' - 3')
106-2A *hcp1* LFF *Sma*I	106-2A *hcp1* region left flank forward	TACCCGGGCAGACTCTTTCGACAGCTTATAG
106-2A *hcp1* LFR *Nde*I	106-2A *hcp1* region left flank reverse	TCCATATGTGGAGTTGGCATAGCTATTTC
106-2A *hcp1* RFF *Nde*I	106-2A *hcp1* region right flank forward	GCCATATGATCGAGGCTTAATCCTCGTC
106-2A *hcp1* RFR *Apa*I	106-2A *hcp1* region right flank reverse	TAGGGCCCGCCCATCTCTTGCAATATCTG
106-2A *hcp2* LFF *Sma*I	106-2A *hcp2* region left flank forward	TTCCCGGGCTTTGCACCGTGATGTATTG
106-2A *hcp2* LFR *Nde*I	106-2A *hcp2* region left flank reverse	TGCATATGATTTGACTGCATGCTAGTCTC
106-2A *hcp2* RFF *Nde*I	106-2A *hcp2* region right flank forward	GGACATATGGGTGTTAAAGGTCAACAAATG
106-2A *hcp2* RFR *Apa*I	106-2A *hcp2* region right flank reverse	GTTGGGCCCTGAAAGATTCGGCTGTTG
hcp1 MutScreen FWD	*hcp1* crossover forward primer	ACATGGTGACAAGGTTGATAG
hcp1 MutScreen REV	*hcp1* crossover reverse primer	CAGAATTCACGCTGAGAAAG
hcp2 MutScreen FWD	*hcp2* crossover forward primer	TACGAGACGATTTGTTACAG
hcp2 MutScreen REV	*hcp2* crossover reverse primer	TTGGCATAGCTTTTGGTCAG
CmR FWD	First crossover forward primer	ATGGAGAAAAAAATCACTGGATATACCACC
CmR REV	First crossover reverse primer	TTACGCCCCGCCCTGCCACTCATCGCAGTA
vgrG1 qPCR FWD	Forward primer for *vgrG1* qPCR	GAAATTGGTGCGAACCAACG
vgrG1 qPCR REV	Reverse primer for *vgrG1* qPCR	CCCACCTGGTCCCTTAATTG
vcgE qPCR FWD	Forward primer for *vcgE* qPCR	AATGATCTCATCACTGCTATCC
vcgE qPCR REV	Reverse primer for *vcgE* qPCR	AATCAAACCCAGGCATAAGC
vvhA qPCR FWD	Forward primer for *vvhA* qPCR	GAGCGTGAGTTTGGTGAG
vvhA qPCR REV	Reverse primer for *vvhA* qPCR	AGGGTTGAACTTCGTCTTATC
sefA qPCR FWD	Forward primer for *sefA* qPCR	TGCAGCTCAGAATACAACATC
sefA qPCR REV	Reverse primer for *sefA* qPCR	GGCTACACCACCAGATAC
vgrG1 RT-PCR FWD	Forward primer for *vgrG1* RT-PCR	ATGGCAAAGTTAACATTCAC
vgrG1 RT-PCR REV	Reverse primer for *vgrG1* RT-PCR	TCTCATCCGGACCATCAG
clpV RT-PCR FWD	Forward primer for *clpV* RT-PCR	ATGTCGAATCTATCACTATCTAC
clpV RT-PCR REV	Reverse primer for *clpV* RT-PCR	TTAGACGATTGAGATAGACAAG

vvhA FWD	*vvhA* forward primer	ATGAAAAAAATGACTCTGTTTACCC
vvhA REV	*vvhA* reverse primer	CTAGAGTTTGACTTGTTGTAATGTG
M13 FWD	pGEM-T Easy forward primer	CCCAGTCACGACGTTGTAAAACG
M13 REV	pGEM-T Easy reverse primer	CAGGAAACAGCTATGAC
pVv3-tmp OE FWD	Forward primer for generating pVv3-tmp	CTCGAATTCACTAGTAACACCCCTTGTATTACTG
pVv3-tmp OE REV	Reverse primer for generating pVv3-tmp	AATACAAGGGGTGTTACTAGTGAATTCGAGCCA

Initial denaturation/polymerase activation – 95 °C for 15 minutes. 35 cycles of denaturation at 94 °C for 30 seconds, annealing at 50 °C for 30 seconds and extension at 72 °C for 1 minute/kb. A final extension was ran at 72 °C for 10 minutes before holding at 4 °C.

All PCR amplified DNA was stored at -20 °C for downstream reactions.

2.3.3. PCR fragment A-tailing

5 – 10 μL of blunt-ended, purified PCR product was mixed with 2 μL 10× ThermoPol® Buffer, 1 μL dATP (10 mM), 0.2 μL Taq DNA polymerase and ddH_2O up to 20 μL (all reagents NEB). The reaction was incubated at 72 °C for 20 minutes. A-tailed DNA was column purified using the Wizard® SV Gel and PCR Clean-Up System kit (Promega) and stored at -20 °C.

2.3.4. Total cellular RNA extraction

Total cellular RNA was extracted from overnight bacterial cultures using the RiboPure™-Bacteria kit (ThermoFisher) according to the manufacturers' instructions. To eliminate traces of gDNA, purified RNA was treated with DNase I (Ambion)

according to the manufacturers' instructions. Purified RNA was stored in RNase-free collection tubes at -80 °C.

2.3.5. Reverse-transcription PCR (RT-PCR)

SuperScript™ III Reverse Transcriptase (Invitrogen) was used to synthesise complementary DNA (cDNA) for RT-PCR. For primer annealing, 50 ng random hexamers (Invitrogen) were mixed with 1 μg total RNA, 1 μL 10 mM dNTPs and ddH_2O to 13 μL. This solution was incubated at 65 °C for 5 minutes and incubated on ice for a further 5 minutes. Following incubation, the following reagents were added to the microcentrifuge tube: 4 μL 5× First-Strand Buffer, 1 μL 0.1 M DTT, 1 μL RNaseOUT™, 1 μL SuperScript™ III RT (all reagents Invitrogen). The solution was incubated at 25 °C for 5 minutes before being incubated for a further 60 minutes at 50 °C to allow primer extension and cDNA generation.

2.3.6. Agarose gel electrophoresis

1 % agarose gels were generated by combining 70 mL 1× TAE (Tris-acetate 40 mM, EDTA 1 mM in ddH_2O to a 1× solution) with 0.7 g of agarose (Sigma) and supplementing with Midori Green nucleic acid gel stain (Nippon Genetics). 100 V was passed across the gel for 45 minutes to separate the negatively charged DNA in a size-selective manner. Separated DNA was visualised using a BioRad ChemiDoc™ UV transilluminator with the Quantity One gel imaging software.

2.3.7. DNA gel purification

DNA bands of interest were excised from 1 % agarose gels using a scalpel and purified using the GeneJET Gel Extraction Kit (ThermoFisher) according to the manufacturer's instructions. Purified DNA was eluted in 30 mL ddH_2O.

2.3.8. Plasmid extraction and ethanol precipitation of plasmid DNA

A list of plasmids used in this study can be seen in Table 2.3. Typical plasmid extractions were performed utilising the Thermo Scientific GeneJET Plasmid Miniprep Kit using 1 mL of overnight bacterial culture. Purified plasmid DNA was eluted in 30 μL ddH_2O and 5 μL visualised by agarose gel electrophoresis. For low copy-number plasmids, 50 mL of overnight bacterial culture was processed using the Promega PureYield™ Plasmid Midiprep System. Purified plasmid DNA was eluted in 500 μL ddH_2O. Midiprepped plasmid DNA was then concentrated via ethanol precipitation.

Briefly, 2 μL glycogen (NEB) was added to 350 μL plasmid DNA along with 1/10 volume 3 M sodium acetate (pH 5.2) and 2× volume 100 % ethanol. Solutions were thoroughly mixed and incubated at -80 °C for 1 hour. Samples were centrifuged at 14,000 rpm, 4 °C, for 30 minutes to pellet plasmid DNA. Supernatant was aspirated and the pellet washed with 700 μl 70 % ethanol. Samples were centrifuged for 15 minutes to wash the pellet and the supernatant aspirated again. Pellets were left to air dry for 15 minutes until no ethanol remained. 30 μL ddH_2O was added and the sample incubated at 65 °C for 1 hour to resuspend plasmid DNA. Concentrated plasmid DNA was visualised using agarose gel electrophoresis and the concentration determined using a NanoDrop™ 1000 (ThermoFisher).

Table 2.3: List of plasmids used in this study.

Plasmid	Description	Source
pGEM-T Easy	Routine cloning plasmid, Amp^r	Promega
pGEM-T Easy-*hcp1*LF	pGEM-T Easy containing 106-2A *hcp1* left flanking region	This study
pGEM-T Easy-*hcp1*RF	pGEM-T Easy containing 106-2A *hcp1* right flanking region	This study
pGEM-T Easy-*hcp2*LF	pGEM-T Easy containing 106-2A *hcp2* left flanking region	This study
pGEM-T Easy-*hcp2*RF	pGEM-T Easy containing 106-2A *hcp2* right flanking region	This study
pGEM-T Easy-*vgrG1*	pGEM-T Easy containing the *vgrG1* fragment amplified by qPCR	This study
pGEM-T Easy-*vcgE*	pGEM-T Easy containing the *vcgE* fragment amplified by qPCR	This study
pGEM-T Easy-*vvhA*	pGEM-T Easy containing the *vvhA* fragment amplified by qPCR	This study
pGEM-T Easy-*sefA*	pGEM-T Easy containing the *sefA* fragment amplified by qPCR	This study
pDM4	Suicide vector, R6K origin, *sacBR*, Cm^r	Lab stock
pDM4-Δ*hcp1*	pDM4 containing ligated 106-2A *hcp1* left and right flanks	This study
pDM4-Δ*hcp2*	pDM4 containing ligated 106-2A *hcp2* left and right flanks	This study
pVv3-kan	*Vibrio* shuttle vector from cryptic *V. vulnificus* plasmid pVN-0126, Kan^r	Dr. S. Hertwig
pVv3-kan-tmp	*Vibrio* shuttle vector from cryptic *V. vulnificus* plasmid pVN-0126, Kan^r, Tmp^r	Dr. S. Hertwig
pVv3-tmp	*Vibrio* shuttle vector from cryptic *V. vulnificus* plasmid pVN-0126, Tmp^r	This study
pRK2013	Helper plasmid for conjugation, Kan^r	Lab stock

2.3.9. Ligations

Appropriate volumes of insert to vector were calculated and combined at a 3:1 insert:vector ratio. 1 μL T4 DNA ligase was added to the solution along with 1 μL 10× T4 DNA ligase buffer (all reagents NEB). Ligation reactions were made up to a final volume of 10 μL with ddH_2O before being incubated overnight at 16 °C.

2.3.10. Calcium chloride chemically competent *E. coli*

1 mL of overnight *E. coli* culture was used to inoculate 50 mL LB broth for growth at 37 °C until an OD_{590nm} of 0.4. The culture was then incubated on ice for 30 minutes before being centrifuged at 3,000 rpm for 10 minutes at 4 °C. Pelleted cells were re-suspended in 25 mL ice cold 0.1 M $CaCl_2$ and incubated on ice for a further hour. Following further centrifugation as previously described, the supernatant was discarded, and pelleted cells re-suspended in 2 mL ice cold 0.1 M $CaCl_2$ with 15 % glycerol (v/v). 100 μl aliquots were frozen and stored at -80 °C.

2.3.11. Chemically competent cell transformation

Chemically competent *E. coli* were thawed on ice and 2 – 4 μL of plasmid DNA or ligation product added. Following 40 minutes incubation on ice, cultures were heat shocked at 42 °C for 45 seconds and incubated on ice for a further 5 minutes. 700 μL pre-warmed LB broth was added, and cultures incubated at 37 °C, 200 rpm, to facilitate expression of antibiotic resistance genes. Cultures were centrifuged, 500 μL of the supernatant removed, and pelleted cells re-suspended in the remaining 400 μL.

200 μL was then spread onto LB agar plates containing the necessary antibiotics and plates incubated overnight at 37 °C.

2.3.12. Electrocompetent cells

Electrocompetent cells were generated and electroporated according to the protocol published by Klevanskaa *et al*., (2014) [279]. 1 mL of overnight bacterial culture was used to inoculate 30 mL LB broth for growth at 37 °C until the OD_{590nm} reached 0.8. Cells were sedimented at 4,000 rpm, 4 °C, for 15 minutes. The supernatant was aspirated, and the pelleted cells resuspended in ice-cold electroporation buffer (1 mM Tris-HCl, pH 6, supplemented with 200 mM sucrose). This wash step was repeated twice, after which pelleted cells were resuspended in 150 μL electroporation buffer. 50 μL aliquots were frozen at -80 °C for future electroporation.

2.3.13. Electrocompetent cell electroporation

Electrocompetent cells (50 μL) were thawed on ice and 400 ng plasmid DNA mixed with the cells. Following 10 minutes incubation on ice, the suspension was added to a pre-chilled electroporation cuvette and electroporation performed at 7.5 kV cm^{-1}, 25 μF and 200 Ω. Immediately after, 950 μL LB broth pre-warmed to 37 °C was added to the cells and the suspension incubated with at 37 °C, 200 rpm, for 1 hour to allow recovery of electroporated cells. Recovered cells were then plated on LB agar plates containing the required antibiotic and incubated at 37 °C overnight to select for successful electroporation.

2.3.14. Tri-parental conjugation

Three bacterial strains were cultured overnight in LB in preparation for tri-parental conjugation. The donor *E. coli* strain, S17-1 λ *pir*, containing the plasmid to be transferred, the helper *E. coli* strain, HB101, containing the kanamycin resistant helper plasmid pRK2013, and the recipient *V. vulnificus* strain. 1 mL of each overnight bacterial culture was pelleted at 14,500 rpm and the supernatant aspirated. To remove antibiotic traces, cells were washed in fresh LB broth. Pelleted cells were resuspended in 200 μL LB broth and combined in a 5:1:1 ratio with the recipient being the higher density. 200 μl of the suspension was spotted on LB agar and incubated overnight at 37 °C. Bacterial growths were scraped off the plate and resuspended in 1 mL phosphate buffered saline (PBS), a water-based salt solution utilised to maintain a consistent pH. 100 μL was spread on a TCBS plate supplemented with the necessary antibiotics and incubated at 37 °C for 2 – 3 days, until colonies were observed. Plasmid DNA was miniprepped from potential transformants to confirm presence of the plasmid and colonies PCR-screened with *V. vulnificus* specific *vvhA* primers.

2.3.15. *V. vulnificus* mutant generation

In-frame deletions of *hcp1* and *hcp2* were constructed using suicide vector pDM4 [285]. Primers were designed to amplify the flanking regions of the genes of interest and to incorporate specific restriction sites to allow downstream ligation (Table 2.2). Flanking regions were cloned into pGEM-T Easy for sequencing. Flanks were excised from pGEM-T Easy using *Sma*I/*Nde*I (left flank) and *Nde*I/*Apa*I (right flank), column purified, and utilised for a three-way ligation into pDM4 linearised using *Sma*I/*Apa*I.

Generated constructs were transformed into *E. coli* S17-1 λ *pir* for conjugation into *V.*

vulnificus as described in section 2.2.11. Successful first cross-over integrants were identified via PCR and respective colonies were subcultured on LB agar plates supplemented with 10 % sucrose to promote second crossover and plasmid excision. PCR using primers flanking the deletion were then used to confirm whether colonies were successful mutants or WT revertants.

2.3.16. Generation of pVv3-tmp by overlap extension PCR (OE-PCR)

pVv3-tmp was constructed from pVv3-kan-tmp according to the protocol published by Hansson *et al*., (2008) [286]. Primers were designed against the 20 bp region immediately up and downstream of the start and stop codons of the kanamycin resistance gene of pVv3-kan-tmp (Appendix 1). Each primer had a 5' tail complementary to the other primer. Overlap-extension PCR (OE-PCR) was set up using 200 ng pVv3-kan-tmp as template, 10 μL 5× Phusion HF buffer, 1 μL dNTPs, 2.5 μL forward and reverse primer (each 10 μM), 0.2 μL Phusion DNA polymerase and ddH_2O up to 50 μL (all reagents NEB). PCR reactions were run at the following conditions. Initial denaturation – 98 °C for 30 seconds. 35 cycles of denaturation at 98 °C for 10 seconds, annealing at 50 °C for 30 seconds and extension at 72 °C for 2 minutes. A final extension was run at 72 °C for 10 minutes before holding at 4 °C.

To digest the methylated template plasmid DNA (pVv3-kan-tmp) and reduce background transformation, PCR reactions were treated with 1 μL *Dpn*I (Agilent) for 1 hour at 37 °C. *Dpn*I was inactivated at 80 °C for 20 minutes and 3 μL of reaction transformed into chemically competent *E. coli* JM109. Transformations were plated on LB agar supplemented with trimethoprim and incubated overnight at 37 °C. Potential transformants were used to inoculate individual wells on a 96-well plate containing

LB/trimethoprim. 96-well plates were incubated at 37 °C, 125 rpm, for 2 hours, to allow outgrowth of potential transformants. Using a colony replicator, cultures were spotted in parallel on LB agar supplemented with either kanamycin or trimethoprim and incubated overnight at 37 °C. Colonies that were able to grow on LB/trimethoprim plates but not LB/kanamycin plates were indicative of kanamycin deletion and taken forward for miniprep and plasmid confirmation by restriction endonuclease digestion.

2.4. Marine snow

2.4.1. Generating natural and artificial marine snow

Natural marine snow was generated according to the technique outlined by Froelich *et al.,* (2013) [249]. 10 $\mu g/L^{-1}$ hyaluronic acid (Merck; MW ≥ 1 MDa) was added to 1 L Nalgene bottles containing 1 L seawater adjusted to 20 ppt salinity. The resulting suspensions were rolled at 12 rpm for 24 hours at 21 °C to facilitate particle collision and aggregate formation.

For artificial marine snow, live phytoplankton cultures were added to 1 L 20 ppt artificial seawater at a final concentration of 10^6 CFU/mL and supplemented with 10 $\mu g/L^{-1}$ hyaluronic acid. For marine snow generated using commercially cultured diatoms two different solutions were utilised. Reef Phytoplankton (ReefPhyto LTD) and TP1800™ (Reed Mariculture). These solutions were added to AMS suspensions in place of laboratory-cultured diatoms to a final concentration of 10^6 cells/mL. Suspensions were incubated at 12 rpm for 24 hours at 21 °C.

2.4.2. Determining the weight of natural marine snow

Natural marine snow was vacuum filtered through Whatman™ qualitative filter paper, Grade 6 (GE Healthcare Life Sciences), to isolate aggregates (Fig. 2.1). Once filtration had isolated the aggregates, filter paper was removed and weighed. The weight was compared to a negative control in which 1 L of artificial seawater was also filtered through the same filter paper. The difference was calculated, and this value constituted the wet mass of the natural marine snow.

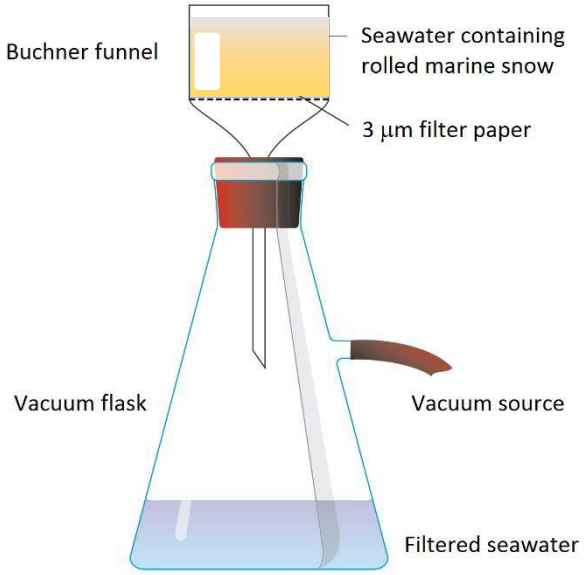

Figure 2.1: Schematic depicting vacuum filtration of marine snow. A vacuum flask was topped with a Buchner funnel loaded with 3 μm pore filter paper. Marine snow was added to the Buchner funnel and vacuum filtered to isolate all aggregates > 3 μm in size. Once completely filtered, filter paper was weight for comparison to a negative control and wet mass of marine snow calculated.

2.4.3. Determining the weight of artificial marine snow

To determine the weight of artificial marine snow, diatom cultures were adjusted to the required concentration and pelleted. The supernatant was aspirated, and the wet mass of the pellet determined. This value was then utilised in conjunction with CFU counts to enumerate bacterial incorporation into aggregates in CFU/g artificial marine snow.

2.4.4. Enumeration bacterial incorporation into marine snow

Aggregates isolated by vacuum filtration were resuspended in 50 mL PBS and vortexed vigorously for 30 seconds to disrupt aggregates and release incorporated *Vibrios.* Samples were centrifuged at 4,000 rpm for 30 minutes and the pellets resuspended in 1 mL PBS. 500 μL of the resuspended solution was diluted serially 10-fold and 100 μL of each dilution spread in triplicate on LB agar. Plates were incubated at 37 °C overnight. The following day colonies were replica plated onto TCBS and incubated overnight at 37 °C for CFU/g marine snow calculations.

2.5. *In vitro* molecular assays

2.5.1. Bacterial growth curves

Overnight bacterial cultures were set up in 5 mL LB broth and grown at 37 °C, 200 rpm. 30 mL fresh LB broth was inoculated to an OD_{590nm} of 0.03 using the overnight bacterial cultures and grown at the required temperature, 200 rpm. Every two hours OD_{590nm} was read and Miles and Misra 10-fold serial dilutions performed in triplicate [287]. Plates were incubated at 37 °C overnight and CFU/mL calculated the following day.

2.5.2. Co-culture killing assays

1 mL of overnight bacterial culture, supplemented with antibiotics where necessary, was used to inoculate 30 mL fresh LB broth to an OD_{590nm} of 0.03. Cultures were incubated at 30 °C, 200 rpm, until they reached an OD_{590nm} of 1.0 where they were then adjusted to an OD_{590nm} of 0.8 and centrifuged for 3 minutes at 14,500 rpm. Pelleted cells were washed twice with 1 mL PBS and resuspended in 1 mL LB to remove any traces of antibiotics. Attacker and prey cultures were combined in a 3:1 ratio, vortexed to mix, and 25 μL of each spotted onto LB agar. LB plates were incubated at either 23 °C, 30 °C or 37 °C for 5 hours to allow contact-dependent killing to take place. Miles and Misra 10-fold serial dilutions of the suspensions were performed and 10 μl spotted in triplicate onto selective agar. Dilution plates were incubated overnight at 37 °C for CFU/mL calculation the following day. After 5 hours, co-culture spots were excised using a flame-sterilised scalpel and resuspended in 1 mL PBS. Miles and Misra 10-fold serial dilutions of the resuspended growths were performed and 10 μL spotted in triplicate onto selective agar. Plates were incubated at 37 °C overnight and CFU/mL calculated the following day.

2.5.3. Plasmid stability assay

V. vulnificus containing either pVv3-kan or pVv3-tmp was cultured in LB supplemented with either kanamycin or trimethoprim at the required temperature overnight. Overnight cultures were used to inoculate 30 mL LB supplemented with antibiotics to an OD_{590nm} of 0.03. Once cultures reached an OD_{590nm} of 1.0 they were adjusted to OD_{590nm} 0.8 and washed twice to remove any traces of antibiotic. 100 μL of each strain was mixed with 300 μL LB and 25 μL of each sample spotted onto LB agar and incubated at the

required temperature for the required length of time. Bacterial growths were excised from LB agar using a flame-sterilised scalpel and resuspended in 1 mL PBS. Miles and Misra 10-fold serial dilutions were performed and 10 μL of the resulting dilutions spotted in triplicate on both LB agar and LB agar supplemented with either kanamycin or trimethoprim. Plates were incubated overnight at 37 °C and CFU/mL calculated the following day.

2.5.4. *D. discoideum* plaque-forming assays

D. discoideum was cultured axenically in HL5 media as described in section 2.1.3. Overnight bacterial cultures were pelleted by centrifugation at 14,500 rpm for 3 minutes and resuspended to an OD_{590nm} of 5.5 in KK2 buffer (0.16 mM KH_2PO_4, 4 mM K_2HPO_4). 1 mL *D. discoideum* culture was pelleted by centrifugation at 2,500 rpm for 5 minutes. Pelleted cells were washed once with KK2, centrifuged for a further 5 minutes and resuspended in 1 mL KK2. Resuspended *D. discoideum* AX3 were added to 1 mL of bacterial culture to a final concentration of 10^2 cells/mL. 200 μL of the resulting suspension was spread on SM agar (Formedium) [288] and incubated at 21 °C for 2 – 3 days to facilitate plaque formation.

2.6. Oyster husbandry

Pacific oysters (*Crassostrea gigas*) were purchased from Lindisfarne oyster farm (Lindisfarne Oysters, Northumberland). Shellfish were thoroughly scrubbed to remove external contaminants and attached organisms. Dead oysters were identified and removed. Oysters were maintained in individual aerated 5 L tanks filled with 20 ppt

salinity artificial seawater. Water was changed daily to prevent build-up of toxic elements. Oysters were fed a concentrated microalgae solution (TP1800, Reed Mariculture) every other day. Oysters were maintained at 21 °C for 5 days to allow them to acclimatise.

2.7. *In vivo* co-culture assays

2.7.1. Uptake of marine snow by oysters

Artificial marine snow was gently added to the individual oyster aquaria, taking care to prevent as much disruption of the aggregates as possible. AMS was generated individually for each bacterial strain prior to addition to oyster tanks. No strains were combined into one batch of AMS. Oysters were left to filter and ingest the marine snow for the required length of time. A circulatory current was generated by the presence of an air stone which maintained the movement of particles around the beaker and prevented settling of the aggregates. In conjunction with this, tank water was manually stirred every hour to maintain particle suspension.

2.7.2. Processing oysters for *Vibrio* plate enumeration

Following exposure to synthetic marine snow, oysters were removed from their tanks using flame sterilised tongs. Shellfish were cleaned with 70 % ethanol and blotted dry. Using a flame-sterilised shucking knife, oysters were shucked, and the tissue separated from the shell by severing the adductor muscle. The stomachs were then isolated by carefully removing the surrounding tissue using flame-sterilised scissors. Stomachs were weighed and placed in plastic bags with 10 mL PBS for homogenisation in a stomacher (Seward 400) on medium speed for 3 minutes.

Homogenate was filtered through a 40 μm cell strainer (Merck) into a clean 50 mL falcon tube to remove tissue debris. The resulting filtrate was utilised for Miles and Misra 10-fold serial dilutions in PBS. 100 μL of each dilution was spread on LB agar and incubated overnight at 37 °C. The following day all colonies were replica plated onto *Vibrio* selective TCBS and incubated overnight at 37 °C. Colonies were then enumerated based off colour and recorded for CFU/g oyster tissue calculations.

2.7.3. DNA extraction from oyster digestive gland homogenates

1 mL of oyster stomach homogenate from section 2.6.2 was placed into a clean microcentrifuge tube and centrifuged at 14,500 rpm for 5 minutes to pellet bacterial cells. Total DNA was extracted using the Wizard DNA extraction kit (Promega) according to the manufacturers' instructions. Extracted DNA was stored at -20 °C for future qPCR quantification.

2.8. qPCR

2.8.1. qPCR probe and primer design

Primer and probe sets were designed against *vgrG1, vcgE, vvhA* and *sefA* of *V. vulnificus* and *S.* Enteritidis. Primers were designed according to the following criteria: a Tm of between 58 – 60 °C, a GC content of between 20 – 80 %, between 9 – 40 base pairs long, < 2 °C difference between the forward and reverse primers and a maximum of two G/Cs in the last five base pairs of the 3' end. Primers were designed to result in an amplicon of ~ 100 bp.

Probes were designed according to the following criteria: a Tm 10 °C higher than the Tm of the primer pair, a GC content of between 20 – 80 %, between 9 – 40 base pairs

long, no G on the 5’ end, < 4 contiguous Gs, less Gs than Cs and the as close to the 3’ end of the forward primer as is possible without overlap. Probes were designed with a 5’ (6)FAM fluorophore and a 3’ TAMRA quencher (Eurofins). Probe sequences are recorded in Table 2.4.

Table 2.4: List of TaqMan qPCR probes used in this study.

Probes	Description	Sequence (5' - 3')
vgrG1	*V. vulnificus* 106-2A *vgrG1* probe, 5' FAM reporter, 3' TAMRA quencher	[FAM] TGAGCGTTGCTAACGAAAGCTACTT [TAM]
vcgE	*V. vulnificus* 99-743 *vcgE* probe, 5' FAM reporter, 3' TAMRA quencher	[FAM] CTCATTGAGCAGTAACGAAAGCACC [TAM]
vvhA	*V. vulnificus vvhA* probe, 5' FAM reporter, 3' TAMRA quencher	[FAM] ATGAACTGCGCCGCCAAGA [TAM]
sefA	*S.* Enteritidis CC012 *sefA* probe, 5' FAM reporter, 3' TAMRA quencher	[FAM] ACAACATCAGCCAACTGGAGTCAG [TAM]

2.8.2. Generation of qPCR positive control material

Positive control material was constructed to allow generation of standard curves for enumeration of *V. vulnificus*. *vvhA, vgrG1* and *vcgE* were PCR amplified using Phusion® High-Fidelity DNA polymerase (NEB) according to the protocol outlined in section 2.2.2. PCR amplicons were column purified and cloned in pGEM®-T Easy (Promega). Constructs were transformed into chemically competent *E. coli* DH5α and successful transformants identified through miniprep of the contrast and excision of the insert with *Eco*RI. Once extracted, plasmid concentration was determined using a

NanoDrop™ 1000 (ThermoFisher) and the constructs serially diluted from 10^8 – 10^1 copies/μL. Purified plasmid DNA was converted to copies/μL using Equation 2.1.

Equation 2.1: Equation for converting plasmid DNA to copies/μl for qPCR standards.

$$\boldsymbol{i})\ Single\ plasmid\ mass\ (g) = (DNA\ size\ (bp))\ x\ (1.096x10^{-21})$$

$$\boldsymbol{ii})\ Mass\ of\ plasmid\ DNA\ needed\ (g)$$
$$= Copy\ number\ of\ interest\ x\ Mass\ of\ a\ single\ plasmid\ (g)$$

$$\boldsymbol{iii})\ Final\ concentration\ of\ plasmid\ DNA\ (g/\mu\mathrm{L}) =$$
$$\frac{Mass\ of\ plasmid\ DNA\ needed\ (g)}{Volume\ of\ plasmid\ DNA\ added\ to\ reaction\ (\mu\mathrm{L})}$$

2.8.3. qPCR protocol

All qPCR reactions were set up in 0.2 mL non-skirted 96-well PCR plates (ThermoFisher) and analysed in a Stratagene Mx3005P qPCR system using the MxPro software (Agilent). Reactions were set up in triplicate according to the following protocol (optimised primer and probe concentrations are listed in section 2.7.4): 10 μL Luna® Universal Probe qPCR Master Mix (NEB), × nM forward primer, × nM reverse primer, × nM TaqMan probe, 5 μL template DNA, and ddH_2O to 20 μL. No-template controls were established using ddH_2O in place of DNA. Samples were run according to the following thermocycler conditions: 95 °C for 10 minutes, then 40 cycles of 95 °C

for 15 seconds, 55 °C for 1 minute and 72 °C for 1 minute. Fluorescence was recorded using the FAM channel.

2.8.4. qPCR optimisation

To optimise qPCR reactions, TaqMan primer and probes combinations were tested at a range of concentrations. Primer concentrations were optimised by generating a primer concentration matrix in a 96-well plate in which forward and reverse primers were combined at combinations of 50, 100, 200, 400, 600, and 800 nM in duplicate. PCRs were set up as described above in section 2.7.3. The optimum combination was determined by whichever combination resulted in a sigmoidal curve at the earliest reaction cycle. Once confirmed, this primer combination was optimised for probe concentration at 50, 100, 200, 400, 600, and 800 nM TaqMan probe. Again, the most suitable concentration was determined by the earliest and most typical sigmoidal curve. The final optimised concentrations for primer and probe sets have been listed in Table 2.5.

Table 2.5: Optimised qPCR primer and probe concentrations.

	vvhA	*vcgE*	*vgrG1*	*sefA*
Forward primer (nM)	200	600	200	100
Reverse primer (nM)	800	600	800	600
TaqMan probe (nM)	800	100	600	800

2.9. Graphing and statistical analysis

All graphing and statistical analysis was performed using GraphPad Prism 8 v8.1.2.

2.10. Scanning Electron Microscopy of marine snow

1 mL samples of artificial marine snow were extracted for processing. Samples were fixed in 2 % glutaraldehyde and 2 % paraformaldehyde in 0.1 M piperazine-N,N′-bis(2-ethanesulfonic acid) (PIPES) buffer (Merck) pH 7.2 and kept at 4 °C until further processing. Using a mild vacuum, fixed samples were transferred onto a 0.1 μm polycarbonate filter. The filter was washed for 5 minutes in Pipes buffer a total of 3 times. The aggregates attached to the filter were then dehydrated using an ethanol gradient. This consisted of washing the filter for 5 minutes in 30, 50, 70, 80, 90 and 95 % ethanol for 5 minutes followed by two final 10- minute washes using 100 % ethanol. Keeping the filter in 100 % ethanol, the filter was incubated for 3 minutes in hexamethyldisilazane before air-drying the filter. Dried filters were mounted onto an aluminium sample pin using carbon conductive tabs. Samples were then sputter-coated with 10 nm gold/palladium (80/20) and imaged using a JEOL JSM 6390 LV scanning electron microscope operated at 5 kV.

Chapter Three

V. vulnificus T6SSs exhibit antibacterial activity at environmental temperature conditions *in vitro*

Introduction and aims

Analysis of a number of *V. vulnificus* genomes led to the identification of two T6SSs, termed the T6SS1 and the T6SS2 [172]. Whilst all strains in the study possessed the T6SS2, only three sequenced strains had the T6SS1 (106-2A, S3-16 and 99-796). The authors established that *V. vulnificus* 106-2A can target and kill both *V. vulnificus* 99-743 and *V. fluvialis* NCTC 11327 in a T6SS1-dependent manner.

This chapter describes the construction of *V. vulnificus* T6SS mutants to enable further characterisation of *V. vulnificus* intra and inter-species killing activity. Following on from previous finding that T6SS1$^+$ *V. vulnificus* strains can target and kill T6SS1$^-$ strains *in vitro,* T6SS1$^+$ strains were labelled 'attackers', and T6SS1$^-$ strains were labelled 'prey'. This study focused primarily on *in vitro* co-culture of relevant attacker and prey strains at environmentally representative temperatures. For ease of comprehension, T6SS genes are referred to by their name most commonly used in the literature e.g. *hcp* instead of *tssD*.

Results

3.1. Generation of *V. vulnificus* 106-2A ΔT6SS1 and ΔT6SS2 mutants

To characterise the role of the T6SSs of *V. vulnificus*, mutants were generated from wild-type (WT) *V. vulnificus* 106-2A through markerless, in-frame deletion of *hcp1* and *hcp2*. In-frame deletion of *hcp1* and *hcp2* prevents T6SS needle assembly, preventing the activity of the T6SS1 and T6SS2. From here on 106-2AΔ*hcp1* and 106-2AΔ*hcp2* will be referred to as ΔT6SS1 and ΔT6SS2.

To generate these strains, up and downstream flanking regions of *hcp1* and *hcp2* were PCR amplified with the primers detailed in Fig. 3.1 and listed in Table 2.2, before being

ligated into commercial holding vector, pGEM-T Easy. Following confirmatory sequencing, flanking regions were excised from pGEM-T Easy using *Sma*I and *Nde*I (left flank) or *Nde*I and *Apa*I (right flank). In parallel, the counterselectable suicide vector, pDM4, was digested with *Sma*I and *Apa*I [285]. The inclusion of these restriction sites ensured that three-way ligation of pDM4, the left flank and the right flank would result in the construction of an in-frame *hcp1* or *hcp2* deletion cassette within pDM4 (Fig. 3.1). Once assembled, pDM4–Δ*hcp1* and pDM4–Δ*hcp2* were sequenced to confirm in-frame assembly and that no mutations or errors had been introduced. Both pDM4–Δ*hcp1* and pDM4–Δ*hcp2* constructs were separately triparentally conjugated into *V. vulnificus* 106-2A and plated on TCBS/Cm to select for first crossover

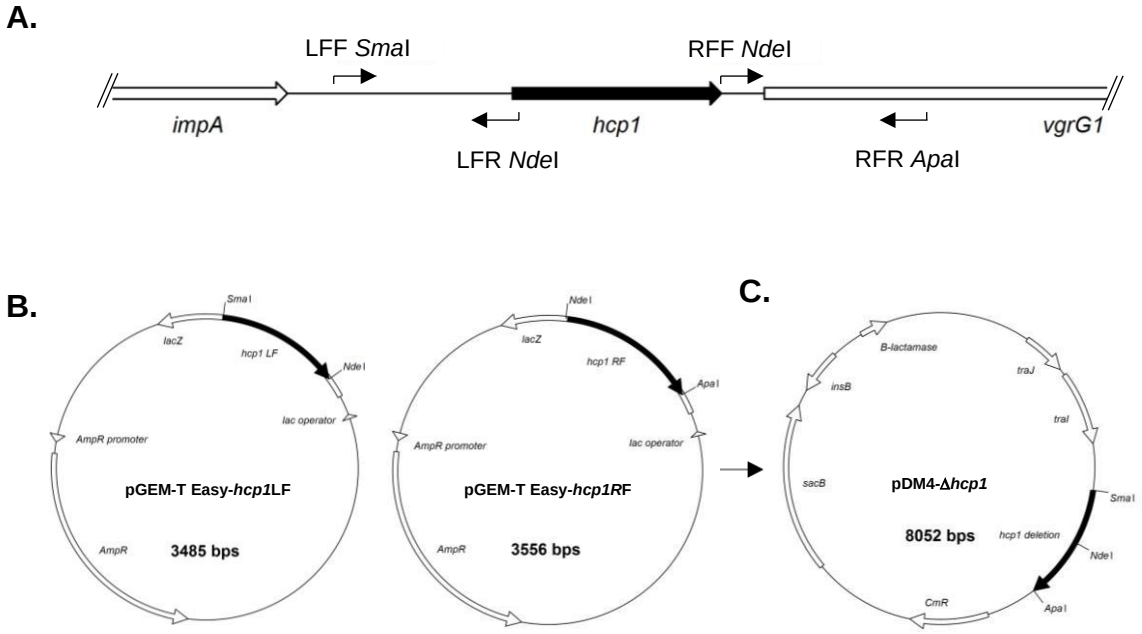

Figure 3.1: Construction of pDM4-based suicide vectors for markerless in-frame deletion of *hcp1* and *hcp2*. This schematic depicts construction of pDM4-Δ*hcp1* but is representative of pDM4-Δ*hcp2* also. **(A)** Left and right flanking regions of *hcp1* and *hcp2* were PCR amplified with primers incorporating restriction endonuclease sites for downstream cloning. **(B)** Amplified flanks were individually cloned into holding vector pGEM-T Easy and sequenced to confirm sequence identity. **(C)** Flanks excised using *Sma*I, *Nde*I and *Apa*I were cloned into pDM4 in a three-way ligation, facilitating ligation of the two flanks into digested pDM4.

integrants. Potential first-crossover integrants were checked using both the MutScreen FWD/CmR REV and MutScreen REV/CmR FWD primers. MutScreen FWD and REV were both designed to bind distally to *hcp1* or *hcp2*, and CmR FWD and REV were designed to the Cm resistance gene in pDM4. Therefore, amplification of a PCR product using both MutScreen and CmR primers would confirm plasmid integration into the genome (Fig. 3.2).

pDM4 is a *sacB*-based suicide vector, expressing *Bacillus subtilis* levansucrase at 10 % sucrose conditions [289]. SacB is lethal to a wide range of Gram-negative bacteria, including *Vibrio* species, allowing for easy pDM4 counter-selection following integration into the genome as described in the methods (section 2.2.16). First-crossover integrants were checked by PCR using the MutScreen primers listed in Table 2.2 and plated onto chloramphenicol plates to confirm resistance. pDM4 excision was promoted by plating successful first crossovers onto LB supplemented with 10 % sucrose. Colonies were plated on chloramphenicol plates and any able to grow on sucrose but susceptible to chloramphenicol were PCR checked to confirm second crossover and *hcp* deletion (Fig. 3.3A). Amplification of *hcp1* and *hcp2* from WT *V. vulnificus* 106-2A resulted in a 1,639 bp and a 1,569 bp band, respectively. Successful deletion of *hcp1* and *hcp2* resulted in reduced band sizes of 1,131 bp and 1,150 bp. DNA bands observable at 500 bp were *V. vulnificus*-specific *vvhA* PCRs to confirm colonies were the correct species. PCRs were performed separately; however, they have been loaded on the gel together for ease of viewing. Successful in-frame deletion mutants were plated on LB/Cm agar to confirm plasmid absence and samples submitted for confirmatory sequencing (Fig. 3.3B/C).

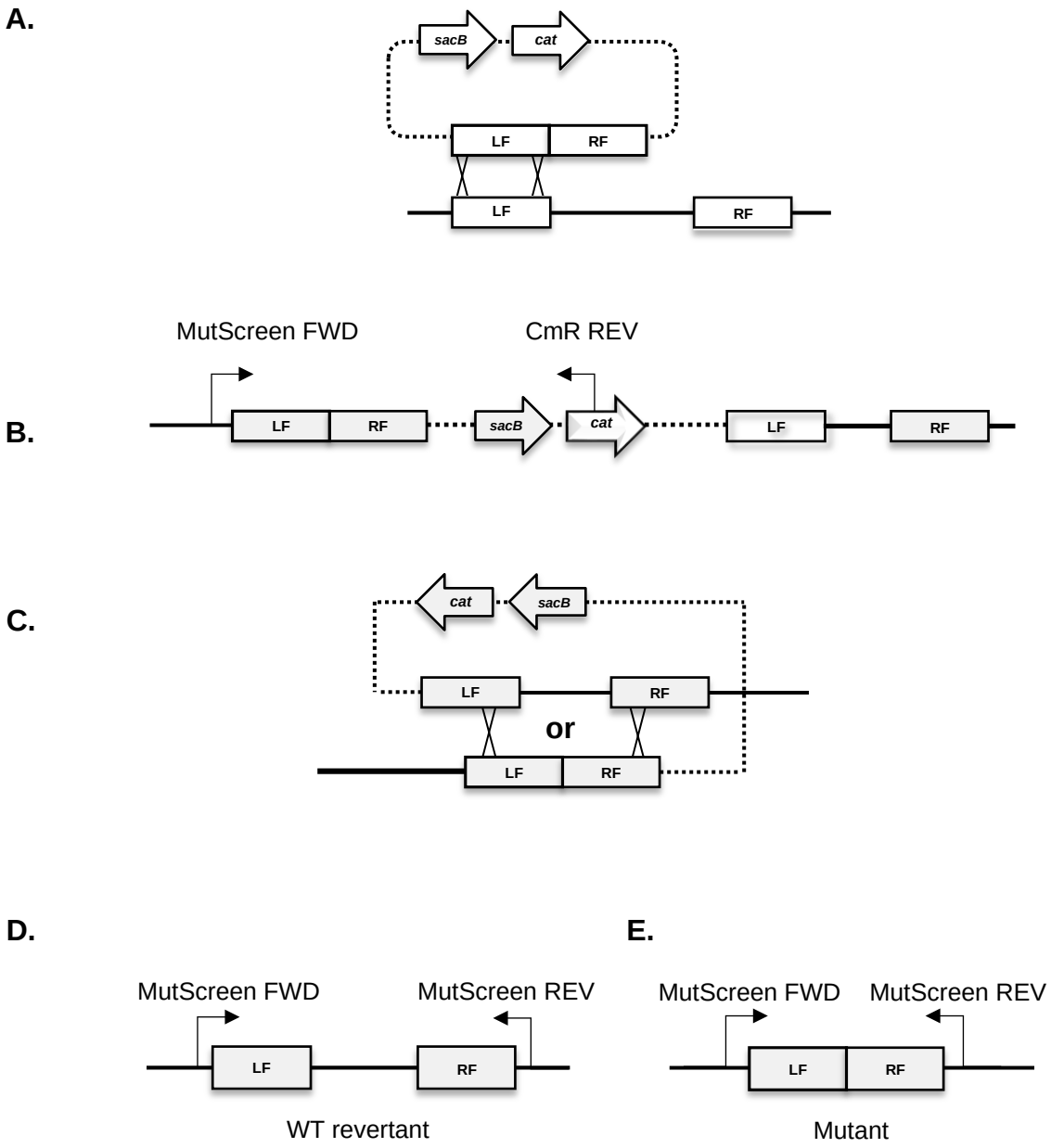

Figure 3.2: pDM4 allelic exchange schematic. (A) Homologous recombination of constructed suicide vectors into the chromosome. The dotted line represents the plasmid backbone. SacB is the *B. subtilis* levansucrase protein, CmR denotes chloramphenicol resistance. The bacterial chromosome is represented by the bold line. **(B)** Merodiploid first crossover strain following recombination of the suicide vector into the genome. Screening primers to identify successfully crossover integrants are labelled, if the construct has not integrated then no amplification is possible. **(C)** The cytotoxic effect of *sacB* expression in the presence of sucrose allows for counter-selection and excision of pDM4 from the chromosome resulting in either a WT revertant **(D)** or a successful mutant **(E)**. MutScreen FWD and REV are designed to bind upstream of the left and right flanks to determine whether mutation has occurred successfully or whether the bacterium has reverted to the WT genotype.

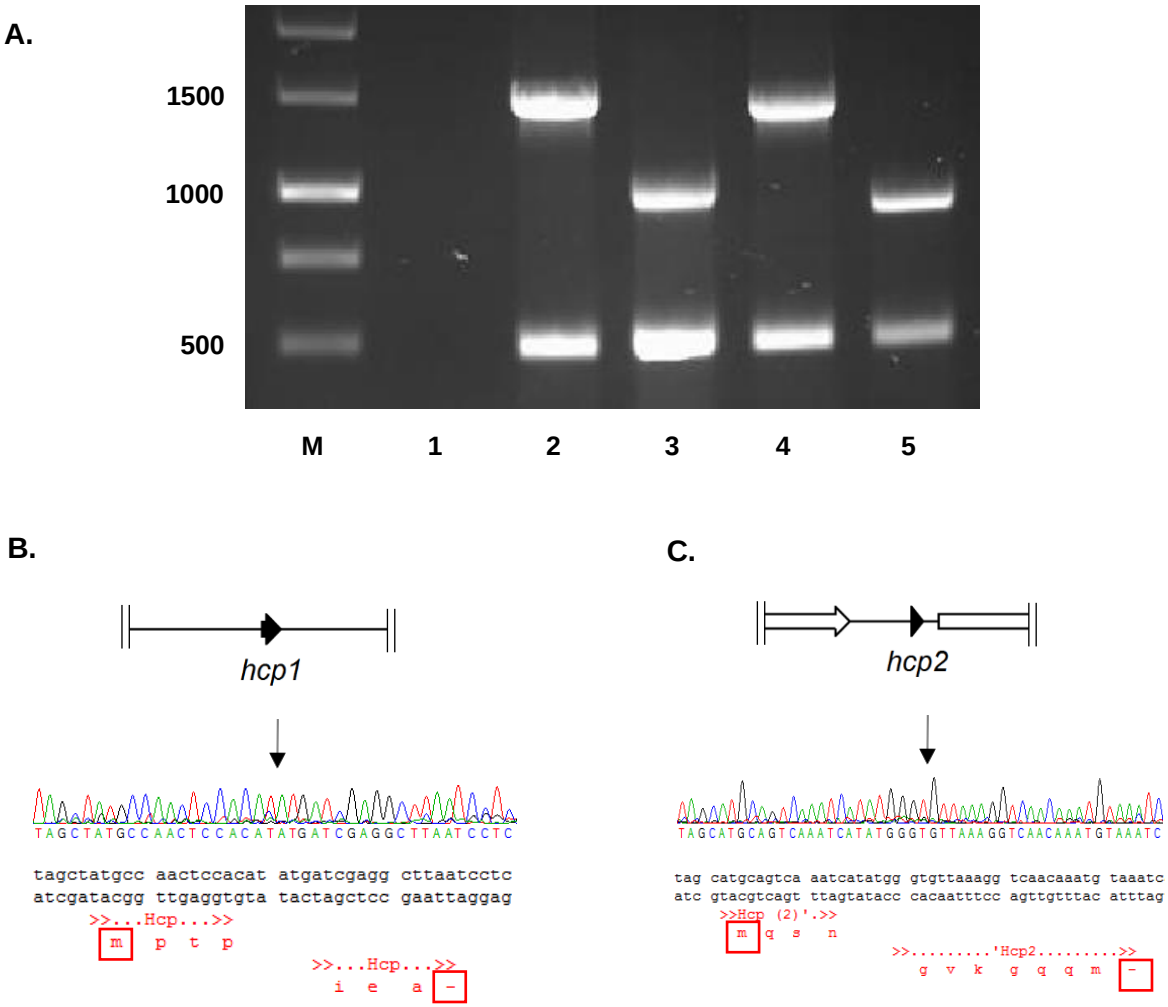

Figure 3.3: Confirmation of ΔT6SS1 and ΔT6SS2 in-frame deletion. (A) PCR confirmation of *V. vulnificus* 106-2A ΔT6SS1 and ΔT6SS2 mutants. Comparison of *hcp1* and *hcp2* regions from WT 106-2A versus successful *hcp* deletions. M – Molecular marker (bp). 1 – Negative control using nuclease free water in place of gDNA. 2 – Positive WT control band for *hcp1* at 1,639 bp. The 500 bp band is the *V. vulnificus* specific *vvhA* control. 3 – Successful Δ*hcp1* mutant band at 1,131 bp and positive *vvhA* band. 4 – Positive WT control band for *hcp2* at 1,569 bp with corresponding *vvhA* control band. 5 – Successful Δ*hcp2* mutant demonstrated by a band at 1,150 bp and confirmatory *vvhA* band.

Hcp regions were PCR amplified and sequenced to confirm no mutations had been introduced during allelic exchange. **(B)** Truncated *hcp1* is marked with both start and stop codons boxed in red. Ligation of the left and right flanks has reduced the gene from 519 bp to 30 bp. The sequence data for the region is displayed above. **(C)** Truncated *hcp2* is marked with both start and stop codons boxed in red. Ligation of the left and right flanks has reduced the gene from 466 bp to 42 bp. The sequence data is displayed above.

3.2. Reverse-transcriptase PCR confirmation of ΔT6SS1 and ΔT6SS2

To confirm that *hcp1* and *hcp2* deletion had not negatively affected expression of downstream genes RNA was extracted from ΔT6SS1 and ΔT6SS2 for reverse-transcriptase PCR (RT-PCR). Primers were designed against *vgrG1* and *clpV2* as the downstream genes for *hcp1* and *hcp2*, respectively. Template complementary DNA (cDNA) was generated from total extracted cellular mRNA according to the methods (section 2.2.5). Fig. 3.4 shows RT-PCR of *vgrG1* and *clpV2* from WT *V. vulnificus* 106-2A and both ΔT6SS1 and ΔT6SS2 mutants. Lane 1 comprises a no template control and lane 2 a no reverse transcriptase control to ensure there was no gDNA contamination.

No bands were observed in either negative control, confirming that there was no reagent contamination or gDNA carry-over. Lanes 3 and 4 show DNA amplified from WT *V. vulnificus* 106-2A using *vgrG1* (2,064 bp) and *clpV2* (2,565) primers respectively. Lane 4 demonstrates successful amplification of *vgrG1* from ΔT6SS1 cDNA as noted by the presence of a band at 2,064 bp. Similarly, in lane 6, *clpV2* has been successfully amplified from ΔT6SS2 cDNA as noted by the presence of a 2,565 bp band. This data confirms that in-frame deletion of *hcp1* and *hcp2* has not affected transcription of downstream T6SS genes.

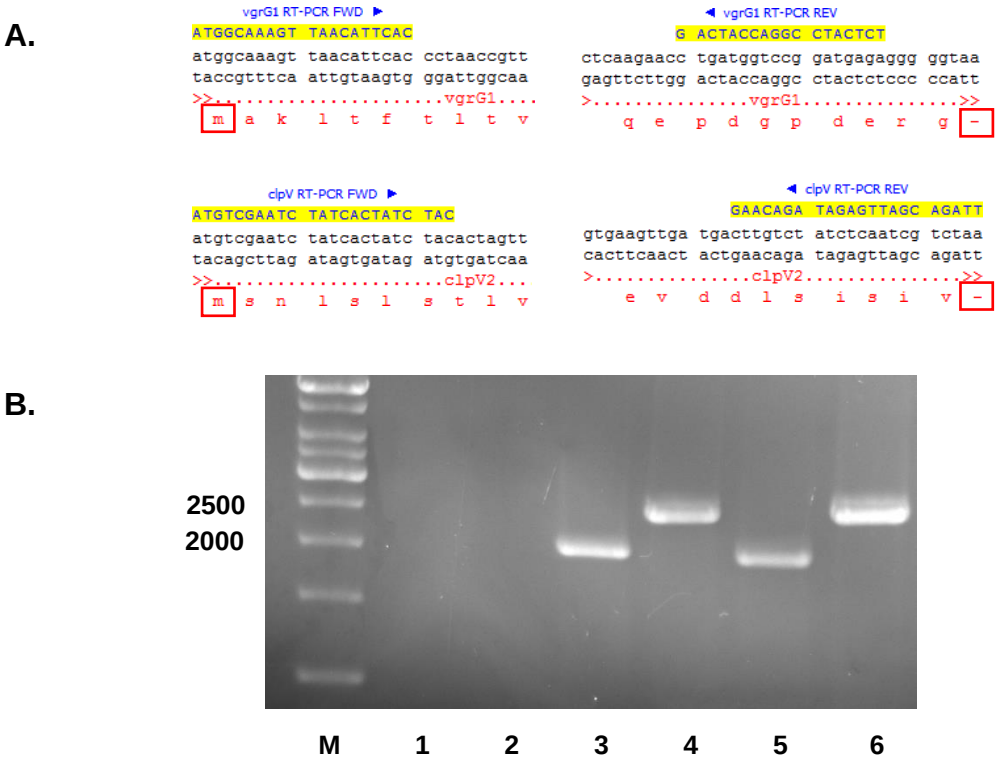

Figure 3.4: RT-PCR of *V. vulnificus* 106-2A ΔT6SS1 and ΔT6SS2. (A) Primer binding sites for *vgrG1* and *clpV2* RT-PCR primers. Gene stop and start codons are highlighted in red boxes. **(B)** Expression of genes downstream of *hcp1* and *hcp2* (*vgrG1* and *clpV* respectively) confirmed using RT-PCR. **M** – molecular marker (bp), **1** – no template control, **2** – no reverse-transcriptase genomic DNA (gDNA) control, **3** – 106-2A WT positive *vgrG1* control (2,056 bp), **4** – 106-2A WT positive *clpV2* control (2,565 bp), **5** – ΔT6SS1 *vgrG1* (2,056 bp), **6** – ΔT6SS2 *clpV2* (2,565 bp). The presence of a 2,056 bp band in lane 5 confirms *vgrG1* transcription in ΔT6SS1. The presence of a 2,565 bp band in lane 6 confirms *clpV2* transcription in ΔT6SS2.

3.3. Growth comparison of WT *V. vulnificus* 106-2A to ΔT6SS mutants

To ascertain whether the introduction of the *hcp* mutations had a phenotypic effect, the growth of all attacker and prey strains was characterised at 21 °C, 30 °C and 37 °C temperatures. 30 °C and 37 °C were selected to confirm that T6SS mutants resulted in similar results to previous studies temperatures. 21 °C was selected as an

environmentally representative temperature ideal for *V. vulnificus* growth in marine environments [290]. Attacker strains tested were *V. vulnificus* 106-2A, ΔT6SS1 and ΔT6SS2, and prey strains were *V. vulnificus* 99-743 and *Salmonella enterica* serovar Enteritidis CC012. These prey strains were selected as they are representative of species with which *V. vulnificus* would come into contact with *in vivo* [2,291].

Strains were cultured in LB broth at 21 °C, 30 °C and 37 °C. Bacterial cultures were incubated for 24 hours and OD_{590nm} absorbance readings taken at T_0, T_2, T_4, T_6, T_8 and T_{24} at each temperature. Samples from each timepoint were serially diluted and plated on LB agar for CFU/mL enumeration (Fig. 3.5). Statistical comparison of WT *V. vulnificus* 106-2A, ΔT6SS1 and ΔT6SS2 at each temperature concluded that there was no significant difference in growth rate. This demonstrates that deletion of *hcp1* and *hcp2* has no negative impact on growth. Equally, prey strain *V. vulnificus* 99-743 showed no significant difference in growth rate relative to 106-2A, ΔT6SS1 or ΔT6SS2.

S. Enteritidis CC012 did demonstrate some significant differences in growth compared *V. vulnificus* at 30 °C and 37 °C. CFU/mL at T_8 and T_{24} were significantly greater than all *V. vulnificus* strains ($p < 0.05$). However, this was not considered as a major obstacle, primarily because the *in vitro* killing assays to be performed at 30 °C and 37 °C would only be incubated for five hours, at which point growth between bacterial species showed no statistical difference. Whilst 21 °C co-culture assays were to be incubated for 24 hours, at these temperature conditions *S.* Enteritidis showed no significant difference in growth compared to *V. vulnificus*.

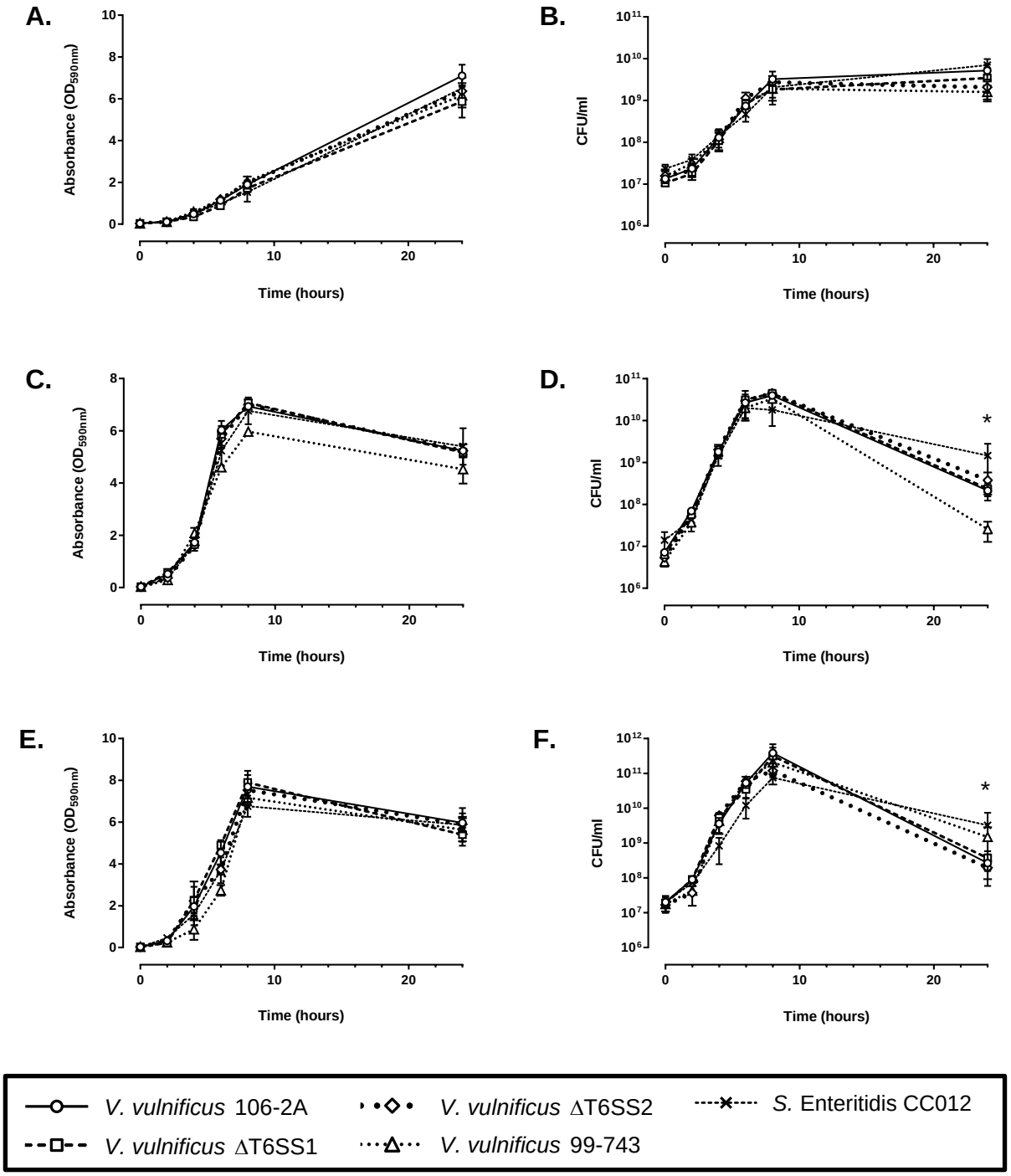

Figure 3.5: Growth curves of *V. vulnificus* and *S.* Enteritidis at 21 °C, 30 °C and 37 °C. Growth curves were performed according to the methods for *V. vulnificus* 106-2A, ΔT6SS1, ΔT6SS2, 99-743 and *S.* Enteritidis CC012. OD590nm readings were taken at T0, T2, T4, T6, T8 and T24. Samples from each time point were serially diluted 10-fold and enumerated on LB agar. Growth curves were performed in triplicate under three individual temperature conditions. (A & B) 21 °C. (C & D) 30 °C. (E & F) 37 °C. Statistics were performed using a two-way ANOVA with Tukey's multiple comparisons corrections, * $p < 0.05$.

3.4. *V. vulnificus* intra-species T6SS activity

3.4.1. Construction of antibiotic resistant *V. vulnificus* using pVv3-kan and pVv3-tmp

Previously, studies performing competition assays using *Vibrio* species have utilised TCBS agar to distinguish between different strains [172]. TCBS contains sucrose, which only particular *V. vulnificus* strains are capable of fermenting. *Vibrio* strains able to degrade sucrose generate a localised acidic environment, resulting in colonies appearing yellow. Therefore, using a sucrose-fermenting prey strain results in yellow prey colonies, whilst non-fermenting attacker strains remain green, allowing for colour-based enumeration of attacker and prey colonies.

However, this was highly unreliable. Fig. 3.6 shows that bacterial cultures plated on TCBS demonstrated a 10,000-fold growth difference relative to the same cultures plated on LB agar. This is not the first study to identify this problem as Tagliava *et al.*, (2019) recently noted that TCBS as a selective medium may be hampering *Vibrio* isolation due to substantial underestimations and even total isolation failures [292]. It was therefore decided to generate antibiotic resistant *V. vulnificus* to enable plate selection following co-culture. No antibiotic resistance was introduced to *S.* Enteritidis CC012 as selection could be performed using *Salmonella* specific chromogenic media which inhibited the growth of *Vibrio* species but had no deleterious effect on *S.* Enteritidis growth (Appendix 2).

To date, the only published shuttle vector for *V. vulnificus* is pVv3, first identified as pVN-0126, a 1,301 bp cryptic plasmid from *V. vulnificus* VN-0126 [293]. Introduction of a kanamycin resistance gene cassette, *lacZ*α gene, polylinker and T7 promoter resulted in construction of pVv3-kan. pVv3-kan can be easily introduced into a number

of *Vibrio* species via electroporation, including *V. parahaemolyticus* and *V. cholerae*. To introduce antibiotic resistance to *V. vulnificus*, pVv3-kan was electroporated into 106-2A, ΔT6SS1 and ΔT6SS2. Plasmid DNA extracted from transformants was confirmed as pVv3-kan by digestion of purified plasmid DNA with *Apa*I, *Kpn*I and *Nde*I.

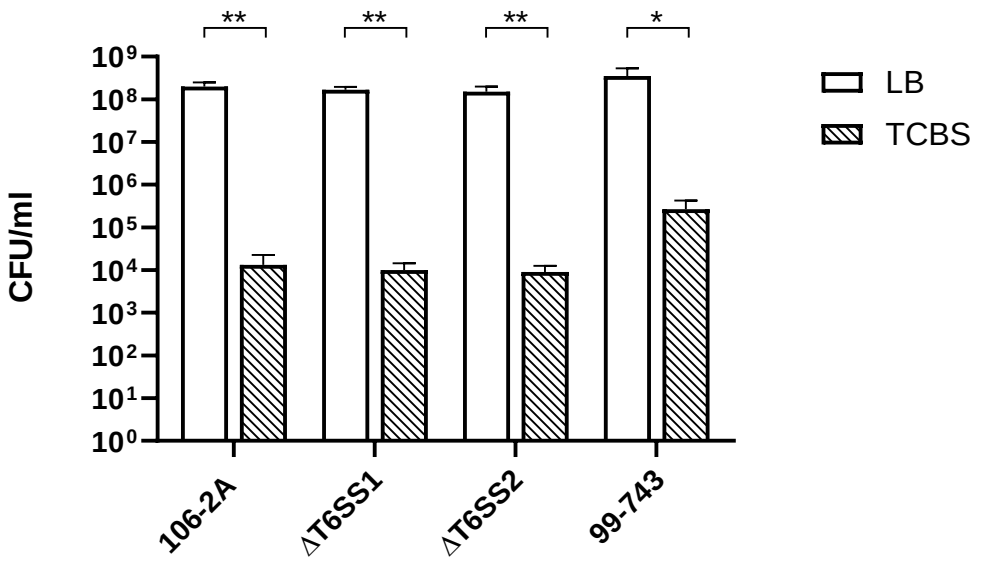

Figure 3.6: *V. vulnificus* growth comparison on LB and TCBS agar. *V. vulnificus* 106-2A, ΔT6SS1, ΔT6SS2 and 99-743 cultures were adjusted to an OD_{590nm} of 0.8 and serially diluted 10-fold for Miles and Misra spot-plate enumeration on LB and TCBS agar. Colonies were enumerated and statistics performed using a t-test with Holm-Sidak's correction for multiple comparisons, * $p < 0.05$. ** $p < 0.01$.

Unfortunately, pVv3-kan contains only a kanamycin resistance cassette. Effective selection of attacker and prey cells required pVv3-kan containing a different antibiotic resistance cassette. The plasmid pVv3-kan-tmp, with a trimethoprim resistance gene inserted outside of the kanamycin resistance gene was modified by *in vitro* mutagenesis to generate a version of pVv3 solely conferring trimethoprim resistance. The kanamycin resistance gene was removed by overlap-extension PCR (OE-PCR),

where OE primers were designed to bind to the DNA directly up and downstream of the kanamycin resistance gene, facilitating PCR amplification of pVv3-kan-tmp but omitting the kanamycin resistance gene). A schematic for this process can be seen in Fig. 3.7.

PCR-amplified plasmid product was incubated with *Dpn*I to digest template DNA before transformation into *E. coli* DH5α. *Dpn*I is a restriction enzyme that recognises and cleaves methylated DNA. As such, *Dpn*I treatment of the PCR product resulted in the degradation of the methylated template plasmid DNA extracted from *E. coli* DH5α [294,295]. As the newly constructed plasmid, pVv3-tmp, had not come into contact with any methyltransferases it was not targeted for degradation by *Dpn*I. This process therefore resulted in the degradation of all template plasmid DNA still containing the kanamycin resistance gene whilst preserving the newly generated construct containing only trimethoprim resistance. pVv3-tmp was transformed into chemically competent *E. coli* and selected for on LB/Tmp. Resistant colonies were subcultured on LB/Kan to confirm kanamycin susceptibility. Transformants that grew on LB/Tmp but not LB/Kan were digested to confirm plasmid integrity.

Before newly generated antibiotic-resistant *V. vulnificus* strains could be used for *in vitro* co-culture assays the impact of pVv3-kan and pVv3-tmp on *V. vulnificus* growth was assessed. No difference in growth rate was observed for any of the resistant *V. vulnificus* strains when compared to the same strain lacking the resistance plasmid (Appendix 3). Plasmid retention assays also demonstrated no significant plasmid loss over 24 hours (Appendix 4).

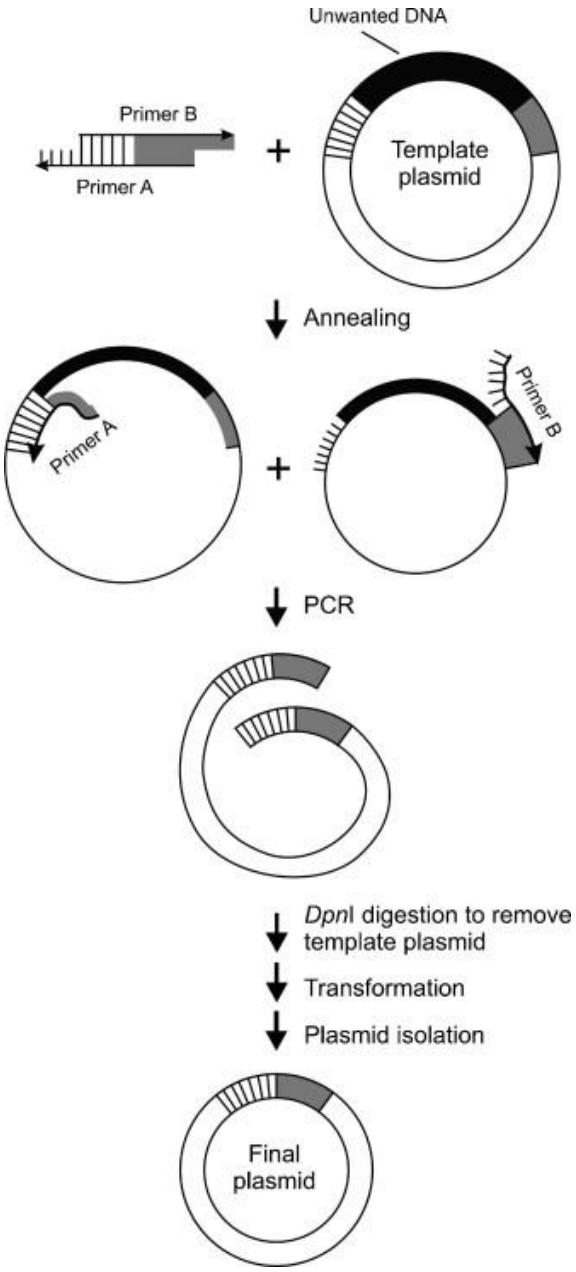

Figure 3.7: Schematic depicting PCR deletion of the kanamycin resistance gene from pVv3-kan-tmp to generate pVv3-tmp. The region of plasmid DNA to be excised is shown in black with the flanking regions indicated by dashed and shaded regions. Plasmid DNA was amplified using primers with complementary 5' tails to facilitate the joining of the two plasmid ends following gene excision. Once amplified, the PCR product was treated with *Dpn*I to digest the template plasmid DNA, leaving only the newly synthesised product lacking the kanamycin resistance gene. The product was transformed into chemically competent *E. coli* DH5α and plasmid DNA extracted from successful transformants. Figure was taken from Hansson *et al*., (2008) [286].

3.4.2. The T6SS1 is active at 30 °C, but not 37 °C

To characterise *V. vulnificus* intra-species killing activity *in vitro*, prey strain 99-743 pVv3-tmp was individually co-cultured on LB agar with 106-2A pVv3-kan, ΔT6SS1 pVv3-kan and ΔT6SS2 pVv3-kan. Bacterial cultures adjusted to an OD_{590nm} of 0.8 were combined at an attacker to prey ratio of 3:1 and incubated for 5 hours at 30 °C and 37 °C on LB agar as described previously for *V. vulnificus* in Church *et al*., (2016) [172]. Growth spots were resuspended and serially diluted for Miles and Misra plate enumeration on either LB/Kan or LB/Tmp to select for attacker and prey strains respectively.

Fig. 3.8 shows viable cell counts of prey 99-743 following co-culture with just LB (negative), 106-2A, ΔT6SS1 or ΔT6SS2 at 30 °C and 37 °C, respectively. Co-culture with LB at 30 °C resulted in recovery of 10^{10} CFU/mL 99-743, demonstrating 100-fold growth from the T_0. Interestingly, when co-cultured with 106-2A and ΔT6SS2, recovery of prey 99-743 was 10^7 CFU/mL, 1,000-fold less than the negative control ($p < 0.01$). This data suggested that prey killing is T6SS1-dependent, as co-culture of 99-743 with ΔT6SS1 resulted in recovery of ~ 10^{10} CFU/mL 99-743, equal to the negative control exposed to no attacker strain.

When incubated at 37 °C, > 10^{11} CFU/mL were recovered from the negative control. 99-743 co-cultured with 106-2A, ΔT6SS1 or ΔT6SS2 showed no significant reduction, with all samples recovered at 10^{11} CFU/mL. This data shows that T6SS1 activity is thermoregulated, demonstrating intra-species killing activity at 30 °C, but not 37 °C. The T6SS2 demonstrated no observable killing activity under any temperature condition tested as has been previously demonstrated.

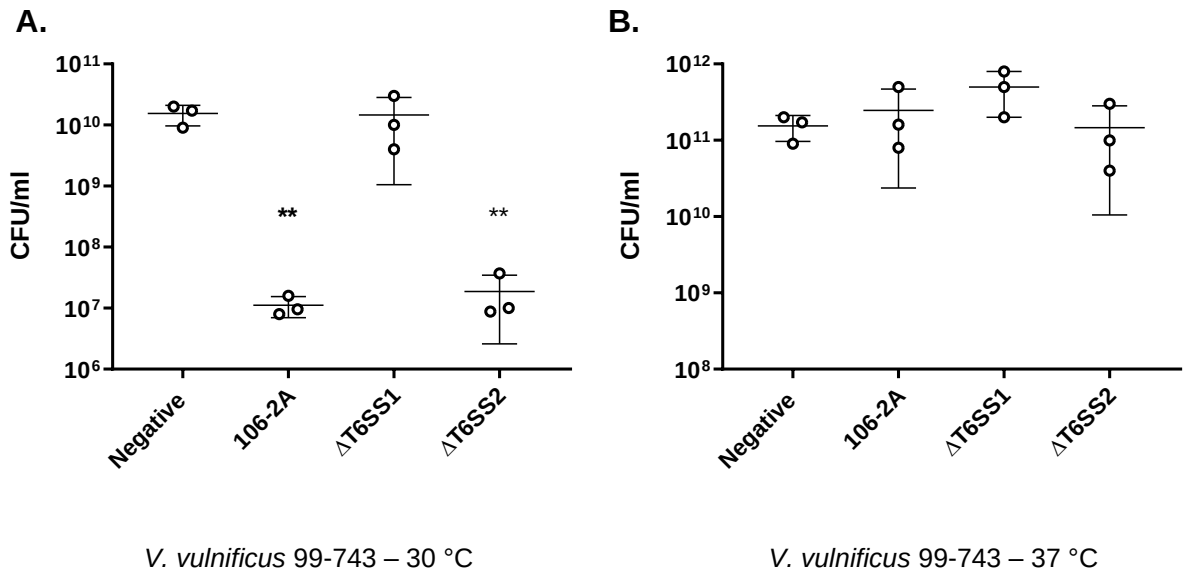

V. vulnificus 99-743 – 30 °C

V. vulnificus 99-743 – 37 °C

Figure 3.8: Recovery of prey *V. vulnificus* following co-culture with attacker *V. vulnificus* at 30 °C and 37 °C. Prey *V. vulnificus* 99-743 was co-cultured with attacker *V. vulnificus* 106-2A, ΔT6SS1 and ΔT6SS2, for 5 hours at 30 or 37 °C. Bacterial spots were resuspended and serially diluted to facilitate 99-743 enumeration. The horizontal lines represent the mean and the error bars represent the standard deviation (n = 3). Statistics were performed using an ordinary one-way ANOVA with Dunnett's corrections for multiple comparisons, ** $p < 0.01$.

Analysing recovered cell counts for attacker strains showed no statistically significant difference, suggesting that there is no reciprocal killing taking place by 99-743 (Appendix 5). 106-2A, ΔT6SS1 and ΔT6SS2 all demonstrate uninhibited growth with no statistical significance observed between the T_5 time points of any strain at either 30 °C or 37 °C relative to their increase from T_0. This result is largely expected as 99-743 only contains the T6SS2, which has been shown to be inactive under these conditions. In conclusion, this data showed that 106-2A is capable of T6SS1-mediated targeting and killing of 99-743 at 30 °C. Under these same conditions no T6SS2 activity was observed, suggesting that intra-species competition at 30 °C is purely T6SS1-dependent. It is therefore likely that T6SS1$^+$ strains possess a competitive

advantage over T6SS1$^-$ strains *in vivo*, impacting *V. vulnificus* populations in habitats such as filter-feeding shellfish.

3.5. The T6SS1 is involved in inter-species competition

It was hypothesised that if *V. vulnificus* can target other *Vibrios* using the T6SS1 then it is possible that it could also target other bacterial species. *S.* Enteritidis CC012 is a rod-shaped, Gram-negative bacterium frequently associated with causing disease in humans, manifesting as diarrhoea, gastroenteritis and feverish symptoms [296]. Whilst not as ubiquitously present in oysters as *Vibrio* species, *Salmonella* species have been identified in oysters previously [256,257,297,298]. CC012 was therefore utilised as the prey strain to investigate inter-species bacterial killing by *V. vulnificus*.

3.5.1. The T6SS1 can target *S.* Enteritidis CC012 at 30 °C

Co-culture assays were conducted using *S.* Enteritidis as prey to explore the inter-species killing activity of the T6SS1. Fig. 3.9A shows co-culture of *S.* Enteritidis CC012 with either *V. vulnificus* 106-2A, ΔT6SS1 or ΔT6SS2 for 5 hours at 30 °C. Co-culture with LB demonstrates that CC012 growth over 5 hours results in 10^{10} CFU/mL from an initial plated concentration of 10^8 CFU/mL. Interestingly, as previously observed, co-culture with 106-2A and ΔT6SS2 resulted in a significant reduction in recovered CC012 CFU/mL, with a 1,000-fold reduction compared to the negative control ($p < 0.01$). Again, co-culture with ΔT6SS1 showed no significant difference compared to the negative control, confirming that *V. vulnificus* inter-species killing of *S.* Enteritidis is T6SS1-dependent.

Fig. 3.9B supports findings from the previous section showing that the T6SS1 is temperature regulated, as co-culture of attacker and prey bacterial strains at 37 °C resulted in no significant reduction in recovery of the prey strain relative to the negative control. Also, no retaliatory killing of attacking *V. vulnificus* strains by *S.* Enteritidis was observed (Appendix 6).

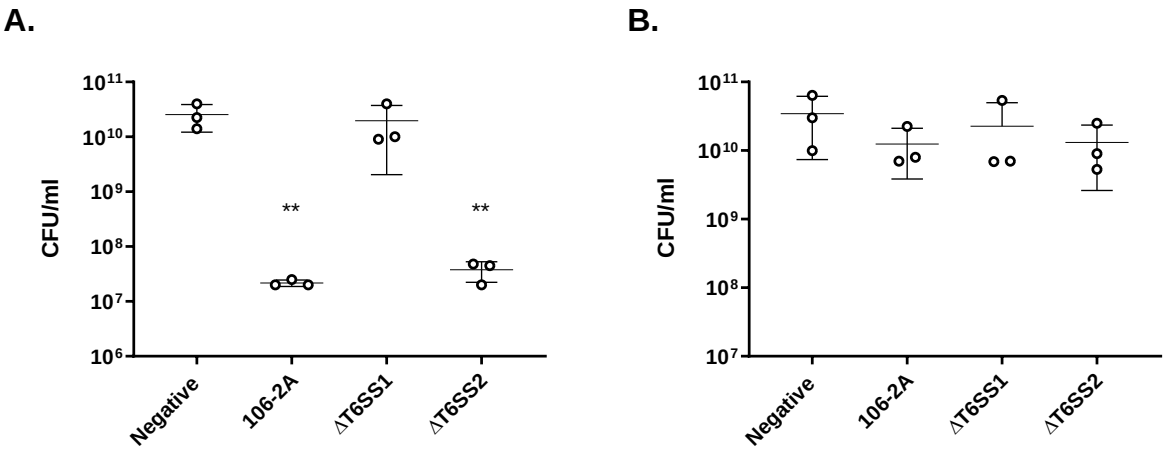

Figure 3.9: Recovery of prey *S.* Enteritidis following co-culture with attacker *V. vulnificus* at 30 °C and 37 °C. (A) Prey *S.* Enteritidis CC012 was co-cultured with attacker *V. vulnificus* 106-2A, ΔT6SS1 and ΔT6SS2, on LB agar for 5 hours at 30 and (B) at 37 °C. Bacterial spots were resuspended and serially diluted to facilitate CC012 enumeration. The horizontal lines represent the mean and the error bars represent the standard deviation (n = 3). Statistics individually comparing each strain to the negative control were performed using an ordinary one-way ANOVA with Dunnett's corrections for multiple comparisons, ** $p < 0.01$.

In conclusion, this study has demonstrated that the T6SS1 of *V. vulnificus* has both intra and inter-species killing activity at 30 °C *in vitro*. The lack of antibacterial activity at 37 °C suggested that the activity of the T6SS1 is temperature regulated. No observable killing at 37 °C implies that the T6SS1 may not be involved in human infection, but rather utilised to provide a competitive edge in environmental conditions.

3.6. *V. vulnificus* ΔT6SS1 demonstrates prey growth inhibition at 21 °C *in vitro*

This study aims to demonstrate that the observed *in vitro* T6SS1 killing is representative of *in vivo* activity in an oyster host. However, currently all co-culture assays have only been performed at 30 °C and 37 °C. Future *in vivo* studies will be performed at 21 °C as it has been shown that this temperature is ideal for *V. vulnificus* growth in seawater [290]. Thus, before embarking on oyster *in vivo* studies, *in vitro* competition assays were performed as previously described at 21 °C for 24 hours. It was decided to incubate co-culture for the longer time period of 24 hours due to the slower growth of the strains under these conditions (Appendix 3).

The recovery of viable prey *V. vulnificus* 99-743 and *S.* Enteritidis CC012 following co-culture at 21 °C with attacker *V. vulnificus* strains 106-2A, ΔT6SS1 or ΔT6SS2 can be seen in Fig. 3.10. Prey recovery when co-cultured with just LB was recorded at 10^{11} CFU/mL for both 99-743 and CC012. However, both prey strains showed a significant, > 10-fold reduction when co-cultured with either 106-2A, ΔT6SS1 or ΔT6SS2 ($p < 0.05$). The inhibition of prey growth when co-cultured with ΔT6SS2 suggested that the T6SS1 is active at 21 °C as it is as 30 °C. No reciprocal growth inhibition of attacker *V. vulnificus* strains by either prey *V. vulnificus* 99-743 or *S.* Enteritidis CC012 was observed at 21 °C (Appendix 7). Interestingly, the reduction in prey growth when co-cultured with ΔT6SS1 suggested that growth inhibition is also T6SS2-mediated at 21 °C. Fascinatingly, this implies that at environmentally representative temperatures of 21 °C both T6SSs are active and demonstrate antibacterial activity.

However, it is possible that 106-2A possesses uncharacterised antibacterial mechanisms active at 21 °C, resulting in the observed inhibition phenotype rather than this being attributable to the T6SS2. Therefore, a 106-2A double mutant in which both *hcp1* and *hcp2* were deleted, inhibiting T6SS activity from both secretion systems, was

generated. If co-culture with the double mutant still demonstrated a reduction in prey strain growth, this implies that growth inhibition is T6SS-independent.

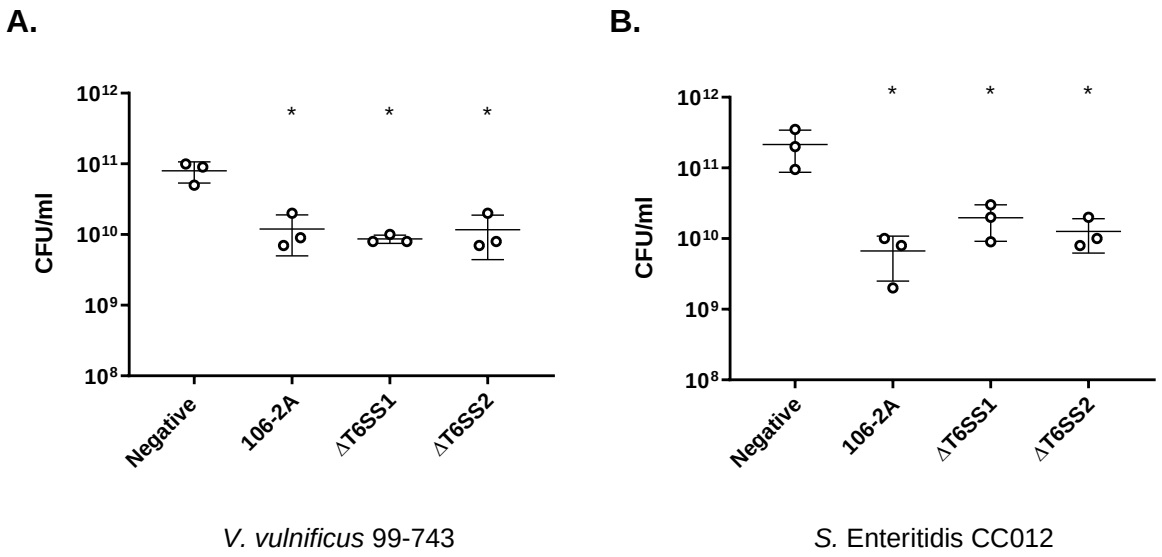

Figure 3.10: Recovery of prey *V. vulnificus* and *S*. Enteritidis following co-culture with attacker *V. vulnificus* at 21 °C. Prey *V. vulnificus* 99-743 (A) and *S*. Enteritidis CC012 (B) were co-cultured with attacker *V. vulnificus* 106-2A, ΔT6SS1 and ΔT6SS2, for 5 hours at 21 °C. Bacterial spots were resuspended and serially diluted to facilitate enumeration of 99-743 and CC012. The horizontal lines represent the mean and the error bars represent the standard deviation (n = 3). Statistics individually comparing each strain to the negative control were performed using an ordinary one-way ANOVA with Dunnett's corrections for multiple comparisons, * $p < 0.05$.

3.7. Generation of a double T6SS mutant in *V. vulnificus* 106-2A (ΔT6SS1/2)

Previously constructed allelic exchange vector, pDM4–Δ*hcp2*, was triparentally conjugated into ΔT6SS1 and an in-frame deletion generated as previously described. Deletion of *hcp1* and *hcp2* was PCR-confirmed and total RNA extracted for RT-PCR of downstream genes. In-frame deletion of *hcp2* was confirmed via sequencing (Appendix 8). From here on the double mutant will be referred to as ΔT6SS1/2. As previously described, pVv3-kan was electroporated into ΔT6SS1/2, conferring

kanamycin resistance. ΔT6SS1/2 growth curves were generated with and without pVv3 to ensure that deletion of both T6SSs had no deleterious impact on growth (Appendix 9). As expected, no significant difference was observed between ΔT6SS1/2 growth and growth of the other *V. vulnificus* strains utilised in this study.

3.8. ΔT6SS1/2 demonstrates that killing at 21 °C is mediated by both T6SS1 and T6SS2

In vitro competition assays were performed at 21 °C with the inclusion of ΔT6SS1/2 to determine whether there was a reduction in prey killing. The results can be seen in Fig. 3.11. The 10-fold reduction in recovery of *V. vulnificus* 99-743 and *S.* Enteritidis CC012 observed following co-culture with attacker *V. vulnificus* strains was not observed following co-culture with the double mutant, ΔT6SS1/2. Instead, recovery of both strains was 10^{11} CFU/mL, consistent with the negative control. This data indicates that the killing demonstrated by 106-2A, ΔT6SS1 and ΔT6SS2 was a result of the activity of the T6SS1 and T6SS2, and not an uncharacterised antibacterial mechanism.

This is the first study to identify a role for the T6SS2 of *V. vulnificus* and these findings suggest that *V. vulnificus* employs both the T6SS1 and the T6SS2 *in vivo* for intra and inter-species killing. This may potentially have a significant impact on the composition of *in vivo* habitats, such as within shellfish.

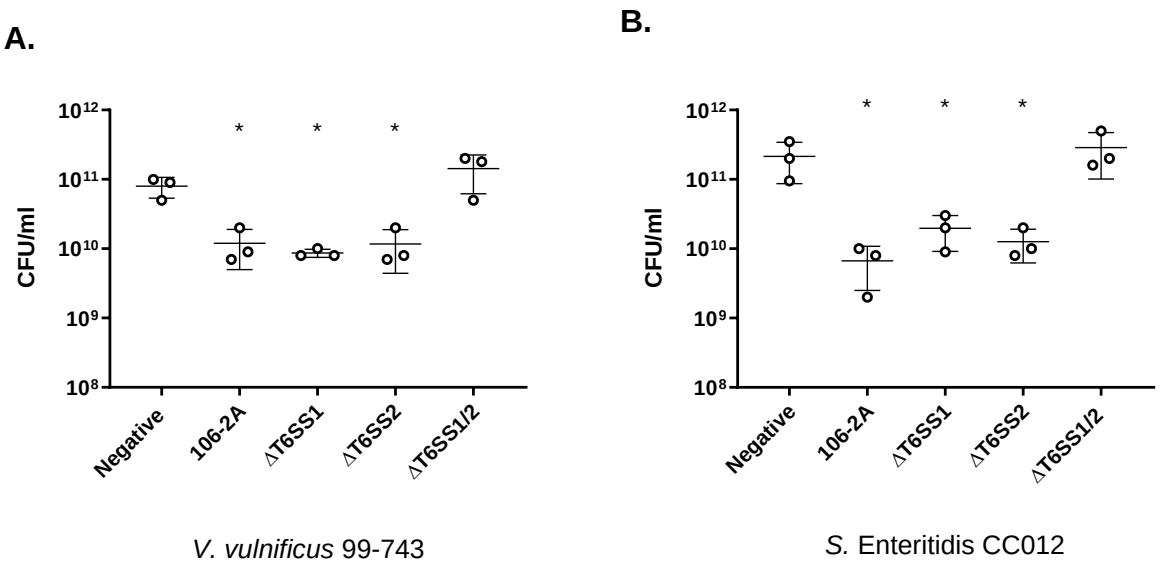

Figure 3.11: *V. vulnificus* and *S.* Enteritidis growth following co-culture with *V. vulnificus* attacker strains at 21 °C. *In vitro* co-culture assays with *V. vulnificus* 99-743 and *S. Enteritidis* CC012 (B) as prey were repeated with the inclusion of ΔT6SS1/2 as an attacking strain. Error bars represent the standard deviation, horizontal bars represent the mean (n = 3). Statistics individually comparing each strain to the negative control were performed using a one-way ANOVA with Dunnett's multiple corrections test, * $p < 0.05$.

3.9. *V. vulnificus* demonstrates no anti-eukaryotic killing activity against *Dictyostelium discoideum*

T6SSs have been shown to have a distinctly wide range of potential target organisms, depending on the activity of the host cell and the environments it commonly encounters [169,173,220,299]. Whilst the data presented so far in this chapter have confirmed the intra and inter-species killing activity of the T6SSs of *V. vulnificus* 106- 2A, it has yet to be investigated whether these secretion systems have anti-eukaryotic killing ability. Exploration into the anti-eukaryotic potential of the T6SSs of *V. vulnificus* had been previously carried out by Church *et al*., (2016) using the larvae of the greater wax moth, *Galleria mellonella*, as an infection model [172]. In this study, the more commonly utilised *Dictyostelium discoideum* model has been employed. *D. discoideum* is a free-living,

eukaryotic amoeba which primarily feeds on bacteria found within soil and decaying matter, such as *E. coli* [300]. *D. discoideum* predation of bacterial lawns results in the formation of phagocytic plaques where the lawn has been cleared by the amoeba, indicating killing. However, T6SS$^+$ anti-eukaryotic bacteria have been shown to target and kill *D. discoideum* before they can be predated, preventing the formation of plaques [169].

D. discoideum AX3 was ordered via DictyBase and upon arrival fruiting bodies were subcultured in HL5 media to generate axenic cultures [284]. Cultures were checked daily using a haemocytometer and subcultured into fresh media before concentrations reached higher than 10^6 cells/mL. Once *D. discoideum* cultures reached mid-log phase, they were resuspended in KK2 buffer and added to bacterial overnight cultures at a final concentration of 10^2 cells/mL. This concentration enables easy distinction of singular amoeba by the formation of a plaque in the bacterial lawn where *D. discoideum* had predated the plated bacteria. Suspensions were plated on SM agar and incubated at 21 °C for 3 days until visible plaque formation was observed.

Fig. 3.12 presents the results of *D. discoideum* plaque forming assays with *V. vulnificus* 106-2A, ΔT6SS1 and ΔT6SS2. *D. discoideum* was plated on *V. cholerae* V52 as a positive control as this bacteria has been previously shown to kill *D. discoideum* in a T6SS-dependent manner, resulting in no plaque formation [169]. Culture of *D. discoideum* on *V. vulnificus* 106-2A, ΔT6SS1 and ΔT6SS2 resulted in the formation of visible plaques, indicative of bacterial predation by the amoeba. To quantify this data, plaque diameters were measured to determine whether there were any empirical differences between strain predation by *D. discoideum* (Fig. 3.12B). This data confirmed that there was no significant difference between average plaque sizes formed through growth on either 106-2A, ΔT6SS1 or ΔT6SS2.

In conclusion, this data demonstrates that neither the T6SS1 nor the T6SS2 of *V. vulnificus* 106-2A can kill *D. discoideum.* This finding serves to further support the lack of anti-eukaryotic activity of *V. vulnificus* T6SS observed when previously put through a *G. mellonella* infection model. From here on, the project will focus purely on elucidating the antibacterial activity of the T6SS and its utilisation both *in vitro* and *in vivo*.

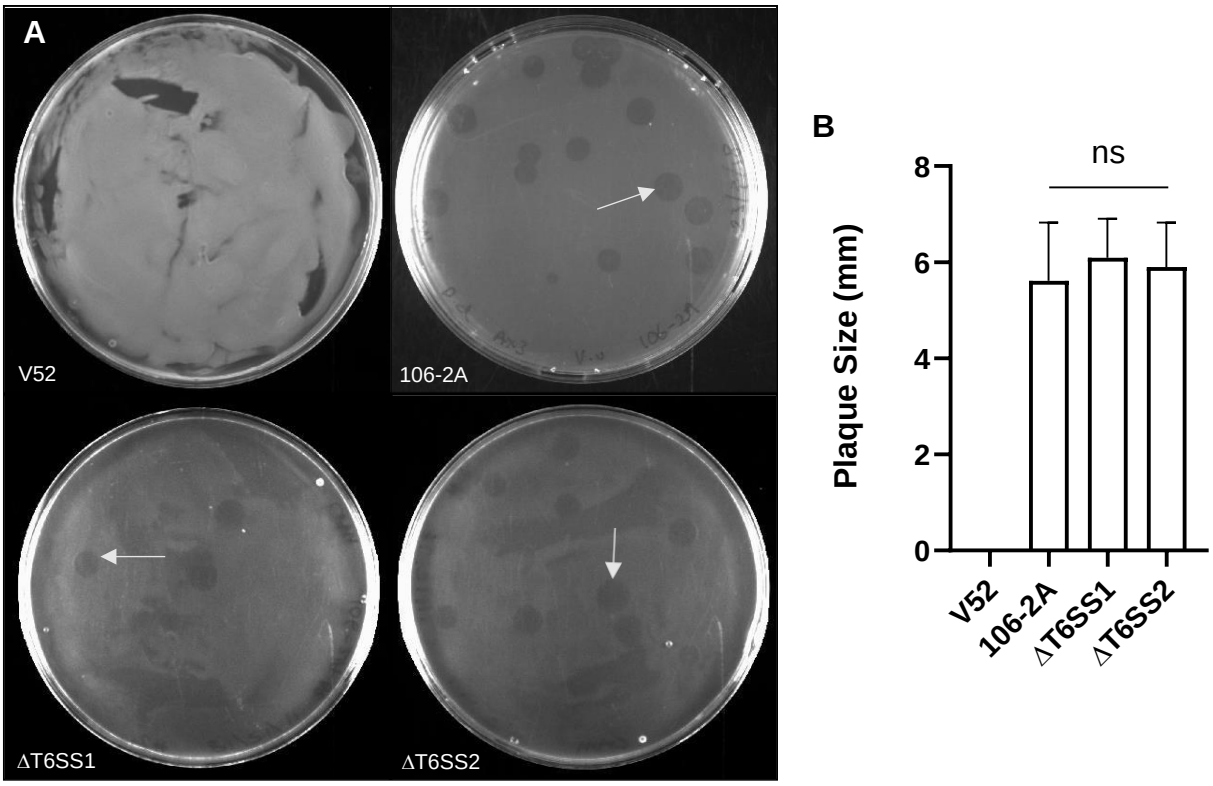

Figure 3.12: *D. discoideum* plaque-forming assays with *V. vulnificus* and *V. cholerae*. **(A)** Cultures of *V. vulnificus* 106-2A, ΔT6SS1, ΔT6SS2 and *V. cholerae* V52 were combined with *D. discoideum* and plated on SM agar at 21 °C until visible plaque formation occurred. No plaques can be seen on the V52 control; however, plaques can be observed on all plates containing *V. vulnificus* strains. Example plaques are marked with white arrows. **(B)** *D. discoideum* plaque diameters were measured following growth on *V. cholerae* V52, *V. vulnificus* 106-2A, ΔT6SS1 and ΔT6SS2 to quantify differences between strains. Statistics were performed using a one-way ANOVA with Tukey's corrections for multiple comparisons, ns – not significant.

Discussion

The T6SS is used by a diverse range of bacteria to target and kill susceptible prokaryotic and eukaryotic cells. To date, two T6SSs have been identified in *V. vulnificus*, namely the T6SS1 and the T6SS2. Previously, the T6SS1 was shown to have antibacterial activity at 30 °C *in vitro* [172]. This chapter aimed to further characterise the *in vitro* activity of the T6SS1 at an environmentally representative temperature to explore the role of the T6SS1 in *V. vulnificus* ecology. Initial co-culture assays at 30 °C demonstrated that *V. vulnificus* 106-2A could target and kill both *V. vulnificus* 99-743 and *S.* Enteritidis CC012 in a T6SS1-dependent manner. However, in an attempt to closer mimic relevant environmental conditions, co-culture assays were performed at 21 °C. This surprisingly led to the finding that both T6SS1 and T6SS2 had antibacterial activity at these temperature conditions. Generation of a *V. vulnificus* double T6SS mutant, ΔT6SS1/2, and co-culture with prey 99-743 and CC012 resulted in no significant reduction in recovered viable prey. This confirmed that the killing observed with 106-2A, ΔT6SS1 and ΔT6SS2 was T6SS-dependent and that both T6SSs were expressed and active.

T6SS expression is regulated at a transcriptional, post-transcriptional, and post-translational level to ensure tight control over T6SS activity [198]. Recognised methods of regulation include temperature, salinity, osmolarity, quorum sensing, nutrient limitation, and biofilm formation [178,180,301–306]. This study focused on the impact of temperature on T6SS activity *in vitro*. It is not yet entirely clear why the T6SS2 is active at 21 °C but remains inactive at 30 °C, whilst the T6SS1 is active at both temperature conditions. Previous investigations of T6SS expression in the closely related *V. cholerae* species, identified the cold-shock protein, CspV, as playing a role in T6SS thermoregulation [307]. Quantification of *hcp* expression at 25 °C showed a 14-fold

decrease in *hcp* transcripts in a Δ*cspV V. cholerae* strain compared to WT *V. cholerae*. Co-culture of Δ*cspV V. cholerae* with prey *E. coli* demonstrated a significant decrease in T6SS-mediated killing at 25 °C and 37 °C. Interestingly, *V. cholerae* T6SS genes were downregulated at 15 °C whereas CspV expression increased 60.9-fold. These results highlight a role for CspV in *V. cholerae* T6SS regulation. Whilst *V. vulnificus* has been shown to contain a CspV homologue, Csp5, no studies have yet explored the regulatory action of Csp5 on the T6SS. It is therefore possible that *V. vulnificus* Csp5 is similarly involved in T6SS regulation as CspV is in *V. cholerae.*

The data presented in this chapter demonstrates thermoregulation of *V. vulnificus* T6SS1 and T6SS2 under different temperature conditions. Differential T6SS regulation is common in microorganisms expressing multiple T6SSs. For example, *V. alginolyticus* expresses two T6SS, named VaT6SS1 and VaT6SS2 [308]. Competition assays between *V. alginolyticus* and *E. coli* at 30 °C showed a reduction of prey *E. coli* as a result of VaT6SS1 activity. An increase in salinity from 1 % to 3 % subsequently resulted in VaT6SS2-mediated killing. Closer investigation into the T6SS1 and T6SS2 operons of *V. vulnificus* may present some clues as to the differential regulation of these two systems. Whilst both operons encode all 13 essential genes as expected, the T6SS2 operon contains a number of accessory genes, *ppkA, pppA* and *fha*. In other T6SS$^+$ microorganisms such as *P. aeruginosa* and *S. marcescens* these genes have been shown to be components of a threonine phosphorylation pathway (TPP) [187,188]. Investigation of *P. aeruginosa* T6SS competition suggested that the TPP pathway plays a role in the 'tit-for-tat' T6SS response [299]. This occurs when a cell attacked by a neighbouring cell in a T6SS-dependent manner launches a counterattack in response. The presence of these genes within the T6SS2 cluster suggests that the T6SS2 may play a role in targeted counterattack against other T6SS$^+$

species. However, it should be noted that the counterattacking phenotype of *P. aeruginosa* is dependent upon the TaqQRST signal sensing complex, which is exclusive to *Pseudomonas*. More in-depth analysis of T6SS regulation and dynamics under a range of variable conditions, such as salinity, would be required to fully understand how these conditions impact T6SS activity.

Surprisingly, these results demonstrate that *V.* vulnificus 106-2A strain can target and kill strain 99-743 in a T6SS2-dependent manner. Typically, T6SS-expressing cells are protected from self-intoxication by T6SS effectors through expression of cognate immunity proteins [209]. This also serves to protect from sister-cells with identical T6SS effector profiles. Since both 106-2A and 99-743 are T6SS2$^+$ it was assumed that 106-2A would be unable to target 99-743 using the T6SS2, as 99-743 would be expressing the necessary immunity proteins. However, co-culture between 106-2A and 99-743 showed T6SS2-mediated killing of 99-743 by 106-2A. A possible explanation for this is that 106-2A expresses T6SS2 effector proteins to which 99-743 does not possess the cognate immunity protein. This has been previously shown in *V. cholerae,* where competing strains possessing dissimilar effector modules were deemed 'incompatible' [309].

There is evidence demonstrating that exchange of effector/immunity modules between T6SS$^+$ bacteria is not only common, but also offers a distinct competitive advantage. Adaption and evolution of bacterial T6SS warfare is largely driven by horizontal gene transfer (HGT), both vertically and horizontally [310]. Recombination analysis of all public *V. cholerae* strains showed that there were a subgroup of strains possessing runs of orphan immunity genes, to which the cognate effector was not present in the genome. Instead the strain encoded just one primary effector [311]. These authors suggested that this is due to homology-facilitated illegitimate recombination, where conserved regions within effectors enable illegitimate insertion of the sequence, including the associated

cognate immunity protein. Interestingly, it appears that addition of novel effectors is minimal, with established effectors being replaced by newly acquired effector genes. This results in a limited effector protein profile coupled with an extensive array of immunity proteins. Also, clearly observed in *V. alginolyticus,* orphan effector/immunity cassettes have been found neighbouring mobile genetic elements, promoting HGT with other bacteria [308]. Therefore, when competing with one another, strain compatibility is determined by the effector/immunity profile of the strains in question.

Given these findings, it is interesting that not all published data supports that T6SS toxin genotypes are sufficient for predicting strain compatibility. Speare *et al*., (2018) explored the co-culture of compatible and incompatible *V. fischeri* strains isolated from squid light-organ crypts [173]. Based on observed toxin alleles, 10 *V. fischeri* strains were separated into six predicted compatibility groups. However, the authors observed intra-group killing in groups 1 and 3, suggesting that toxin genotypes are not guaranteed indicators of strain compatibility.

These studies support the idea that 106-2A can target and kill 99-743 in a T6SS2-dependent manner due to expression of effector proteins to which 99-743 is susceptible. As all *V. vulnificus* are T6SS2$^+$, this suggested that all *V. vulnificus* strains possess a means of T6SS-mediated competition. Therefore, the distribution of effector/immunity modules is a primary factor in colonisation and population dynamics. Future work to explore this will involve the sequencing of a panel of *V. vulnificus* strains, both T6SS1$^+$/T6SS1$^-$, for comparative genomics and elucidation of effector distribution and interactions.

Having established the intra-species killing activity of the T6SS1 and the T6SS2, *V. vulnificus* was co-cultured with prey *S.* Enteritidis CC012 to explore the roles of the T6SSs in inter-species competition. Co-culture assays showed reductions in *S.*

Enteritidis prey following co-culture with attacker *V. vulnificus* at both 21 °C and 30 °C. This killing was confirmed as T6SS-dependent using a ΔT6SS1/2 double mutant. Interestingly, no reciprocal killing of *V. vulnificus* by *S.* Enteritidis was observed during competition, despite *S. enterica* serovars containing T6SSs [312]. This may be due to a 24 kb deletion in the *Salmonella* pathogenicity island, SPI-19. SPI-19 encodes a T6SS locus and has been identified in *S. enterica* serovars Dublin, Gallinarum, Agona, Weltervreden and Enteritidis [313]. Activity of SPI-19 T6SS has been demonstrated in *S.* Gallinarum, the causative agent of fowl typhoid, where the T6SS mediates survival within macrophages [314]. Conversely, the same *S.* Gallinarum strain demonstrated no antibacterial activity in co-culture assays. The deletion of a 24 kb region in this pathogenicity island suggests that the activity of this T6SS may be impaired if not entirely deleted. An alternative explanation is that the SPI-19 T6SS has no antibacterial activity. *S. enterica* serovars such as serovars Typhi and Typhimurium encode their T6SS on an alternative pathogenicity island, SPI-6, and have demonstrated both antibacterial and anti-eukaryotic T6SS activity [315,316]. It is therefore possible that SPI-19 is geared towards anti-eukaryotic activity, facilitating establishment and disease in a eukaryotic host, and consequently may be non-antibacterial.

Based on the data showing *V. vulnificus* T6SS antibacterial activity, it was hypothesised that *V. vulnificus* may employ the T6SS to target eukaryotic cells. T6SS-mediated anti-eukaryotic activity has been observed in a variety of microorganisms with extremely diverse target ranges. For example, the T6SS of *V. cholerae* has been shown to cross-link actin in phagocytic cells, immobilising the immune cell and protecting sister *V. cholerae* [317]. The role of actin cross-linking in *V. cholerae* infection was further established in a recent study showing *V. cholerae* clearance of *Aeromonas*

veronii from monocolonised Zebrafish intestines through T6SS-driven stimulation of intestinal movements, resulting in *A. veronii* ejection [318]. Anti-eukaryotic activity of *V. vulnificus* T6SSs has been previously explored in a *Galleria mellonella* model of infection [172]. The authors observed no anti-eukaryotic activity following infection of larvae at 37 °C. However, the data presented here has shown that neither T6SS is active under these conditions supportive of these previous observations. To test the potential anti-eukaryotic capabilities of *V. vulnificus* T6SSs, attacker strains were co-cultured with the social amoeba, *D. discoideum,* at 21 °C. Predation of *V. vulnificus* by *D. discoideum* suggested that *V. vulnificus* was unable to target *D. discoideum,* further supporting the hypothesis that neither T6SS was capable of targeting anti-eukaryotic activity under these temperature conditions. Recently, a study demonstrated for the first time an anti-fungal T6SS phenotype exhibited by *S. marcescens* Db10 [218]. Expression of two anti-fungal T6SS effectors, Tfe1 and Tfe2, was shown to induce cell death in *Candida* species through disruption of nutrient uptake, induction of autophagy, and loss of plasma membrane potential. Whilst *S. marcescens* Db10 has shown significant virulence against *Caenorhabditis elegans*, *G. mellonella* and *D. discoideum* eukaryotic models of infection, this killing showed no reduction when challenged with a non-functional T6SS mutant [175]. It is therefore possible that *V. vulnificus* T6SSs may demonstrate some form of anti-fungal activity despite the lack of virulence against *D. discoideum* shown in this study.

Conclusion

In conclusion, this chapter demonstrates that *V. vulnificus* 106-2A utilises the T6SS1 and T6SS2 to kill prey *V. vulnificus* and *S.* Enteritidis at 21 °C *in vitro*. This temperature is representative of typical environmental conditions and suggests that the T6SSs may play an important role in *V. vulnificus* ecology. Whilst T6SS1 activity has been demonstrated at 23 °C and 30 °C, this is the first study to show activity at 21 °C. Furthermore, this is the first time that any role has been identified for the T6SS2. The presence of a T6SS2 in every sequenced *V. vulnificus* strain indicates that the T6SS2 may be essential for inter-bacterial competition by T6SS1$^-$ strains.

The ability of strain 106-2A to target and kill strain 99-743 in a T6SS2-dependent manner suggests that these two strains contain different effector/immunity profiles. In this instance, 106-2A appears to encode T6SS2-associated effectors to which 99-743 lacks cognate immunity proteins, allowing T6SS2-mediated killing of prey 99-743. Therefore, distribution of effector/immunity genes between *V. vulnificus* strains may play an important role in the establishment and interactions in *in vivo* populations.

V. vulnificus anti-eukaryotic activity was explored through plaque forming assays with the phagocytic amoeba, *D. discoideum.* As antibacterial activity had been demonstrated by both T6SSs at 21 °C it was assessed whether *V. vulnificus* 106-2A could also target eukaryotic cells under these conditions. However, plaques indicative of predation of *V. vulnificus* were observed for 106-2A, ΔT6SS1 and ΔT6SS2, confirming no anti-eukaryotic activity at 21 °C against *D. discoideum*. Future work will explore the reproduction of these *in vitro* killing assays in a representative *in vivo* model.

Chapter Four

Development of a natural marine snow model for bacterial incorporation

Introduction and aims

In this study it has been successfully demonstrated that *V. vulnificus* 106-2A T6SSs can kill *V. vulnificus* and *S.* Enteritidis *in vitro* at 21 °C. Thus, it was sought to explore whether this *in vitro* killing was representative of *in vivo* interactions through the development of an oyster model of infection. Being bioaccumulators, oysters facilitate uptake and concentration of microorganisms from the surrounding water column within their stomachs, presenting the ideal model for studying bacterial interactions *in vivo* [319]. Furthermore, oyster consumption is a common source of *Vibrio* infection in humans, demonstrating that this model is representative of environmental *Vibrio* interactions [320,321]. To undertake competition assays *in vivo,* sufficient uptake of *V. vulnificus* by oysters for contact-dependent killing between attacker and prey bacteria is required. Due to the filter-feeding mechanism of oysters, particles too large are rejected as pseudofaeces whereas those too small pass through the gills without being retained [247,249,322]. Planktonic *V. vulnificus* fall below the optimal size range for ingestion and therefore uptake is sub-optimal [249].

Previous studies have shown that bacterial cultures can be incorporated into marine snow in order to promote ingestion by oysters [249,268,322]. Marine snow are microcosms composed of aggregated particulate matter into which bacteria can incorporate. Being larger structures, marine snow is far more conducive to retention by filter-feeders, therefore incorporation of attacker and prey bacteria into marine snow to facilitate robust, high-level uptake of bacteria was investigated.

Results

4.1. Developing a natural marine snow model

Marine snow consists of a diverse range of matter, including dust, sand, microorganisms, diatoms, algae, protists, faecal matter and inorganics [260,261,267,268,323,324]. These components are brought together at random by Brownian motion, differential settling and shear forces, resulting in particle collision and formation of larger aggregates [260,267,276]. There has been a collection of studies that have attempted to generate marine snow in a laboratory environment. Froelich *et al.,* (2013) describe the optimisation of a method initially put forward by Shanks and Edmundson (1989) and adapted by Ward and Kach (2009) [322,324]. This technique involved supplementing seawater with hyaluronic acid, a ubiquitous carbohydrate polymer commonly found in bacterial extracellular matrices, to promote particle adhesion and aggregation. The method explored here was rolling of suspensions overnight to facilitate aggregation of particles into larger marine snow microcosms as described in the methods (section 2.3.1). Marine snow formed using seawater as a substrate will be referred to as natural marine snow (NMS) for the remainder of the study. Seawater was collected from Dawlish (Devon, UK) to provide the substrate for aggregate formation. Care was taken to ensure that seawater was collected from the same location at the same point in the tide to ensure consistency. A representative micrograph of laboratory-generated NMS is shown in Fig. 4.1. Sizes of formed aggregates were typically < 1 cm in diameter; however, this was shown to vary between seawater samples collected, with some samples not generating any aggregates > 0.1 cm in diameter.

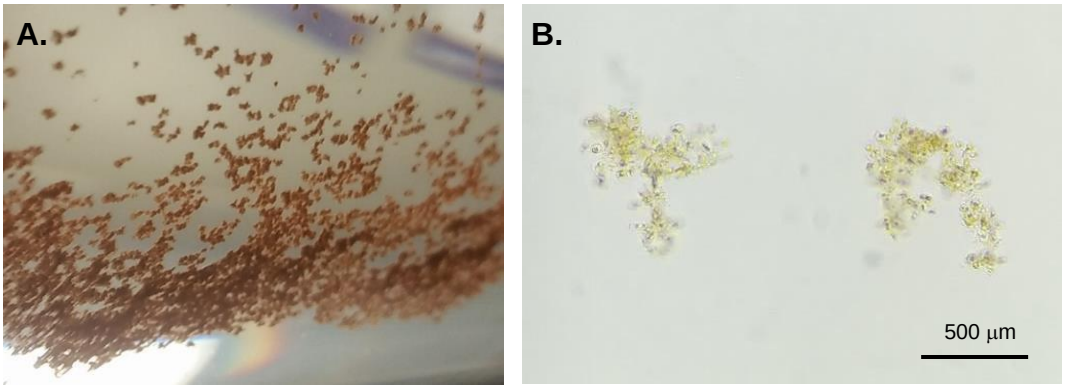

Figure 4.1: Natural marine snow generated using seawater as a substrate. Seawater from Dawlish was supplemented with hyaluronic acid and rolled overnight to promote particle aggregation and NMS formation. **(A)** Visible NMS microcosms. **(B)** NMS visualised using a light microscope. Magnification × 400.

4.2. Variation in natural marine snow formation utilising different seawater samples

NMS formation was typically consistent when using the same batch of seawater for aggregate generation. However, there was notable variation in size and number of aggregates using seawater collected on different days. To quantify this variation, the difference in aggregate mass formed using different seawater samples was analysed. Seawater samples collected over a period of five days were used to generate NMS. NMS was isolated via filtration and the wet weight recorded. Results were recorded as milligrams of wet aggregate mass.

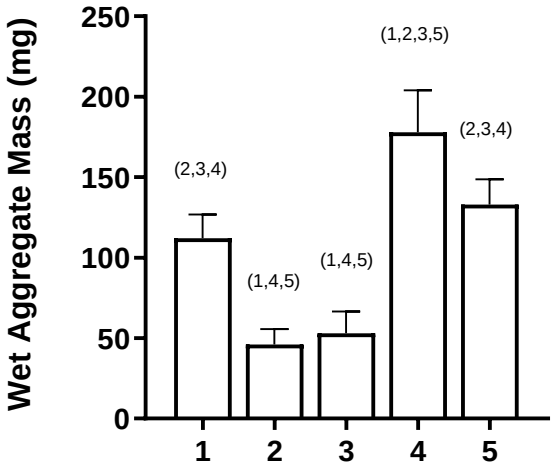

Figure 4.2: Variability in mass of natural marine snow produced using seawater as a substrate. NMS was generated from five individually collected seawater samples and aggregate mass determined (n = 3). Horizontal bars represent the mean, error bars represent the standard deviation. Statistics comparing every strain individually to every other strain were performed using a one-way ANOVA with Tukey's corrections for multiple comparisons. The numbers above the bars indicate the samples to which that sample is significantly different ($p < 0.05$).

As can be seen in Fig. 4.2, wet aggregate mass of samples ranged from 50 – 200 mg. It was observed that each sample had significantly different mass to at least three other samples, with sample 4 significantly different to every other sample tested ($p < 0.05$). This variation in total aggregate mass between samples is likely due to compositional differences. External elements such as sea-surface conditions, weather, temperature, precipitation and wave volume/frequency all play a role in seawater composition at the time and point of collection [325]. The use of seawater to generate NMS therefore presented a challenge in terms of standardisation and comparison of results obtained using different seawater samples. For the remainder of this chapter seawater from sample 4 was utilised as this sample resulted in the greatest aggregate mass and should therefore facilitate the highest bacterial incorporation.

4.3. *V. vulnificus* enumeration from marine snow on TCBS

As previously discussed in Chapter 3, *Vibrio* enumeration on TCBS agar is inaccurate and results in significantly different CFU/mL values relative to enumeration on LB agar. However, a method of isolating *V. vulnificus* from NMS whilst allowing distinction between attacker and prey strains was required. Despite having developed *V. vulnificus* strains with antibiotic resistances in the previous chapter, future oyster model work would not allow for plasmid selection throughout the assay, potentially promoting plasmid loss prior to attacker and prey strain enumeration. Therefore, a replica-plating method was assessed, in which *V. vulnificus* cultures were plated on LB to facilitate accurate growth of bacteria, before being replica-plated onto TCBS for

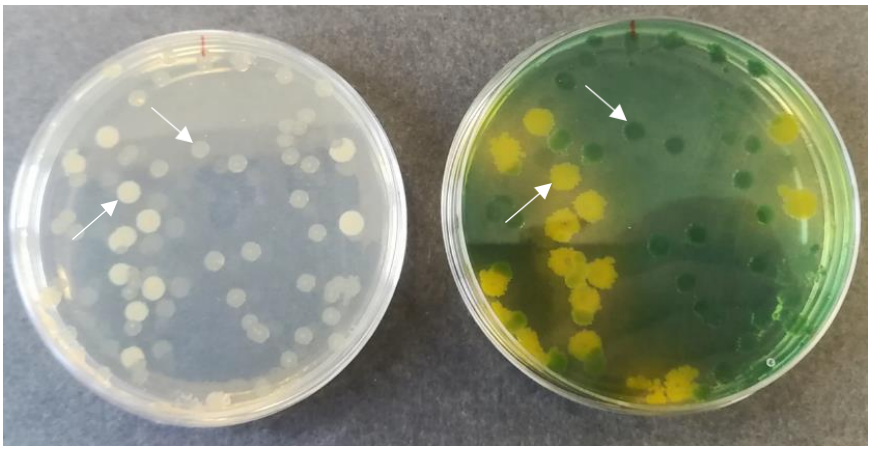

Figure 4.3: Replica plating *V. vulnificus* onto TCBS agar from LB agar. *V. vulnificus* 106-2A and 99-743 bacterial cultures were combined, spread onto LB agar, and incubated overnight (left plate). The following day, colonies were replica-plated onto TCBS agar (right plate) to facilitate colour-based enumeration as 106-2A grows green on TCBS, whereas 99-743 grows yellow. Matching colonies have been marked with arrows to highlight the difference between the two *V. vulnificus* strains on each media.

colour-based enumeration of attacker and prey strains. Fig. 4.3 demonstrates an example of mixed overnight cultures of *V. vulnificus* 106-2A (green) and 99-743 (yellow) plated on LB and then replica-plated onto TCBS. As can be seen, colonies that have grown on LB have transferred to TCBS and can now be differentiated from one another by colony colour.

4.4. Incorporation of *V. vulnificus* into natural marine snow

To test the incorporation efficiency of *V. vulnificus* into NMS, rolling tubes containing 1 L seawater supplemented with hyaluronic acid were inoculated with *V. vulnificus* to final concentrations of 10^3, 10^5, and 10^7 CFU/mL. Tubes were rolled for 24 hours at 21 °C and aggregates isolated by filtration for plate-enumeration the following day. Filtration was performed using a Buchner funnel with 3 μm pore filter paper (Whatman). *V. vulnificus* measures ~ 2 μm and therefore any planktonic *V. vulnificus* cells not associated with NMS should pass through the filter. Conversely, *V. vulnificus* cells incorporated into the larger NMS aggregates would be unable to pass through the pores and be retained for enumeration.

Despite successful incorporation and recovery of *V. vulnificus* from every sample, the total number of bacteria incorporated appeared surprisingly low (Fig. 4.4). NMS inoculated to a final *V. vulnificus* concentration of 10^3 CFU/mL resulted in $1 – 4 \times 10^3$ CFU/g NMS. As expected, NMS inoculated with higher concentrations of *V. vulnificus* resulted in greater bacterial incorporation, with 10^5 CFU/mL resulting in $3 \times 10^3 – 2 \times 10^4$ CFU/g NMS and 10^7 CFU/mL resulting in $5 \times 10^3 – 3 \times 10^4$ CFU/g NMS (Figs. 4.4B & 4.4C). However, given that there was a 10,000-fold increase in *V. vulnificus* inoculation concentrations between 10^3 CFU/mL and 10^7 CFU/mL, a significantly

greater difference in incorporation than a 10-fold increase was expected.

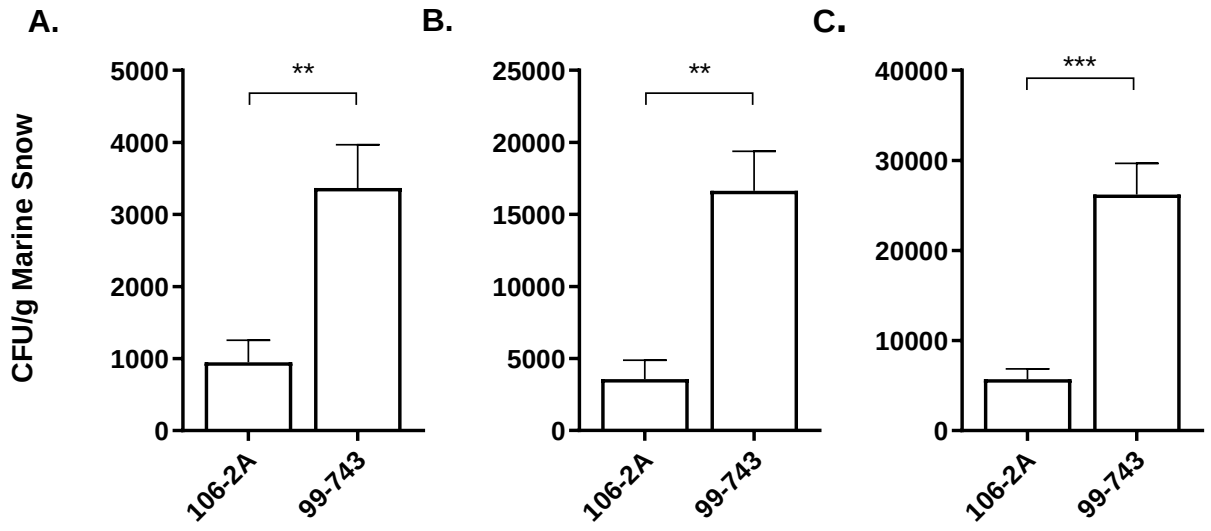

Figure 4.4: Incorporation of *V. vulnificus* into natural marine snow. *V. vulnificus* 106-2A and 99-743 were incorporated into NMS formed using seawater as a substrate. **(A)** 10^3 CFU/mL **(B)** 10^5 CFU/mL **(C)** 10^7 CFU/mL. Viable *V. vulnificus* recovered from aggregates was enumerated in triplicate for each sample. Error bars represent the standard deviation (n = 3). Statistics comparing the aggregation efficiency of 99-743 and 106-2A were performed using an unpaired, two-tailed t-test, ** $p < 0.01$, *** $p < 0.001$.

Interestingly, 99-743 demonstrated significantly greater incorporation into NMS than 106-2A, despite equal concentrations of each being added under identical conditions. It is worthy to note that the two strains were of different genotypes, with 99-743 being an E-type (environmental) and 106-2A being a C-type (clinical), according to a classification system described by Warner and Oliver, (1999) [42]. Studies demonstrate that strain genotype impacts integration into NMS, with E-type strains showing significantly greater inclusion [249]. The results here also show that E-type 99-743 incorporates into NMS significantly more effectively than C-type 106-2A and that this is consistent following inoculation at a range of concentrations. As the aim was to

assess NMS as a model for *Vibrio* uptake by oysters, these results present two obstacles: low-level *V. vulnificus* incorporation, and differences in incorporation between genotypes.

4.5. Co-incorporation of E-type and C-type *V. vulnificus* into natural marine snow

Given the greater individual incorporation of E-type 99-743 into NMS than C-type 106-2A, it was investigated whether the presence of an E-type strain would impact integration of a C-type strain into NMS during co-incorporation. Significantly greater incorporation of E-type *V. vulnificus* strains into NMS would present a potential explanation for the higher presence of E-type *V. vulnificus* in oysters, compared to C-type [33]. NMS rolling tubes containing 1 L seawater supplemented with hyaluronic acid were inoculated with both *V. vulnificus* 106-2A and 99-743 to final concentrations of 10^7 CFU/mL each and rolled for 24 hours at 21 °C (Fig. 4.5).

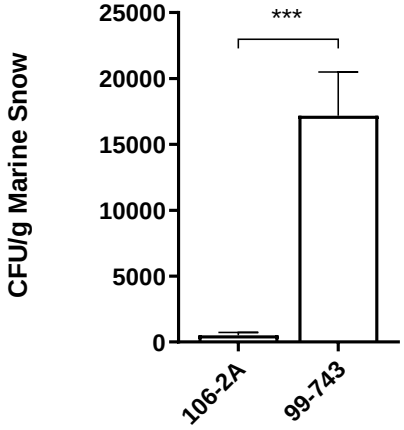

Figure 4.5: Co-incorporation of *V. vulnificus* into natural marine snow. *V. vulnificus* 106-2A and 99-743 were added to NMS rolling tubes at a 1:1 ratio (10^7 CFU/mL each). Generated NMS was filtered, and incorporated bacteria enumerated (n = 3). Error bars represent the standard deviation. Statistics were performed using an unpaired, two-tailed t-test, *** $p < 0.001$.

106-2A integration into NMS was dramatically reduced compared to single strain incorporation experiments previously performed. When incorporated into NMS individually, 106-2A recovery was < 10^4 CFU/g NMS. However, co-incorporation with E-type 99-743, reduced this to < 10^3 CFU/g NMS. 99-743 still demonstrated significantly greater integration than 106-2A, with recovery of ≤ 2×10^4 CFU/g NMS ($p < 0.001$). These findings may explain the discrepancy in numbers between E- and C-type *V. vulnificus* in oysters.

4.6. Natural microorganisms outcompete *V. vulnificus* for incorporation into natural marine snow

The ability to generate NMS and show incorporation of two *V. vulnificus* strains has been demonstrated in this study. However, incorporation rates were extremely low compared to the inocula. This study theorised that this low-level incorporation may have been the result of using seawater as a substrate for aggregate formation. Seawater collected from Dawlish was inherently variable in terms of composition, with respect to particulate matter and bacterial species present within it. Previous studies have shown that seawater has been shown to contain microorganisms at concentrations > 10^5 CFU/mL [326]. Consequently, it is very likely that there is competition for incorporation from a diverse range of marine microorganisms. To explore the extent that natural bacteria were incorporating into NMS, uninoculated NMS was generated and enumerated on LB and TCBS agar.

Fig. 4.6 shows enumeration of natural bacteria incorporated into NMS generated using five separately collected seawater samples. For every sample recovery of natural bacteria was ≥ 10^5 CFU/g NMS, with sample 1 containing > 10^7 CFU/g NMS, significantly greater than every other sample (p < 0.001). Enumeration on TCBS showed that whilst samples 2 and 5 contained no detectable *Vibrio* species, samples 1, 3 and 4 all contained 10^2 – 10^3 CFU/g NMS, although the exact species were unknown. This data demonstrates that the presence of incorporated natural *Vibrios* would impact NMS colonisation by exogenous *V. vulnificus* and confound enumeration of bacteria selected for study. Moreover, the data here shows that this approach was unable to achieve incorporation of exogenous *V. vulnificus* into oysters at

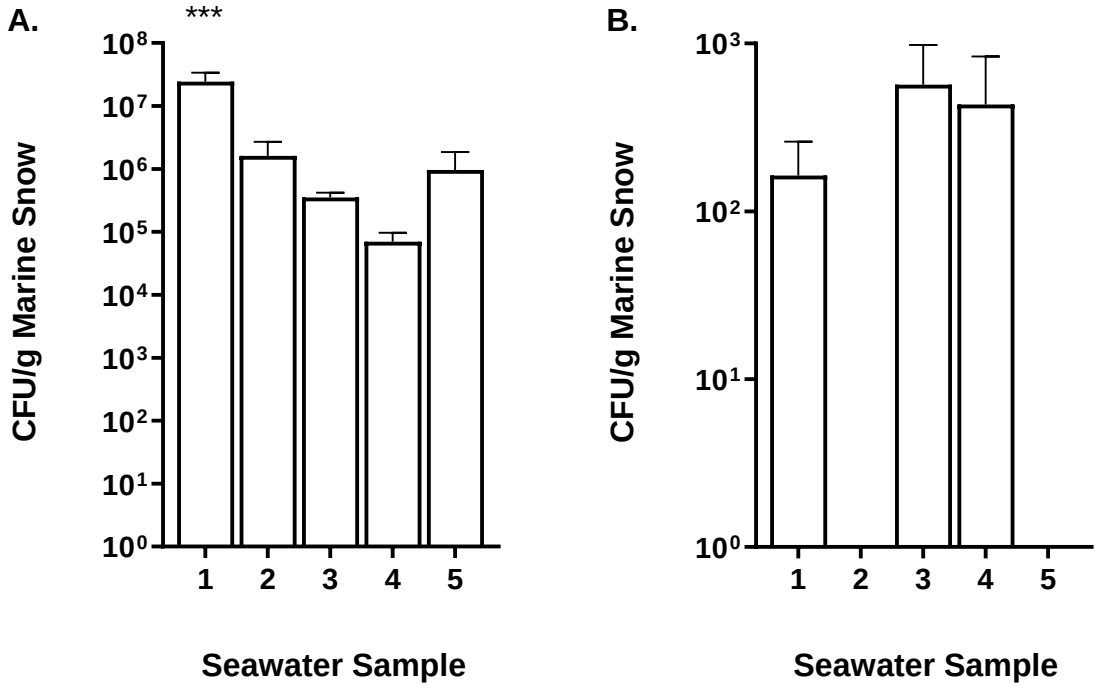

Figure 4.6: Enumeration of natural bacteria and *Vibrio* species from natural marine snow. Laboratory-generated NMS with no added bacteria was enumerated on LB and TCBS agar to assess concentrations of naturally occurring microorganisms per gram of NMS. **(A)** Enumeration on LB agar. **(B)** Enumeration on TCBS agar. Five individually collected seawater samples were assessed (n = 3). Error bars represent the standard deviation. Statistics comparing every strain to every other strain were performed using a one-way ANOVA with Tukey's corrections for multiple comparisons, *** p < 0.001.

concentrations significantly higher than the concentrations at which natural *Vibrio* species were already present.

In conclusion, whilst the generation of NMS using seawater presented numerous obstacles to future *in vivo* assays. These included inconsistent aggregation, variation in aggregate formation between seawater samples, competition for incorporation with natural bacteria, genotype-dependent variation in *V. vulnificus* incorporation and disparate incorporation of *V. vulnificus* between seawater samples.

Discussion

This chapter explores *V. vulnificus* incorporation into an NMS model for future uptake by oysters. Seawater collected from Dawlish was shown to act as a suitable substrate for formation of aggregates into which *V. vulnificus* incorporation was demonstrated. However, it was discovered that *V. vulnificus* incorporation was extremely low-level, being largely outnumbered by natural bacteria present in the seawater. Combined with the compositional variability of seawater resulting in significantly different aggregate formation between seawater samples, NMS was deemed ineffective for the purpose of this study.

Enumeration of natural bacteria from NMS demonstrated significantly greater incorporation than exogenous *V. vulnificus* strains. NMS is a naturally forming microenvironment and it is therefore likely that the natural bacteria incorporated into NMS were already adhered to the particles within the seawater before NMS generation. Kiørbe *et al*., (2003) examined the dynamics of microbial communities on marine aggregates and found that bacteria already attached to NMS demonstrate

greatly increased growth and reduced detachment rates compared to exogenous bacteria [268]. The presence of the detritosphere, a microscopic nutrient sphere surrounding aggregates, promotes growth and survival of incorporated microorganisms, generating pressure to maintain incorporation [269]. The use of seawater will have resulted in natural bacteria already having been in contact with the substrate matter, resulting in colonisation and inhibiting *V. vulnificus* incorporation. Bochdansky *et al*., (2017) explored the distribution of prokaryotic and eukaryotic microbes on marine snow recovered from the bathyal zone (1,000 – 3,000 m below the surface). The study found that, whilst prokaryotes numerically exceeded eukaryotes, the biomass of eukaryotic organisms was greater, with fungi and labyrinthulomycetes (marine protists) dominating [327]. There is therefore a significant number of a diverse microorganisms competing with exogenous *V. vulnificus* for incorporation into NMS, resulting in extremely low-level incorporation of attacker and prey strains. The variability of seawater is also affected by seasonal changes, with different bacteria demonstrating prevalence throughout the year. This fluctuation is particularly apparent with *Vibrio* species, who have demonstrated observable association with SST through spiking CFU counts in summer and falling to often undetectable levels in winter [4,48,57]. Consequently, an NMS model employing seawater as a substrate would suffer further inconsistency over time as a result of changing bacterial populations within collected seawater.

These findings help explain the results put forth by Warner and Oliver, (2008) highlighting the elevated presence of E-type *V. vulnificus* compared to C-type strains in oysters [33]. Despite being present at similar concentrations in the surrounding water (E-type – 46.9 %, C-type – 53.1 %), E-type *V. vulnificus* outnumbered their C-type counterparts 84.4 % to 15.6 % when isolated from oyster tissues. The significant

incorporation advantage for E-type *V. vulnificus* into NMS suggests that E-type *V. vulnificus* are successfully outcompeting C-type *V. vulnificus* strains *in situ* and are consequently present in much higher concentrations in oysters. This offers a potential explanation for the disparity between E-type and C-type presence in oysters, and the low clinical occurrence observed despite the organism's ubiquity. Reduced C-type presence in oysters as a result of E-type competition would serve to result in reduced human exposure to pathogenic strains.

Conclusions

This study has explored the use of seawater to generate an NMS model for the high-level uptake of bacteria by oysters. Incorporation studies showed that despite inoculation concentration to a final concentration of 10^7 CFU/mL, incorporation was < 10^5 CFU/g NMS. NMS presents a starting point for the development of a marine snow model to facilitate the high-level uptake of bacteria by oysters. However, the model presents too many challenges to be considered a viable model as it stands. Future work will look at developing a more defined model which address the issues of aggregate consistency, low incorporation levels, and presence of natural bacteria.

Chapter Five

Development of an artificial marine snow model for bacterial incorporation

Introduction and aims

The previous chapter confirmed that whilst *V. vulnificus* incorporation into NMS is possible, due to presence of natural microorganisms and variation in seawater composition the method is ineffective. Therefore, it was decided to explore the possibility of generating a defined 'artificial' marine snow (AMS) using diatom monocultures as a substrate. Diatoms are common components of natural marine aggregates and a common oyster food. Two diatom species, *Thalassiosira pseudonana* CCMP 1335 and *Phaeodactylum tricornutum* UTEX 646, were investigated to determine whether they were a suitable substrate for AMS generation. It was hypothesised that using defined diatoms would facilitate precise control over the volume of substrate (diatoms/mL) as diatom cultures could be enumerated prior to aggregation to ensure concentration consistency. The use of laboratory-grown diatom cultures would also enable greater control over the sterility of the substrate, removing the issue of contaminating natural microorganisms. Thus, the aim was to generate a reproducible AMS model into which *V. vulnificus* and *S.* Enteritidis could be reliably incorporated for future uptake by oysters.

Results

5.1. *V. vulnificus* incorporation into diatom-based artificial marine snow

AMS was generated using the same methodology as previously described for NMS, with the exception of using 1 L artificial seawater supplemented with diatoms to a final concentration of 10^6 cells/mL in place of seawater (methods, section 2.3.1). Diatom suspensions formed visible aggregates after overnight incubation, a representative micrograph of which can be seen in Fig. 5.1.

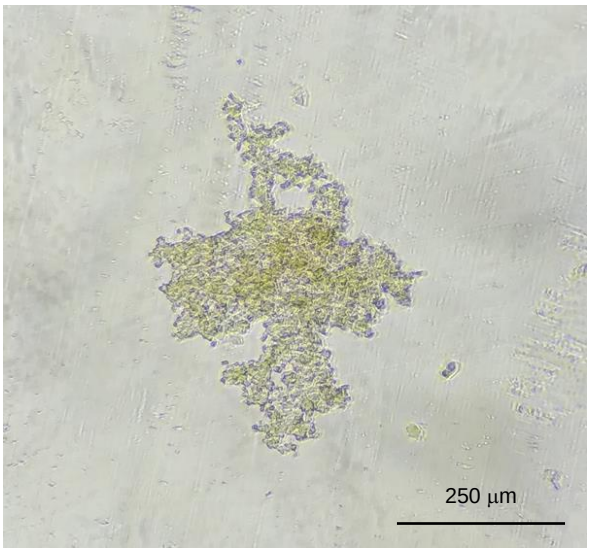

Figure 5.1: Light micrograph of *T. pseudonana* artificial marine snow. Diatom AMS was generated by incubating 1 L suspensions consisting of artificial seawater, 10^6 cells/mL diatom culture, and hyaluronic acid at 16 rpm for 24 hours. Magnification × 100.

Bacteria-free negative controls were established for *T. pseudonana* and *P. tricornutum* and plated on LB agar. A lack of colonies recovered from either negative control confirmed the sterility of the AMS model. Once aggregation of *T. pseudonana* and *P. tricornutum* had been assessed, diatom AMS suspensions were supplemented with bacterial cultures to a final concentration of 10^5 CFU/mL. Remarkably, *V. vulnificus* incorporation into AMS was extremely successful (Fig. 5.2). 99-743 demonstrated > 10^8 CFU/g AMS, 10,000-fold greater than 99-743 incorporation into NMS (Fig. 4.4). Similarly, 106-2A demonstrated consistently > 10^7 CFU/g AMS, 1,000-fold greater than incorporation into NMS. As observed with NMS, there was a significant difference between incorporation of 99-743 and 106-2A into AMS. This difference was observed with both *T. pseudonana* and *P. tricornutum* aggregates, and in each instance 99-743 demonstrated a 10-fold greater integration than 106-2A (*P. tricornutum* $p < 0.05$, *T. pseudonana* $p < 0.01$).

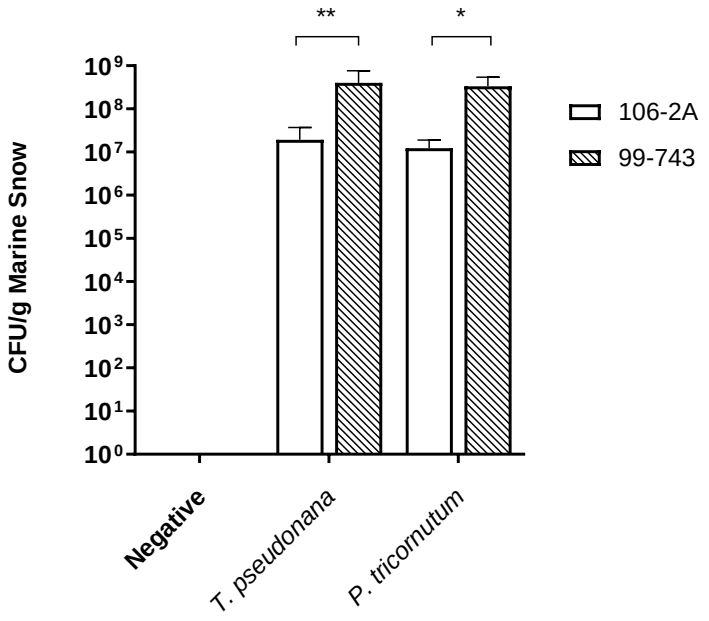

Figure 5.2: Incorporation of *V. vulnificus* into diatom-based artificial marine snow. *V. vulnificus* 106-2A and 99-743 were incorporated into AMS generated using cultures of two separate diatom species, *T. pseudonana* CCMP 1135 and *P. tricornutum* UTEX 646 for 24 hours at 21 °C. Bacteria-free negative controls were established and enumerated in parallel on LB agar. Error bars represent the standard deviation (n = 3). Statistics were performed using t-tests, * $p < 0.05$, ** $p < 0.01$.

Despite the success of this diatom based AMS model, diatom growth rate was a major limitation. Due to the high concentrations of diatom cells required, laboratory-grown cultures typically took 14 days to reach a suitable density in sufficient volume for extensive AMS generation and testing. It was therefore decided to continue using diatoms as an AMS substrate but in a more time-effective and easily manageable manner.

5.2. *V. vulnificus* incorporation into Reef Phytoplankton-based artificial marine snow

To replace laboratory-grown diatom cultures, a highly concentrated commercial phytoplankton stock was procured. Reef Phytoplankton (RP) is a concentrated (5×10^8 cells/mL) blend of five phytoplankton genera, *Isochrysis, Pavlova, Tetraselmis, Thalassiosira* and *Nannochloropsis*. RP was added to marine snow tubes in place of laboratory-grown diatom cultures and AMS generated as previously described. Curiously, no visible AMS formation was recorded following overnight aggregation of RP. A possible explanation for this was the non-viability of the phytoplankton cells contained within the phytoplankton blend (as stated by the manufacturer). Being non-viable, these phytoplankton retain their structure and nutritional content, but no longer grow and replicate. It was theorised that, being non-viable, these cells may lack some component for promoting aggregation. However, this study hypothesised that formation of large aggregates may not be entirely essential for facilitating uptake by oysters. As long as exogenous bacteria can adhere to phytoplankton cells, they will be within the optimal size range for ingestion by oysters. AMS was therefore generated as previously described, with the use of RP in place of a live diatom culture.

Fig. 5.3 shows incorporation of *V. vulnificus* 106-2A and 99-743 into RP-based AMS. Bacteria-free controls demonstrated incorporation of natural bacteria at ~ 10^4 CFU/g AMS, however absence of bacterial colonies on TCBS confirmed that no natural bacteria were *Vibrio* species. 106-2A was consistently recovered from AMS at concentrations > 10^7 CFU/g AMS, and 99-743 at concentrations > 10^8 CFU/g AMS. 99-743 demonstrated significantly greater integration than 106-2A, with bacterial loads consistently 10-fold higher ($p < 0.01$). Reassuringly, RP was equally successful as laboratory-cultured diatoms for bacterial incorporation. It is necessary to note that

negative controls plated on LB agar indicated presence of natural bacteria at 10^3 – 10^4 CFU/g AMS. However, the extremely high-level uptake of 106-2A and 99-743 into AMS demonstrated that, despite the presence of natural microorganisms, exogenous *V. vulnificus* could be incorporated into RP-based AMS in extremely high concentrations.

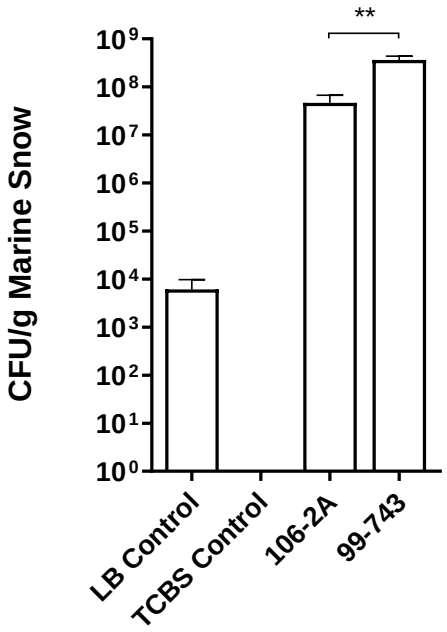

Figure 5.3: Incorporation of *V. vulnificus* into Reef Phytoplankton-based artificial marine snow. *V. vulnificus* 106-2A and 99-743 were incorporated into AMS generated using RP as a substrate for 24 hours at 21 °C. Suspensions were supplemented with 10^5 CFU/mL of either 106-2A or 99-743. Bacteria-free controls were established and plated on LB and TCBS agar. Error bars represent the standard deviation (n = 3). Statistics were performed using an ordinary one-way ANOVA with Tukey's corrections for multiple comparisons, ** $p < 0.01$.

5.3. Scanning-electron microscopy visualisation of *V. vulnificus* incorporated into Reef Phytoplankton-based artificial marine snow

To visually confirm incorporation of *V. vulnificus* into AMS, inoculated aggregates were subjected to scanning electron microscopy (SEM). Processed samples consisted of 106-2A in AMS, 99-743 in AMS, a bacteria-free AMS control and an adhesion control. The purpose of the adhesion control was to confirm that bacteria visually observed incorporated into AMS were not simply unincorporated cells that had settled on AMS aggregates during sample processing for SEM, giving the appearance of integration. Adhesion control AMS was supplemented with *V. vulnificus* immediately prior to sampling, preventing sufficient time for incorporation into AMS to occur. Observation of bacteria in the adhesion control would therefore indicate planktonic bacteria that had been retained during sample processing and that this would have to be taken into account for all other samples.

AMS samples were processed according to the methods, section 2.9, and visualised using a JEOL JSM 6390 LV scanning electron microscope operated at 5 kV. Figs. 5.4 and 5.5 show SEM micrographs of *V. vulnificus* 99-743 and 106-2A incorporation into AMS, respectively. *V. vulnificus* cells have been false-coloured in Photoshop for ease of identification; 99-743 – blue, 106-2A – pink (unprocessed images can be observed in Appendix 10 and 11). Figs. 5.4A and 5.5A show examples of some of the phytoplankton species contained within RP, including *Tetraselmis, Nannochloropsis* and *Thalassiosira*. Figs. 5.4B and 5.5B show representative micrographs of 99-743 and 106-2A adhesion controls. The absence of bacteria present in these samples confirmed that planktonic bacteria were not settling on AMS during sample processing and therefore all bacteria observed in other samples were legitimately incorporated into phytoplankton aggregates.

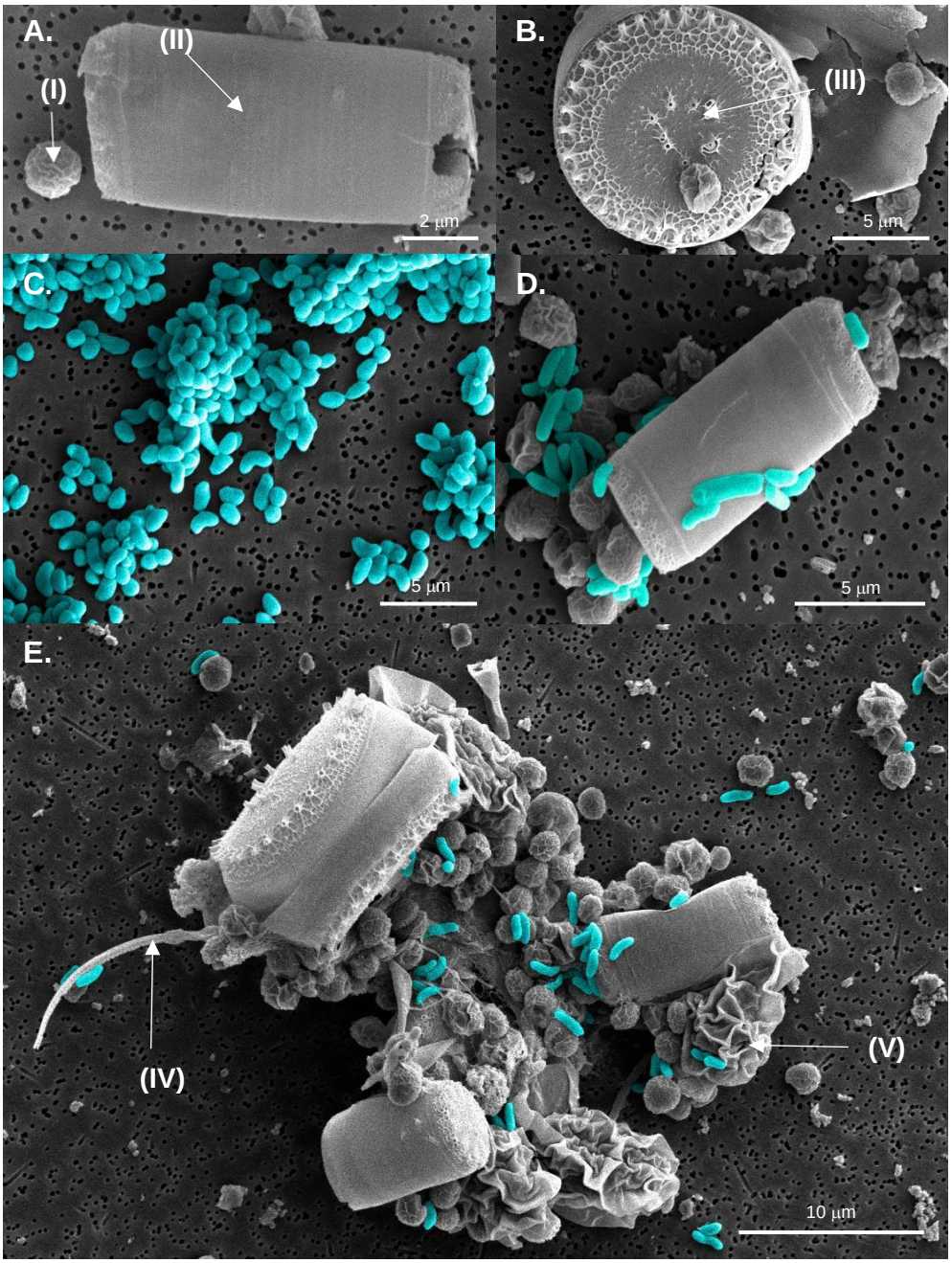

Figure 5.4: Scanning electron microscopy visualisation of *V. vulnificus* 99-743 incorporated into Reef Phytoplankton-based artificial marine snow. *V. vulnificus* 99-743 was incorporated into RP-based AMS and processed for SEM visualisation. **(A)** RP-only negative control, magnification × 9,000. **(B)** Adhesion control, magnification × 7,000. **(C)** 99-743 only control, magnification × 7,000. **(D & E)** 99-743 incorporated into AMS, magnification × 9,000 and × 3,000 respectively. (I) *Nannochloropsis,* (II) *Thalassiosira,* (III) *T. weissfloggi,* (IV) *Isochrysis* (flagella), (V) unknown.

Figs. 5.4D/E and 5.5D/E illustrate successful incorporation of 99-743 and 106-2A into AMS. Initially, there were no AMS aggregates visible with the naked eye following overnight aggregation of RP, which was theorised to be due to phytoplankton non-viability. However, these images confirm that aggregation is occurring, but merely on a far smaller scale than was observed with viable diatom cultures. Whilst AMS aggregates using laboratory-grown diatom cultures were up to 250 μm in diameter, RP-based AMS resulted in the formation of far smaller aggregates, ~ 10 – 30 μm in diameter.

These SEM images confirm successful *V. vulnificus* incorporation into AMS. However, there were numerous unidentified constituents within samples alongside the expected phytoplankton species (all indicated with arrows). I – IV are *Nannochloropsis, Thalassiosira, Tetraselmis,* and *Isochrysis*, respectively, all of which were expected to be identified as they are listed amongst the five phytoplankton species contained within RP. However, V is unidentified and does not appear to be any of the listed phytoplankton species.

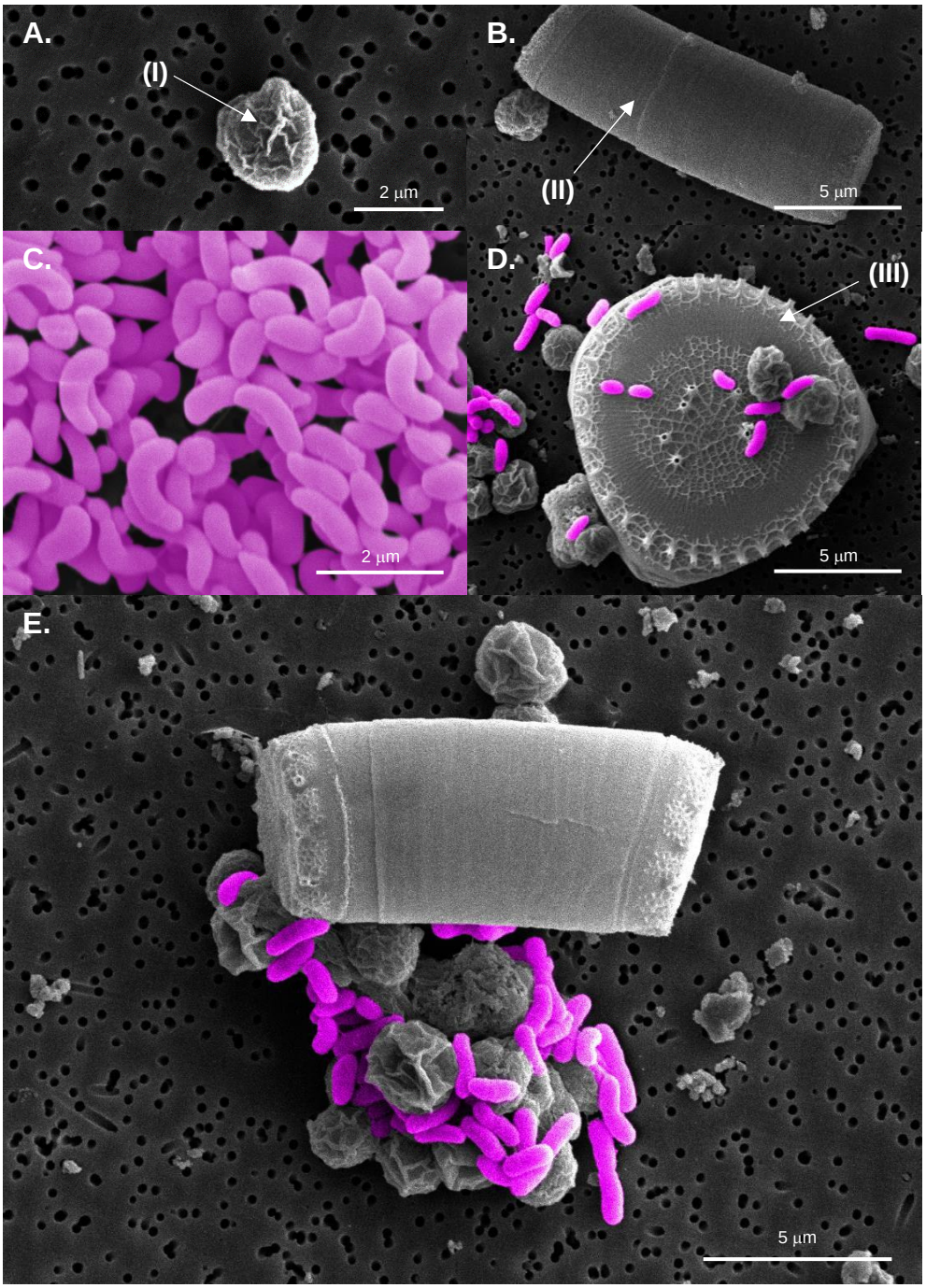

Figure 5.5: Scanning electron microscopy visualisation of *V. vulnificus* 106-2A incorporated into Reef Phytoplankton-based artificial marine snow. (A) RP-only control, magnification × 11,000. **(B)** Adhesion control, magnification × 7,000. **(C)** 106-2A only control, magnification × 15,000. **(D & E)** 106-2A Incorporated into AMS, magnification × 7,000 and × 6,500, respectively. (I) *Nannochloropsis,* (II) *Thalassiosira,* (III) *Tetraselmis.*

5.4. Inconsistent bacterial incorporation into artificial marine snow due to variable Reef Phytoplankton composition

The previous section demonstrates that phytoplankton provide a highly effective substrate for generating AMS, facilitating significant *V. vulnificus* incorporation. However, microscopic analysis of different RP stocks revealed disparities in the ratios of phytoplankton within. Fig. 5.6 shows incorporation of *V. vulnificus* 106-2A and 99-743 into AMS using three separate RP stocks. Results showed consistent incorporation into AMS between replicates from the same stock solution, however incorporation was far more varied between stock solutions. Integration of 106-2A into RP sample 1 resulted in > 10^7 CFU/g AMS, however the same bacterial inocula added to RP sample 2 resulted in < 10^6 CFU/g AMS.

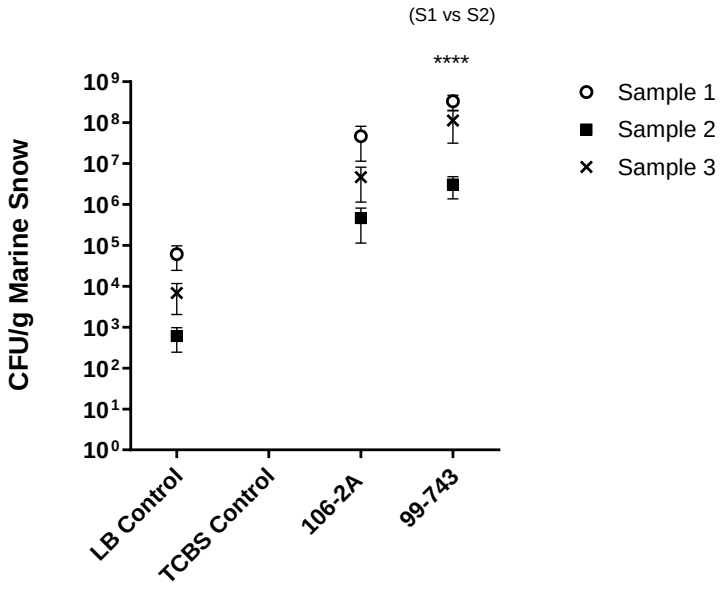

Figure 5.6: *V. vulnificus* incorporation into artificial marine snow using separate Reef Phytoplankton samples. *V. vulnificus* 106-2A and 99-743 were incorporated into AMS formed using three individual RP samples at 21 °C for 24 hours. Negative controls were plated on LB and TCBS agar. Error bars represent the standard deviation (n = 3). Statistics comparing every strain to every other strain were performed using a two-way ANOVA with Tukey's corrections for multiple comparisons, **** $p < 0.0001$.

Whilst not statistically significant, this difference could have a major impact on ensuring uptake and co-culture of consistent ratios of attacker and prey bacteria in oysters. Similarly, 99-743 incorporation into RP sample 1 resulted in > 10^8 CFU/g AMS, whereas in RP sample 3 99-743 was < 10^7 CFU/g AMS ($p < 0.0001$). These results confirm that RP composition variability had a direct effect on bacterial incorporation. This is potentially due to particular phytoplankton species within the blend binding *V. vulnificus* with greater affinity than others. Observation of the SEM images (Figs. 5.4 and 5.5) appeared to suggest that *V. vulnificus* commonly bound to *Nannochloropsis* in greater volumes than other species, however this could not be confirmed without further testing.

This variability introduced a question of consistency around AMS generated with different RP stocks and the complication of comparisons between assays using different stocks. One possible solution was to perform incorporation assays for every new batch of RP to determine the incorporation efficiency, however this is time consuming. It was therefore decided to further optimise the model by switching to a phytoplankton concentrate consisting of only *T. pseudonana*. Controlling one diatom species would prevent discrepancies caused by varying ratios of different species and help ensure consistent *V. vulnificus* incorporation.

5.5. *V. vulnificus* incorporation into *T. pseudonana* artificial marine snow

Commercially cultured *T. pseudonana* (TP1800, Reed Mariculture) was obtained in a highly concentrated suspension (10^9 cells/mL). *T. pseudonana* was primarily chosen as it has previously been demonstrated to be a highly effective substrate for marine snow formation and bacterial incorporation (Fig. 5.2). Similarly to RP, *T. pseudonana*

cells from TP1800 were non-viable, and as such would maintain their structure but no longer grow or replicate. AMS was generated as previously described but with the addition of 1 mL TP1800 in place of RP to a final concentration of 10^6 cells/mL. A bacteria-free negative control was also established in parallel for enumeration of bacteria present in TP1800 naturally.

As observed with RP, no visible aggregates formed following overnight agglomeration of *T. pseudonana*. Given that both RP and TP1800 consist of non-viable phytoplankton cells this was not unexpected. Remarkably, enumeration of bacteria-free negative controls resulted in no recovery of contaminating bacteria, either on LB or TCBS (Fig. 5.7). This lack of natural microorganisms was surprising as some level of contamination was expected as observed with the RP stock. *V. vulnificus* 106-2A

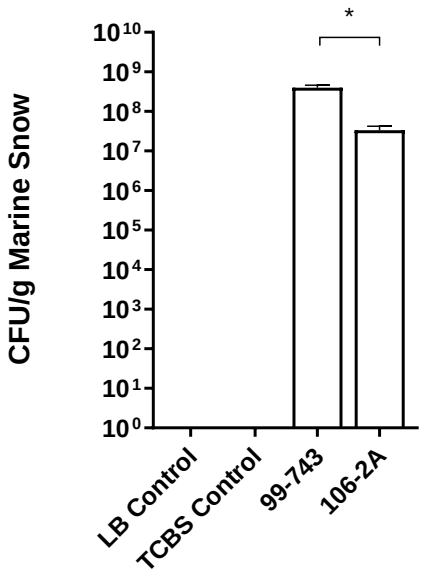

Figure 5.7: Incorporation of *V. vulnificus* into artificial marine snow using TP1800 as a substrate. *V. vulnificus* 106-2A, and 99-743 were incorporated into TP1800 AMS over 24 hours at 21 °C. Bacteria-free controls were established and enumerated on LB and TCBS agar. Error bars represent the standard deviation (n = 3). Statistics were performed using an ordinary one-way ANOVA with Tukey's corrections for multiple comparisons, * $p < 0.05$.

incorporated at > 10^7 CFU/g AMS, again 99-743 incorporation was significantly higher than 106-2A as seen previously, demonstrating > 10^8 CFU/g AMS ($p < 0.05$). Comparison of different TP1800 batches confirmed that bacterial incorporation was consistent between batches (Appendix 12).

These data confirmed development of a defined and reproducible AMS model for incorporation of *V. vulnificus* at concentrations 10,000-fold greater than NMS. From here on all AMS referenced consists of this *T. pseudonana* TP1800 model.

5.6. Dose-dependent incorporation of *V. vulnificus* into artificial marine snow

Whilst this chapter has described the development of a robust AMS model for high-level bacterial incorporation, significantly greater 99-743 incorporation into aggregates than 106-2A is always observed with both NMS and AMS models. Future *in vivo* killing assays will require oyster exposure to defined ratios of attacker and prey bacteria. Given this, *V. vulnificus* 106-2A and 99-743 incorporation into AMS was tested at final concentration of 10^5, 10^6 and 10^7 CFU/mL to determine whether increased inocula results in increased incorporation. Fig. 5.8 shows a consistent increase in *V. vulnificus* recovered from AMS relative to the increase in inoculation concentration. When supplemented at 10^5 CFU/mL, 106-2A was recovered at > 10^7 CFU/g AMS, when inoculation was increased 100-fold to 10^7 CFU/mL, 106-2A recovery from AMS also increased 100-fold to > 10^9 CFU/mL. 99-743 demonstrated similar activity, with inoculation at 10^5 CFU/g AMS resulting in > 10^8 CFU/g AMS, and 10^7 CFU/mL resulting in > 10^{10} CFU/g AMS. At every inoculation concentration tested, 99-743 demonstrated significantly greater incorporation than 106-2A ($p < 0.05$).

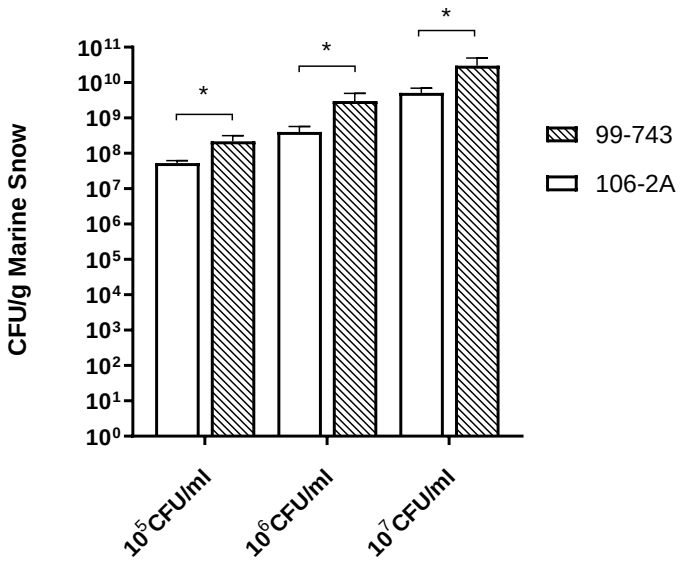

Figure 5.8: Incorporation of *V. vulnificus* into artificial marine snow at increasing concentrations. *V. vulnificus* 106-2A and 99-743 were incorporated into AMS at 10^5, 10^6, and 10^7 CFU/ml. AMS was enumerated and CFU counts taken following 24 hours rolling at 21 °C. Error bars represent the standard deviation (n = 3). Statistics were performed using unpaired t-tests, * $p < 0.05$.

5.7. Equal incorporation of *V. vulnificus* strains into artificial marine snow

Having demonstrated dose-dependent incorporation of *V. vulnificus* 106-2A and 99-743 into AMS, bacterial inoculation concentrations were selected to facilitate equal incorporation of attacker and prey strains. Fig. 5.9A demonstrates incorporation of *V. vulnificus* 106-2A, ΔT6SS1, ΔT6SS2, ΔT6SS1/2, and 99-743 into AMS at a final concentration of 10^8 CFU/ml. Bacteria-free controls plated on LB and TCBS agar recovered no contaminating microorganisms.

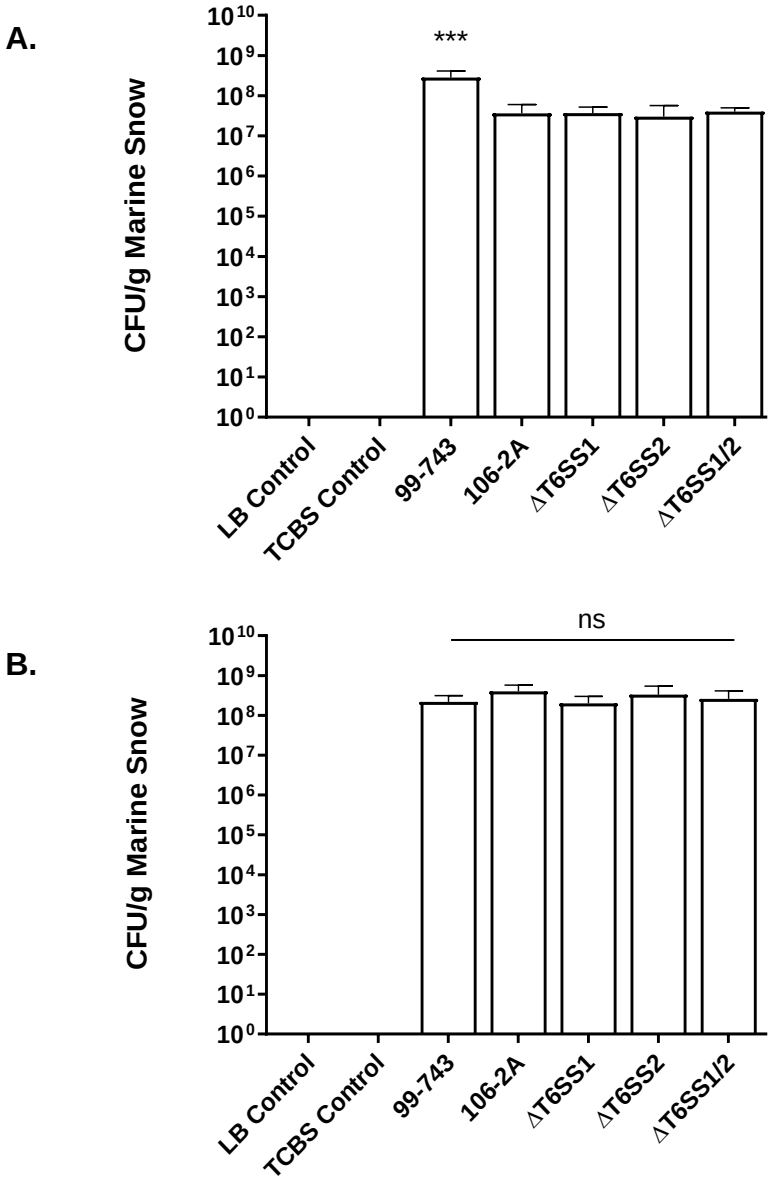

Figure 5.9: Incorporation of adjusted *V. vulnificus* concentrations into artificial marine snow. (A) 10^5 CFU/mL *V. vulnificus* 99-743, 106-2A, ΔT6SS1, ΔT6SS2 and ΔT6SS1/2 were incorporated into AMS for 24 hours at 21 °C. (B) *V. vulnificus* 99-743 (10^5 CFU/ml), 106-2A, ΔT6SS1, ΔT6SS2 and ΔT6SS1/2 (10^6 CFU/ml) were incorporated into AMS for 24 hours at 21 °C. Bacteria-free negative controls were plated on LB and TCBS agar. Error bars represent the standard deviation (n = 3). Statistics comparing every strain to every other strain were performed using a one-way ANOVA with Tukey's corrections for multiple comparisons, *** $p < 0.001$, ns – not significant.

As expected, 99-743 demonstrated significantly greater incorporation than the respective attacker strains with > 10^8 CFU/g AMS (p < 0.001). Interestingly, enumeration of wild type *V. vulnificus* 106-2A and the isogenic T6SS mutants from AMS demonstrated no significant difference in incorporation efficacy. This data suggests that the T6SS is not involved in *V. vulnificus* integration into AMS. Fig. 5.9B shows that increasing inoculation concentrations for attacker *V. vulnificus* results in equal incorporation of attacker and prey strains into AMS at 10^8 CFU/g AMS.

5.8. *S.* Enteritidis incorporation into artificial marine snow

Having demonstrated the effectiveness of AMS for *V. vulnificus* incorporation, it was investigated whether *S.* Enteritidis CC012 would show similar incorporation for future *in vivo* inter-species killing assays. AMS was inoculated with *S.* Enteritidis to a final concentration of 10^5 CFU/mL and rolled at 21 °C for 24 hours. Bacteria-free negative controls were plated on LB and *Salmonella*-selective ChromoSelect agar. Fig. 5.10 shows recovery of *S.* Enteritidis from AMS relative to *V. vulnificus* 106-2A and the T6SSs mutants. CC012 was consistently recovered from AMS at ~ 10^9 CFU/g AMS, demonstrating significantly greater incorporation than 99-743 (p < 0.05), 106-2A, and the T6SSs mutants (p < 0.0001).

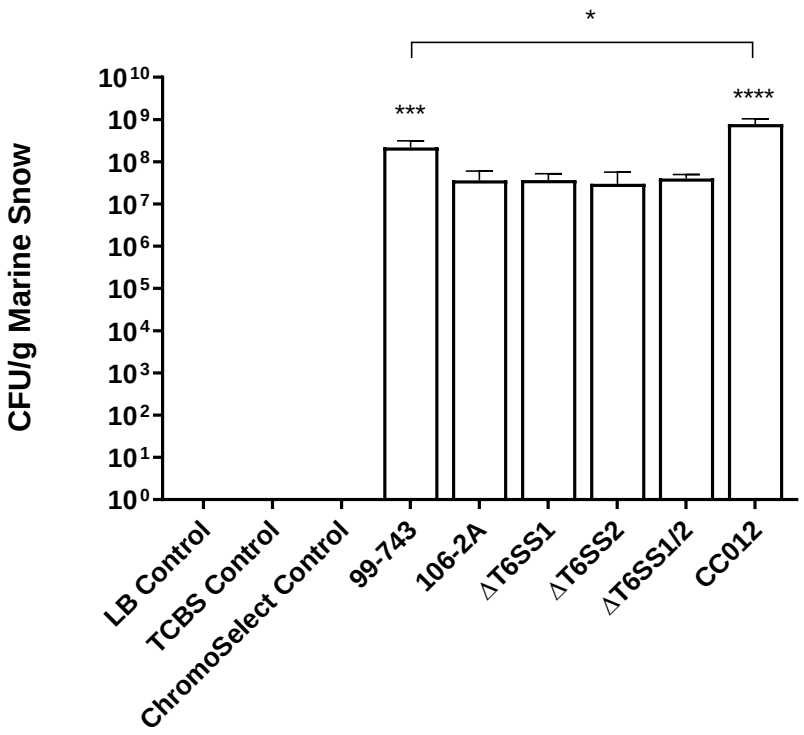

Figure 5.10: Incorporation of *V. vulnificus* and *S*. Enteritidis into artificial marine snow. 10^5 CFU/mL *S*. Enteritidis CC012 was incorporated into AMS for 24 hours at 21 °C before enumeration on TCBS or ChromoSelect agar. Bacteria-free negative controls were plated on LB and ChromoSelect agar. This graph compares incorporation data for *S.* Enteritidis CC012 to previously obtained incorporation data for *V. vulnificus* (Fig.5.9A). Error bars represent the standard deviation (n = 3). Statistics comparing every strain to every other strain were performed using a one- way ANOVA with Tukey's corrections for multiple comparisons, * $p < 0.05$, *** $p < 0.001$,
**** $p < 0.0001$.

S. Enteritidis incorporation into AMS was tested at a range of concentrations to determine the required concentrations for downstream *in vivo* assays (Fig. 5.11). As previously observed with *V. vulnificus*, dose-dependent inoculation of AMS resulted in a relative increase in bacterial incorporation into aggregates. Inoculation of AMS to a final *S.* Enteritidis concentration of 10^5 CFU/mL resulted in 10^8 – 10^9 CFU/g AMS. 100-fold increase in inocula to a final concentration of 10^5 CFU/mL resulted in a similar 100-fold increase in incorporated *S.* Enteritidis at 10^{10} – 10^{11} CFU/g AMS.

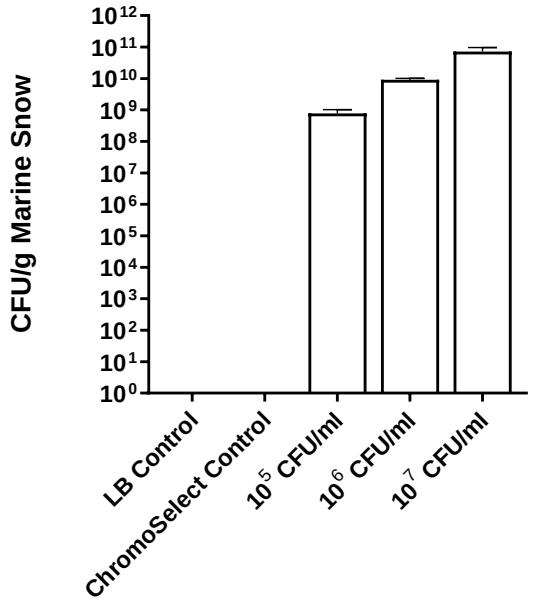

Figure 5.11: Dose-dependent incorporation of *S.* Enteritidis CC012 into artificial marine snow. *S*. Enteritidis CC012 was incorporated in AMS at final concentrations of 10^5, 10^6 and 10^7 CFU/mL. A bacteria-free negative control was also established and plated on LB and *Salmonella*-selective ChromoSelect agar. Error bars represent the standard deviation (n = 3).

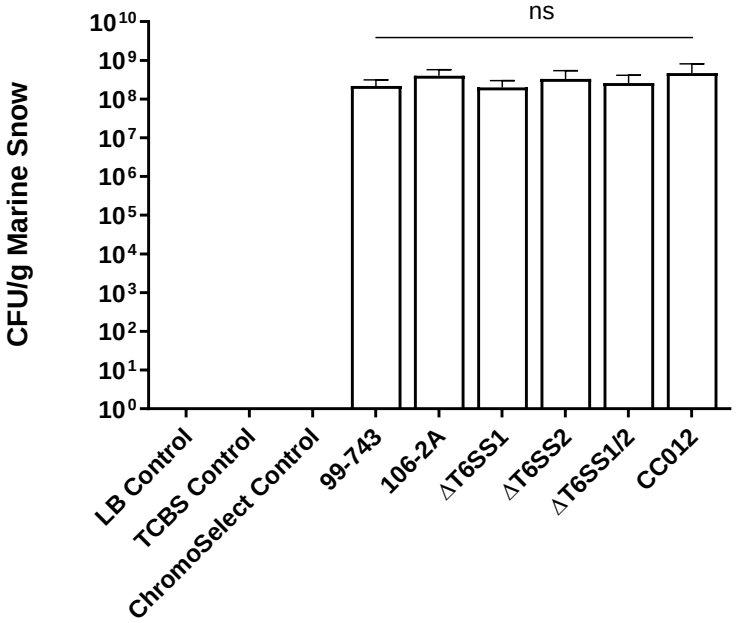

Figure 5.12: Comparison of dose adjusted *S.* Enteritidis CC012 incorporation into artificial marine snow versus *V. vulnificus* attacker and prey strains. Error bars represent the standard deviation (n = 3). Statistics were performed using a one-way ANOVA with Tukey's corrections for multiple comparisons, ns – not significant.

Given this, *S.* Enteritidis inocula was reduced from a final concentration of 10^5 CFU/mL to 10^4 CFU/mL to facilitate equal incorporation into AMS as *V. vulnificus*. Fig. 5.12 shows the standardised incorporation of *V. vulnificus* and *S.* Enteritidis into AMS in which no significant difference was observed between any of the strains tested.

5.9. Scanning-electron microscopy visualisation of *V. vulnificus* and *S.* Enteritidis in artificial marine snow

Following confirmation of *V. vulnificus* and *S.* Enteritidis incorporation into AMS, samples were processed for SEM visualisation (Fig. 5.13). Fig. 5.13A shows a representative micrograph of the adhesion control in which no bacteria were observed. As previously described in this study, this confirms that all the bacteria observed in experimental samples are genuinely associated with AMS, and not present as an artefact of the sample preparation process. Figs. 5.13B-D show individual incorporation of *V. vulnificus* and *S.* Enteritidis into AMS. Bacterial cells have been false-coloured in Photoshop for ease of identification (106-2A – pink, 99-743 – blue, CC012 – green). In all images *V. vulnificus* and *S.* Enteritidis incorporation into AMS aggregates is clearly observable, confirming quantitative data. Unprocessed SEM images can be seen in Appendix 13.

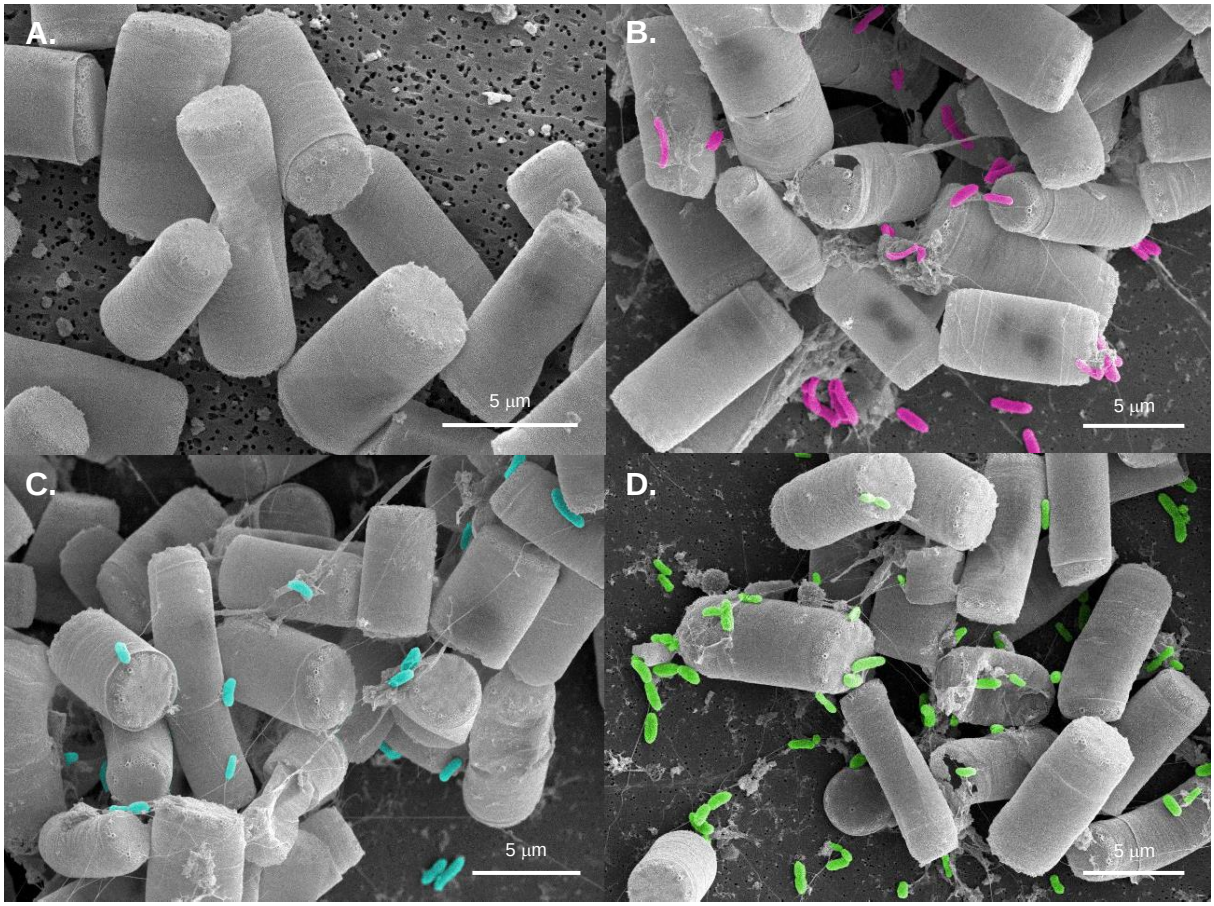

Figure 5.13: SEM visualisation of *V. vulnificus* and *S*. Enteritidis incorporation into artificial marine snow. *V. vulnificus* 106-2A, 99-743 and *S.* Enteritidis CC012 were incorporated into AMS generated using *T. pseudonana* as a substrate at 21 °C for 24 hours. **(A)** Adhesion control, magnification × 5,000. **(B)** *V. vulnificus* 106-2A (pink) incorporated into AMS, magnification × 4,000. **(C)** *V. vulnificus* 99-743 (blue) incorporated into AMS, magnification × 4,000. **(D)** *S*. Enteritidis CC012 (green) incorporated into AMS, magnification × 4,000.

The data presented so far in this study demonstrates the development of a highly reproducible model for bacterial incorporation into diatom AMS. Controlling the substrate ensures consistent aggregate formation and equally consistent incorporation of attacker and prey bacteria. Furthermore, removal of seawater as a component has ensured complete reduction of natural bacteria and the impact they may have posed in future killing assays.

5.10. Co-incorporation of attacker and prey bacteria into artificial marine snow

Having observed *in vitro* killing activity of the T6SS1 and T6SS2 of *V. vulnificus,* it was hypothesised that these systems may be active when incorporated into AMS. This would present an opportunity for attacker strains to kill prey strains before oyster uptake. To control for this possibility, attacker *V. vulnificus* 106-2A, ΔT6SS1, ΔT6SS2 and ΔT6SS1/2 were co-incorporated into AMS with either *V. vulnificus* 99-743 or *S.* Enteritidis CC012 prey strains (Fig. 5.14). All strains demonstrated incorporation of ~ 10^8 CFU/g AMS, with no strain outcompeting the other. No significant reduction of either prey strain was observed following co-incorporation with WT 106-2A when compared to individual uptake observed previously in this chapter. This data suggested that no T6SS-dependent killing was taking place.

Previously in this study, E-type *V. vulnificus* 99-743 was shown to outcompete C-type 106-2A for integration into NMS during co-incorporation (Fig. 4.4). Furthermore, 106-2A competition with 99-743 was shown to result in reduced incorporation of 106-2A relative to previous single-strain incorporation studies (Fig. 4.5). A similar interaction was not observed using this AMS model. Instead, co-incorporation of E- and C-type *V. vulnificus* was shown to have no significant impact on C-type incorporation, with total integration comparable to single-strain controls.

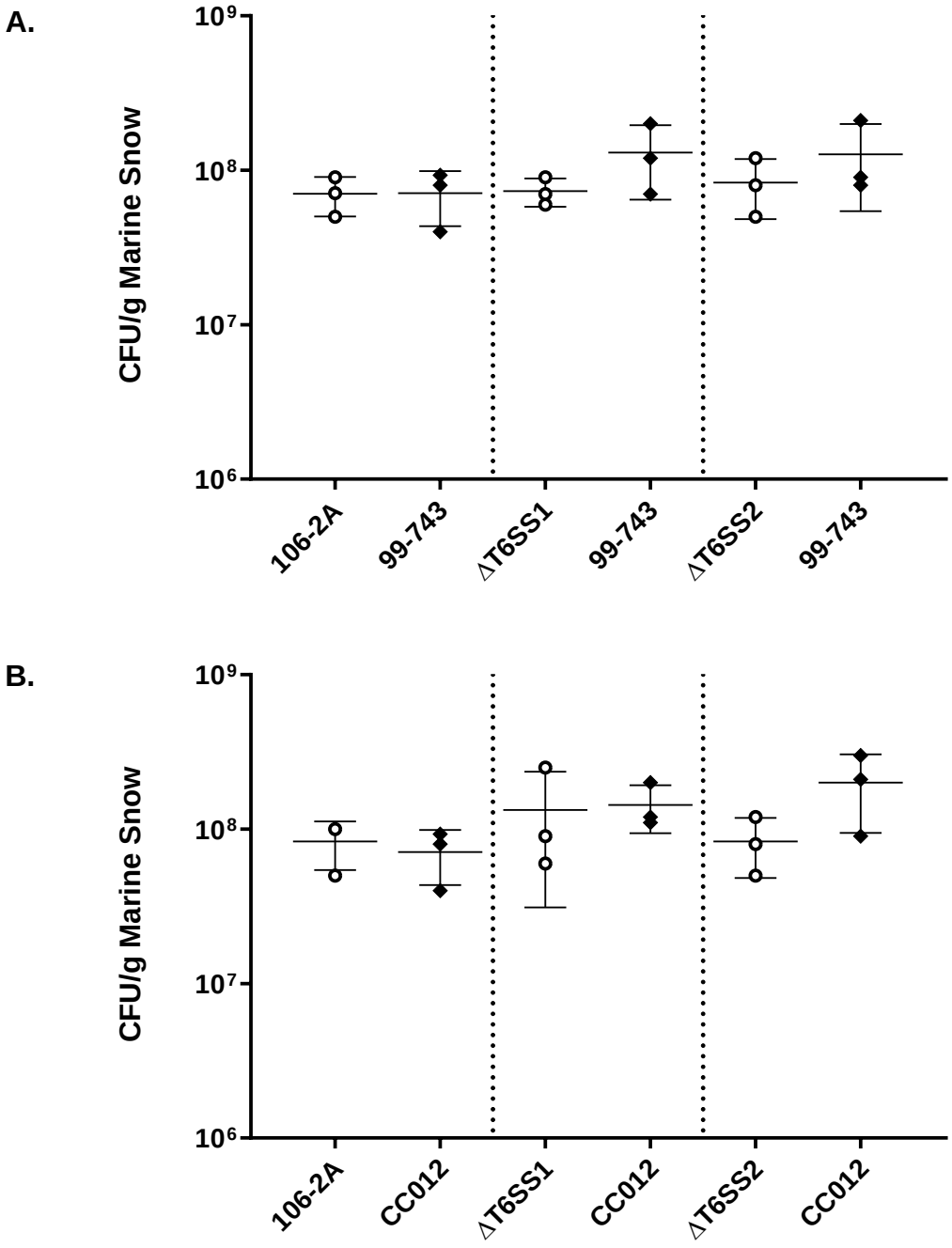

Figure 5.1: Co-incorporation of attacker and prey bacteria into artificial marine snow. Attacker *V. vulnificus* 106-2A, ΔT6SS1 and ΔT6SS2 were co-incorporated into AMS with either **(A)** *V. vulnificus* 99-743 or **(B)** *S*. Enteritidis CC012 for 24 hours at 21 °C. Vertical dotted lines separate co-cultures. Each dot represents a replicate performed in triplicate. Attacker strains are marked with empty circles, prey strains with black diamonds. Error bars represent the standard deviation (n = 3). Statistics comparing recovered attacker versus prey for each co-culture were performed using a nested one-way ANOVA with Tukey's corrections for multiple comparisons. No samples were significantly different to one another.

Discussion

This chapter describes the development of a defined and highly controllable AMS model through aggregation of the cosmopolitan diatom, *T. pseudonana*. This diatom-based model facilitated the incorporation of *V. vulnificus* and *S.* Enteritidis into aggregates at significantly greater concentrations than previously observed with NMS in this study.

Diatoms are unicellular eukaryotes found ubiquitously in wet and moist environments, with an estimated 100,000 species across 200 genera [328]. Diatoms and other phytoplankton are common constituents of marine snow, with phytoplankton blooms and diatom mats directly influencing marine snow formation [329–331]. Furthermore, this chapter shows that successful aggregate formation only requires a singular diatom species, allowing for strict control over the volume of substrate utilised to generate diatom-based AMS [332]. Bacterial incorporation into AMS using diatoms as a substrate was highly successful, demonstrating 10,000-fold greater incorporation into AMS than NMS as previously explored in this study. Use of a diatom model also facilitated straightforward dose-dependent incorporation of different bacterial species and strains into aggregates. As a result, concentrations of attacker and prey bacteria with different incorporation efficiencies can be easily adjusted to achieve required incorporation concentrations.

AMS addresses all the issues presented by NMS. Artificial seawater supplemented with diatoms circumvented both seawater variability and natural bacteria presence, as observed for NMS. AMS generation using diatom species, *T. pseudonana* and *P. tricornutum,* showed > 10^7 CFU/g incorporation of *V. vulnificus*, 10,000-fold greater than incorporation into NMS. Most importantly, bacterial incorporation was extremely consistent, demonstrating that utilising equal volumes of diatom substrate facilitated

highly reproducible bacterial incorporation between replicates. However, the downside to this method was the slow rate of growth of both diatom species, limiting the rate at which diatom based AMS studies could progress.

Therefore, this study explored the use of commercial phytoplankton concentrates to provide the substrate for AMS generation. Initial tests utilised RP, a blend of *Thalassiosira, Nannochloropsis, Tetraselmis, Pavlova* and *Isochrysis* species. Despite initial success incorporating high concentrations of *V. vulnificus* into RP-based AMS, further replicates demonstrated significant variation between *V. vulnificus* incorporation into separate RP stocks. Microscopic analysis of RP samples demonstrated that the ratios of the contained phytoplankton species were typically unequal, with one species often more frequent. Previous studies have demonstrated that particular bacterial colonisers demonstrate distinct affinities for specific phytoplankton. For example, Behringer *et al*., (2018) utilised 16S metabarcoding to assess four *Asterionellopsis glacialis* and three *Nitzschia longissima* phytoplankton strains over a year to observe changes in their bacterial composition [333]. They recorded only very minimal changes in bacterial populations despite strong pressures from culturing conditions, indicating significant associations between diatom hosts and bacterial communities. These findings were supported by subsequent data demonstrating similar short and long-term associations between bacterial communities and *Thalassiosira* species [334]. The preferential association of bacteria with certain phytoplankton would likely result in significant differences in the number of incorporated bacteria between RP stocks in accordance with which species of diatom was most prevalent within the suspension. To circumvent this, a concentrated *T. pseudonana* monoculture was investigated as a suitable substrate for AMS. Bacterial incorporation into *T. pseudonana* aggregates using laboratory-grown *T.*

pseudonana cultures had been explored previously in this chapter, and the use of a diatom monoculture would prevent phytoplankton species variation from impacting incorporation. AMS studies using *T. pseudonana* in place of RP were extremely successful, demonstrating significant and reproducible incorporation of both *V. vulnificus* and *S.* Enteritidis into diatom aggregates.

Every marine snow model investigated in this study demonstrated significantly greater incorporation of E-type *V. vulnificus* 99-743 than C-type 106-2A. One theory highlights the enhanced chitin-binding ability of E-type strains promoting adhesion to chitin-rich aggregates [276]. Chitin is the second most abundant polysaccharide on earth behind cellulose and is present in marine snow due to being an important structural component of marine zooplankton and phytoplankton [335]. Bacteria such as *Vibrio harveyi* have recently been shown to be critical for chitin recycling, utilising a 'chitoporin' membrane protein, ChiP, for uptake of chito-oligosaccharides [336]. Many *Vibrionaceae* utilise only chitin as a source of energy, whilst other *Vibrio* species such as *V. cholerae* have been demonstrated to regulate particular cellular process such as natural competence when in association with chitinous surfaces [337]. Activity of chitinolytic bacteria (particularly from the *Vibrionaceae* family), is so extensive that, despite the high prevalence of chitin within vertically falling marine snow, chitin accumulation on the ocean floor is extremely minimal [336,338]. Williams *et al*., (2014) explored the role of surface proteins in chitin attachment, notably the type 4 pilus [276]. Two *V. vulnificus* type 4 pilus mutants, Δ*pilA* and Δ*pilD*, displayed significantly reduced attachment to chitin-coated beads versus wild type *V. vulnificus*. To determine whether this was genotype-specific, E- and C-type strains were incubated with chitin fragments and relative gene expression monitored. Their results demonstrated that E-type strains expressed 23-fold more PilA and 9-fold more PilD than C-type strains,

supporting the hypothesis of enhanced chitin binding resulting in greater E-type incorporation into marine snow. Furthermore, chitin attachment assays performed at both 30 °C and 37 °C showed increased C-type binding at 37 °C, in conjunction with decreased E-type attachment [278]. This suggests that C-type chitin binding activity may be predominantly geared towards human infection, as opposed to environmental interactions. This hypothesis is further supported by the elevated expression of *gpbA* in C-type strains. GbpA is a chitin binding protein expressed 46- fold greater in C-type strains which has been associated with host colonisation in host colonisation by *V. cholerae* [279]. Combined with the data presented by this study, these results suggest that greater incorporation of E-type *V. vulnificus* into AMS may be facilitated by an increased affinity of E-type strains to chitin compared to C-type *V. vulnificus*.

The overall aim of this thesis is to explore the role of the T6SS of *V. vulnificus* on both intra and inter-species killing activity in an *in vivo* oyster model. As such, this chapter also demonstrates *S.* Enteritidis incorporation into AMS. Assessment of *S.* Enteritidis CC012 incorporation demonstrated significantly greater levels than *V. vulnificus*, even E-type *V. vulnificus* 99-743. As the mechanics behind bacterial incorporation into marine snow are not well understood it is unclear why this is the case. As previously discussed, chitin binding ability has been identified as a possible factor in determining aggregation into marine snow. *Salmonella* species chitin binding has been primarily explored in *S. enterica* serovar Typhimurium [339–341]. Brandl *et al*., (2011) demonstrated that pre-incubation of *S.* Typhimurium with chitin reduced binding to chitin beads by 727-fold [339]. However further assays comparing the chitin binding abilities of attacker and prey strains would be required to understand the significance of chitin-binding ability on the data presented in this chapter.

Finally, co-incorporation of T6SS1^{+} attacker *V. vulnificus* (106-2A, ΔT6SS1, ΔT6SS2, ΔT6SS1/2) and T6SS1^{-} prey *V. vulnificus* (99-743) and prey *S.* Enteritidis CC012 into AMS resulted in no observable T6SS-dependent killing of *V. vulnificus* and *S.* Enteritidis prey strains. Whilst initially believed to be due to the conditions not being conducive to T6SS activity, analysis of SEM images (Fig. 5.13) suggested that the lack of killing may be insufficient contact between attacker and prey bacteria. T6SS killing requires cell-cell contact to facilitate the translocation of cytotoxic effectors from the host cell into the periplasm of the prey cell [169,232,299]. However, SEM micrographs indicate that bacteria are not incorporated into AMS in high enough densities to facilitate ample cell-cell contact, but rather are typically spread out over the aggregates. It therefore appears likely that any T6SS activity in AMS would be of too low a level to accurately record. This is perhaps unsurprising as 10^9 *T. pseudonana* cells were exposed to only 10^8 CFU bacterial cells. Future work would look at either increasing the bacterial inoculation or reducing the number of diatom cells used. Either of these solutions would ensure increased colonisation of aggregates by attacker and prey strains, facilitating interaction between attacker and prey bacteria.

Conclusions

This chapter has developed a defined model for incorporating bacterial cultures into phytoplankton based AMS for future uptake by oysters. Use of *T. pseudonana* monocultures has eliminated the compositional variability issues presented by NMS, resulting in a highly reproducible and controllable AMS model into which both *V. vulnificus* and *S.* Enteritidis are effectively incorporated. Bacterial concentrations in AMS significantly outweigh loads incorporated into NMS as explored by this study.

Moving forwards, AMS uptake by oysters will be assessed to determine the applicability of this model for facilitating bacterial uptake by oysters and exploring *in vivo* interactions.

Chapter Six

V. vulnificus T6SS1 and T6SS2 have antibacterial activity in an *in vivo* oyster model

Introduction and aims

This chapter focuses on the uptake and retention of bacteria from AMS by the Pacific oyster, *C. gigas*. Previous chapters have demonstrated that *V. vulnificus* employs both the T6SS1 and the T6SS2 to kill prey *V. vulnificus* and *S.* Enteritidis strains *in vitro* and as such this chapter will also explore whether these *in vitro* results are reproducible *in vivo*. This will be conducted by co-culture of attacker and prey strains within oysters and subsequent *in vivo* killing assays. This chapter also describes the development of a series of qPCR assays designed to enumerate *V. vulnificus* and *S. Enteritidis* from oyster homogenates. qPCRs will be used to confirm data obtained from *V. vulnificus* and *S.* Enteritidis plate-counts following *in vivo* co-culture.

Results

6.1. Oyster uptake of *V. vulnificus* and *S.* Enteritidis from artificial marine snow

Having demonstrated that *V. vulnificus* and *S.* Enteritidis could be successfully incorporated into AMS at high concentrations, the subsequent step was to confirm this facilitated high-level uptake of bacteria by oysters. *V. vulnificus* and *S.* Enteritidis were incorporated into AMS at 10^8 CFU/g AMS for uptake by oysters according to the workflow shown in Fig. 6.1 (methods, section 2.6). It should be noted that AMS was individually generated for each bacterial strain to prevent any potential bacterial competition in the aggregates prior to oyster uptake. Six oysters were exposed to AMS containing bacteria for each strain to account for variance in bacterial populations found within oysters. Each assay was performed in triplicate, resulting in a total of 18 oysters per sample. Control oysters were exposed to bacteria-free AMS. After

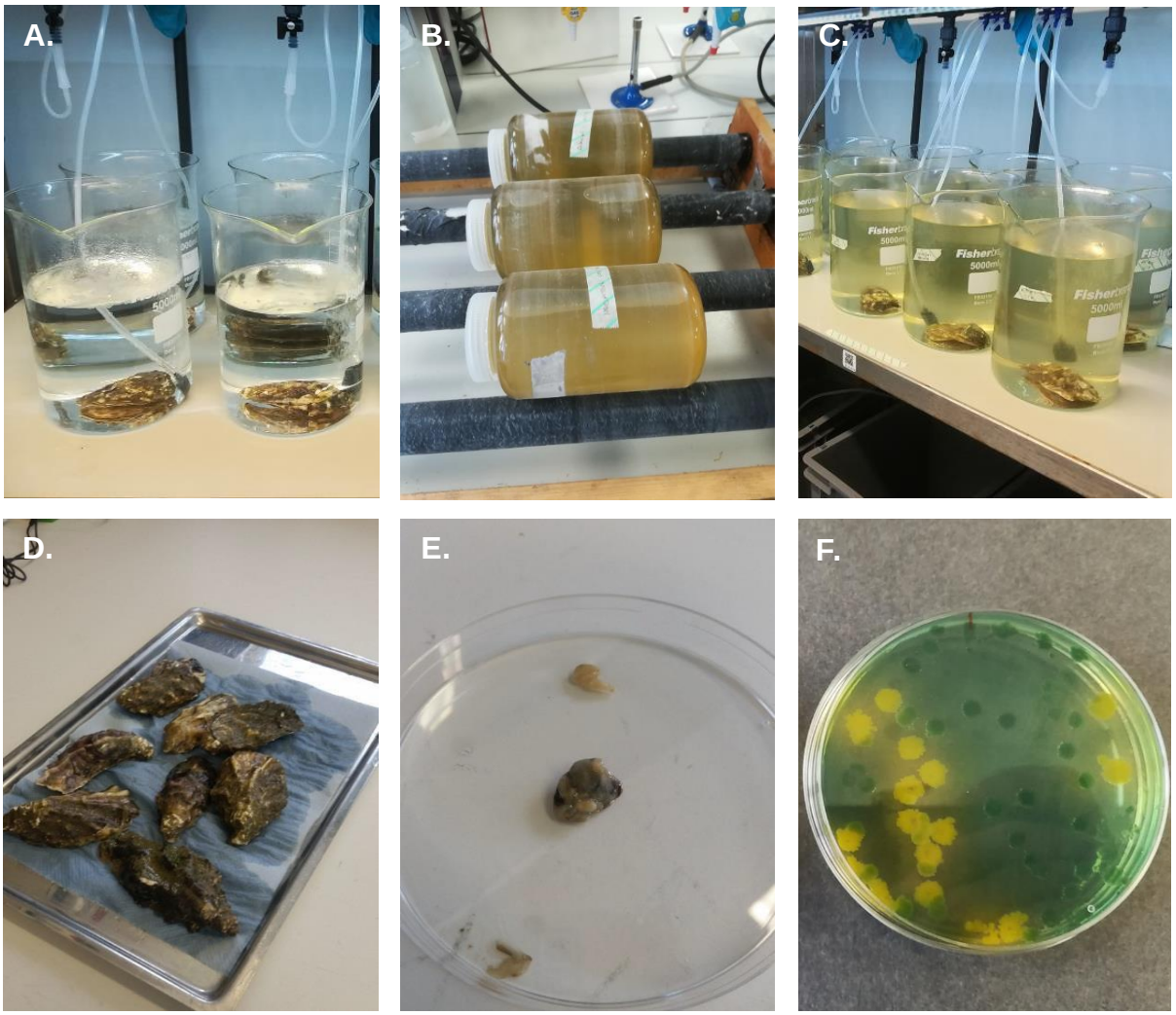

Figure 6.1: Oyster *in vivo* co-culture killing assay workflow. (A) Oysters were cleaned upon arrival to remove any fouling organisms and placed into individual aquaria to acclimatise to 21 °C, 20 ppt salinity conditions. **(B)** Once oysters had acclimatised for five days, AMS was generated as required. **(C)** Oysters were exposed to AMS for 24 hours at 21 °C. Circulation was maintained with the presence of an air stone and regular manual stirring. **(D)** After 24 hours oysters were removed and washed with 70 % ethanol to remove non-ingested bacteria. **(E)** Oysters were shucked with a sterile shucking knife and the stomach isolated. Stomachs were weighed and homogenised in PBS. **(F)** Homogenates were serially diluted and plated on LB agar. Once colonies had grown, LB plates were replica-plated onto TCBS to select for *Vibrio* species. Assays requiring *Salmonella* selection were plated on ChromoSelect agar.

exposure for 24 hours, oyster stomachs were excised, homogenised and plated on the relevant selective media for enumeration.

Numbers of bacterial strains taken up by oysters from AMS are shown in Fig. 6.2. Despite professional depuration of oysters prior to delivery, natural bacteria were isolated from control oysters at 10^2 – 10^4 CFU/g tissue. Enumeration of bacteria-free AMS oyster controls on TCBS and ChromoSelect agar demonstrated < 10^3 CFU/g

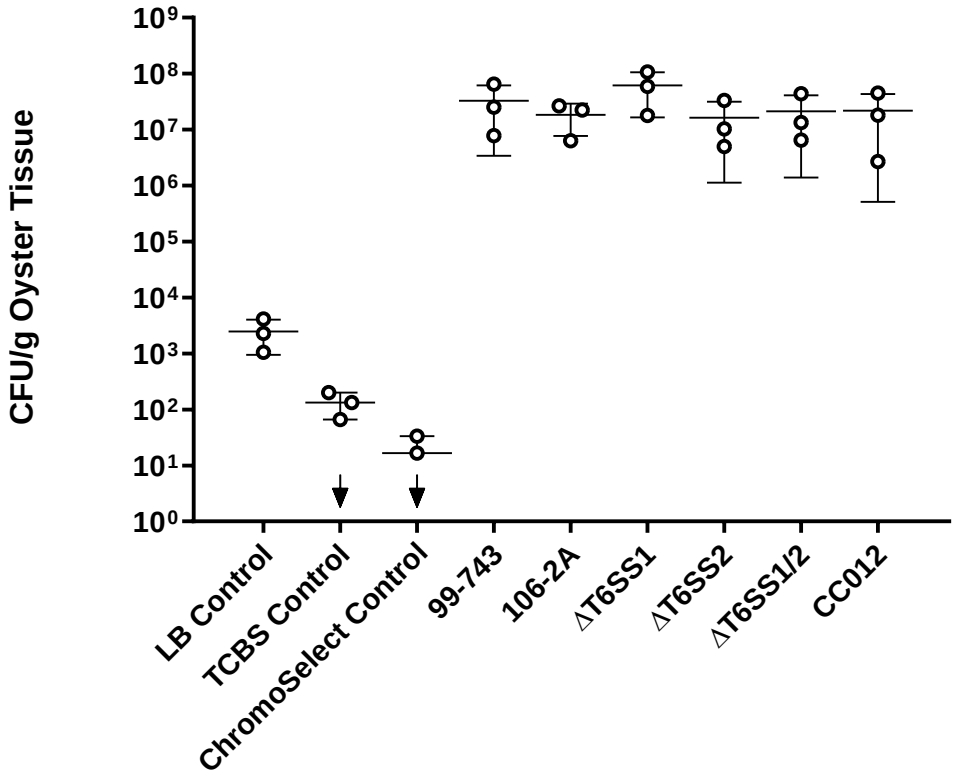

Figure 6.1: Oyster uptake of *V. vulnificus* and *S.* Enteritidis from artificial marine snow. *V. vulnificus* 99-743, 106-2A, ΔT6SS1, ΔT6SS2, ΔT6SS1/2 and *S.* Enteritidis CC012 were incorporated into AMS and added to oyster tanks for uptake over 24 hours. Control oysters were exposed to bacteria-free AMS and plated on LB, TCBS and ChromoSelect agar. Each circle represents the mean of six oysters (n = 3). Horizontal bars represent the mean, error bars represent the standard deviation. Downward arrows indicate that one or more samples were below the limit of detection (100 CFU/g tissue). Statistics comparing every strain to every other strain were performed using a nested one-way ANOVA with Tukey's corrections for multiple comparisons, no samples were significantly different to one another.

tissue and < 10^2 CFU/g tissue for *Vibrio* and *Salmonella* species, respectively. However, not all oysters contained contaminating *Vibrio* or *Salmonella* species, as indicated by downward arrows on the graph (Fig. 6.2). Excitingly, uptake of *V.*

vulnificus and *S.* Enteritidis from AMS was extremely successful. Bacterial uptake ranged from 10^6 – 10^8 CFU/g tissue and was highly consistent between replicates. Importantly, there was no significant difference in uptake observed between any strains or species. Therefore, no AMS inocula adjustment was required to compensate for dissimilar ingestion of different strains. This demonstrated the development of an extremely robust and reproducible AMS model for facilitating high volume ingestion of bacterial cultures by oysters.

6.1.1. Uptake of *V. vulnificus* and *S.* Enteritidis over 48 hours

Having demonstrated that AMS facilitates effective bacterial uptake by oysters, rate of bacterial ingestion was explored over 48 hours to determine whether there were significant differences in uptake between different strains as this would impact downstream co-culture assays. Bacterial loads in oysters exposed to AMS were enumerated at T_0, T_4, T_8, T_{24} and T_{48} hours to establish the rates at which different strains were ingested from AMS. Fig. 6.3 shows rapid initial uptake of bacteria from AMS, with bacterial concentrations rising from 10^2 CFU/g tissue at T_0 to 10^5 – 10^7 CFU/g tissue at T_4. This rapid uptake was expected as depuration had reduced native oyster microflora, enabling colonisation by exogenous bacteria. Ingested bacterial concentrations peaked at T_8, ranging from 5×10^6 – 5×10^8 CFU/g tissue. T_{24} shows *V. vulnificus* and *S.* Enteritidis concentrations plateauing at 10^6 – 10^8 CFU/g tissue. Enumeration at T_{48} demonstrated a decrease in total number of *V. vulnificus* and *S.*

Enteritidis present within the oysters, concentrations observed ranged from 5×10^4 – 5×10^7 CFU/g tissue. Reassuringly, no significant difference was observed between the rates at which *V. vulnifcus* and *S.* Enteritidis strains are taken up by oysters.

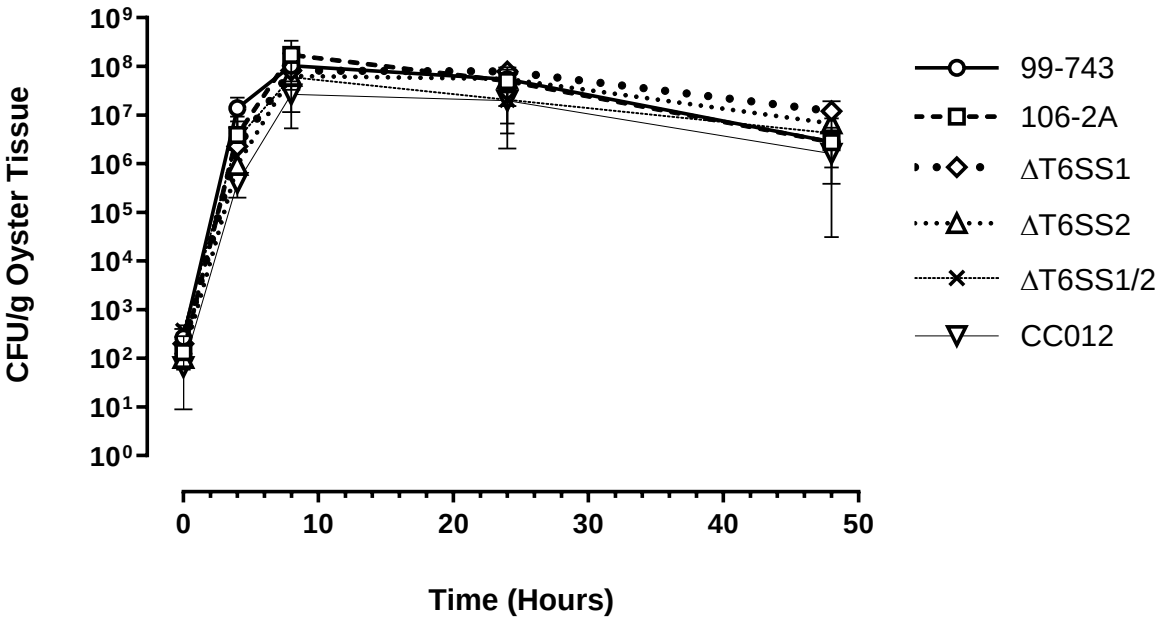

Figure 6.2: Oyster uptake of *V. vulnificus* and *S.* Enteritidis from artificial marine snow over 48 hours. Oyster uptake of *V. vulnificus* 99-743, 106-2A, ΔT6SS1, ΔT6SS2, ΔT6SS1/2 and *S.* Enteritidis CC012 from AMS over 48 hours. Each point on the graph represents the mean of six oysters (n = 3), error bars represent the standard deviation. Bacterial loads were enumerated at T_0, T_4, T_8, T_{24} and T_{48} hours post exposure to AMS.

6.1.2. *V. vulnificus* and *S.* Enteritidis depuration from oysters

An aim of this study was to develop an *in vivo* model that would enable study of bacterial interactions in oysters, specifically to reproduce *in vitro* data that showed T6SS1 and T6SS2 antibacterial activity at 21 °C. Two key problems typically encountered by previous studies in this field are extremely low uptake of planktonic bacteria by oysters and very rapid depuration of ingested bacteria following uptake [249]. Having demonstrated successful uptake of *V. vulnificus* and *S.* Enteritidis from AMS,

this study sought to compare the uptake and depuration of bacteria from AMS with the uptake and depuration of planktonic bacteria by oysters. This would elucidate whether incorporation into AMS is advantageous for bacterial retention in oysters during depuration.

Oysters were exposed to inoculated AMS for 24 hours to facilitate uptake of incorporated bacteria as previously described. Planktonic control oysters had their tank water supplemented with equal concentrations of *V. vulnificus* to those incorporated into AMS. Following exposure (T_{24}), tanks were cleaned and replaced with fresh artificial seawater to promote depuration of ingested bacteria. This process was repeated at 8 hours, then again after 24 hours, and then finally again after 48 hours. Six oysters per strain were removed and homogenised at T_0, T_{24} (0 hours post-depuration), T_{32} (8 hours post-depuration), T_{56} (24 hours post-depuration), and T_{80} (48 hours post-depuration) to enumerate the bacterial load (Fig. 6.4). As previously described for uptake experiments in section 6.1.1, all assays were performed in triplicate, resulting in a total of 18 oysters per strain, per timepoint.

As previously observed, bacterial concentrations in oysters following exposure to inoculated AMS for 24 hours was 10^6 – 10^8 CFU/g tissue. The planktonic control was far less effective, demonstrating < 10^5 CFU/g tissue uptake of *V. vulnificus* and *S.* Enteritidis, up to 1,000-fold less than AMS-exposed animals. Enumeration of *V. vulnificus* and *S.* Enteritidis from oysters at T_{24}, T_{32}, T_{56} and T_{80} hours showed a steady reduction in bacterial load within oyster stomachs. Final enumeration at T_{80}, after 48 hours of depuration, showed a 10,000-fold reduction in bacteria compared to oyster samples enumerated at T_{24}. No strains incorporated into AMS demonstrated significantly faster or increased depuration from oysters than any other. The planktonic control achieved background levels of bacteria far more rapidly as was expected due

to the low initial levels of uptake. Bacterial loads after 24-hour depuration (T_{56}) showed < 10^3 CFU/g tissue, similar to natural bacteria levels observed at T_0. Depuration rates were similar between the planktonic control and the AMS-exposed oysters. The planktonic control dropped from 5×10^4 CFU/g tissue at T_{24} to 5×10^2 CFU/g tissue at T_{56} (24-hour depuration). This 100-fold reduction was also observed in all oysters exposed to inoculated AMS whose recorded bacterial loads dropped from 5×10^7 CFU/g tissue at T_{24} to 5×10^5 CFU/g tissue at T_{56}. This suggests that AMS does not provide a significant advantage in bacterial retention during depuration and that oyster expulsion of microflora is not concentration dependent.

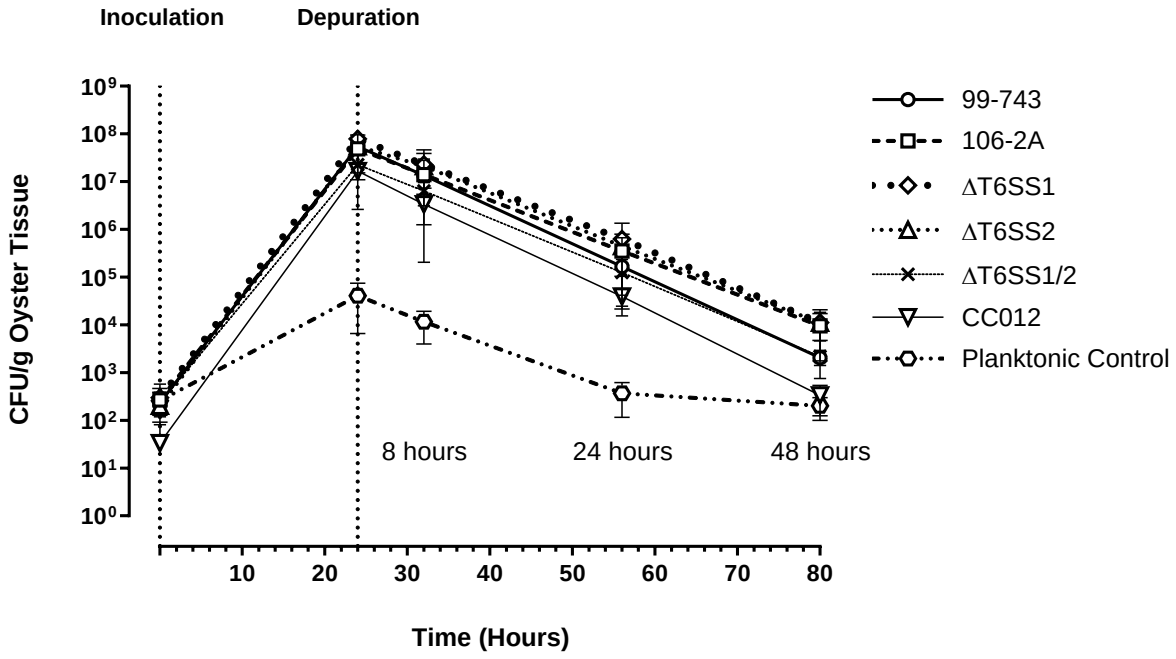

Figure 6.3: Depuration of *V. vulnificus* and *S*. Enteritidis from oysters over 48 hours. Oysters were exposed to AMS containing *V. vulnificus* 99-743, 106-2A, ΔT6SS1, ΔT6SS2, ΔT6SS1/2 and *S*. Enteritidis CC012 for 24 hours at 21 °C to facilitate uptake of incorporated bacteria. A subset of oysters were also exposed to planktonic *V. vulnificus* to act as a control for typical oyster inoculation protocols (planktonic control; *V. vulnificus* 106-2A). At 24 hours, tanks were cleaned and filled with sterile artificial seawater to stimulate depuration. This process was repeated at T_{32}, T_{56} and T_{80} hours. Six oysters were assessed per strain at each timepoint (n = 3). Timepoints consisted of T_0, T_{24} (0 hours post-depuration), T_{32} (8 hours post-depuration), T_{56} (24 hours post-depuration) and T_{80} (48 hours post-depuration).

6.2. *In vivo* intra-species *V. vulnificus* co-culture assays

6.2.1. Attacker to prey ratio of 1:1

This chapter has demonstrated that incorporation of bacteria into AMS facilitates uptake by oysters to concentrations ranging from 10^6 – 10^8 CFU/g tissue. Furthermore, there has been no observed difference in uptake rate between different bacterial strains and species. Given these data, this study proceeded to perform bacterial co-culture assays in oysters to explore the activity of the T6SSs *in vivo*. Initially, oysters were exposed to AMS containing attacker and prey *V. vulnificus* at a 1:1 ratio for 24 hours to facilitate uptake and competition between competing *V. vulnificus* strains. Whilst previous *in vitro* co-culture assays had been performed at an attacker to prey ratio of 3:1, it was decided to initially test a 1:1 ratio to be more representative of a natural situation. Negative control oysters were exposed to bacteria-free AMS and plated on LB and TCBS agar to enumerate natural microorganisms. Simultaneously, individual strain uptake controls were performed to ensure that each batch of oysters demonstrated consistent uptake and that there were no extraneous factors impacting the assay.

Fig. 6.5 shows enumeration of attacker and prey *V. vulnificus* from oyster stomach tissue following co-culture at 21 °C for 24 hours. Bacteria-free AMS control oyster enumeration identified natural microorganisms at 10^3 – 10^4 CFU/g tissue. Again, this was expected as depuration of established bacteria from oysters is difficult. Of these bacteria, plating on TCBS agar confirmed < 10^3 CFU/g tissue to be *Vibrio* species. Several oysters returned no colonies on TCBS at all.

All single strain control oysters demonstrated previously observed levels of *V. vulnificus* uptake (Fig. 6.2), with concentrations between 10^6 – 10^8 CFU/g tissue. Comparison of prey 99-743 recovered from co-culture oysters demonstrated no

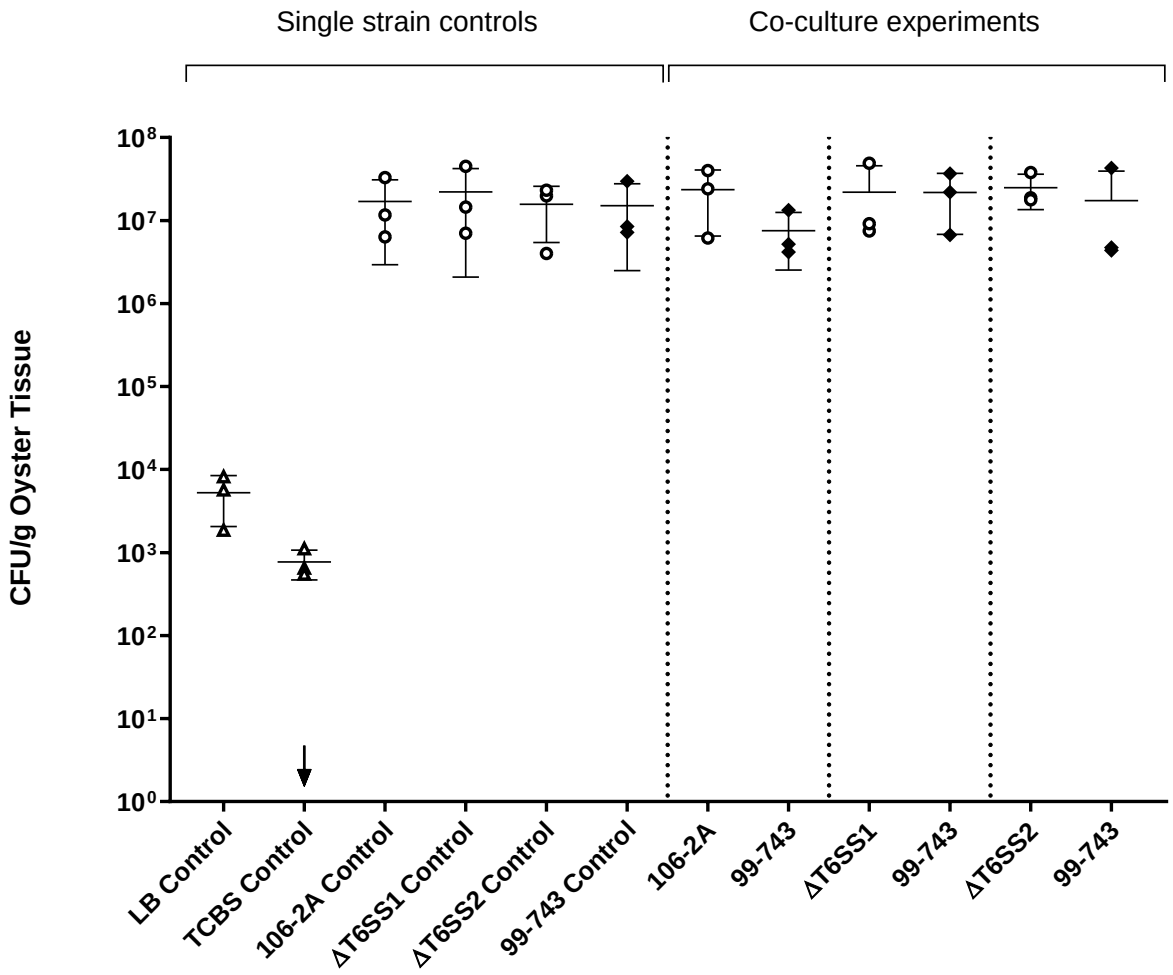

Figure 6.4: *In vivo* intra-species *V. vulnificus* co-culture at an attacker to prey ratio of 1:1. *In vivo* co-culture assays were performed between attacker *V. vulnificus* strains, 106-2A, ΔT6SS1, ΔT6SS2 or ΔT6SS1/2, and prey *V. vulnificus* 99-743 for 24 hours at 21 °C at an attacker to prey ratio of 1:1. Control oysters were exposed to either bacteria-free AMS or AMS containing a single bacterial strain. Each mark represents a biological replicate consisting of six technical oyster replicates processed per strain/co-culture (n = 3). Clear triangles mark bacteria-free controls, clear circles mark attacker strains, black diamonds mark prey strains. Downward arrows indicate some replicates are below the 10^2 CFU/g tissue limit of detection. Vertical dotted lines separate the co-culture assays and controls. Horizontal lines represent the mean of the three replicates, error bars represent the standard deviation. Statistics comparing all prey strain data from the co-cultures with the prey data from the prey control and all co-culture attacker strain data with their respective attacker strain control data were performed using a nested one-way ANOVA with Dunnett's corrections for multiple comparisons.

significant reduction when compared to the single strain 99-743 oyster control subset, with consistently 10^6 – 10^8 CFU/g AMS recovered. This contrasted with the *in vitro* data where prey 99-743 showed a 1,000-fold reduction following co-culture with attacker *V. vulnificus* (Fig. 3.9). Enumeration of *V. vulnificus* attacker strains from co- culture oysters showed no significant difference in concentration of 106-2A, ΔT6SS1 and ΔT6SS2 compared to single strain controls also. It was hypothesised that killing of prey 99-743 may have simply been occurring on too small a scale to be significant. The ratio of attacker to prey cells was therefore increased from 1:1 to both 5:1 and 10:1 to determine whether dose-dependent killing could be observed with higher attacker concentrations.

6.2.2. Attacker to prey ratios of 5:1 and 10:1

To achieve an attacker to prey ratio of 5:1, inocula of attacker strains was increased from 10^8 CFU/g AMS (initial inocula: 10^8 CFU/mL) to 5×10^8 CFU/g AMS (initial inocula: 5×10^8 CFU/mL) and co-culture assays performed as previously described (methods, section 2.6). Oysters exposed to bacteria-free AMS were plated on LB and TCBS agar (Fig. 6.6).

Background bacteria were recovered at 10^4 CFU/g tissue, of which 10^2 – 10^3 CFU/g tissue were confirmed to be *Vibrio* species by plating on TCBS. These results were similar to those previously obtained (section 6.2.1), demonstrating relative consistency between oysters utilised in these assays. Single strain controls consistently demonstrated > 10^7 CFU/g tissue uptake into oysters, with no strains showing significantly increased or reduced uptake relative to each other and previous uptake experiments. However, 99-743 co-culture with *V. vulnificus* 106-2A, ΔT6SS1, and

ΔT6SS2 at an attacker to prey ratio of 5:1 resulted in 99-743 recovery at $10^5 – 10^6$ CFU/g tissue, significantly lower than the 99-743 single strain control ($p < 0.0001$). This reduction was T6SS-dependent, as co-culture assays performed between 99-743 and the double mutant, ΔT6SS1/2, resulted in no significant killing of prey 99-743, with recovery of $10^6 – 10^8$ CFU/g tissue, equal to the single strain control.

It was considered that the observed 99-743 reduction may be a result of increasing attacker to prey ratios to 5:1, simply increasing the levels of attacker strain available for uptake. However, if this was the case a reduction of 99-743 would also be expected following co-culture with ΔT6SS1/2. Isolation of 99-743 from co-culture with ΔT6SS1/2 at concentrations equal to the single strain control confirmed that increased attacker to prey ratios did not impact co-culture results in ways other than T6SS-dependent killing.

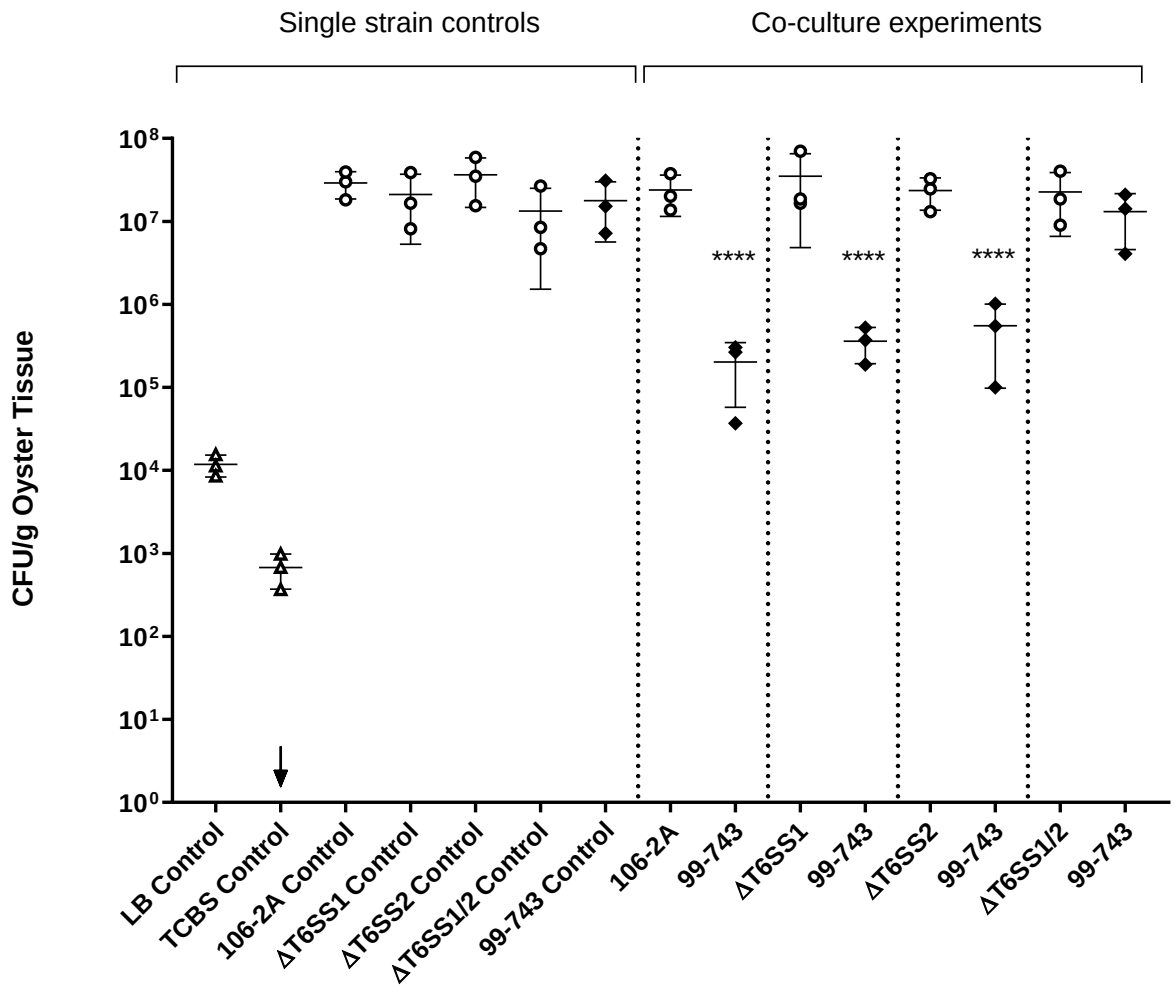

Figure 6.5: *In vivo* intra-species *V. vulnificus* co-culture at an attacker to prey ratio of 5:1. *In vivo* co-culture assays were performed between attacker *V. vulnificus* strains, 106-2A, ΔT6SS1, ΔT6SS2 or ΔT6SS1/2, and prey *V. vulnificus* 99-743 for 24 hours at 21 °C at an attacker to prey ratio of 5:1. Control oysters were exposed to either bacteria-free AMS or AMS containing a single bacterial strain. Each mark represents a biological replicate consisting of six technical oyster replicates processed per strain/co-culture (n = 3). Clear triangles mark bacteria-free controls, clear circles mark attacker strains, black diamonds mark prey strains. Downward arrows indicate some replicates are below the 10^2 CFU/g tissue limit of detection. Vertical dotted lines separate the co-culture assays and controls. Horizontal lines represent the mean of the three replicates, error bars represent the standard deviation. Statistics comparing all prey strain data from the co-cultures with the prey data from the prey control and all co-culture attacker strain data with their respective attacker strain control data were performed using a nested one-way ANOVA with Dunnett's corrections for multiple comparisons, **** $p < 0.0001$.

These results therefore confirm that the reduction in prey 99-743 observed following co-culture with 106-2A, ΔT6SS1, and ΔT6SS2 was as a result of T6SS dependent killing, mediated by both the T6SS1 and the T6SS2. This is the first time that *V. vulnificus* T6SSs have been demonstrated to have intra-species killing activity *in vivo*.

Having demonstrated T6SS-dependent killing of prey 99-743 at attacker to prey ratios of 5:1, co-culture assays were repeated at 10:1 (Fig. 6.7). 99-743 co-culture with 106-2A, ΔT6SS1, and ΔT6SS2 resulted in a significant decrease to 10^2 – 10^4 CFU/g tissue ($p < 0.0001$). This reduction in 99-743 was 1,000-fold greater than the reduction observed at 5:1, and 10,000-fold greater than the single strain controls. Due to the enumeration method, the limit of detection for plate-enumeration was 10^2 CFU/g tissue. Downward arrows in Fig. 6.7 indicate that there were one or more samples in which concentrations were < 10^2 CFU/g tissue, resulting in no recovery of prey colonies.

Interestingly, 99-743 co-culture with ΔT6SS1/2, resulted in a semi-log reduction of 99-743 to 5×10^6 CFU/g tissue ($p < 0.01$). This reduction was not observed at 5:1, suggesting that exposure of oysters to increased attacker *V. vulnificus* concentrations was resulting in significantly greater uptake of attacker strains and impacting uptake of 99-743. However, this study still observed significantly greater reduction of 99-743 when co-cultured with 106-2A, ΔT6SS1, and ΔT6SS2 compared to ΔT6SS1/2, confirming that these strains are killing 99-743 *in vivo* in a T6SS-dependent manner.

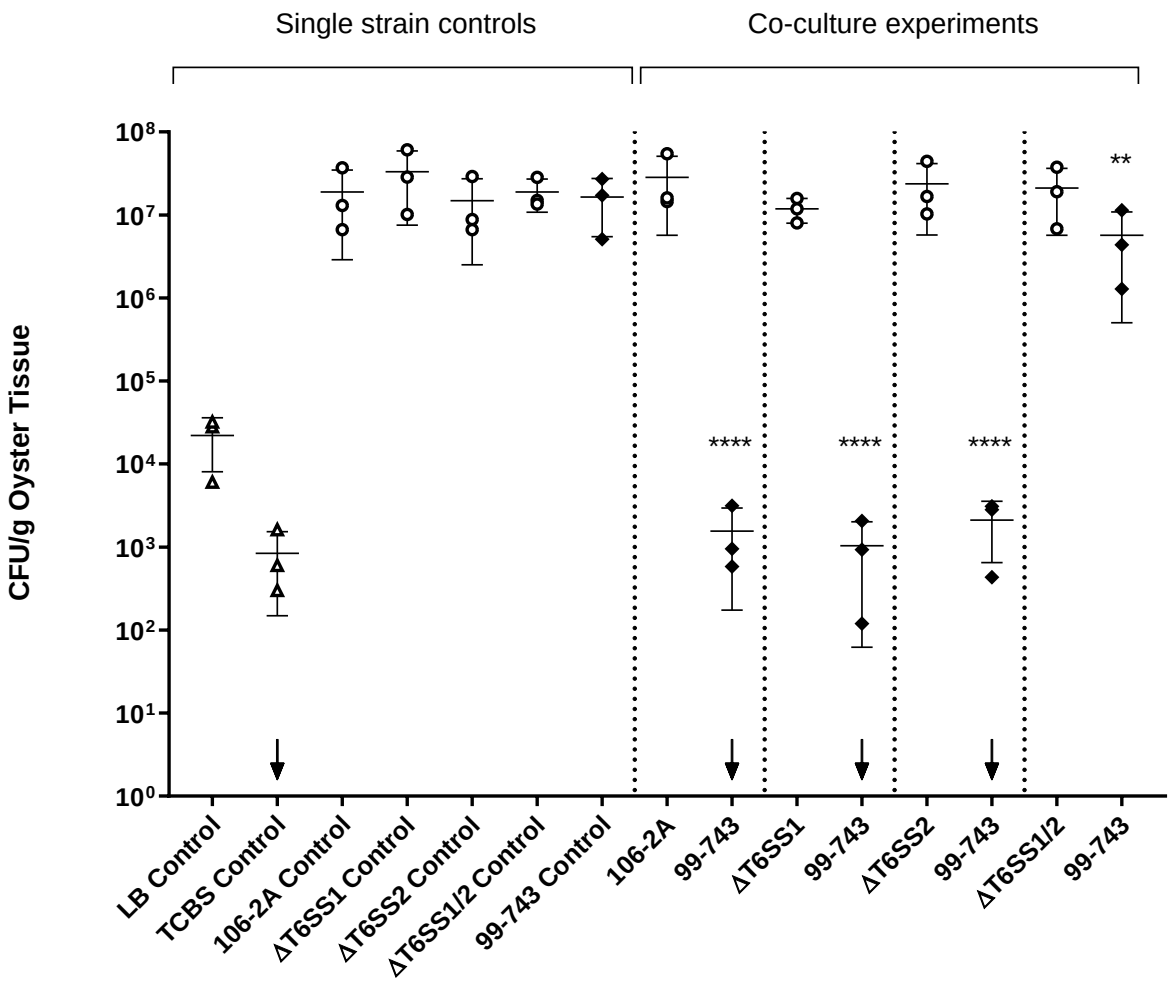

Figure 6. 6: *In vivo* intra-species *V. vulnificus* co-culture at an attacker to prey ratio of 10:1. *In vivo* co-culture assays were performed between attacker *V. vulnificus* strains, 106-2A, ΔT6SS1, ΔT6SS2 or ΔT6SS1/2, and prey *V. vulnificus* 99-743 for 24 hours at 21 °C at an attacker to prey ratio of 10:1. Control oysters were exposed to either bacteria-free AMS or AMS containing a single bacterial strain. Each mark represents a biological replicate consisting of six technical oyster replicates processed per strain/co-culture (n = 3). Clear triangles mark bacteria-free controls, clear circles mark attacker strains, black diamonds mark prey strains. Downward arrows indicate some replicates are below the 10^2 CFU/g tissue limit of detection. Vertical dotted lines separate the co-culture assays and controls. Horizontal lines represent the mean of the three replicates, error bars represent the standard deviation. Statistics comparing all prey strain data from the co-cultures with the prey data from the prey control and all co-culture attacker strain data with their respective attacker strain control data were performed using a nested one-way ANOVA with Dunnett's corrections for multiple comparisons, ** $p < 0.01$, **** $p < 0.0001$.

6.3. *V. vulnificus* inter-species competition assays *in vivo*

6.3.1. Attacker to prey ratios of 5:1 and 10:1

Having demonstrated *V. vulnificus* 106-2A and the isogenic single T6SS deletion mutants were able to kill prey *V. vulnificus in vivo,* co-culture assays were performed investigating inter-species competition with prey *S.* Enteritidis CC012. As no significant killing was observed at an attacker to prey ratio of 1:1 for intra-species killing it was decided to only test 5:1 and 10:1 attacker to prey ratios for inter-species assays.

Fig. 6.8 shows enumeration of *V. vulnificus* and *S.* Enteritidis from oysters following co-culture at an attacker to prey ratio of 5:1 for 24 hours at 21 °C. Control oysters exposed to bacteria-free AMS were enumerated and numbers of natural microorganisms enumerated on LB agar and ChromoSelect agar. Whilst oysters tended to contain natural microorganisms at around the same $10^2 – 10^4$ CFU/g tissue concentrations observed in other assays, *S.* Enteritidis concentrations were generally lower than was observed for *Vibrio* species. Typically, *Vibrios* were enumerated at $< 5 \times 10^3$ CFU/g tissue with 7 oysters out of the 36 control oysters utilised in the 5:1 and 10:1 assays containing no *Vibrios* at all. However, *S.* Enteritidis was always present at $< 4 \times 10^2$ CFU/g tissue, and only identified in 15 out of 36 control oysters assessed over the two co-culture assays.

Single strain control oysters demonstrated uptake of *V. vulnificus* and *S.* Enteritidis at $10^6 – 10^8$ CFU/g tissue. *S.* Enteritidis enumeration from co-culture with106-2A, ΔT6SS1, and ΔT6SS2 demonstrated significant reduction of prey *S.* Enteritidis. Bacterial loads showed a reduction from $10^6 – 10^8$ CFU/g tissue in the single strain

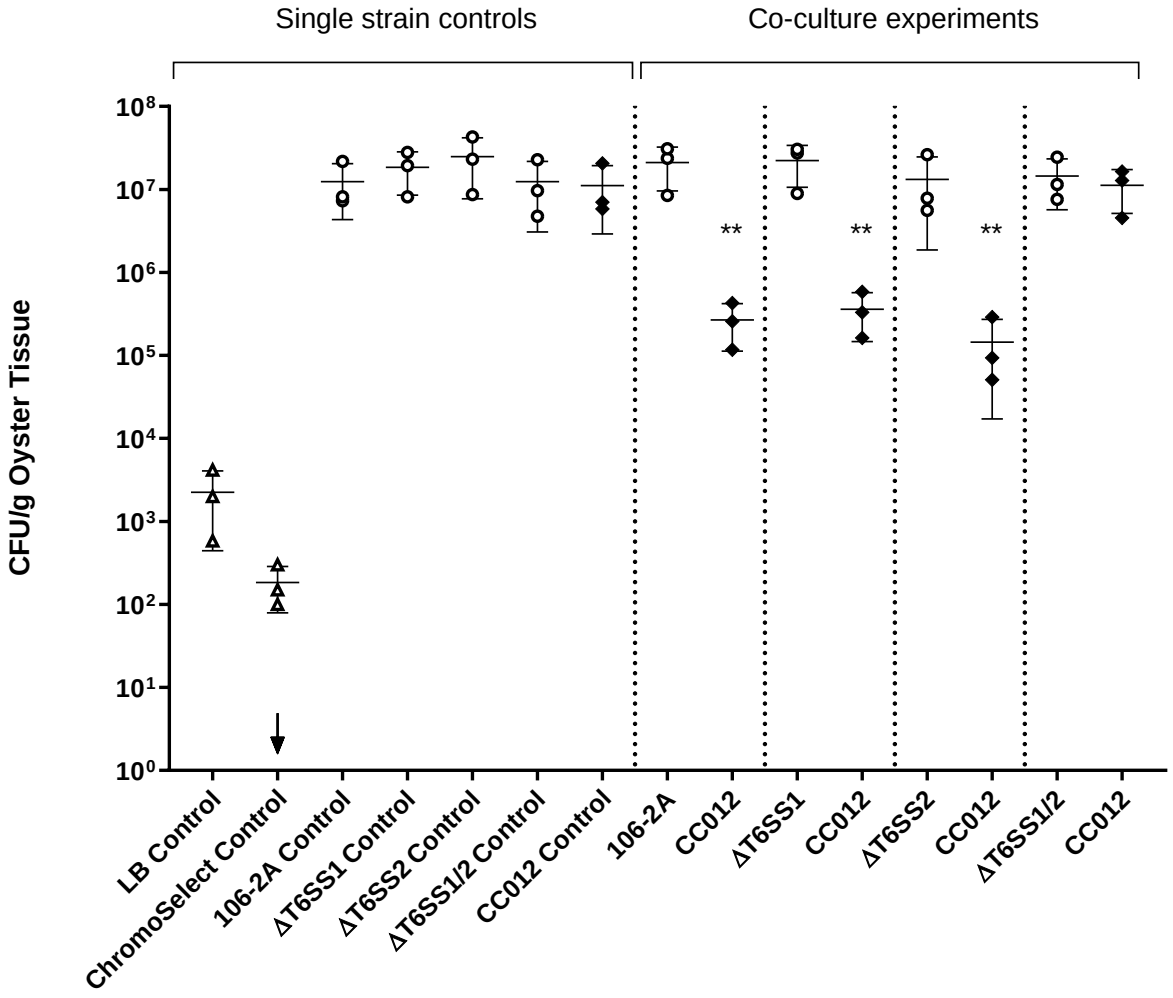

Figure 6.7: *In vivo* inter-species *V. vulnificus* co-culture with *S*. Enteritidis at an attacker to prey ratio of 5:1. *In vivo* co-culture assays were performed between attacker *V. vulnificus* strains, 106-2A, ΔT6SS1, ΔT6SS2 or ΔT6SS1/2, and prey *S*. Enteritidis CC012 for 24 hours at 21 °C at an attacker to prey ratio of 5:1. Control oysters were exposed to either bacteria-free AMS or AMS containing a single bacterial strain. Each mark represents a biological replicate consisting of six technical oyster replicates processed per strain/co-culture (n = 3). Clear triangles mark bacteria-free controls, clear circles mark attacker strains, black diamonds mark prey strains. Downward arrows indicate some replicates are below the 10^2 CFU/g tissue limit of detection. Vertical dotted lines separate the co-culture assays and controls. Horizontal lines represent the mean of the three replicates, error bars represent the standard deviation. Statistics comparing all prey strain data from the co-cultures with the prey data from the prey control and all co-culture attacker strain data with their respective attacker strain control data were performed using a nested one-way ANOVA with Dunnett's corrections for multiple comparisons, ** $p < 0.01$.

control to 10^4 – 10^6 CFU/g tissue when co-cultured with 106-2A, ΔT6SS1, or ΔT6SS2 ($p < 0.01$). This 100-fold reduction demonstrated *V. vulnificus* T6SS1 and T6SS2 have inter-species killing activity *in vivo,* complementing previous *in vitro* data from this study. Furthermore, no reduction in *S.* Enteritidis recovery when cultured with the ΔT6SS1/2 double mutant confirmed that killing observed by wild type 106-2A and the two single T6SS mutants was T6SS-dependent.

In vivo inter-species assays were repeated at an attacker to prey ratio of 10:1 to determine whether reduction of prey *S.* Enteritidis was dose-dependent, as previously shown for intra-species competition. Negative control oysters exposed to bacteria-free AMS were enumerated on LB and ChromoSelect agar. LB agar returned natural microorganisms at 10^2 – 10^4 CFU/g tissue. Of these, ChromoSelect agar confirmed *Salmonella* species to be < 10^3 CFU/g tissue. Single strain uptake of *V. vulnificus* and *S.* Enteritidis from AMS was consistently > 10^7 CFU/g tissue and demonstrated no significant difference between samples or replicates. *In vivo* co-culture of *S.* Enteritidis with *V. vulnificus* 106-2A, ΔT6SS1, or ΔT6SS2 resulted in a significant reduction in recovered *S.* Enteritidis from > 10^7 CFU/g tissue in the single strain control to 10^2 – 10^4 CFU/g tissue ($p < 0.001$). In no oysters were *S.* Enteritidis completely removed from the oyster as was observed with intra-species competition.

To confirm that this reduction was T6SS-dependent *S.* Enteritidis was co-cultured with the ΔT6SS1/2 double mutant. Interestingly, this resulted in a significant *S.* Enteritidis reduction, with a reduction from > 10^7 CFU/g tissue in the single strain control to 5 × 10^6 CFU/g tissue in the co-culture ($p < 0.05$). Although statistically significant, the change in concentration is minimal respective to the reduction observed following co-culture with wild-type *V. vulnificus* or either single T6SSs deletion mutant. Given that

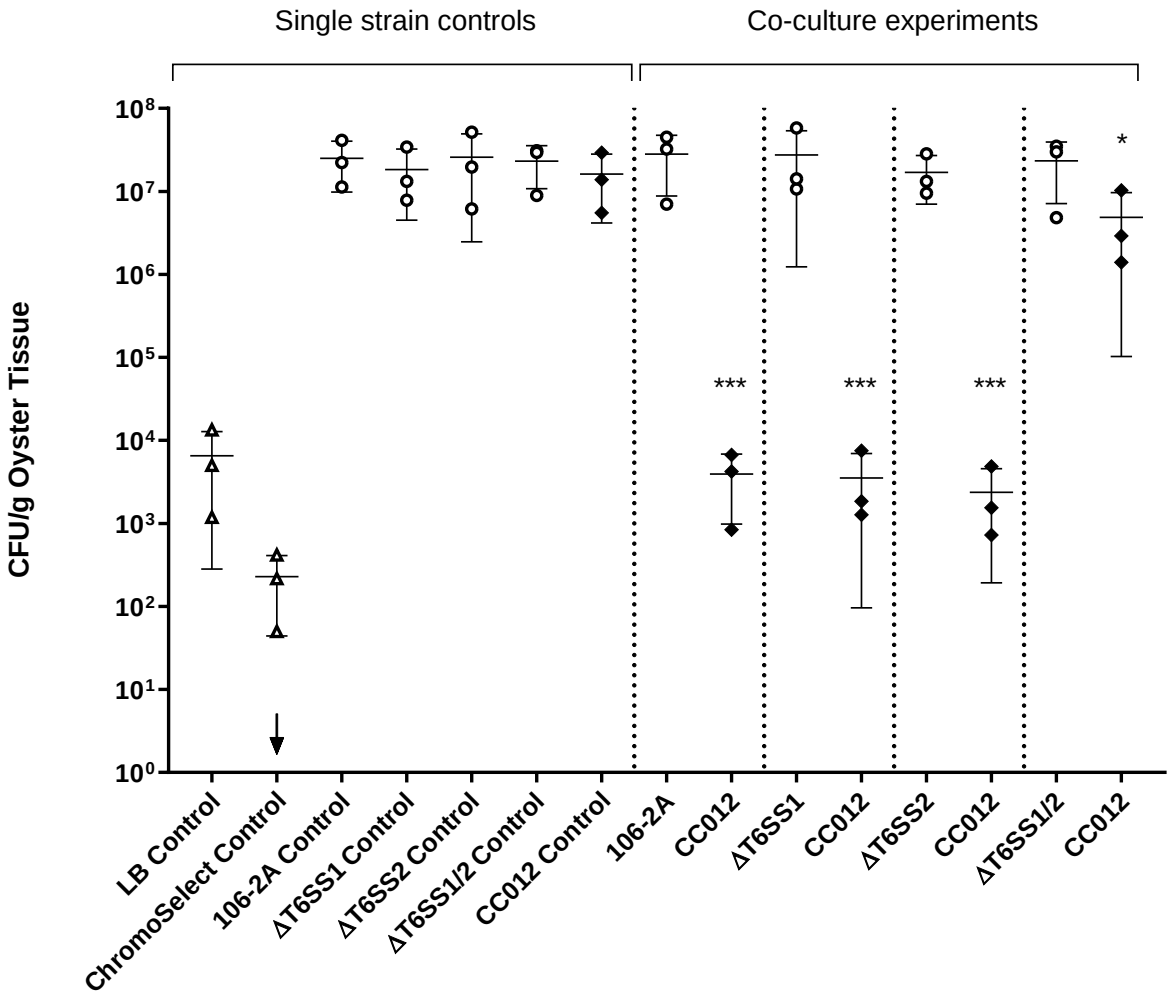

Figure 6.8: *In vivo* inter-species *V. vulnificus* co-culture with *S*. Enteritidis at an attacker to prey ratio of 10:1. *In vivo* co-culture assays were performed between attacker *V. vulnificus* strains, 106-2A, ΔT6SS1, ΔT6SS2 or ΔT6SS1/2, and prey *S.* Enteritidis CC012 for 24 hours at 21 °C at an attacker to prey ratio of 10:1. Control oysters were exposed to either bacteria-free AMS or AMS containing a single bacterial strain. Each mark represents a biological replicate consisting of six technical oyster replicates processed per strain/co-culture (n = 3). Clear triangles mark bacteria-free controls, clear circles mark attacker strains, black diamonds mark prey strains. Downward arrows indicate some replicates are below the 10^2 CFU/g tissue limit of detection. Vertical dotted lines separate the co-culture assays and controls. Horizontal lines represent the mean of the three replicates, error bars represent the standard deviation. Statistics comparing all prey strain data from the co-cultures with the prey data from the prey control and all co-culture attacker strain data with their respective attacker strain control data were performed using a nested one-way ANOVA with Dunnett's corrections for multiple comparisons, * $p < 0.05$, *** $p < 0.001$.

similar significance was observed following *V. vulnificus* 99-743 co-culture with ΔT6SS1/2, this difference was suggested to be a result of the greater concentration of attacker strain to which oysters were exposed. The extent of prey killing by 106-2A, ΔT6SS1, and ΔT6SS2 clearly demonstrated that T6SS-depedent killing was the cause of the reduction in prey numbers.

6.4. qPCR quantification of *V. vulnificus* and *S.* Enteritidis from *in vivo* oyster matrices

Probe-based TaqMan qPCR is a highly sensitive and accurate technique for microorganism enumeration from a range of environments where plate-culture may not always be possible [342]. Whilst dye-based SYBR qPCR is popular, this study employed a TaqMan probe-based qPCR due to the increased sensitivity of the sequence-specific fluorescent probe. The aim of the TaqMan qPCR was to utilise a molecular enumeration method to confirm plate-count data demonstrating antibacterial T6SS activity *in vivo*. A schematic of qPCR primer and probe binding sites can be seen in Appendix 15.

6.4.1. Generation of standard curve material

TaqMan qPCR primers and probes were designed as described in the methods (section 2.7.1) against *vvhA, vgrG1, vcgE* and *sefA*. These genes were each carefully selected to identify both 106-2A and the T6SS mutants (*vgrG1*), 99-743 (*vcgE*), *V. vulnificus* species (*vvhA*), or *S.* Enteritidis species (*sefA*). VvhA is an extracellular *V.*

vulnificus haemolysin pore-forming toxin commonly used as a marker for the species [343–345]. This probe was employed as a *V. vulnificus* species control to identify natural *V. vulnificus* in negative controls. VgrG1 forms part of the tip complex of the T6SS1 and is therefore only present in T6SS1$^+$ attacker *V. vulnificus* strains, 106-2A, ΔT6SS1, ΔT6SS2, and ΔT6SS1/2 [346]. Whilst *vcgE* does not encode a protein, it is only identified in E-type *V. vulnificus,* such as 99-743 [43]. SefA is a *S.* Enteritidis fimbrin protein involved in actin-cross-linking and was therefore utilised as a *Salmonella*-specific probe [347].

To enable absolute quantification of *V. vulnificus* and *S.* Enteritidis from oyster matrices, standard curves were generated against which experimental samples could be plotted to determine copy number/μL and total CFU/oyster. Standards were generated by cloning the fragments of *vvhA, vgrG1, vcgE* and *sefA* amplified by the qPCR primers designed for the assay into holding vector, pGEM-T Easy. Plasmid maps for pGEM-T Easy–*vvhA,* pGEM-T Easy–*vgrG1,* pGEM-T Easy–*vcgE* and pGEM-T Easy–*sefA* are shown in Appendix 14. Once constructed, purified plasmid DNA was adjusted to a series of standard concentrations, ranging from 10^8 – 10^3 copies/μL for *vgrG1* and 10^8 – 10^1 copies/μL for *vcgE, sefA* and *vvhA* as these samples required greater sensitivity due to lower concentrations observed using plate-counts.

6.4.2. qPCR optimisation and standard curve generation

To ensure accurate absolute quantification of *V. vulnificus* and *S.* Enteritidis from oyster matrices TaqMan qPCR primer and probe concentrations were optimised to ensure the consistent generation of a standard curve with an r^2 value ≥ 0.99. Any curve

< 0.99 was not determined accurate enough for enumeration purposes. Primers and probes were designed according to the methods (section 2.7.1) (Appendix 15).

Primer concentration was first optimised through combination of forward and reverse primers at 50, 100, 200, 400, 600 and 800 nM so that every concentration of the forward primer was tested with every concentration of the reverse primer. Fig. 6.10A/B shows the optimisation of *vgrG1* as a representative example for all qPCRs. The optimal combination of forward and reverse primer concentrations was determined by which combination resulted in a sigmoidal curve at the earliest cycle number. The results varied between qPCRs and can be seen in Table 2.5. Once established, probe concentration was optimised by testing at 50, 100, 200, 400, 600 and 800 nM (Fig. 6.10C). The probe concentration resulting in a sigmoidal curve at the earliest cycle number was deemed optimal. Finalised probe concentrations for *vvhA, vcgE, vgrG1,* and *sefA* are also listed in Table 2.5.

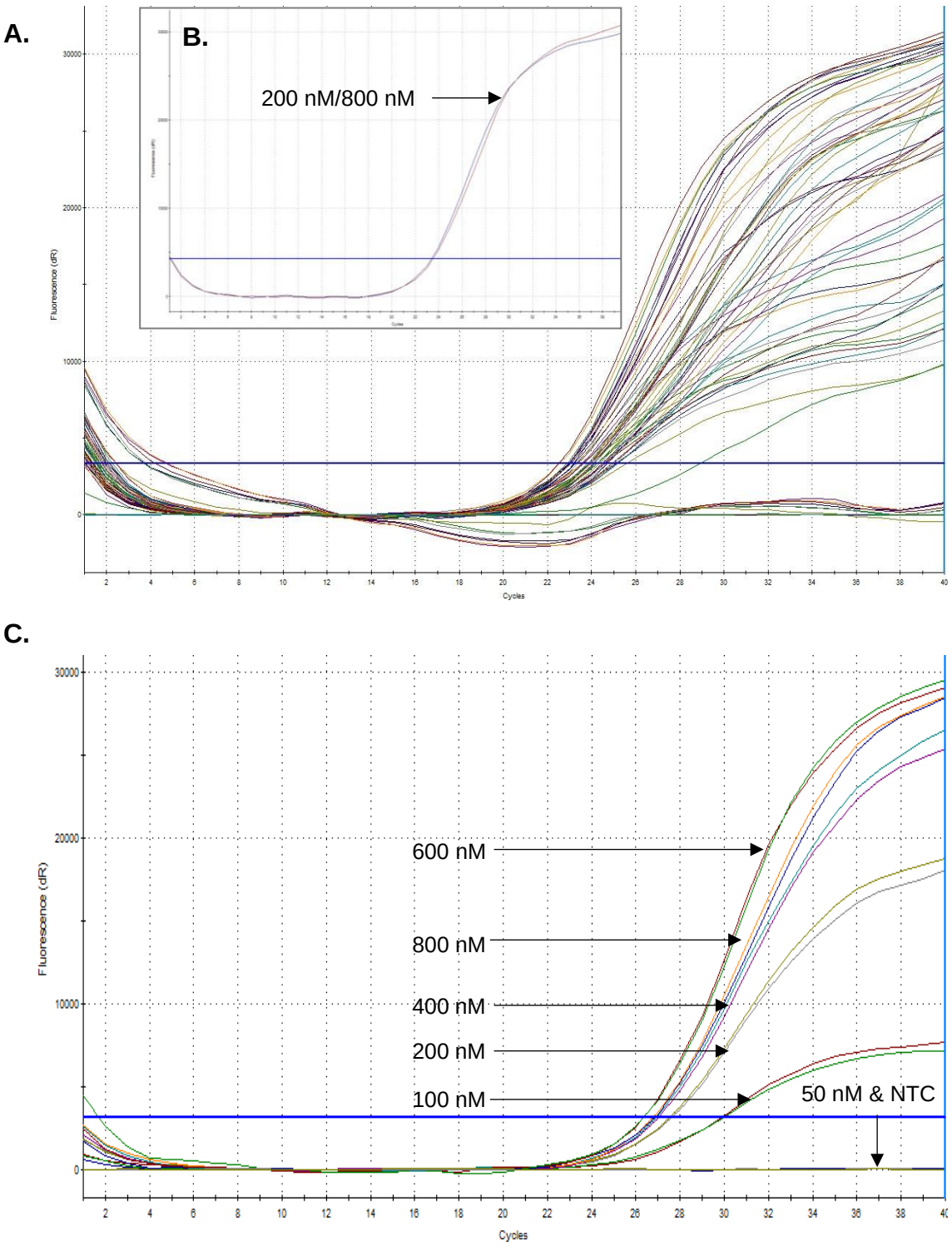

Figure 6.10: *vgrG1* qPCR primer and probe optimisation. (A) Primer optimisation amplification plots. The horizontal blue line represents the cycle threshold (Ct). **(B)** Optimised *vgrG1* primer concentrations and the resulting sigmoidal curve. FWD primer – 200nM, REV primer – 800 nM. **(C)** Probe optimisation plots utilising the optimised primer concentration. Probe concentration was assessed at 50, 100, 200, 400, 600, and 800 nM. A no-template control (NTC) using H_2O in place of template DNA was included.

Having optimised primer and probe concentrations, standard curves for quantification were generated. A representative standard curve can be seen in Fig. 6.11 for *vgrG1* following optimisation. Each standard was loaded in triplicate to account for pipetting error. As can be seen, amplification of 10^8 – 10^3 copies/μL standards generates a robust standard curve with an r^2 value of 0.994, meeting the > 0.99 value required for absolute quantification. To ensure standard curve generation was consistent, each curve was generated in triplicate on separate days and using different reagents and template DNA stocks.

Unfortunately, this study was unable to effectively generate standard curves for *vcgE, sefA* and *vvhA* which included 10^2 and 10^1 copies/μL standards. Despite optimisation there appeared to be too much variability at these low concentrations to generate a consistent curve with an acceptable r^2 value of > 0.99. The lowest standard for these curves was therefore 10^3 copies/μL. An example of these ineffective standard curves including the 10^2 and 10^1 standards can be seen in Appendix 16. This presented a problem in that the limit of detection for these qPCRs was limited to 10^3 copies/μL of extracted DNA. However, oyster homogenates had been diluted 10-fold, and the extracted DNA dissolved in 100 μL ddH_2O (of which 5 μL was used as template). Therefore, qPCR quantification data had to be multiplied by 200 to calculate the concentration of bacteria in the original samples. This resulted in 10^5 CFU/g tissue being the lowest bacterial concentration possible to enumerate. It was decided to perform the qPCR assays regardless and simply denote samples where amplification was < 10^5 CFU/g tissue with a downwards arrow.

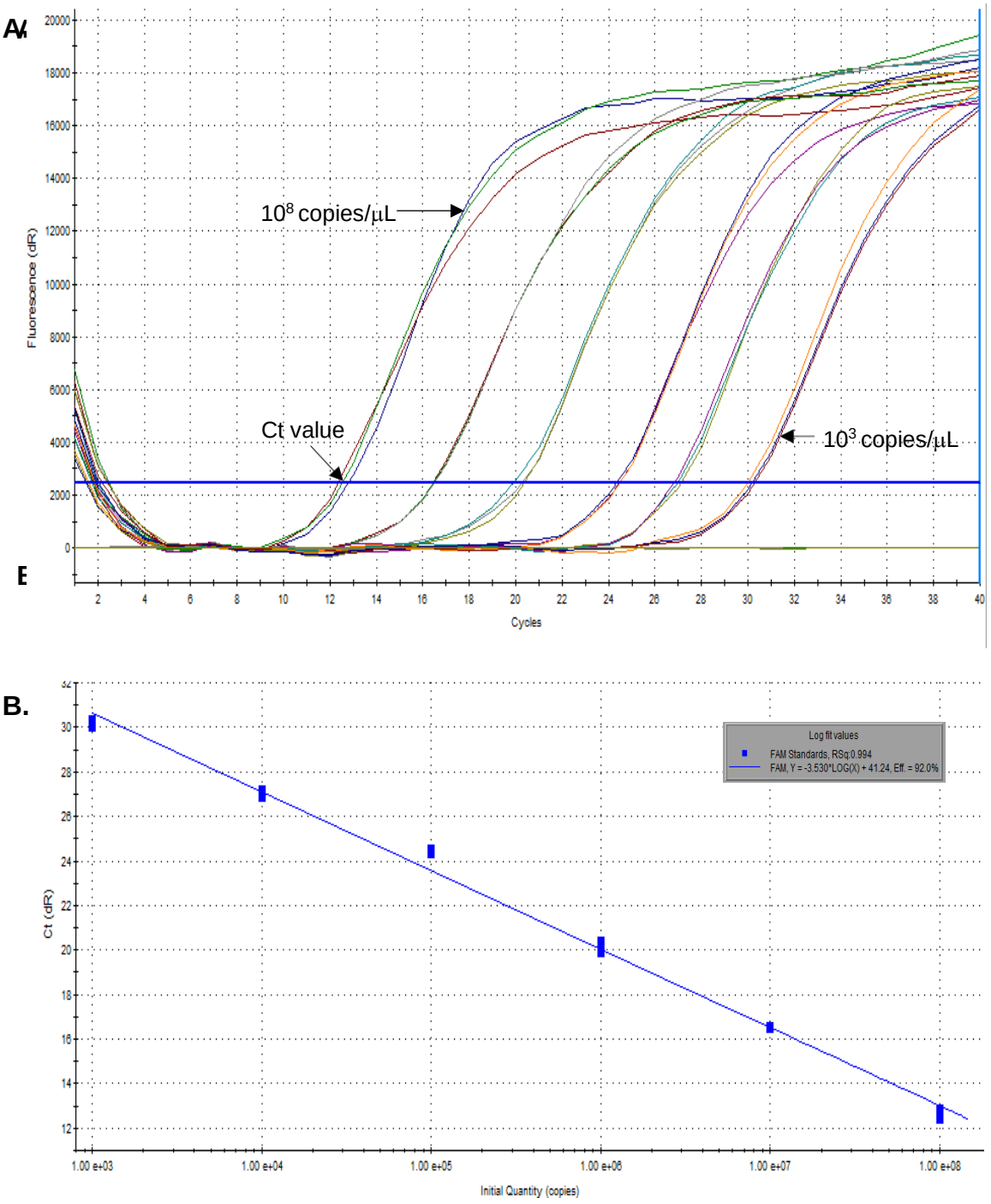

Figure 6.11: Optimised *vgrG1* standard curve. (A) Amplification of qPCR standards from 10^8 – 10^3 copies/µL. Each standard was run in triplicate to account for pipetting error. **(B)** A representative *vgrG1* standard curve generated using the amplification from the top image. Higher copy number standards result in lower Ct values due to increased amplification resulting in greater fluorescence. As lower concentration standards have less template material it take a greater number of cycles for fluorescence to cross the Ct and for amplification to be detected. An r^2 value of 0.994 indicates that this curve would be suitable for quantification.

6.4.3. qPCR quantification of *V. vulnificus* and *S.* Enteritidis from single strain uptake experiments

Once *vvhA, vgrG1, vcgE* and *sefA* qPCRs had been successfully optimised, DNA extracted from oyster homogenates was utilised as template for qPCR enumeration of *V. vulnificus* and *S.* Enteritidis CC012. Firstly, *V. vulnificus* and *S.* Enteritidis were enumerated from the single strain uptake controls shown previously in Fig. 6.2. Comparison of qPCR quantification data and plate count enumeration can be seen in Fig. 6.12. As observed, qPCR quantification resulted in highly similar CFU/g tissue results compared to plate enumeration with none of the assessed strains demonstrating significantly different results following comparison.

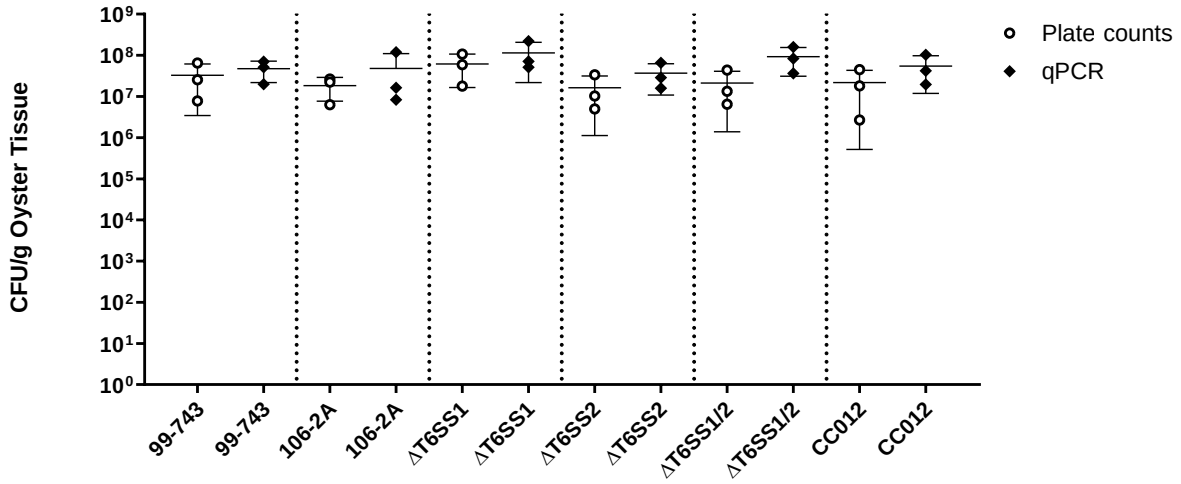

Figure 6.9: Comparison of qPCR and plate count enumeration of *V. vulnificus* and *S.* Enteritidis from oysters matrices. Optimised qPCR assays were utilised to quantify *V. vulnificus* 99-743, 106-2A, ΔT6SS1, ΔT6SS2, ΔT6SS1/2, and *S.* Enteritidis CC012 from oyster homogenates previously enumerated using plate-counts (Fig. 6.2). Plate counts are represented by clear circles, qPCR counts by black diamonds. Each mark represents the mean of six technical oyster replicates (n = 3). Horizontal lines represent the mean, error bars represent the standard deviation, vertical lines separate comparisons between strains. Statistics comapring plate count data versus qPCR data for each strain were performed using individual unpaird t-tests, no data showed significant differences.

6.4.4. qPCR quantification of *V. vulnificus* from *in vivo* intra-species co-culture assays

DNA extracted from oyster homogenates from 5:1 and 10:1 bacterial co-culture assays was utilised as template DNA in qPCR assays to quantify *V. vulnificus* loads in oyster tissue. qPCR data was compared to plate-count data to confirm that observed results were consistent across different methods of enumeration. Quantification of intra-species killing between *V. vulnificus* attacker and prey strains can be seen in Fig. 6.13. As previously discussed, qPCR reactions had a 10^3 copies/μL accuracy limit, and therefore could not enumerate bacteria present at < 10^5 CFU/g tissue. For this reason, qPCR was unable to quantify the levels of natural *V. vulnificus* in the oyster samples using the *vvhA* probe and this has been indicated with a downwards arrow.

Quantification of single strain controls confirmed uptake of attacker and prey *V. vulnificus* strains by oysters at concentrations > 10^7 CFU/g tissue (Fig. 6.13). Attacker strain concentrations remained > 10^7 CFU/g tissue following co-culture with prey *V. vulnificus* 99-743 for 24 hours at 21 °C. However, prey 99-743 demonstrated a significant reduction from > 10^7 CFU/g tissue to 10^5 – 10^7 CFU/g tissue following co-culture with 106-2A, ΔT6SS1, and ΔT6SS2 ($p < 0.05$, $p < 0.01$). No significant

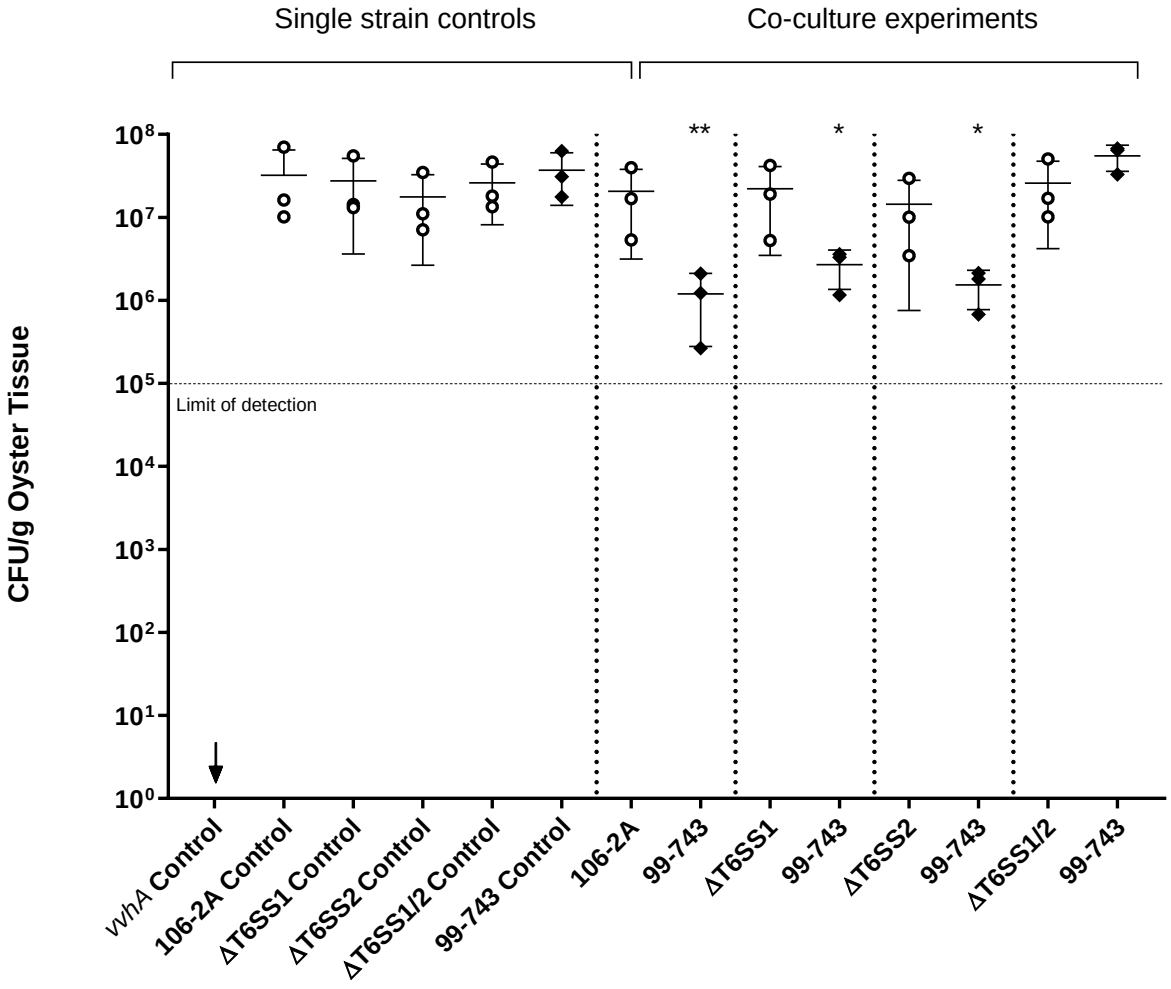

Figure 6.10: qPCR quantification of *V. vulnificus* from *in vivo* intra-species co-culture. *In vivo* co-culture assays were performed between attacker *V. vulnificus* strains, 106-2A, ΔT6SS1, ΔT6SS2 or ΔT6SS1/2, and prey *V. vulnificus* 99-743 for 24 hours at 21 °C at an attacker to prey ratio of 5:1. Control oysters were exposed to either bacteria-free AMS or AMS containing a single bacterial strain. Each mark represents a biological replicate consisting of six technical oyster replicates processed per strain/co-culture (n = 3). Clear circles mark attacker strains, black diamonds mark prey strains. Downward arrows indicate some replicates are below the 10^5 CFU/g tissue limit of detection. Vertical dotted lines separate the co-culture assays and controls. Horizontal lines represent the mean of the three replicates, error bars represent the standard deviation. Statistics comparing all prey strain data from the co-cultures with the prey data from the prey control and all co-culture attacker strain data with their respective attacker strain control data were performed using a nested one-way ANOVA with Dunnett's corrections for multiple comparisons, * $p < 0.05$, ** $p < 0.01$.

reduction in prey 99-743 was observed when co-cultured with the double mutant, ΔT6SS1/2, confirming that this killing was T6SS-dependent. This data confirms plate count enumeration results and supports the finding that *V. vulnificus* T6SS1 and T6SS2 are active and employed in intra-species competition in an environmentally representative model.

Quantification of 99-743 from 10:1 co-culture assays by qPCR confirmed consistent uptake of attacker and prey strains at > 10^7 CFU/g tissue (Fig. 6.14). As demonstrated by plate enumeration, 99-743 showed significantly greater reduction at an attacker to prey ratio of 10:1 compared to 5:1. Due to the limitations of the qPCR assay at these low bacterial concentrations no data was recovered for these samples. However, the absence of qPCR data confirms that these samples were below the 10^3 copies/μL threshold, indicating that 99-743 was not present in oysters at > 10^5 CFU/g tissue. Interestingly, whilst plate-count enumeration of 10:1 intra-species competition showed a small but significant reduction of 99-743 when co-cultured with ΔT6SS1/2 ($p < 0.01$) (Fig. 6.7), qPCR quantification shows no significant difference between 99-743 from co-culture vs 99-743 from single strain controls.

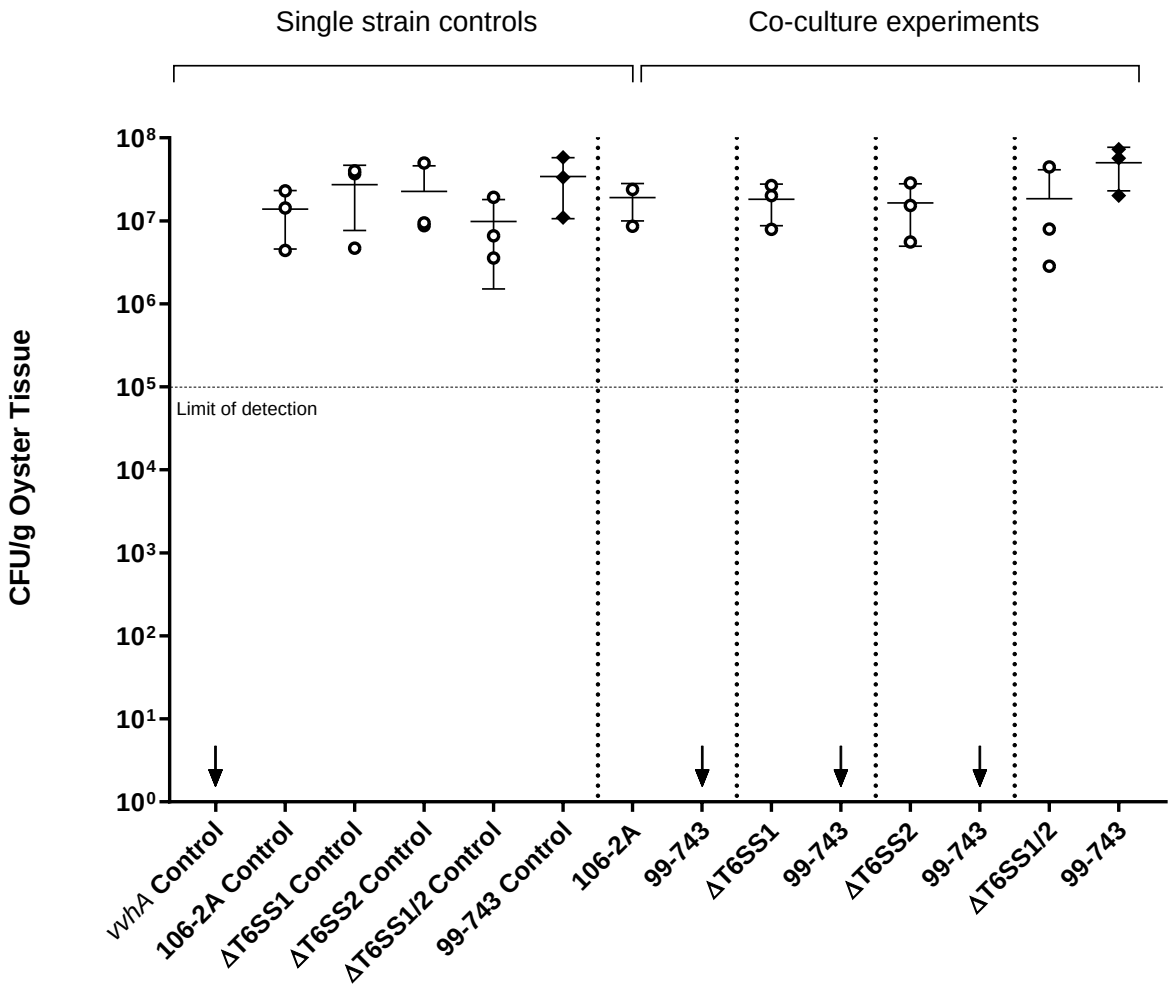

Figure 6.11: qPCR quantification of *V. vulnificus* from *in vivo* intra-species co-culture. *In vivo* co-culture assays were performed between attacker *V. vulnificus* strains, 106-2A, ΔT6SS1, ΔT6SS2 or ΔT6SS1/2, and prey *V. vulnificus* 99-743 for 24 hours at 21 °C at an attacker to prey ratio of 10:1. Control oysters were exposed to either bacteria-free AMS or AMS containing a single bacterial strain. Each mark represents a biological replicate consisting of six technical oyster replicates processed per strain/co-culture (n = 3). Clear circles mark attacker strains, black diamonds mark prey strains. Downward arrows indicate some replicates are below the 10^5 CFU/g tissue limit of detection. Vertical dotted lines separate the co-culture assays and controls. Horizontal lines represent the mean of the three replicates, error bars represent the standard deviation. Statistics comparing all prey strain data from the co-cultures with the prey data from the prey control and all co-culture attacker strain data with their respective attacker strain control data were performed using a nested one-way ANOVA with Dunnett's corrections for multiple comparisons.

6.4.5. qPCR quantification of *V. vulnificus* and *S.* Enteritidis from *in vivo* inter-species co-culture assays

Inter-species *in vivo* killing assays between *V. vulnificus* attacker strains and prey *S.* Enteritidis CC012 were similarly assessed via qPCR using the *sefA* probe to quantify CC012. Fig. 6.15 shows qPCR quantification of attacker and prey strains following co-culture at an attacker to prey ratio of 5:1. As previously discussed, the developed qPCRs lacked the sensitivity to detect bacterial loads < 10^5 CFU/g tissue and therefore this study was unable to accurately enumerate CC012 from negative control oysters. Whilst this confirms bacterial loads are < 10^5 CFU/g tissue, it is unable to accurately identify an exact concentration.

Single strain uptake controls demonstrated consistent uptake of attacker and prey strains at > 10^7 CFU/g tissue, as observed previously in intra-species co-culture assays. Attacker bacterial loads remain > 10^7 CFU/g tissue in all co-culture oysters also, demonstrating no reduction from co-culture with CC012. However, quantification of prey CC012 showed a significant reduction from > 10^7 CFU/g tissue to as low as 10^5 CFU/g tissue when co-cultured with 106-2A, ΔT6SS1 and ΔT6SS2 ($p < 0.05$, $p < 0.01$). Co-culture of CC012 with ΔT6SS1/2 shows no significant CC012 reduction compared to the CC012 single strain control, confirming that CC012 reduction with other attacker strains, ΔT6SS1 and ΔT6SS2, was T6SS-dependent.

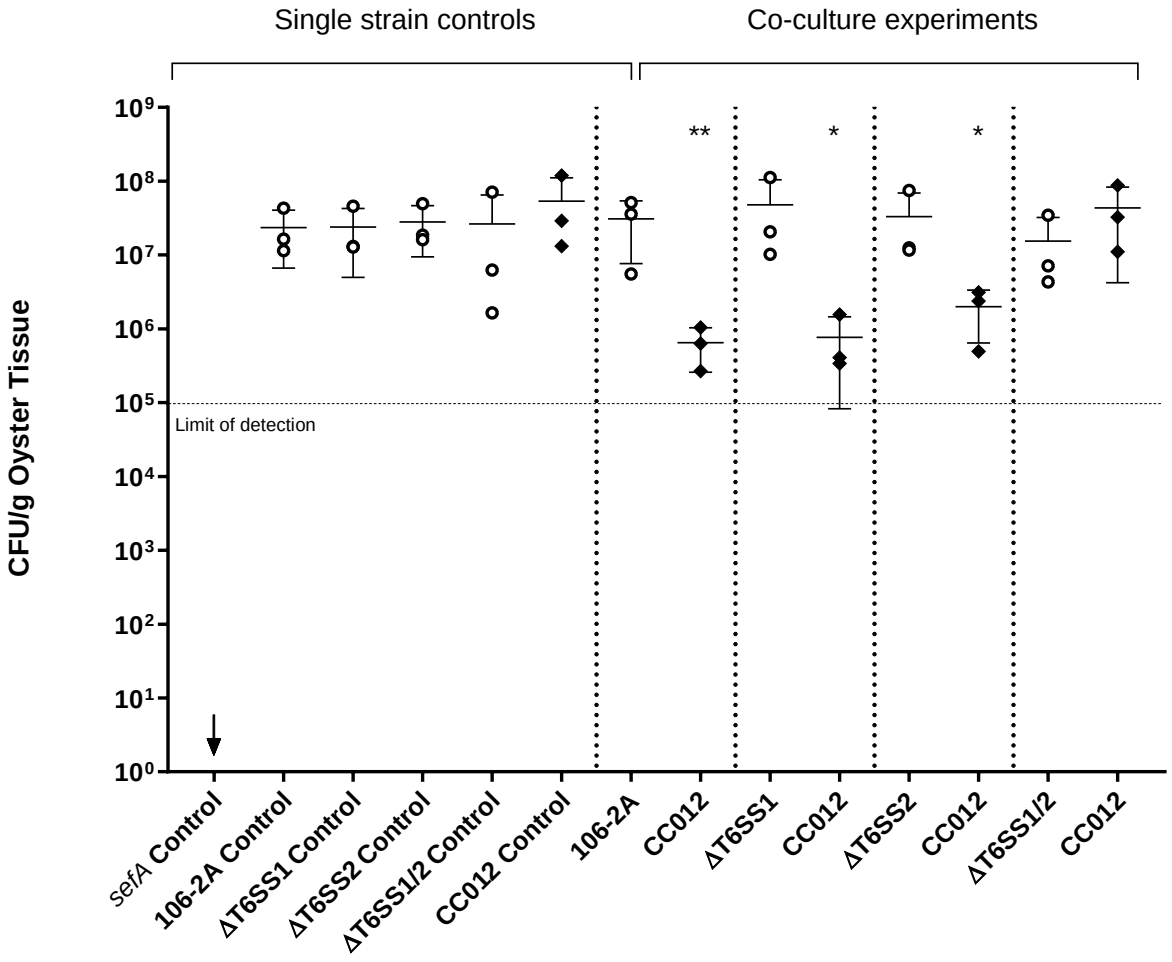

Figure 6.12: qPCR quantification of *V. vulnificus* and *S.* Enteritidis from *in vivo* inter-species co-culture. *In vivo* co-culture assays were performed between attacker *V. vulnificus* strains, 106-2A, ΔT6SS1, ΔT6SS2 or ΔT6SS1/2*,* and prey *S*. Enteritidis CC012 for 24 hours at 21 °C at an attacker to prey ratio of 5:1. Control oysters were exposed to either bacteria-free AMS or AMS containing a single bacterial strain. Each mark represents a biological replicate consisting of six technical oyster replicates processed per strain/co-culture (n = 3). Clear circles mark attacker strains, black diamonds mark prey strains. Downward arrows indicate some replicates are below the 10^5 CFU/g tissue limit of detection. Vertical dotted lines separate the co-culture assays and controls. Horizontal lines represent the mean of the three replicates, error bars represent the standard deviation. Statistics comparing all prey strain data from the co-cultures with the prey data from the prey control and all co-culture attacker strain data with their respective attacker strain control data were performed using a nested one-way ANOVA with Dunnett's corrections for multiple comparisons, * $p < 0.05$, ** $p < 0.01$.

Fig. 6.16 shows *V. vulnificus* and *S.* Enteritidis enumeration from oysters following co-culture at an attacker to prey ratio of 10:1. Single strain controls showed uptake of attacker and prey strains at 10^6 – 10^8 CFU/g tissue. However, quantification of CC012 following co-culture with 106-2A, ΔT6SS1, and ΔT6SS2 resulted in no detection of CC012 by qPCR, indicating that bacterial concentrations within oysters were < 10^5 CFU/g tissue. Whilst qPCR was unable to accurately determine the exact concentrations of CC012 within oyster matrices, this data did confirm that CC012 reduction was greater at an attacker to prey ratio of 10:1 than 5:1, as expected and demonstrated previously by plate count enumeration. Interestingly, no significant CC012 reduction was observed following co-culture with the double T6SS mutant as was previously seen for the 10:1 assay plate count data (Fig. 6.9).

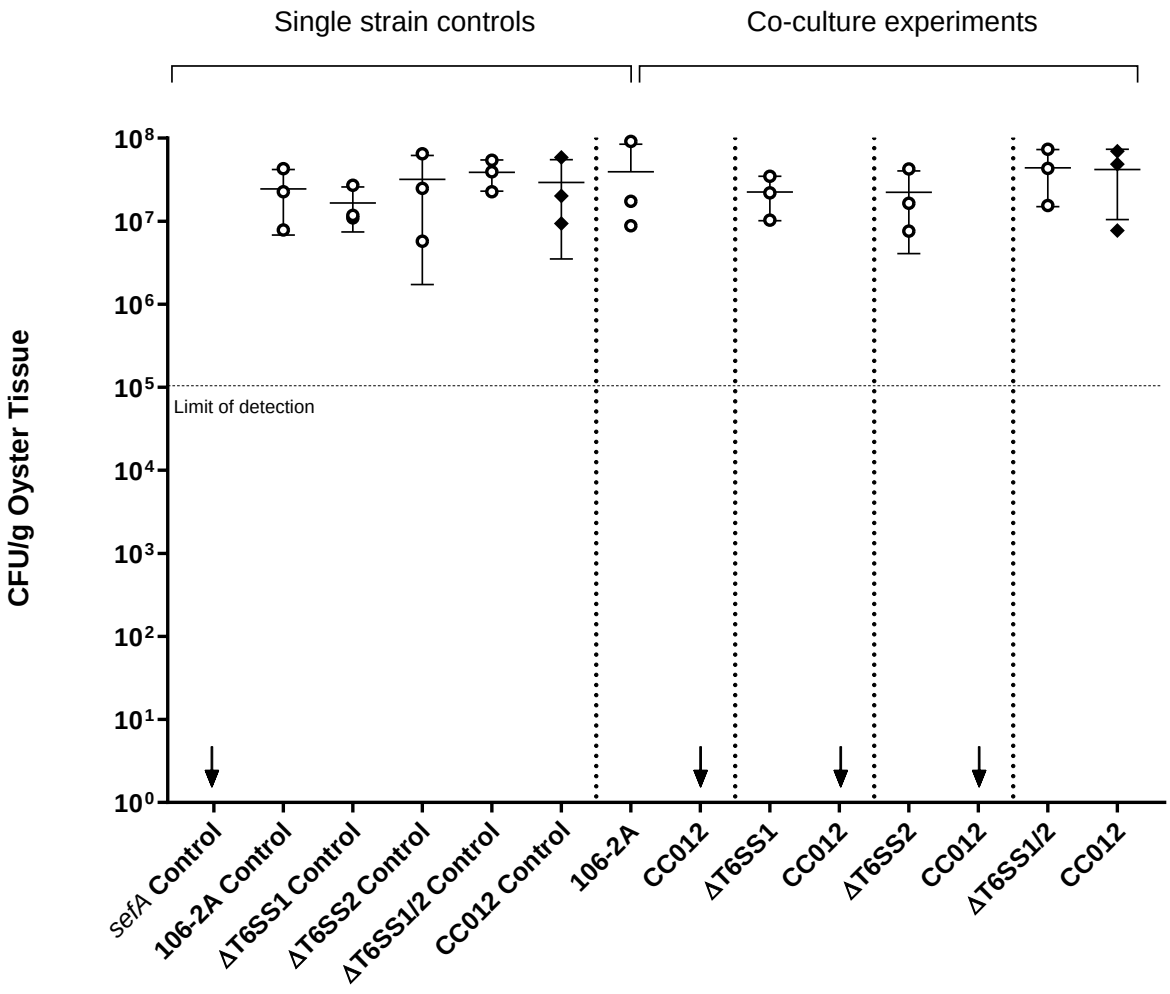

Figure 6.13: qPCR quantification of *V. vulnificus* and *S.* Enteritidis from *in vivo* inter-species co-culture. *In vivo* co-culture assays were performed between attacker *V. vulnificus* strains, 106-2A, ΔT6SS1, ΔT6SS2 or ΔT6SS1/2, and prey *S*. Enteritidis CC012 for 24 hours at 21 °C at an attacker to prey ratio of 10:1. Control oysters were exposed to either bacteria-free AMS or AMS containing a single bacterial strain. Each mark represents a biological replicate consisting of six technical oyster replicates processed per strain/co-culture (n = 3). Clear circles mark attacker strains, black diamonds mark prey strains. Downward arrows indicate some replicates are below the 10^5 CFU/g tissue limit of detection. Vertical dotted lines separate the co-culture assays and controls Horizontal lines represent the mean of the three replicates, error bars represent the standard deviation. Statistics comparing all prey strain data from the co-cultures with the prey data from the prey control and all co-culture attacker strain data with their respective attacker strain control data were performed using a nested one-way ANOVA with Dunnett's corrections for multiple comparisons

This chapter confirms that the T6SS1 and T6SS2 of *V. vulnificus* 106-2A are active in an oyster *in vivo* model, where the systems demonstrate antibacterial activity against both *V. vulnificus* and *S.* Enteritidis strains. These results support *in vitro* findings previously described in this study (Chapter 3) which show that both the T6SS1 and the T6SS2 have antibacterial activity at 21 °C. This is first study to describe the activity of the T6SS2 of *V. vulnificus* and the first to characterise the activity of both *V. vulnificus* T6SSs *in vivo*.

Discussion

This chapter describes the application of AMS for facilitating oyster uptake of bacteria. Animals exposed to AMS inoculated with *V. vulnificus* and *S.* Enteritidis demonstrated significantly higher bacterial uptake than previous studies in which oysters' tanks were simply inoculated with planktonic bacteria. Using this *in vivo* oyster model, a role for the T6SS1 and the T6SS2 of *V. vulnificus* in intra-species killing *in vivo* has been identified. Furthermore, similar killing activity was demonstrated against *S.* Enteritidis, showing that *V. vulnificus* T6SSs are antibacterial and are involved in both intra and inter-species competition *in vivo*.

Vibrios are ubiquitous aquatic microorganisms that have the potential to cause fatal human disease, thus it is essential to understand their ecology and apply this knowledge to manage disease spread and prevention. Investigating *Vibrio* ecology is important for food security concerns due to the threat pathogenic *Vibrios* present to the aquaculture industry. The State of the World Fisheries and Aquaculture (SOFIA) report (2018) describes 80 million tonnes of aquaculture produced in 2016, of which molluscs totalled 17.1 million tonnes (47 % of global production) [348]. However,

intensive farming practices are resulting in large-scale seasonal losses due to pathogenic *Vibrio* species [349,350]. *Vibrio splendidus* is an oyster pathogen that has been responsible for consistent seasonal oyster losses of up to 80 % over a 10-year period in the bay of Morlaix, France [351].

For this reason, it is important that studies can effectively explore bacteria-host interactions using an oyster model. However, many of these studies rely on the uptake of planktonic bacteria by oysters, which is inefficient and results in low-level bacterial uptake [246,253,255,257]. This is due to filter-feeding shellfish preferentially retaining particles above a certain size threshold, which planktonic bacteria do not attain [249]. Marine snow was first characterised in 1930s, and its role in nutrient transport in the ocean is well understood [258,331,352]. Froelich and Oliver, (2013) were the first to explore incorporation of bacteria, specifically *V. vulnificus*, into NMS for uptake by oysters [249]. However, incorporation into NMS and subsequent uptake by oysters was low-level, at ~ 10^5 CFU/mL in NMS and 10^2 – 10^3 CFU/g tissue, respectively. The data presented in this study demonstrates that aggregation of *T. pseudonana* results in a significantly more effective and reproducible AMS model for bacterial incorporation. Subsequent exposure of inoculated AMS to oysters for uptake of incorporated bacteria resulted in highly successful uptake and retention, with all strains ingested at > 10^7 CFU/g tissue on average. Bacterial loads in oysters > 10^7 CFU/g tissue uptake is significantly higher than any other study published to date and demonstrates the superiority of AMS to all current oyster inoculation techniques. Furthermore, as levels of naturally occurring bacteria in oysters were ~ 10^4 CFU/g tissue, this model ensures that exogenous bacteria greatly outnumber native microorganisms, reducing the impact potentially presented by any interactions between native and exogenous bacteria. No significant difference in uptake between different bacterial strains and species over 48 hours

indicates that this model facilitates even uptake of whichever strain or species has been incorporated, allowing for easy co-culture of various strains and species. Interestingly, despite oysters being exposed to 10-fold higher bacterial concentrations in the 10:1 assays versus the 1:1 assays, no significant difference was observed in bacterial uptake between the groups. This suggests that there may be a physical limit to the volumes of bacteria which oysters can accommodate.

The success of the AMS model reported in this thesis suggests potential use in a wider range of applications outside of research. Global awareness regarding the reduction of antibiotic use in agriculture and aquaculture has led to a directed effort to identify novel methods of pathogen control. One such application is the use of 'probiotic' bacteria that either kill or directly compete with dangerous pathogens, reducing their impact and viability. A recent study by Stevick *et al*., (2019) showed that the addition of probiotic *Bacillus pumilus* to oyster rearing tanks aided in larval survival following challenge with the oyster pathogen, *Vibrio coralliilyticus* [353]. Similarly, Kang *et al*., (2018) identified novel applicable probiotic activity of *Enterococcus faecium* [354]. Co-culture of *E. faecium* and *V. parahaemolyticus* in oysters at 10^5 CFU/mL resulted in a 10-fold decrease in recovered *V. parahaemolyticus*. However, *E. faecium* incorporation into AMS would result in greater uptake by oysters, potentially facilitating more effective reduction of *V. parahaemolyticus* numbers and increasing food safety.

As expected, natural bacteria were always isolated from control oysters exposed to bacteria-free AMS, despite professional depuration. Bivalve depuration involves placing shellfish in continuously circulating, UV-treated water to eliminate any expunged microorganisms [355]. Whilst effective for reducing natural bacteria to safe concentrations for human consumption, microflora are never entirely cleared [233]. It was initially theorised that this endogenous natural population may have some impact on

in vivo killing assays, whether through killing of either attacker or prey strains, or competing with exogenous bacteria for oyster colonisation. However, comparison of natural bacteria levels to levels of exogenous bacteria showed that the uptake of exogenous bacteria from AMS was so significantly greater that it was not considered to be a conflicting factor. Uptake of AMS containing exogenous bacteria resulted in attacker and prey strain concentrations in oysters at 10,000-fold greater levels than the natural population. No significant difference was observed between levels of attacker and prey bacteria individually introduced into oysters using AMS. This indicates that no exogenous strain or species was negatively impacted by any naturally occurring microorganisms within the oysters. Uptake of exogenous bacteria from AMS was so effective that a small population of native microorganisms would be unlikely to noticeably impact the viability of exogenous populations.

Significant T6SS-dependent killing of prey *V. vulnificus* 99-743 was observed following co-culture with 106-2A, ΔT6SS1 or ΔT6SS2 within oysters. A lack of prey reduction when co-cultured with the double mutant, ΔT6SS1/2, confirmed that this killing was due to activity of the T6SS1 and T6SS2 of *V. vulnificus*. Having demonstrated *in vivo* intra-species competition, further studies were performed to confirm that *V. vulnificus* was also capable of utilising its T6SSs for inter-species competition. Oysters were exposed to AMS inoculated with *S.* Enteritidis CC012 and attacker *V. vulnificus* strains. As observed for intra-species co-culture, a significant reduction of prey *S.* Enteritidis was recorded following co-culture with 106-2A, ΔT6SS1, and ΔT6SS2 but not ΔT6SS1/2, confirming inter-species *in vivo* killing activity of the *V. vulnificus* T6SS1 and T6SS2.

All plate count enumeration data in this study was confirmed using qPCR. Four qPCR assays were designed and optimised for absolute quantification of all *V. vulnificus* species, all *Salmonella* species, and *V. vulnificus* 106-2A, *V. vulnificus* ΔT6SS1, *V. vulnificus* ΔT6SS2, *V. vulnificus* ΔT6SS1/2, and *V. vulnificus* 99- 743. Initially, it was expected that qPCRs would identify significantly greater bacterial concentrations than plate count enumeration. This was because qPCR would also quantify free DNA from dead bacteria and DNA from VBNC bacteria not detected by plate culture. However, whilst qPCR quantification was typically higher than respective plate counts, the increase was marginal, confirming the reliability of the plate count data described by this study. It was expected that there would be a greater difference between the plate count data and the qPCR data when enumerating bacteria from oysters due to the ability of qPCR to also enumerate free DNA released from dead cells. Jana *et al*., (2019) describes the discovery of a widespread DNase toxin domain in a range of Gram-negative and Gram-positive bacteria, termed PoNe (Polymorphic Nuclease effector) [224]. PoNe domains are commonly fused to delivery domains of T6SS proteins and suggest that *V. vulnificus* may employ nuclease effectors to kill target bacteria. The degradation of bacterial DNA upon death would limit the volume of free DNA released from dead cells, therefore reducing the final counts provided by the qPCR assay. Further genomic investigation would be required to identify whether PoNe domains are found in *V. vulnificus*. Their identification in close *V. vulnificus* relative, *V. parahaemolyticus,* suggests it is a possibility, however more research is required.

Significantly greater killing of prey bacteria was observed *in vivo* compared to *in vitro* assays. The most obvious explanation for which was the increased volumes of attacker to prey bacteria utilised. *In vitro* assays were performed at an attacker to prey

ratio of 3:1, whereas *in vivo* assays were performed at both 5:1 and 10:1. As T6SS activity is contact dependent it is expected that increasing the concentrations of the attacking strain would increase contact between attacker and prey strains, facilitating increased prey strain killing. However, it is also possible that the oyster stomach environment plays a role in promoting T6SS activity. More specifically, that the less nutrient-rich oyster stomach may promote up-regulation of *V. vulnificus* T6SSs to facilitate more effective competition with neighbouring microorganisms. Recently, the T6SSs of *B. thailandensis, P. aeruginosa* and *Yersinia pseudotuberculosis* have all been shown to secrete effectors involved in the acquisition of essential nutrients such as iron, zinc and manganese [228,305,356]. In *P. aeruginosa,* iron down-regulates H2-T6SS expression by binding to two ferric uptake repressor (Fur) sequences, known as Fur boxes, overlapping predicted σ^{70} promoters [356]. High iron concentration results in increased binding of Fur proteins to the Fur boxes, reducing HS-T6SS expression. *Y. pseudotuberculosis* RelA, a stress-response protein also found in *V. vulnificus*, directly upregulates expression of the T6SS4 in response to nutrient starvation conditions [305,357]. Whilst a simple model, the conditions within the oyster stomach are not well characterised and therefore it is hard to say to exactly which conditions ingested bacteria are exposed. It is possible that the T6SS1 and T6SS2 of *V. vulnificus* are upregulated under *in vivo* conditions, resulting in the observed increase in T6SS-dependent killing, although further work would be required to test this hypothesis.

Whilst this is the first study to date to demonstrate *V. vulnificus* intra and inter-species competition in an oyster model, this is not the first study to demonstrate the role of a *Vibrio* T6SS in *in vivo* competition. Speare *et al.,* (2018) demonstrate that *V. fischeri* employs a T6SS2 to target and kill competing strains in the light-organ crypts of a *Euprymna scolopes* squid model [173]. Interestingly, that study showed that whilst 'lethal'

and ‘nonlethal’ strains were unable to coexist due to killing of the nonlethal strain, two lethal strains were able to coexist with one another due to continued killing of the other strain [173]. This further supports a possible role for the T6SS in *V. vulnificus* ecology, where even though two ‘attacker’ strains may possess lethal T6SS machinery to which the other strain does not express the requisite immunity proteins, reciprocal killing of each strain by the other ensures that both strains are equally capable of surviving within that niche.

Conclusions

This chapter successfully demonstrates that the defined AMS model developed by this study facilitates efficient and reproducible uptake of incorporated bacteria by oysters. This model was shown to function for both *V. vulnificus* and *S.* Enteritidis strains and presents a novel methodology for promoting bacterial uptake by oysters for both research and aquaculture purposes. AMS was utilised to ensure uptake of attacker and prey *V. vulnificus* and *S.* Enteritidis for *in vivo* co-culture assays. The results of these assays confirm previous *in vitro* data that the T6SSs of *V. vulnificus* 106-2A have antibacterial activity *in vivo*. This data suggests that the T6SS may play a significant role in the establishment of *V. vulnificus,* and other T6SS^{+} bacteria, *in vivo*.

Chapter Seven

Concluding remarks and future work

V. vulnificus is an opportunistic human pathogen, capable of causing severe fulminating infection and death if not treated rapidly. Previous studies attempting to characterise the virulence potential of environmental and clinical *V. vulnificus* isolates identified two T6SSs, named the T6SS1 and the T6SS2 [172]. The T6SS has been identified across a wide range of Gram-negative bacteria and has been shown to have roles in bacterial competition, nutrient acquisition, natural competence and immune cell killing. The aim of this PhD was to characterise the roles of the T6SS1 and T6SS2 of *V. vulnificus* under environmental conditions to assess the roles of these T6SSs in the ecology of this bacterium.

In vitro bacterial co-culture killing assays demonstrated that attacker *V. vulnificus* 106-2A (T6SS1$^+$/T6SS2$^+$) was able to target and kill prey *V. vulnificus* 99-743 (T6SS1$^-$/T6SS2$^+$), and prey *S.* Enteritidis CC012 using both the T6SS1 and T6SS2. Interestingly, the two systems were differentially thermoregulated. The T6SS1 being active at both 21 °C and 30 °C, whereas the T6SS2 was active only at a more environmentally representative 21 °C. This is the first described role for the T6SS2 of *V. vulnificus,* suggesting that it may play an important role in bacterial competition *in vivo*. Despite significant anti-prokaryotic killing activity, no anti-eukaryotic killing was observed following co-culture with the phagocytic amoeba, *D. discoideum*, suggesting that the role of these T6SSs is primarily antibacterial. This data supports previous studies that have explored *V. vulnificus* T6SS anti-eukaryotic activity using alternative models of infection, such as the larvae of the greater wax moth, *G. mellonella* [172].

Of interest, this study observed T6SS2-dependent killing of T6SS2$^+$ prey *V. vulnificus*. One possible explanation for this is that *V. vulnificus* 106-2A may possess different T6SS2 effector/immunity modules to prey 99-743. Future work would look at undertaking genomic comparisons between T6SS1$^+$/T6SS2$^+$ and T6SS1$^-$/T6SS2$^+$ *V.*

vulnificus to identify differences in effector/immunity modules and the impact this may have on bacterial co-culture killing assays. To facilitate this, WGS has been performed on *V. vulnificus* strains for future analysis, however no further research into this area was performed during this study. Furthermore, it would be interesting to support bioinformatic data with a proteomics-based approach in which *V. vulnificus* secretomes are investigated using mass-spectrometry to identify potential secreted effectors of interest.

Having demonstrated that *V. vulnificus* employs both the T6SS1 and the T6SS2 to target and kill neighbouring bacteria in an intra and inter-species manner, it was hypothesised that the T6SSs may play a key role in determining *V. vulnificus* population structure within shellfish hosts. To test this hypothesis, this study aimed to characterise *V. vulnificus* T6SS activity using an *in vivo* oyster model for replication of the natural environment. A marine snow model using seawater as a substrate was tested to facilitate sufficient uptake of attacker and prey bacterial strains for *in vivo* co-culture. However, low-level bacterial incorporation into aggregates, contaminating natural bacteria, and inconsistent aggregate formation resulted in this being an ineffective and unsuitable model. Therefore, a more defined and highly controllable artificial marine snow (AMS) model was developed using phytoplankton cultures as a substrate for aggregate formation. AMS enabled significant incorporation of attacker and prey bacteria into aggregates with none of the drawbacks previously described with the NMS model.

This study identified significant differences in the effectiveness of different bacterial strains when incorporating into both NMS and AMS. Previous studies have shown that *V. vulnificus* genotype is an indicator of incorporation efficiency, with E-type *V. vulnificus* demonstrating significantly greater incorporation than their C-type *V.*

vulnificus counterparts. There has been surprisingly little research into the mechanics by which *V. vulnificus* incorporates into marine snow aggregates. Currently, the only avenue of exploration has identified the role of the T4SS pilus in binding chitin to mediate attachment. Future work should investigate the mechanisms behind bacterial incorporation into marine snow to understand how this may shape microbial communities within shellfish hosts. As *S.* Enteritidis was shown to incorporate into AMS significantly more effectively than even E-type 99-743, chitin adhesion assays could be performed using *V. vulnificus* 106-2A, 99-743 and *S.* Enteritidis CC012. If chitin adhesion is the driving factor behind incorporation into aggregates, then results would demonstrate significantly greater *S.* Enteritidis adhesion to chitin. However, a non-significant or even significantly reduced binding to chitin by *S.* Enteritidis would indicate that there are other factors mediating bacterial incorporation to marine snow aggregates to be considered.

AMS was demonstrated to act a suitable substrate for both *V. vulnificus* and *S.* Enteritidis incorporation and uptake by oysters. Uptake experiments demonstrated that incorporation of bacteria into AMS facilitated bacterial uptake into oysters at significantly greater concentrations than has been achieved by any other study to date. This demonstrates that this study has developed a highly efficient and robust model for the inoculation of oysters with bacteria for *in vivo* study. Due to the versatile nature of this model, future work would explore incorporation of different bacterial species into these aggregates and how this may be used in downstream research or aquaculture applications.

Having developed an optimised AMS model for the high-level uptake of *V. vulnificus* and *S.* Enteritidis, this study demonstrated that *V. vulnificus* 106-2A T6SS1 and T6SS2 have intra and inter-species killing activity in an oyster model. Significant killing of prey

V. vulnificus and *S.* Enteritidis was observed following co-culture with wild type 106-2A and the two single T6SS mutants, ΔT6SS1 and ΔT6SS2. This was confirmed as T6SS-dependent through the inclusion of the double mutant, ΔT6SS1/2, with which no reduction in prey bacteria was observed. This study therefore demonstrates that *V. vulnificus* utilises both the T6SS1 and the T6SS2 to mediate antibacterial activity *in vivo*, resulting in significant killing of competing bacterial strains. The T6SS is regulated by a range of conditions, such as temperature and salinity. Future work would be required to characterise the modulation of T6SS activity *in vivo* under a wider range of environmental conditions. There is also a potential question here about how well this model may represent genuine *in vivo* interactions between attacker and prey strains in oysters in a natural, non-depurated state. It may therefore be interesting to repeat these *in vivo* studies in a non-depurated oyster model to elucidate further the impact of the natural microflora on these interactions.

Appendices

A.

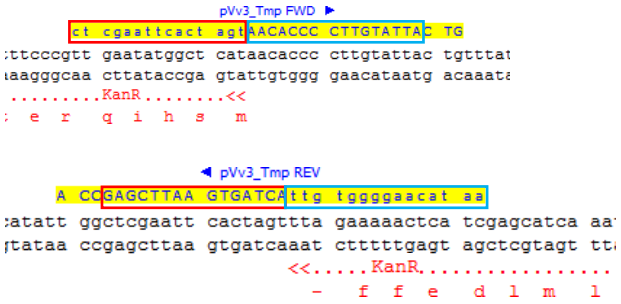

Appendix 1: Schematic demonstrating generation of pVv3-tmp by overlap-extension PCR. (A) Overlap-extension primers were designed to amplify pVv3-kan-tmp whilst removing the kanamycin resistance cassette from the plasmid. Primers are highlighted in yellow, capitalised bases represent those that bind to the plasmid DNA template, lowercase letters indicate the 5' primer tails. Primers were designed so that each 5' tail is complementary to the DNA-binding region (capitalised letters) of the opposing primer. These complementary regions are highlighted in boxes of matching colours.

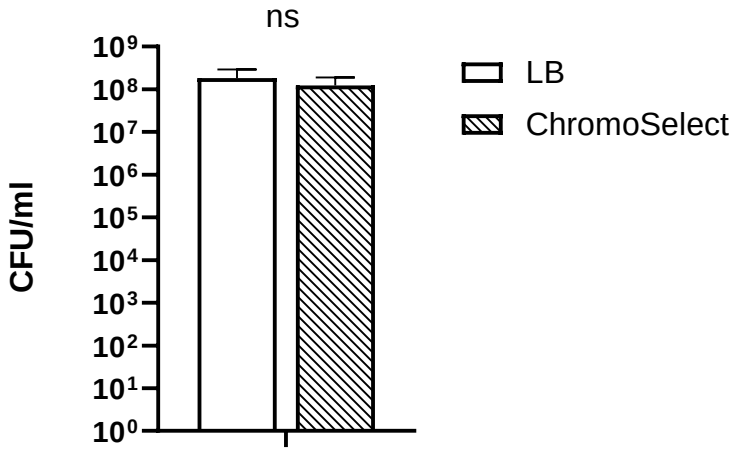

Appendix 2: *S.* Enteritidis CC012 growth on LB agar compared to ChromoSelect agar. *S*. Enteritidis overnight cultures were adjusted to an OD_{590nm} of 0.03 and incubated at 37 °C, 200 rpm, until the OD_{590nm} reached 1.0. Cultures were adjusted to an OD_{590nm} of 0.8 and plated for Miles and Misra enumeration on LB and ChromoSelect agar. Plates were incubated overnight at 37 °C and CFU/mL counts determined the following day. Statistics performed using an ordinary t-test, ns – not significant.

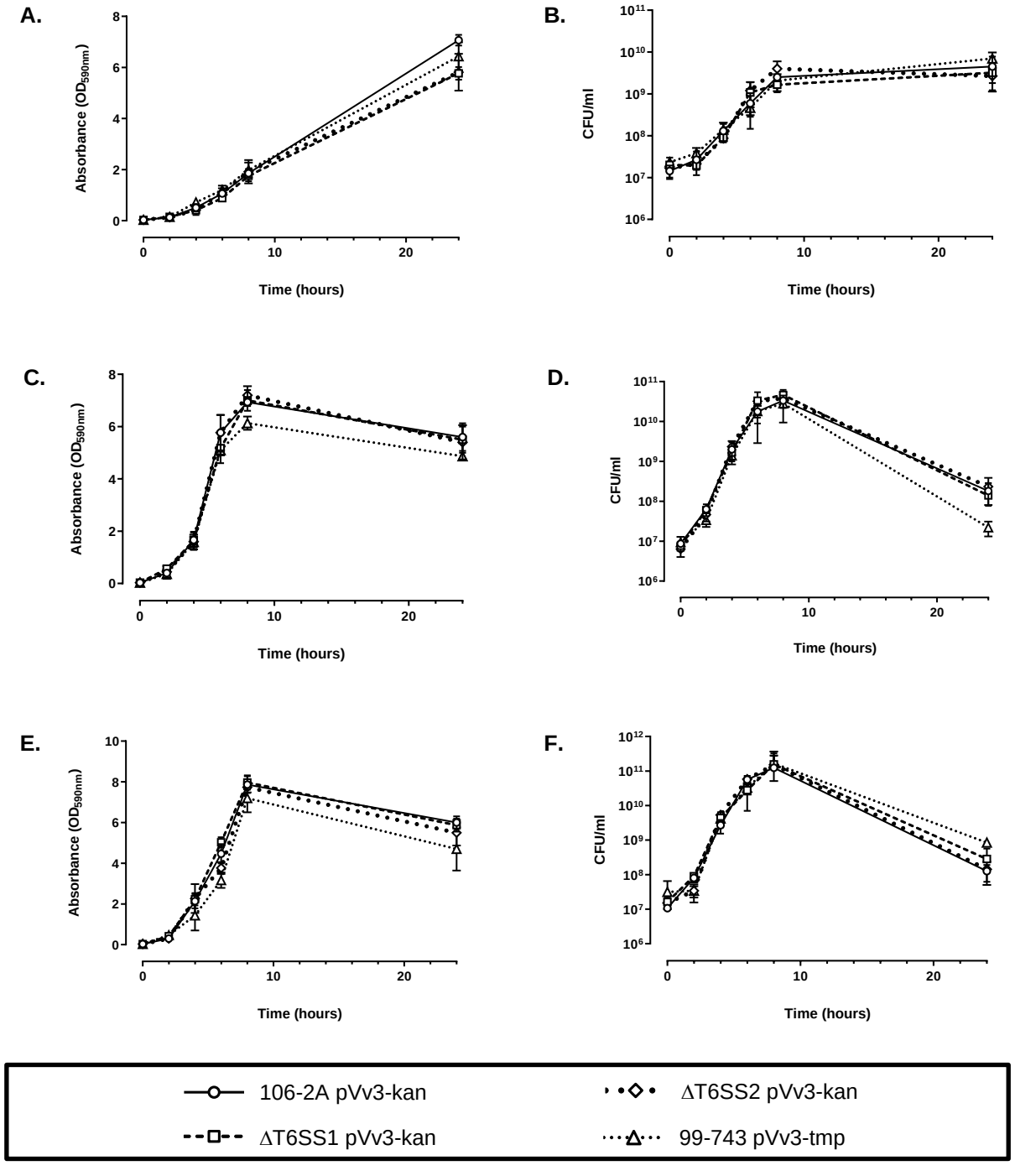

Appendix 1: Growth curves of antibiotic resistant *V. vulnificus* at 21, 30 and 37 °C. Growth curves were performed for *V. vulnificus* 106-2A pVv3-kan, ΔT6SS1 pVv3-kan, ΔT6SS2 pVv3-kan, and 99-743 pVv3-tmp, according to the Materials and Methods (section 2.4.1). OD_{590nm} readings were taken at T_0, T_2, T_4, T_6, T_8 and T_{24} hours before samples were serially diluted and plated on LB agar supplemented with the required antibiotic for enumeration. Growth curves were performed in triplicate at three individual temperature conditions. (A & B) 21 °C. (C & D) 30 °C. (E & F) 37 °C.

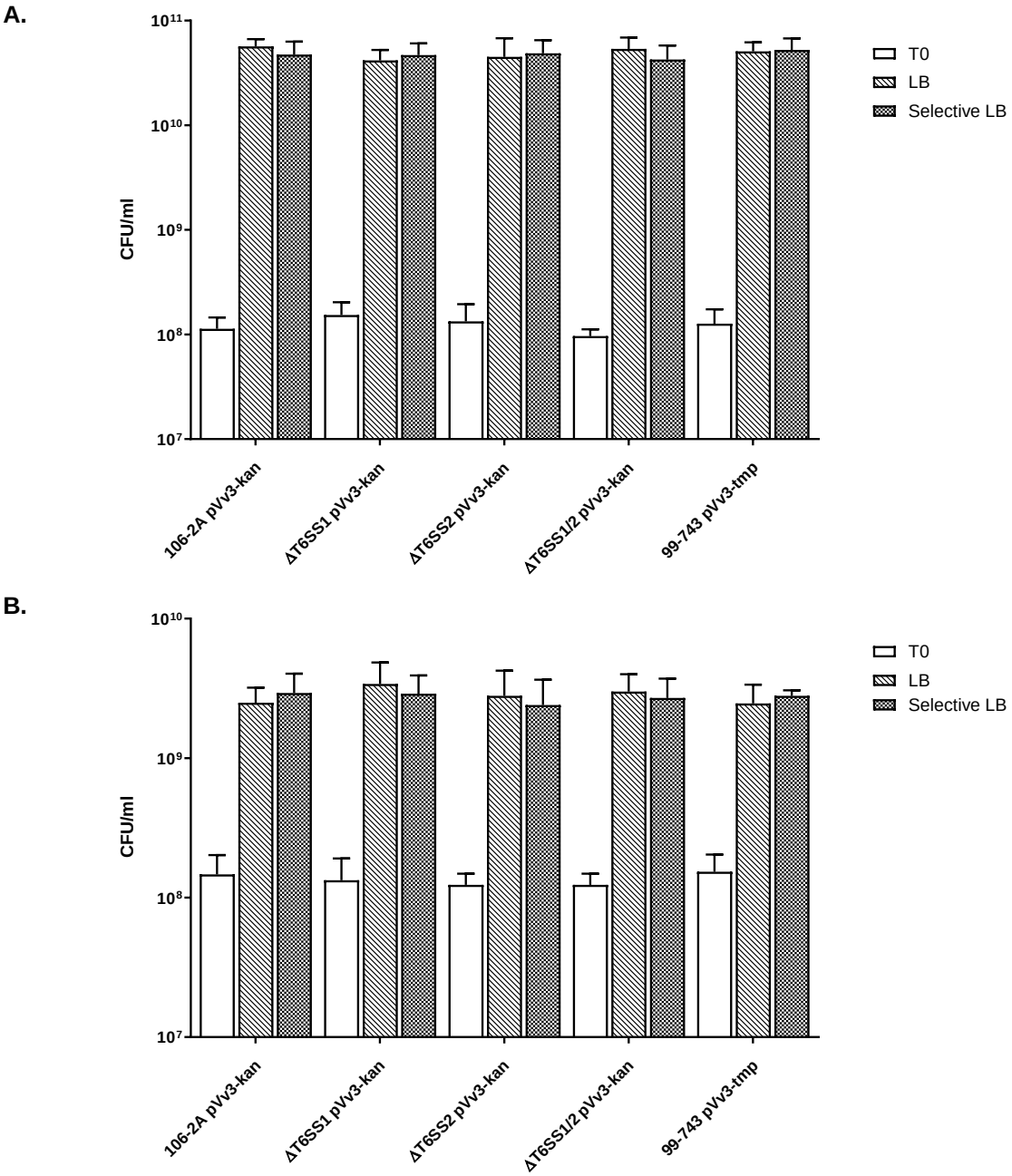

Appendix 2: Plasmid retention assay of pVv3-Kan and pVv3-Tmp in *V. vulnificus* over 5 hours at 30 °C and 24 hours at 21 °C. Overnight V. vulnificus 106-2A pVv3-kan, ΔT6SS1 pVv3-kan, ΔT6SS2 pVv3-kan, ΔT6SS1/2 pVv3-kan, and 99-743 pVv3-tmp cultures were adjusted to an OD_{590nm} of 0.03 and grown to an OD_{590nm} of 1.0. Cultures were adjusted to an OD_{590nm} of 0.8 and spotted onto selective LB and LB agar with no antibiotics for incubation at the required temperature for 5 hours at 30 °C **(A)** and 24 hours at 21 °C **(B)**. T_0 cultures were enumerated to quantify the initial concentration of V. vulnificus present. Bacterial growths were resuspended and plated onto selective media to determine whether there had been a loss in plasmid retention compared to bacteria cultured on selective LB. No significant loss of plasmid was noted for either plasmid under either temperature/time condition. Statistics were performed using a nested one-way ANOVA, no results were significant different to one another.

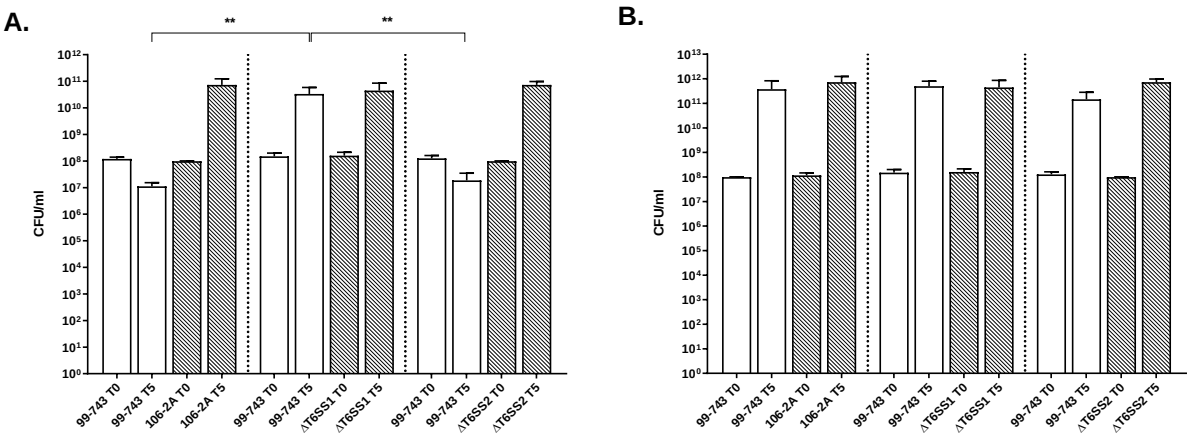

Appendix 4: Total data from *in vitro* intra-species *V. vulnificus* co-cultures at 30 and 37 °C. Attacker *V. vulnificus* 106-2A, ΔT6SS1, and ΔT6SS2 were co-cultured for 5 hours at 30 °C and 37 °C with prey *V. vulnificus* 99-743. **(A)** Co-culture performed at 30 °C. **(B)** Co-culture performed at 37 °C. Vertical dotted lines group strains that were co-cultured together. Error bars represent the mean (n = 3). Statistics were performed using an unpaired, two-tailed student's t-test, ** $p < 0.01$.

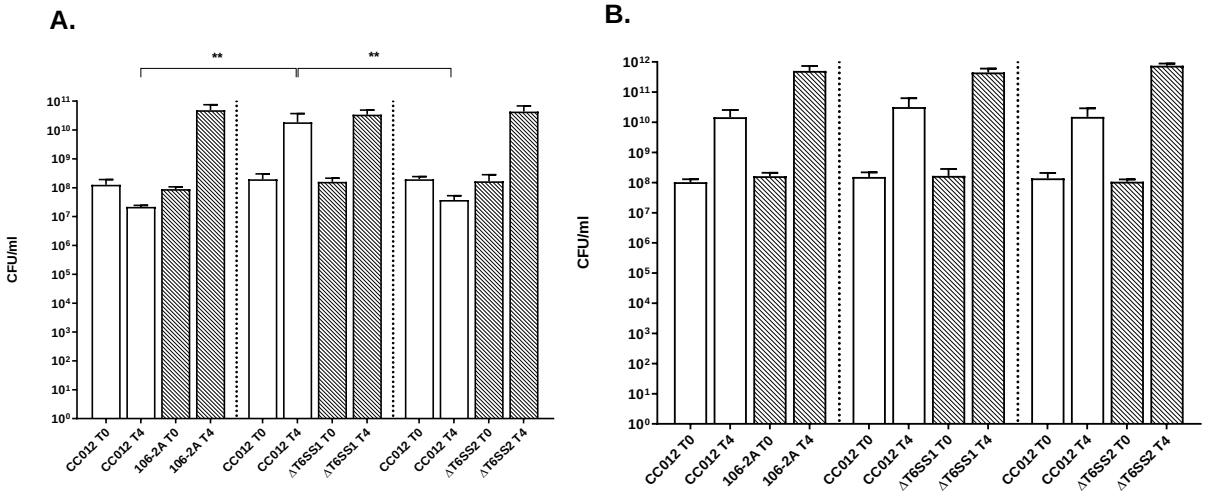

Appendix 4: Total data from *in vitro* inter-species co-cultures between *V. vulnificus* and *S*. Enteritidis at 30 and 37 °C. Attacker *V. vulnificus* 106-2A, ΔT6SS1, and ΔT6SS2 were co-cultured for 5 hours at 30 °C and 37 °C with prey *S*. Enteritidis CC012. **(A)** Co-culture performed at 30 °C. **(B)** Co-culture performed at 37 °C. Vertical dotted lines group strains that were co-cultured together. Error bars represent the mean (n = 3). Statistics were performed using an unpaired, two-tailed student's t-test, ** $p < 0.01$.

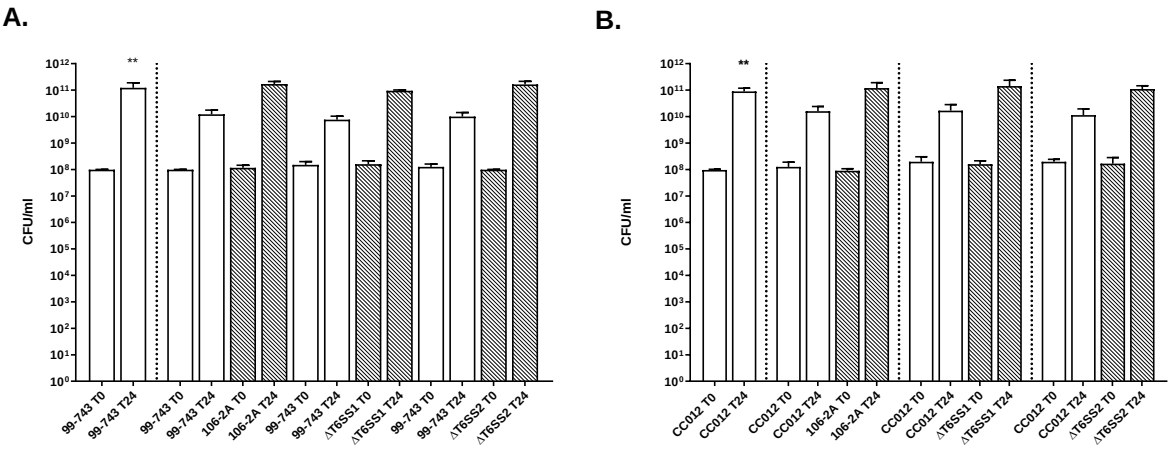

Appendix 7: Total data from *in vitro* intra and inter-species co-culture killing assays at 21 °C. Attacker *V. vulnificus* 106-2A, ΔT6SS1, and ΔT6SS2 were co-cultured for 24 hours at 21 °C with either **(A)** *V. vulnificus* 99-743 or **(B)** *S.* Enteritidis CC012 prey strains. Vertical dotted lines group strains that were co-cultured together. Error bars represent the mean (n = 3). Statistics were performed using an unpaired, two-tailed student's t-test,** $p < 0.01$.

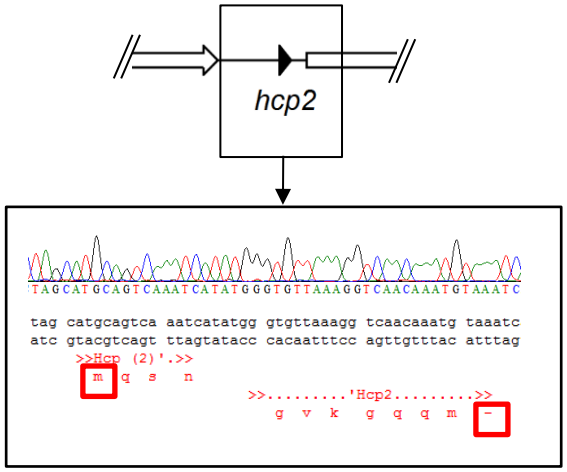

Appendix 8: Sequence confirmation of in-frame *hcp2* deletion in *V. vulnificus* ΔT6SS1 to generate ΔT6SS1/2. The *hcp2* region was PCR amplified and sequenced to confirm no mutations had been introduced during allelic exchange. Truncated *hcp2* is marked with both start and stop codons boxed in red. Ligation of the left and right flanks has reduced the gene from 466 bp to 42 bp. The sequence data for the region is displayed above.

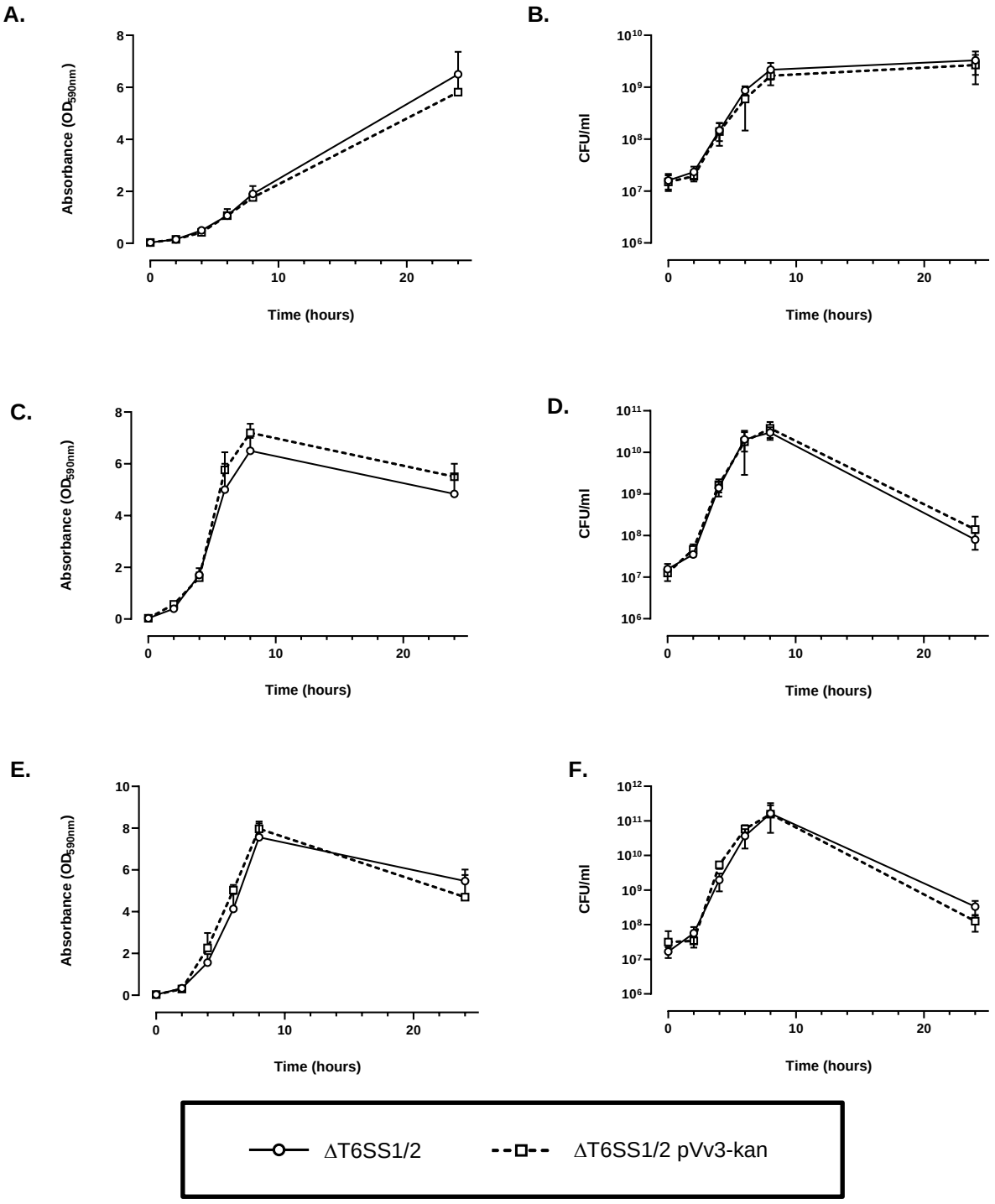

Appendix 5: Growth curves of ΔT6SS1/2 and ΔT6SS1/2 pVv3-kan at 21, 30 and 37 °C. Growth curves were performed for V. vulnificus ΔT6SS1/2 pVv3-kan and ΔT6SS1/2 pVv3-kan according to the Materials and Methods (section 2.4.1). OD_{590nm} readings were taken at T_0, T_2, T_4, T_6, T_8 and T_{24} hours before samples were serially diluted and plated on LB agar supplemented with kanamycin for enumeration. Growth curves were performed at **(A & B)** 21 °C. **(C & D)** 30 °C. **(E & F)** 37 °C.

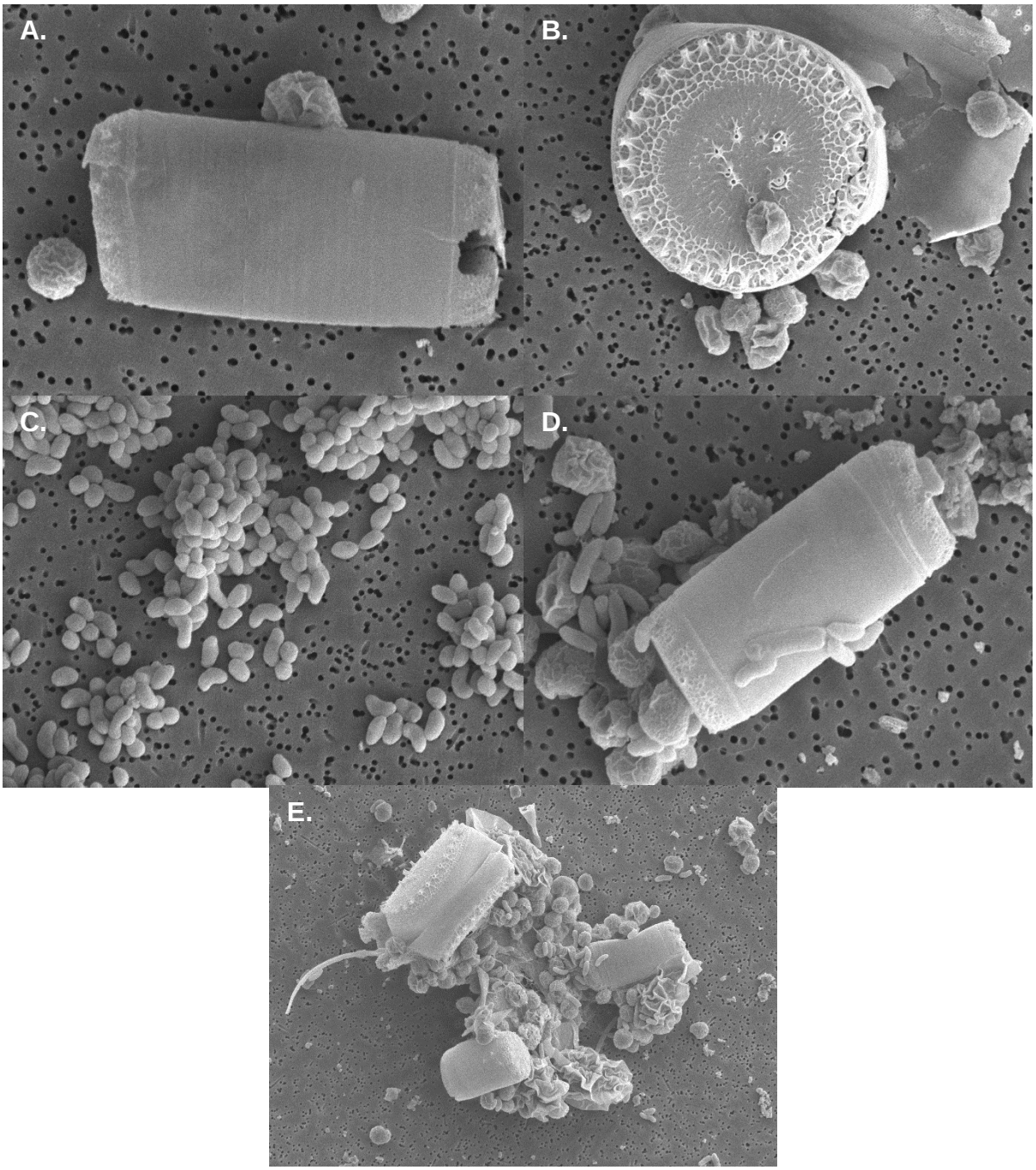

Appendix 10: SEM visualisation of *V. vulnificus* 99-743 incorporation into RP-based artificial marine snow. *V. vulnificus* 99-743 was incorporated into RP-based AMS and processed for SEM visualisation. **(A)** RP-only negative control, magnification × 9,000. **(B)** Adhesion control, magnification × 7,000. **(C)** 99-743 only control, magnification × 7,000. **(D & E)** 99-743 incorporated into AMS, magnification × 9,000 and × 3,000 respectively.

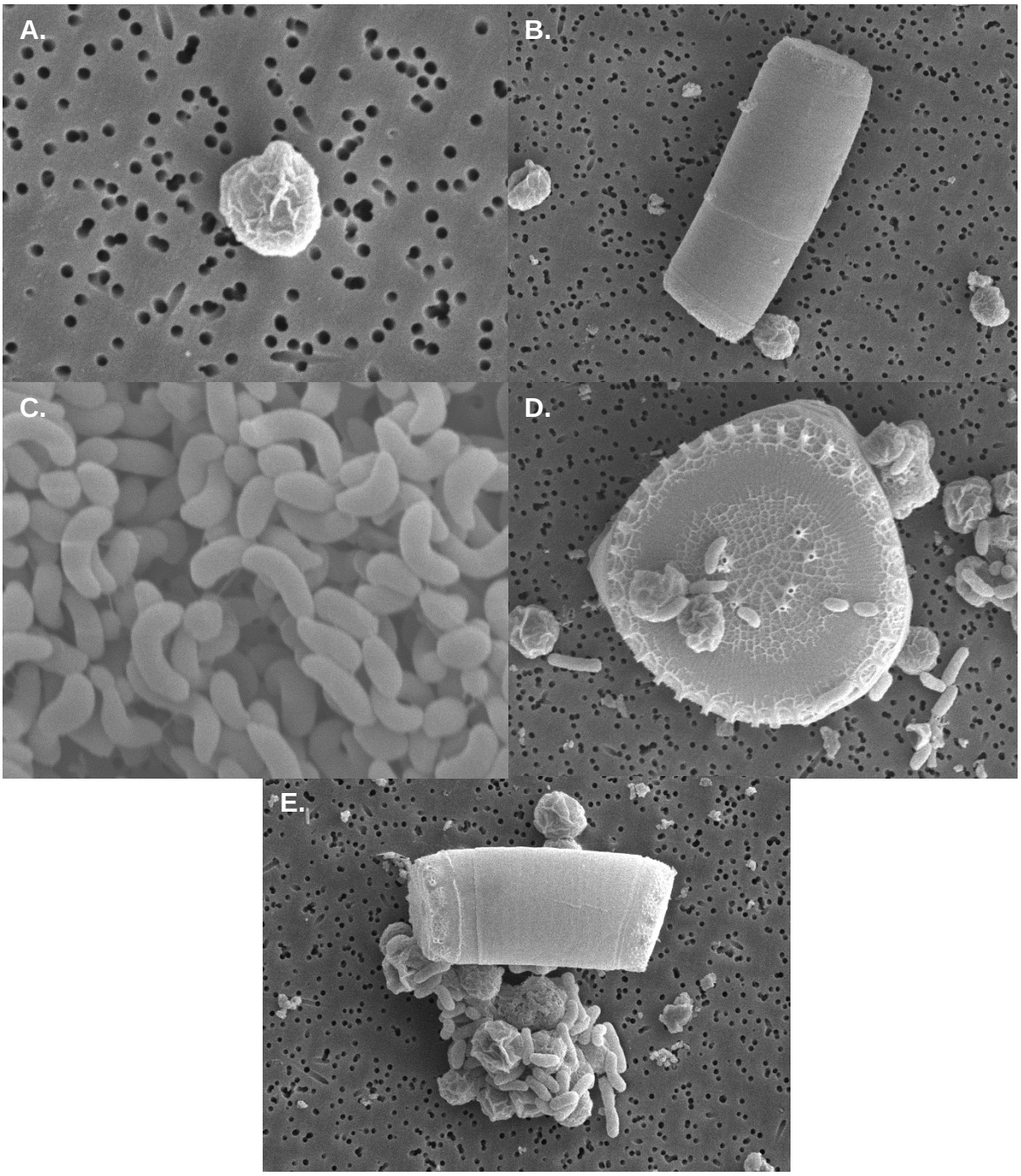

Appendix 11: SEM visualisation of *V. vulnificus* 106-2A incorporation into RP-based artificial marine snow. *V. vulnificus* 106-2A was incorporated into RP-based AMS and processed for SEM visualisation. **(A)** RP-only control, magnification × 11,000. **(B)** Adhesion control, magnification × 7,000. **(C)** 106-2A only control, magnification × 15,000. **(D & E)** 106-2A Incorporated into AMS, magnification × 7,000.

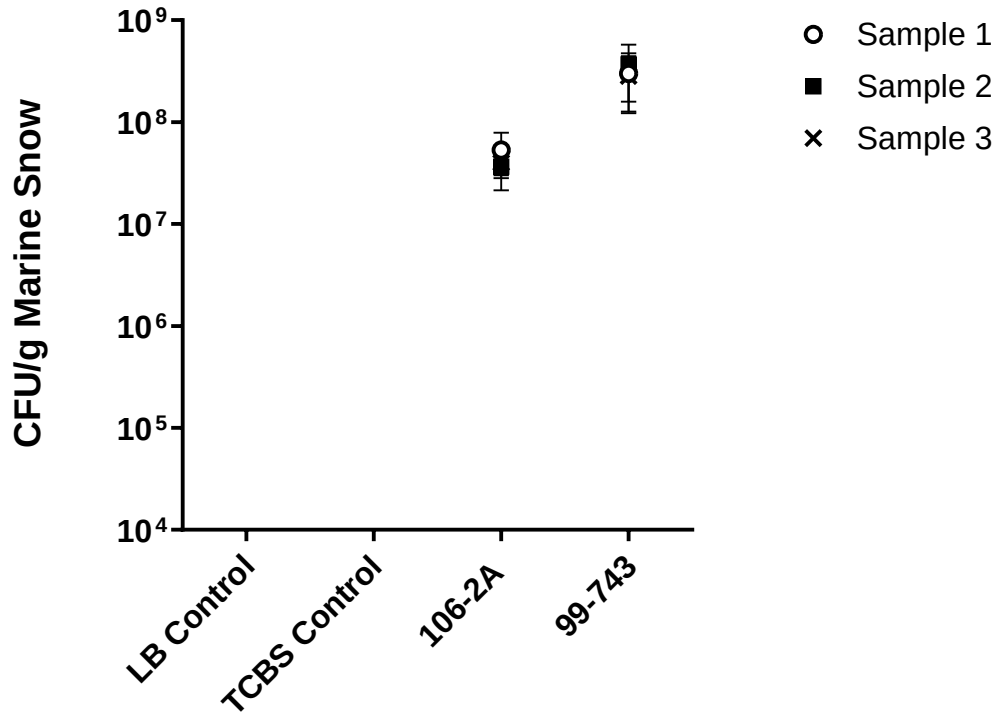

Appendix 6: *V. vulnificus* incorporation into *T. pseudonana* artificial marine snow using separate TP1800 batches. *V. vulnificus* 106-2A and 99-743 were incorporated into AMS formed using three individual TP1800 samples at 21 °C for 24 hours. Negative controls were plated on LB and TCBS agar. Error bars represent the standard deviation (n = 3).

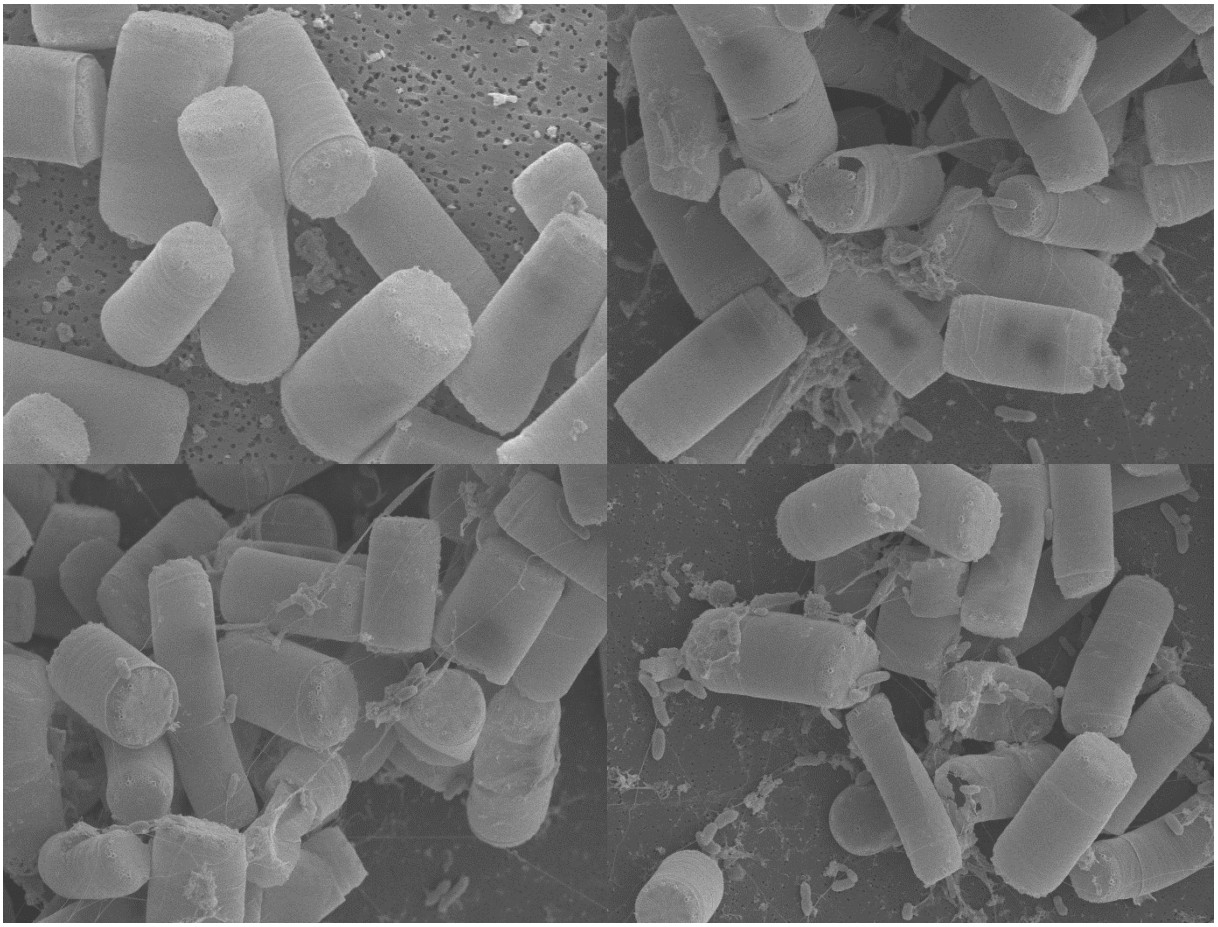

Appendix 13: SEM visualisation of *V. vulnificus* and *S.* Enteritidis incorporation into *T. pseudonana* artificial marine snow. *V. vulnificus* 106-2A, 99-743, and *S*. Enteritidis CC012 were incorporated into AMS using *T. pseudonana* as a substrate for 24 hours at 21 °C. **(A)** Adhesion control, magnification × 5,000. **(B)** *V. vulnificus* 106-2A incorporated into AMS, magnification × 4,000. **(C)** *V. vulnificus* 99-743 incorporated into AMS, magnification × 4,000. **(D)** *S*. Enteritidis CC012 incorporated into AMS, magnification × 4,000.

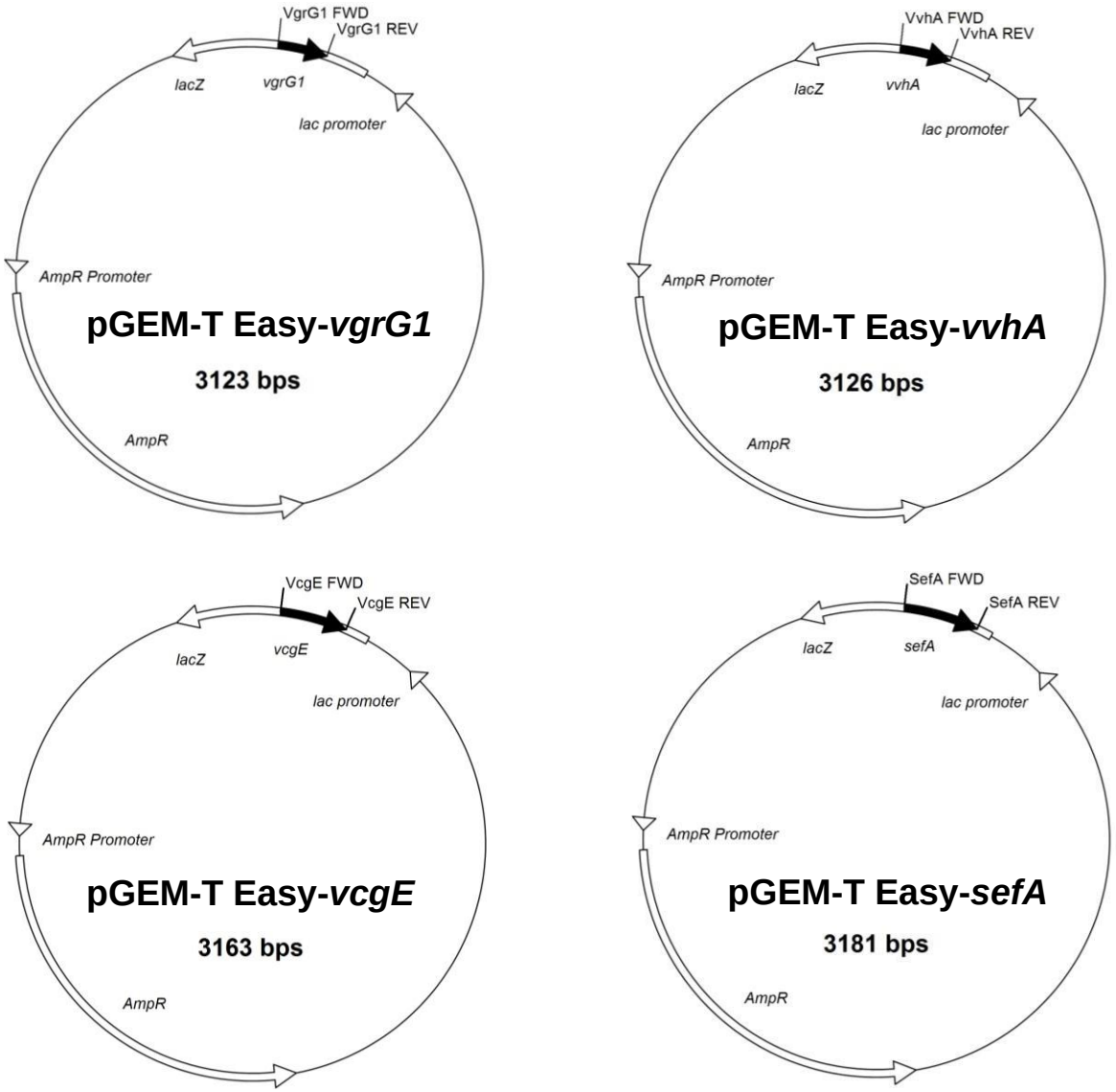

Appendix 14: Plasmid maps for qPCR standard curve material. *vvhA*, *vgrG1*, *vcgE* and *sefA* gene regions were cloned into pGEM-T Easy to generate constructs for qPCR standard curves. Primer binding sites for qPCR primers have been labelled.

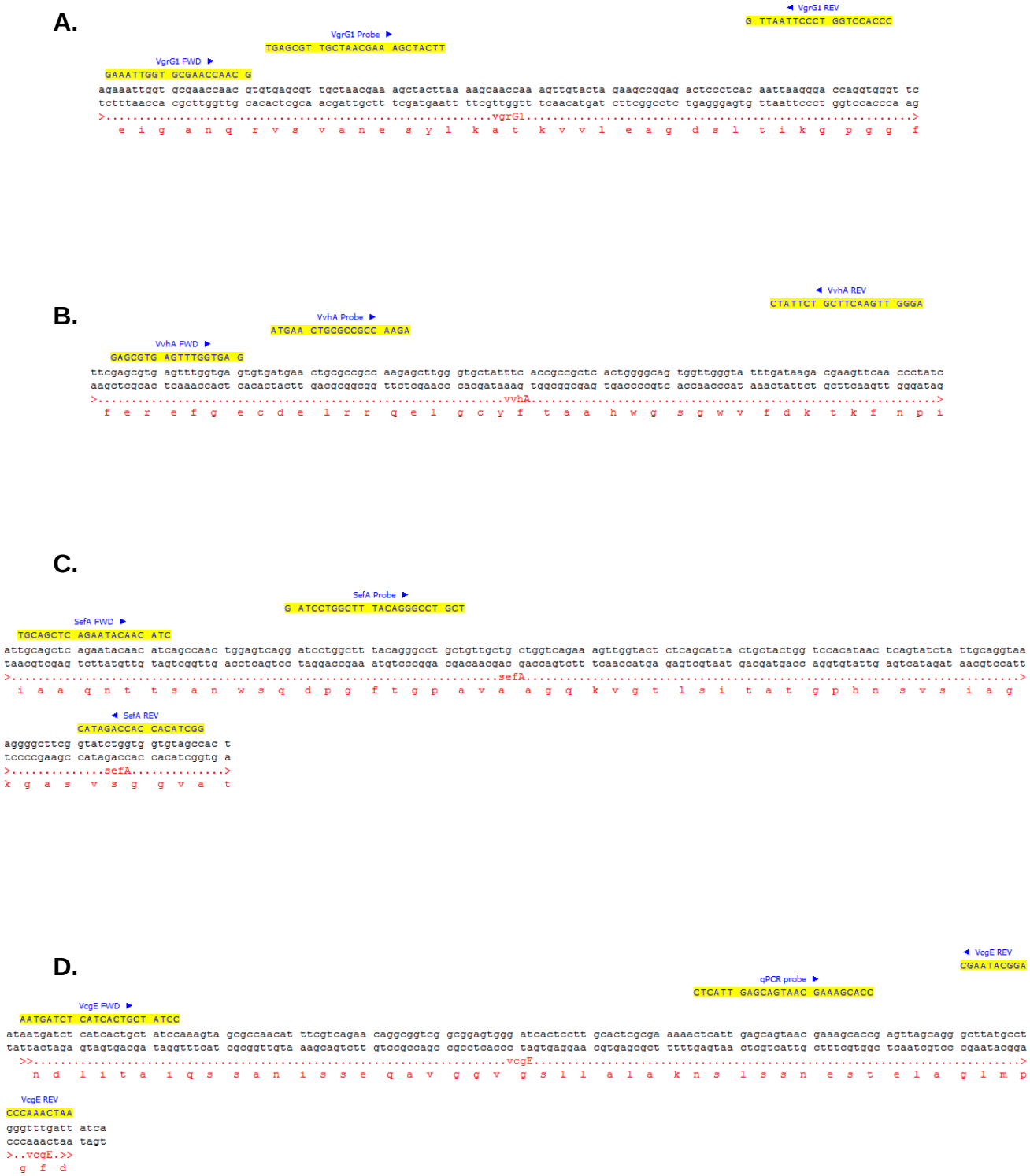

Appendix 15: qPCR primer and probe binding sites. Gene regions for *vvhA*, *vgrG1*, *vcgE*, and *sefA* regions are shown with the qPCR forward/reverse primers and probes binding sites marked.

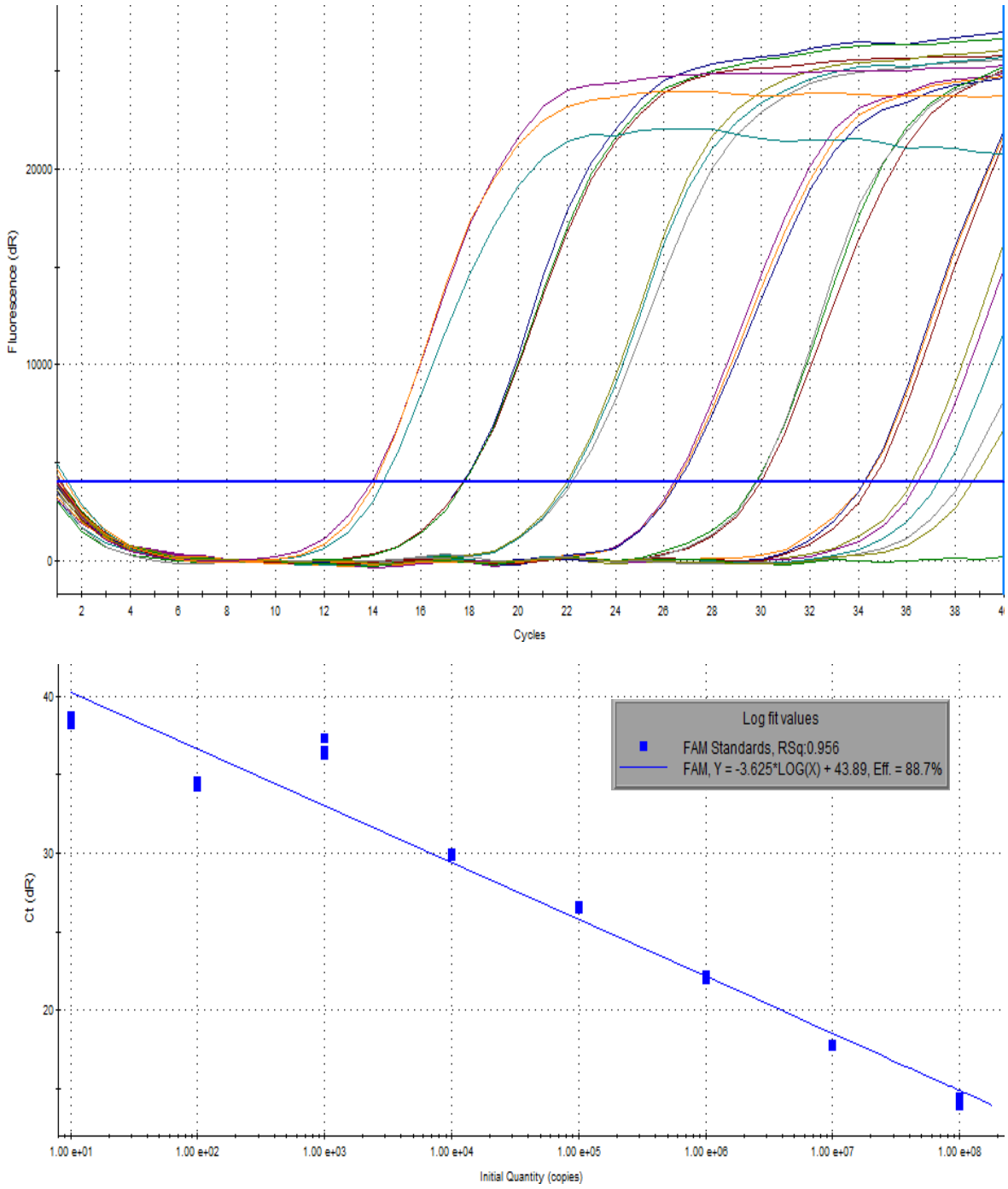

Appendix 16: *vcgE* qPCR standard curve showing ineffective amplification of 10^2 and 10^1 copies/µL standards. (A) Amplification of qPCR standards from 10^8 – 10^1 copies/µL. Each standard was run in triplicate to account for pipetting error. **(B)** A representative *vcgE* standard curve generated using the amplification from the top image. An r^2 value of 0.956 indicates that this curve would be unsuitable for quantification as it does not reach the required 0.99 value.

References

1. Maugeri, T., Carbone, M., Fera, M. & Gugliandolo, C. Detection and differentiation of *Vibrio vulnificus* in seawater and plankton of a coastal zone of the Mediterranean Sea. *Res. Microbiol.* **157**, 194–200 (2006).
2. DePaola, A. *et al.* Analysis of *Vibrio vulnificus* from market oysters and septicemia cases for virulence markers. *Appl. Environ. Microbiol.* **69**, (2003).
3. Jones, M. & Oliver, J. *Vibrio vulnificus*: disease and pathogenesis. *Infect. Immun.* **77**, 1723–33 (2009).
4. Ceccarelli, D. & Colwell, R. *Vibrio* ecology, pathogenesis and evolution. *Front. Microbiol.* (2014).
5. Lippi, D. & Gotuzzo, E. The greatest steps towards the discovery of *Vibrio cholerae*. *Clin. Microbiol. Infect.* **20**, 191–195 (2014).
6. Thompson, F., Iida, T. & Swings, J. Biodiversity of *Vibrios*. *Microbiol. Mol. Biol. Rev.* **68**, 403–31 (2004).
7. Thode, S., Rojek, E., Kozlowski, M., Ahmad, R. & Haugen, P. Distribution of siderophore gene systems on a Vibrionaceae phylogeny: Database searches, phylogenetic analyses and evolutionary perspectives. *PLoS One* **13**, e0191860 (2018).
8. Beaz-Hidalgo, R. *et al. Vibrio celticus* sp. nov., a new *Vibrio* species belonging to the Splendidus clade with pathogenic potential for clams. *Syst. Appl. Microbiol.* **33**, 311–315 (2010).
9. Romalde, J., Dieguez, A., Lasa, A. & Balboa, S. New *Vibrio* species associated to molluscan microbiota: a review. *Front. Microbiol.* **4**, 413 (2014).
10. Restrepo, L. *et al.* PirVP genes causing AHPND identified in a new *Vibrio* species (*Vibrio punensis*) within the commensal *Orientalis* clade. *Sci. Rep.* **8**, 13080 (2018).
11. Strom, M. & Paranjpye, R. Epidemiology and pathogenesis of *Vibrio vulnificus*. *Microbes Infect.* **2**, 177–88 (2000).
12. Drake, S., DePaola, A. & Jaykus, L.-A. An overview of *Vibrio vulnificus* and *Vibrio parahaemolyticus*. *Compr. Rev. Food Sci.Food Saf.* **6**, 120–144 (2007).
13. Hollis, D., Weaver, R., Baker, C. & Thornsberry, C. Halophilic *Vibrio* species isolated from blood cultures. *J. Clin. Microbiol.* **3**, 425–31 (1976).
14. Reichelt, J., Baumann, P. & Baumann, L. Study of genetic relationships among marine species of the genera *Beneckea* and *Photobacterium* by means of in vitro DNA/DNA hybridization. *Arch. Microbiol.* **110**, 101–20 (1976).
15. Farmer, J. *Vibrio 'Benekea' vulnificus*, the bacterium associated with sepsis, septicaemia and the sea. *Lancet* **314**, 903 (1979).
16. Chen, C.-Y. *et al.* Comparative genome analysis of *Vibrio vulnificus*, a marine pathogen. *Genome Res.* **13**, 2577–87 (2003).
17. Bier, N. *et al.* Genotypic diversity and virulence characteristics of clinical and environmental *Vibrio vulnificus* isolates from the Baltic Sea region. *Appl. Environ. Microbiol.* **79**, 3570–81 (2013).
18. Koton, Y., Gordon, M., Chalifa-Caspi, V. & Bisharat, N. Comparative genomic analysis of clinical and environmental *Vibrio vulnificus* isolates revealed biotype 3 evolutionary relationships. *Front. Microbiol.* **5**, 803 (2014).
19. Kim, Y. *et al.* Characterization and pathogenic significance of *Vibrio vulnificus* antigens preferentially expressed in septicemic patients. *Infect. Immun.* **71**, 5461–5471 (2003).

20. Gulig, P. *et al.* SOLiD sequencing of four *Vibrio vulnificus* genomes enables comparative genomic analysis and identification of candidate clade-specific virulence genes. *BMC Genomics* **11**, 512 (2010).
21. Makino, K. *et al.* Genome sequence of *Vibrio parahaemolyticus*: a pathogenic mechanism distinct from that of *V cholerae*. *Lancet* **361**, 743–749 (2003).
22. Fraser, C. *et al.* DNA sequence of both chromosomes of the cholera pathogen *Vibrio cholerae*. *Nature* **406**, 477–483 (2000).
23. Blake, P., Weaver, R. & Hollis, D. Diseases of humans (other than Cholera) caused by *Vibrios*. *Annu. Rev. Microbiol.* **34**, 341–367 (1980).
24. Tison, D., Nishibuchi, M., Greenwood, J. & Seidler, R. *Vibrio vulnificus* biogroup 2: new biogroup pathogenic for eels. *Appl. Environ. Microbiol.* **44**, 640–6 (1982).
25. Veenstra, J. *et al.* Infection by an indole-negative variant of *Vibrio vulnificus* transmitted by eels. *J. Infect. Dis.* **166**, 209–10 (1992).
26. Amaro, C. & Biosca, E. *Vibrio vulnificus* biotype 2, pathogenic for eels, is also an opportunistic pathogen for humans. *Appl. Environ. Microbiol.* **62**, 1454–7 (1996).
27. Amaro, C., Biosca, E., Fouz, B. & Garay, E. Electrophoretic analysis of heterogeneous lipopolysaccharides from various strains of *Vibrio vulnificus* biotypes 1 and 2 by silver staining and immunoblotting. *Curr. Microbiol.* **25**, 99–104 (1992).
28. Amaro, C., Biosca, E., Esteve, C., Fouz, B. & Toranzo, A. Comparative study of phenotypic and virulence properties in *Vibrio vulnificus* biotypes 1 and 2 obtained from a European eel farm experiencing mortalities. *Dis. Aquat. Organ.* **13**, 29–35 (1992).
29. Bisharat, N. *et al.* Clinical, epidemiological, and microbiological features of *Vibrio vulnificus* biogroup 3 causing outbreaks of wound infection and bacteraemia in Israel. Israel *Vibrio* Study Group. *Lancet (London, England)* **354**, 1421–4 (1999).
30. Ziolo, K. *et al. Vibrio vulnificus* biotype 3 multifunctional autoprocessing RTX toxin is an adenylate cyclase toxin essential for virulence in mice. *Infect. Immun.* **82**, 2148–57 (2014).
31. Kim, B., Gavin, H. & Satchell, K. Variable virulence of Biotype 3 *Vibrio vulnificus* due to MARTX toxin effector domain composition. *mSphere* **2**, (2017).
32. Efimov, V. *et al.* Insight into the evolution of *Vibrio vulnificus* biotype 3's genome. *Front. Microbiol.* **4**, 393 (2013).
33. Warner, E. & Oliver, J. Population structures of two genotypes of *Vibrio vulnificus* in oysters (*Crassostrea virginica*) and seawater. *Appl. Environ. Microbiol.* **74**, 80–5 (2008).
34. Roig, F., Sanjuán, E., Llorens, A. & Amaro, C. *pilF* polymorphism-based PCR to distinguish *Vibrio vulnificus* strains potentially dangerous to public health. *Appl. Environ. Microbiol.* **76**, 1328–33 (2010).
35. González-Escalona, N., Jaykus, L.-A. & DePaola, A. Typing of *Vibrio vulnificus* strains by variability in their 16S-23S rRNA intergenic spacer regions. *Foodborne Pathog. Dis.* **4**, 327–337 (2007).
36. Aznar, R., Ludwig, W., Amann, R. & Schleifer, K. Sequence determination of rRNA genes of pathogenic *Vibrio* species and whole-cell identification of *Vibrio vulnificus* with rRNA-targeted oligonucleotide probes. *Int. J. Syst. Bacteriol.* **44**, 330–337 (1994).

37. Wright, A. *et al.* Differential expression of *Vibrio vulnificus* capsular polysaccharide. *Infect. Immun.* **67**, 2250–7 (1999).
38. Han, F. & Ge, B. Multiplex PCR assays for simultaneous detection and characterization of *Vibrio vulnificus* strains. *Lett. Appl. Microbiol.* **51**, no-no (2010).
39. Farmer, J. & Hickman-Brenner, F. The genera *Vibrio* and *Photobacterium*. in *The Prokaryotes* 508–563 (Springer New York, 2006). doi:10.1007/0-387-30746-X_18.
40. Baker-Austin, C. *et al. pilF* polymorphism-based real-time PCR to distinguish *Vibrio vulnificus* strains of human health relevance. *Food Microbiol.* **30**, 17–23 (2012).
41. Nilsson, W., Paranjype, R., DePaola, A. & Strom, M. Sequence polymorphism of the 16S rRNA gene of *Vibrio vulnificus* is a possible indicator of strain virulence. *J. Clin. Microbiol.* **41**, 442–6 (2003).
42. Warner, J. & Oliver, J. Randomly amplified polymorphic DNA analysis of clinical and environmental isolates of *Vibrio vulnificus* and other *Vibrio* species. *Appl. Environ. Microbiol.* **65**, 1141–4 (1999).
43. Rosche, T., Yano, Y. & Oliver, J. A rapid and simple PCR analysis indicates there are two subgroups of *Vibrio vulnificus* which correlate with clinical or environmental isolation. *Microbiol. Immunol.* **49**, 381–9 (2005).
44. Reynaud, Y., Pitchford, S., De Decker, S., Wikfors, G. H. & Brown, C. L. Molecular typing of environmental and clinical strains of *Vibrio vulnificus* isolated in the northeastern USA. *PLoS One* **8**, e83357 (2013).
45. Fujiwara-Nagata, E. & Eguchi, M. Significance of Na+ in the fish pathogen, *Vibrio anguillarum,* under energy depleted condition. *FEMS Microbiol. Lett.* **234**, 163–167 (2004).
46. Osaka, K., Komatsuzaki, M., Takahashi, H., Sakano, S. & Okabe, N. *Vibrio vulnificus* septicaemia in Japan: an estimated number of infections and physicians' knowledge of the syndrome. *Epidemiol. Infect.* **132**, 993–6 (2004).
47. Paydar, M. & Thong, K. Prevalence and genetic characterization of Vibrio vulnificus in raw seafood and seawater in Malaysia. *J. Food Prot.* **76**, 1797–1800 (2013).
48. Veenstra, J., Rietra, P., Coster, J., Slaats, E. & Dirks-Go, S. Seasonal variations in the occurrence of *Vibrio vulnificus* along the Dutch coast. *Epidemiol. Infect.* **112**, 285–90 (1994).
49. Paz, S., Bisharat, N., Paz, E., Kidar, O. & Cohen, D. Climate change and the emergence of *Vibrio vulnificus* disease in Israel. *Environ. Res.* **103**, 390–396 (2007).
50. Melhus, A., Holmdahl, T. & Tjernberg, I. First documented case of bacteremia with *Vibrio vulnificus* in Sweden. *Scand. J. Infect. Dis.* **27**, 81–2 (1995).
51. França, J. *et al. Vibrio vulnificus* infection in Southern Brazil -- case report. *An. Bras. Dermatol.* **88**, 424–6 (2013).
52. Oliver, J., Warner, R. & Cleland, D. Distribution of *Vibrio vulnificus* and other lactose-fermenting *Vibrios* in the marine environment. *Appl. Environ. Microbiol.* **45**, 985–98 (1983).
53. Dalsgaard, A., Frimodt-Møller, N., Bruun, B., Høi, L. & Larsen, J. L. Clinical manifestations and molecular epidemiology of *Vibrio vulnificus* infections in Denmark. *Eur. J. Clin. Microbiol. Infect. Dis.* **15**, 227–32 (1996).
54. Torres, L., Escobar, S., Lopez, A., Marco, M. & Pobo, V. Wound Infection due to *Vibrio vulnificus* in Spain. *Eur. J. Clin. Microbiol. Infect. Dis.* **21**, 537–538 (2002).
55. Huehn, S. *et al.* Pathogenic *Vibrios* in environmental, seafood and clinical sources in Germany. *Int. J. Med.*

Microbiol. **304**, 843–850 (2014).

56. Vezzulli, L., Höfle, M., Pruzzo, C., Pezzati, E. & Brettar, I. Effects of global warming on *Vibrio* ecology. *Microbiol. Spectr.* **3**, (2015).
57. Mahmud, Z. H. *et al.* Occurrence, seasonality and genetic diversity of *Vibrio vulnificus* in coastal seaweeds and water along the Kii Channel, Japan. *FEMS Microbiol. Ecol.* **64**, 209–218 (2008).
58. Randa, M. A., Polz, M. F. & Lim, E. Effects of temperature and salinity on *Vibrio vulnificus* population dynamics as assessed by quantitative PCR. *Appl. Environ. Microbiol.* **70**, 5469–76 (2004).
59. Whitesides, M. D. & Oliver, J. D. Resuscitation of *Vibrio vulnificus* from the Viable but Nonculturable State. **63**, 1002–5 (1997).
60. Brenzinger, S. *et al.* Structural and proteomic changes in viable but non-culturable *Vibrio cholerae*. *Front. Microbiol.* **10**, (2019).
61. Motes, M. L. *et al.* Influence of water temperature and salinity on *Vibrio vulnificus* in Northern Gulf and Atlantic Coast oysters (*Crassostrea virginica*). *Appl. Environ. Microbiol.* **64**, 1459–65 (1998).
62. Takemura, A., Chien, D. & Polz, M. Associations and dynamics of *Vibrionaceae* in the environment, from the genus to the population level. *Front. Microbiol.* **5**, 38 (2014).
63. Greenfield, D. *et al.* Temporal and environmental factors driving *Vibrio vulnificus* and *V. parahaemolyticus* populations and their associations with harmful algal blooms in South Carolina detention ponds and receiving tidal creeks. *GeoHealth* **1**, 306–317 (2017).
64. Thickman, J. & Gobler, C. The ability of algal organic matter and surface runoff to promote the abundance of pathogenic and non-pathogenic strains of *Vibrio parahaemolyticus* in Long Island Sound, USA. *PLoS One* **12**, e0185994 (2017).
65. Fabiano L. Thompson, Brian Austin, J. S. *The biology of* Vibrios. (American Society of Microbiology, 2006). doi:10.1128/9781555815714.
66. Givens, C., Bowers, J., DePaola, A., Hollibaugh, J. & Jones, J. Occurrence and distribution of *Vibrio vulnificus* and *Vibrio parahaemolyticus* - potential roles for fish, oyster, sediment and water. *Lett. Appl. Microbiol.* **58**, 503–510 (2014).
67. Baker-Austin, C. *et al.* Emerging *Vibrio* risk at high latitudes in response to ocean warming. *Nat. Clim. Chang.* **3**, 73–77 (2012).
68. Baker-Austin, C., Trinanes, J., Gonzalez-Escalona, N. & Martinez-Urtaza, J. Non-cholera *Vibrios*: The microbial barometer of climate change. *Trends Microbiol.* **25**, 76–84 (2017).
69. Deeb, R., Tufford, D., Scott, G., Gooch Moore, J. & Dow, K. Impact of climate change on *Vibrio vulnificus* abundance and exposure risk. *Estuaries and Coasts* **41**, 2289–2303 (2018).
70. Lipp, E., Huq, A. & Colwell, R. Effects of global climate on infectious disease: the cholera model. *Clin. Microbiol. Rev.* **15**, 757–70 (2002).
71. Sterk, A., Schets, F., de Roda Husman, A., de Nijs, T. & Schijven, J. Effect of climate change on the concentration and associated risks of *Vibrio* spp. in Dutch recreational waters. *Risk Anal.* **35**, 1717–1729 (2015).
72. Vezzulli, L. *et al.* Climate influence on *Vibrio* and associated human diseases during the past half-century in the

coastal North Atlantic. *Proc. Natl. Acad. Sci. U. S. A.* **113**, E5062-71 (2016).

73. Baker-Austin, C. *et al.* Heat wave-associated Vibriosis, Sweden and Finland, 2014. *Emerg. Infect. Dis.* **22**, 1216–20 (2016).
74. Herrfurth, D. *et al.* Uptake and localization of *Vibrio cholerae*, *Vibrio parahaemolyticus*, and *Vibrio vulnificus* in blue mussels (*Mytilus edulis*) of the Baltic Sea. *J. Shellfish Res.* **32**, 855 (2013).
75. Dore, M. Climate change and changes in global precipitation patterns: What do we know? *Environ. Int.* **31**, 1167–1181 (2005).
76. Esteves, K. *et al.* Rapid proliferation of *Vibrio parahaemolyticus*, *Vibrio vulnificus*, and *Vibrio cholerae* during freshwater flash floods in French Mediterranean coastal lagoons. *Appl. Environ. Microbiol.* **81**, 7600–9 (2015).
77. Rahmstorf, S. Rising hazard of storm-surge flooding. *Proceedings of the National Academy of Sciences of the United States of America* vol. 114 11806–11808 (2017).
78. Rhoads, J. Post-hurricane Katrina challenge: *Vibrio vulnificus*. *J. Am. Acad. Nurse Pract.* **18**, 318–324 (2006).
79. Bopp, C., Mintz, E., Sobel, J., Arvelo, W. & Gaffga, N. Vibrio illnesses after hurricane Katrina --- Multiple states, August--September 2005. *Morb. Mortal. Wkly.* **54**, 928–931 (2005).
80. Froelich, B. A. & Noble, R. T. *Vibrio* bacteria in raw oysters: managing risks to human health. *Philos. Trans. R. Soc. B Biol. Sci.* **371**, 20150209 (2016).
81. Andrews, L., Park, D. & Chen, Y. Low temperature pasteurization to reduce the risk of *Vibrio* infections from raw shell-stock oysters. *Food Addit. Contam.* **17**, 787–791 (2000).
82. Wright, A., Simpson, L. & Oliver, J. Role of iron in the pathogenesis of *Vibrio vulnificus* infections. *Infect. Immun.* **34**, 503–7 (1981).
83. Horseman, M. & Surani, S. A comprehensive review of *Vibrio vulnificus*: an important cause of severe sepsis and skin and soft-tissue infection. *Int. J. Infect. Dis.* **15**, e157–e166 (2011).
84. Haq, S. M. & Dayal, H. H. Chronic liver disease and consumption of raw oysters: A potentially lethal combination—A review of *Vibrio vulnificus* septicemia. *Am. J. Gastroenterol.* **100**, 1195–1199 (2005).
85. Chiang, C., Chiang, S.-R. & Chuang, Y.-C. *Vibrio vulnificus* infection: clinical manifestations, pathogenesis, and antimicrobial therapy. *J. Microbiol. Immunol. Infect.* **36**, 81–88 (2003).
86. Zückert, W. Secretion of bacterial lipoproteins: through the cytoplasmic membrane, the periplasm and beyond. *Biochim. Biophys. Acta* **1843**, 1509–16 (2014).
87. Zoued, A. *et al.* Architecture and assembly of the Type VI secretion system. *Biochim. Biophys. Acta - Mol. Cell Res.* **1843**, 1664–1673 (2014).
88. Shapiro, R. L. *et al.* The role of Gulf Coast oysters harvested in warmer months in *Vibrio vulnificus* infections in the United States, 1988-1996. *J. Infect. Dis.* **178**, 752–9 (1998).
89. Bross, M., Soch, K., Morales, R. & Mitchell, R. *Vibrio vulnificus* infection: diagnosis and treatment. *Am. Fam. Physician* **76**, 539–44 (2007).
90. Hendren, N., Sukumar, S. & Glazer, C. S. Vibrio vulnificus septic shock due to a contaminated tattoo. *BMJ Case Rep.* **2017**, 199–220 (2017).
91. Kotton, Y., Soboh, S. & Bisharat, N. *Vibrio vulnificus* necrotizing fasciitis associated with acupuncture. *Infect. Dis. Rep.* **7**, (2015).

92. Oliver, J. Wound infections caused by *Vibrio vulnificus* and other marine bacteria. *Epidemiol. Infect.* **133**, 383–91 (2005).
93. Baethge, B. & West, B. *Vibrio vulnificus*: did Hippocrates describe a fatal case? *Rev. Infect. Dis.* **10**, 614–5.
94. Menon, M., Yu, P., Iwamoto, M. & Painter, J. Pre-existing medical conditions associated with *Vibrio vulnificus* septicaemia. *Epidemiol. Infect.* **142**, 878–81 (2014).
95. Hor, L., Chang, T. & Wang, S. Survival of *Vibrio vulnificus* in whole blood from patients with chronic liver diseases: association with phagocytosis by neutrophils and serum ferritin Levels. *J. Infect. Dis.* **179**, 275–278 (1999).
96. Chen, Y., Satoh, T. & Tokunaga, O. *Vibrio vulnificus* infection in patients with liver disease: report of five autopsy cases. *Virchows Arch.* **441**, 88–92 (2002).
97. Muldrew, K. L., Miller, R. R., Kressin, M., Tang, Y.-W. & Stratton, C. Necrotizing fasciitis from *Vibrio vulnificus* in a patient with undiagnosed hepatitis and cirrhosis. *J. Clin. Microbiol.* **45**, 1058–62 (2007).
98. Nazir, S., Brown, K., Shin, A. & Donato, A. *Vibrio vulnificus* infection and liver cirrhosis: a potentially lethal combination. *BMJ Case Rep.* **2016**, (2016).
99. Kim, C., Park, Y. & Shin, S. A widespread deferoxamine-mediated iron-uptake System in *Vibrio vulnificus*. *J. Infect. Dis.* **196**, 1537–1545 (2007).
100. Kim, C., Park, R., Choi, M., Sun, H. & Shin, S. Ferrophilic characteristics of *Vibrio vulnificus* and potential usefulness of iron chelation therapy. *J. Infect. Dis.* **195**, 90–98 (2007).
101. Fan, J., Shao, C., Ho, Y., Yu, C. & Hor, L. Isolation and characterization of a *Vibrio vulnificus* mutant deficient in both extracellular metalloprotease and cytolysin. *Infect. Immun.* **69**, 5943–8 (2001).
102. Merkel, S., Alexander, S., Zufall, E., Oliver, J. & Huet-Hudson, Y. Essential role for estrogen in protection against *Vibrio vulnificus*-induced endotoxic shock. *Infect. Immun.* **69**, 6119–22 (2001).
103. Matsuoka, Y. *et al.* Accurate diagnosis and treatment of *Vibrio vulnificus* infection: a retrospective study of 12 cases. *Brazilian J. Infect. Dis.* **17**, 7–12 (2013).
104. Lee, J.-Y. *et al.* Clinical usefulness of Real-Time Polymerase Chain Reaction for the diagnosis of *Vibrio vulnificus* infection using skin and soft tissues. *Am. J. Trop. Med. Hyg.* **97**, 443–446 (2017).
105. Gilliss, D. *et al.* Vital signs: Incidence and trends of infection with pathogens transmitted commonly through food --- Foodborne diseases active surveillance network, 10 U.S. sites, 1996--2010. *Morb. Mortal. Wkly. Rep.* **60**, 749–755 (2011).
106. *Vibrio vulnificus* | Natural disasters and severe weather. https://www.cdc.gov/disasters/vibriovulnificus.html.
107. People at Risk | *Vibrio* Illness (Vibriosis) | CDC. https://www.cdc.gov/vibrio/people-at-risk.html.
108. Scallan, E. *et al.* Foodborne illness acquired in the United States--major pathogens. *Emerg. Infect. Dis.* **17**, 7–15 (2011).
109. Marano, N. *et al.* A survey of stool culturing practices for *Vibrio* species at clinical laboratories in Gulf Coast states. *J. Clin. Microbiol.* **38**, 2267–70 (2000).
110. Yun, N. & Kim, D.-M. *Vibrio vulnificus* infection: a persistent threat to public health. *Korean J. Intern. Med.* **33**, 1070–1078 (2018).

111. Han, L. *et al.* Biochemical characterization and phylogenetic analysis of the virulence factor lysine decarboxylase from *Vibrio vulnificus*. *Front. Microbiol.* **9**, (2018).
112. Kim, C.-M. *et al. Vibrio vulnificus* vulnibactin, but not metalloprotease VvpE, is essentially required for iron-uptake from human holotransferrin. *Biol. Pharm. Bull.* **29**, 911–8 (2006).
113. Rhee, J., Kim, K. & Choi, S. CadC activates pH-dependent expression of the *Vibrio vulnificus cadBA* operon at a distance through direct binding to an upstream region. *J. Bacteriol.* **187**, 7870–7875 (2005).
114. Rhee, J., HRhee, J., Ryu, P. & Choi, S. Identification of the *cadBA* operon from *Vibrio vulnificus* and its influence on survival to acid stress. *FEMS Microbiol. Lett.* **208**, 245–251 (2002).
115. Kovacikova, G., Lin, W. & Skorupski, K. The LysR-type virulence activator AphB regulates the expression of genes in *Vibrio cholerae* in response to low pH and anaerobiosis. *J. Bacteriol.* **192**, 4181–4191 (2010).
116. Kim, J.-S., Sung, M.-H., Kho, D.-H. & Lee, J. K. Induction of manganese-containing superoxide dismutase is required for acid tolerance in *Vibrio vulnificus*. *J. Bacteriol.* **187**, 5984–5995 (2005).
117. Yu, J., Yu, X. & Liu, J. A thermostable manganese-containing superoxide dismutase from pathogen *Chlamydia pneumoniae*. *FEBS Lett.* **562**, 22–26 (2004).
118. Sheng, Y. *et al.* Superoxide dismutases and superoxide reductases. *Chem. Rev.* **114**, 3854–918 (2014).
119. Barnes, A., Balebona, C., Horne, M. & Ellis, A. Superoxide dismutase and catalase in *Photobacterium damselae* subsp. piscicida and their roles in resistance to reactive oxygen species. *Microbiology* **145**, 483–494 (1999).
120. Kim, S., Lee, D., Ho, S. & Choi, S. H. Evidence that the *Vibrio vulnificus* flagellar regulator FlhF is regulated by a quorum sensing master regulator SmcR. *Microbiology* **158**, 2017–2025 (2012).
121. Kim, S. *et al.* Contribution of six flagellin genes to the flagellum biogenesis of *Vibrio vulnificus* and *in vivo* invasion. *Infect. Immun.* **82**, 29–42 (2014).
122. Paranjpye, R. & Strom, M. A *Vibrio vulnificus* type IV pilin contributes to biofilm formation, adherence to epithelial cells, and virulence. *Infect. Immun.* **73**, 1411–22 (2005).
123. Goo, S. *et al.* Identification of OmpU of *Vibrio vulnificus* as a fibronectin-binding protein and its role in bacterial pathogenesis. *Infect. Immun.* **74**, 5586–5594 (2006).
124. Willis, L. & Whitfield, C. Structure, biosynthesis, and function of bacterial capsular polysaccharides synthesized by ABC transporter-dependent pathways. *Carbohydr. Res.* **378**, 35–44 (2013).
125. Larson, T. & Yother, J. *Streptococcus pneumoniae* capsular polysaccharide is linked to peptidoglycan via a direct glycosidic bond to β-D-*N*-acetylglucosamine. *Proc. Natl. Acad. Sci. U. S. A.* **114**, 5695–5700 (2017).
126. Campos, M. *et al.* Capsule polysaccharide mediates bacterial resistance to antimicrobial peptides. *Infect. Immun.* **72**, 7107–14 (2004).
127. Chan, Y., Kim, H., Schneewind, O. & Missiakas, D. The capsular polysaccharide of *Staphylococcus aureus* is attached to peptidoglycan by the LytR-CpsA-Psr (LCP) family of enzymes. *J. Biol. Chem.* **289**, 15680–90 (2014).
128. Whitfield, C. Biosynthesis and assembly of capsular polysaccharides in *Escherichia coli*. *Annu. Rev. Biochem.* **75**, 39–68 (2006).
129. Hilton, T., Rosche, T., Froelich, B., Smith, B. & Oliver, J. Capsular polysaccharide phase variation in *Vibrio*

vulnificus. *Appl. Environ. Microbiol.* **72**, 6986–93 (2006).

130. Wright, A., Simpson, L., Oliver, J. & Morris, J. Phenotypic evaluation of acapsular transposon mutants of *Vibrio vulnificus*. *Infect. Immun.* **58**, 1769–73 (1990).
131. Mayer, A. *et al. Vibrio vulnificus* MO6-24/O lipopolysaccharide stimulates superoxide anion, thromboxane B_2, matrix metalloproteinase-9, cytokine and chemokine release by rat brain microglia *in vitro*. *Mar. Drugs* **12**, 1732–56 (2014).
132. McPherson, V., Watts, J., Simpson, L. & Oliver, J. Physiological effects of the lipopolysaccharide of *Vibrio vulnificus* on mice and rats. *Microbios* **67**, 141–9 (1991).
133. Park, K.-H. *et al.* Low-density lipoprotein protects *Vibrio vulnificus*-induced lethality through blocking lipopolysaccharide action. *Exp. Mol. Med.* **39**, 673–678 (2007).
134. Payne, S., Mey, A. & Wyckoff, E. *Vibrio* iron transport: evolutionary adaptation to life in multiple environments. *Microbiol. Mol. Biol. Rev.* **80**, 69–90 (2016).
135. Martin, J., Gordon, M. & Fitzwater, S. The case for iron. *Limnol. Oceanogr.* **36**, 1793–1802 (1991).
136. Bogard, R. & Oliver, J. Role of iron in human serum resistance of the clinical and environmental *Vibrio vulnificus* genotypes. *Appl. Environ. Microbiol.* **74**, 3322–3322 (2008).
137. Viveiros, A. *et al.* Transferrin as a predictor of survival in cirrhosis. *Liver Transpl.* **24**, 343–351 (2018).
138. Alice, A., Naka, H. & Crosa, J. Global gene expression as a function of the iron status of the bacterial cell: influence of differentially expressed genes in the virulence of the human pathogen *Vibrio vulnificus*. *Infect. Immun.* **76**, 4019–37 (2008).
139. Escolar, L., Pérez-Martín, J. & de Lorenzo, V. Opening the iron box: transcriptional metalloregulation by the Fur protein. *J. Bacteriol.* **181**, 6223–9 (1999).
140. Litwin, C., Rayback, T. & Skinner, J. Role of catechol siderophore synthesis in *Vibrio vulnificus* virulence. *Infect. Immun.* **64**, 2834–8 (1996).
141. Duong-Nu, T. M. *et al.* All three TonB systems are required for *Vibrio vulnificus* CMCP6 tissue invasiveness by controlling flagellum expression. *Infect. Immun.* **84**, 254–265 (2015).
142. Postle, K. & Larsen, R. A. TonB-dependent energy transduction between outer and cytoplasmic membranes. in *BioMetals* vol. 20 453–465 (2007).
143. Minandri, F. *et al.* Role of iron uptake systems in *Pseudomonas aeruginosa* virulence and airway infection. *Infect. Immun.* **84**, 2324–2335 (2016).
144. Kustusch, R. J., Kuehl, C. J. & Crosa, J. H. The *ttpC* gene is contained in two of three TonB systems in the human pathogen *Vibrio vulnificus*, but only one is active in iron transport and virulence. *J. Bacteriol.* **194**, 3250–3259 (2012).
145. Song, E. J. *et al. Vibrio vulnificus* VvhA induces autophagy-related cell death through the lipid raft-dependent c-Src/NOX signaling pathway. *Sci. Rep.* **6**, (2016).
146. Lee, S. J. *et al.* VvpE mediates the intestinal colonization of *Vibrio vulnificus* by the disruption of tight junctions. *Int. J. Med. Microbiol.* **306**, 10–19 (2016).
147. Jeong, H. G. & Satchell, K. J. F. Additive function of *Vibrio vulnificus* MARTXVv and VvhA cytolysins promotes

rapid growth and epithelial tissue necrosis during intestinal infection. *PLoS Pathog.* **8**, (2012).

148. Kwon, K.-B. *et al. Vibrio vulnificus* cytolysin induces superoxide anion-initiated apoptotic signaling pathway in human ECV304 Cells. *J. Biol. Chem.* **276**, 47518–47523 (2001).
149. Kim, B.-S. & Kim, J.-S. Cholesterol induce oligomerization of *Vibrio vulnificus* cytolysin specifically. *Exp. Mol. Med.* **34**, 239–242 (2002).
150. Kang, M.-K. *et al.* Induction of nitric oxide synthase expression by *Vibrio vulnificus* cytolysin. *Biochem. Biophys. Res. Commun.* **290**, 1090–1095 (2002).
151. Lee, B., Kim, S., Choi, S. & Kim, T. Induction of interleukin-8 production via nuclear factor-kappaB activation in human intestinal epithelial cells infected with *Vibrio vulnificus*. *Immunology* **115**, 506–515 (2005).
152. Gray, L. & Kreger, A. Mouse skin damage caused by cytolysin from *Vibrio vulnificus* and by *V. vulnificus* infection. *J. Infect. Dis.* **155**, 236–41 (1987).
153. Kim, H. *et al.* Hemolytic mechanism of cytolysin produced from *Vibrio vulnificus*. *Life Sci.* **53**, 571–7 (1993).
154. Chang, A. *et al. Vibrio vulnificus* secretes a broad-specificity metalloprotease capable of interfering with blood homeostasis through prothrombin activation and fibrinolysis. *J. Bacteriol.* **187**, 6909–16 (2005).
155. Kim, H. *et al.* Procaspase-3 activation by a metalloprotease secreted from *Vibrio vulnificus*. *Int. J. Mol. Med.* **20**, 591–5 (2007).
156. Wright, A. & Morris, J. The extracellular cytolysin of *Vibrio vulnificus* inactivation and relationship to virulence in mice. *Infect. Immun.* **59**, 192–7 (1991).
157. Lee, J. *et al.* Identification and characterization of the *Vibrio vulnificus* rtxA essential for cytotoxicity *in vitro* and virulence in mice. *J. Microbiol.* **45**, 146–52 (2007).
158. Lin, W. *et al.* Identification of a *Vibrio cholerae* RTX toxin gene cluster that is tightly linked to the cholera toxin prophage. *Proc. Natl. Acad. Sci. U. S. A.* **96**, 1071–6 (1999).
159. Boardman, B., Meehan, B. & Fullner Satchell, K. Growth phase regulation of *Vibrio cholerae* RTX toxin export. *J. Bacteriol.* **189**, 1827–35 (2007).
160. Kwak, J., Jeong, H.-G. & Satchell, K. *Vibrio vulnificus* rtxA1 gene recombination generates toxin variants with altered potency during intestinal infection. *Proc. Natl. Acad. Sci. U. S. A.* **108**, 1645–50 (2011).
161. Kim, Y. *et al. Vibrio vulnificus* RTX toxin kills host cells only after contact of the bacteria with host cells. *Cell. Microbiol.* **10**, 848–862 (2008).
162. Abby, S. S. *et al.* Identification of protein secretion systems in bacterial genomes. *Sci. Rep.* **6**, (2016).
163. Coburn, B., Sekirov, I. & Finlay, B. B. Type III secretion systems and disease. *Clinical Microbiology Reviews* vol. 20 535–549 (2007).
164. Park, D. *et al.* Visualization of the type III secretion mediated <i>Salmonella<i>–host cell interface using cryo-electron tomography. *Elife* **7**, (2018).
165. Lombardi, C. *et al.* Structural and functional characterization of the Type three secretion system (T3SS) needle of *Pseudomonas aeruginosa*. *Front. Microbiol.* **10**, 573 (2019).
166. Sato, K. *et al.* A protein secretion system linked to *Bacteroidete* gliding motility and pathogenesis. *Proc. Natl. Acad. Sci. U. S. A.* **107**, 276–281 (2010).
167. Cascales, E. & Cambillau, C. Structural biology of type VI secretion systems. *Philosophical Transactions of the*

Royal Society B: Biological Sciences vol. 367 1102–1111 (2012).

168. Maffei, B., Francetic, O. & Subtil, A. Tracking proteins secreted by bacteria: What's in the toolbox? *Front. Cell. Infect. Microbiol.* **7**, (2017).
169. Pukatzki, S. *et al.* Identification of a conserved bacterial protein secretion system in *Vibrio cholerae* using the *Dictyostelium* host model system. *Proc. Natl. Acad. Sci. U. S. A.* **103**, 1528–33 (2006).
170. Boyer, F., Fichant, G., Berthod, J., Vandenbrouck, Y. & Attree, I. Dissecting the bacterial type VI secretion system by a genome wide *in silico* analysis: What can be learned from available microbial genomic resources? *BMC Genomics* **10**, (2009).
171. Lennings, J., West, T. E. & Schwarz, S. The *Burkholderia* type VI secretion system 5: Composition, regulation and role in virulence. *Front. Microbiol.* **9**, 3339 (2019).
172. Church, S. R., Lux, T., Baker-Austin, C., Buddington, S. P. & Michell, S. L. *Vibrio vulnificus* Type 6 Secretion System 1 contains anti-bacterial properties. *PLoS One* **11**, e0165500 (2016).
173. Speare, L. *et al.* Bacterial symbionts use a type VI secretion system to eliminate competitors in their natural host. *Proc. Natl. Acad. Sci.* **115**, E8528–E8537 (2018).
174. Zhao, W., Caro, F., Robins, W. & Mekalanos, J. J. Antagonism toward the intestinal microbiota and its effect on *Vibrio cholerae* virulence. *Science (80-.).* **359**, 210–213 (2018).
175. Murdoch, S. L. *et al.* The opportunistic pathogen *Serratia marcescens* utilizes type VI secretion to target bacterial competitors. *J. Bacteriol.* **193**, 6057–69 (2011).
176. Hood, R. D. *et al.* A type VI secretion system of *Pseudomonas aeruginosa* targets a toxin to bacteria. *Cell Host Microbe* **7**, 25–37 (2010).
177. Carruthers, M. D., Nicholson, P. A., Tracy, E. N. & Munson, R. S. *Acinetobacter baumannii* utilizes a type VI secretion system for bacterial competition. *PLoS One* **8**, (2013).
178. Salomon, D., Gonzalez, H., Updegraff, B. L. & Orth, K. *Vibrio parahaemolyticus* type VI secretion system 1 is activated in marine conditions to target bacteria, and is differentially regulated from system 2. *PLoS One* **8**, e61086 (2013).
179. Aubert, D. F., Flannagan, R. S. & Valvano, M. A. A novel sensor kinase-response regulator hybrid controls biofilm formation and type VI secretion system activity in *Burkholderia cenocepacia*. *Infect. Immun.* **76**, 1979–1991 (2008).
180. Moscoso, J. A., Mikkelsen, H., Heeb, S., Williams, P. & Filloux, A. The *Pseudomonas aeruginosa* sensor RetS switches Type III and Type VI secretion via c-di-GMP signalling. *Environ. Microbiol.* **13**, 3128–3138 (2011).
181. Brunet, Y. R., Bernard, C. S., Gavioli, M., Lloubès, R. & Cascales, E. An epigenetic switch involving overlapping Fur and DNA methylation optimizes expression of a Type VI secretion gene cluster. *PLoS Genet.* **7**, e1002205 (2011).
182. Chakraborty, S., Sivaraman, J., Leung, K. Y. & Mok, Y. K. Two-component PhoB-PhoR regulatory system and ferric uptake regulator sense phosphate and iron to control virulence genes in type III and VI secretion systems of *Edwardsiella tarda*. *J. Biol. Chem.* **286**, 39417–39430 (2011).
183. Pieper, R. *et al.* Temperature and growth phase influence the outer-membrane proteome and the expression of a type VI secretion system in *Yersinia pestis*. *Microbiology* **155**, 498–512 (2009).

184. Gueguen, E. *et al.* Expression of a *Yersinia pseudotuberculosis* type VI secretion system is responsive to envelope stresses through the OmpR transcriptional activator. *PLoS One* **8**, e66615 (2013).
185. Zheng, J., Shin, O. S., Cameron, D. E. & Mekalanos, J. J. Quorum sensing and a global regulator TsrA control expression of type VI secretion and virulence in *Vibrio cholerae*. *Proc. Natl. Acad. Sci. U. S. A.* **107**, 21128–21133 (2010).
186. Kitaoka, M., Miyata, S. T., Brooks, T. M., Unterweger, D. & Pukatzki, S. VasH Is a transcriptional regulator of the Type VI Secretion System functional in endemic and pandemic *Vibrio cholerae*. *J. Bacteriol.* **193**, 6471–6482 (2011).
187. Mougous, J. D., Gifford, C. A., Ramsdell, T. L. & Mekalanos, J. J. Threonine phosphorylation post-translationally regulates protein secretion in *Pseudomonas aeruginosa*. *Nat. Cell Biol.* **9**, 797–803 (2007).
188. Ostrowski, A. *et al.* Killing with proficiency: Integrated post-translational regulation of an offensive Type VI secretion system. *PLoS Pathog.* **14**, e1007230 (2018).
189. Basler, M., Pilhofer, M., Henderson, G., Jensen, G. & Mekalanos, J. Type VI secretion requires a dynamic contractile phage tail-like structure. *Nature* **483**, 182–186 (2012).
190. Zoued, A. *et al.* Priming and polymerization of a bacterial contractile tail structure. *Nature* **531**, 59–63 (2016).
191. Brackmann, M., Wang, J. & Basler, M. Type VI secretion system sheath inter-subunit interactions modulate its contraction. *EMBO Rep.* **19**, 225–233 (2018).
192. Brunet, Y. R., Hénin, J., Celia, H. & Cascales, E. Type VI secretion and bacteriophage tail tubes share a common assembly pathway. *EMBO Rep.* **15**, 315–321 (2014).
193. Brunet, Y. R., Zoued, A., Boyer, F., Douzi, B. & Cascales, E. The type VI secretion TssEFGK-VgrG phage-like baseplate is recruited to the TssJLM membrane complex via multiple contacts and serves as assembly platform for tail tube/sheath polymerization. *PLoS Genet.* **11**, (2015).
194. Hachani, A., Allsopp, L. P., Oduko, Y. & Filloux, A. The VgrG proteins are 'à la carte' delivery systems for bacterial type VI effectors. *J. Biol. Chem.* **289**, 17872–17884 (2014).
195. Durand, E. *et al.* Biogenesis and structure of a type VI secretion membrane core complex. *Nature* **523**, 555–560 (2015).
196. Durand, E. *et al.* Structural characterization and oligomerization of the TssL protein, a component shared by bacterial type VI and type IVb secretion systems. *J. Biol. Chem.* **287**, 14157–14168 (2012).
197. Arisaka, F., Yap, M. L., Kanamaru, S. & Rossmann, M. G. Molecular assembly and structure of the bacteriophage T4 tail. *Biophysical Reviews* vol. 8 385–396 (2016).
198. Chen, L., Zou, Y., She, P. & Wu, Y. Composition, function, and regulation of T6SS in *Pseudomonas aeruginosa*. *Microbiological Research* vol. 172 19–25 (2015).
199. Mougous, J. D. *et al.* A virulence locus of *Pseudomonas aeruginosa* encodes a protein secretion apparatus. *Science (80-.).* **312**, 1526–1530 (2006).
200. Kostyuchenko, V. A. *et al.* The tail structure of bacteriophage T4 and its mechanism of contraction. *Nat. Struct. Mol. Biol.* **12**, 810–813 (2005).
201. Navarro-Garcia, F., Ruiz-Perez, F., Cataldi, A. & Lazarbal, M. Type VI secretion system in pathogenic

Escherichia coli: Structure, role in virulence, and acquisition. *Front. Microbiol.* **10**, (2019).

202. Shneider, M. M. *et al.* PAAR-repeat proteins sharpen and diversify the type VI secretion system spike. *Nature* **500**, 350–353 (2013).
203. Bröms, J. E., Ishikawa, T., Wai, S. N. & Sjöstedt, A. A functional VipA-VipB interaction is required for the type VI secretion system activity of *Vibrio cholerae* O1 strain A1552. *BMC Microbiol.* **13**, 96 (2013).
204. Bönemann, G., Pietrosiuk, A., Diemand, A., Zentgraf, H. & Mogk, A. Remodelling of VipA/VipB tubules by ClpV-mediated threading is crucial for type VI protein secretion. *EMBO J.* **28**, 315–325 (2009).
205. Cianfanelli, F. R., Monlezun, L. & Coulthurst, S. J. Aim, load, fire: The Type VI Secretion System, a bacterial nanoweapon. *Trends Microbiol.* **24**, 51–62 (2016).
206. Basler, M. & Mekalanos, J. J. Type 6 secretion dynamics within and between bacterial cells. *Science* **337**, 815 (2012).
207. Leiman, P. G. *et al.* Type VI secretion apparatus and phage tail-associated protein complexes share a common evolutionary origin. *Proc. Natl. Acad. Sci. U. S. A.* **106**, 4154–4159 (2009).
208. Nguyen, V. S. *et al.* Type VI secretion TssK baseplate protein exhibits structural similarity with phage receptor-binding proteins and evolved to bind the membrane complex. *Nat. Microbiol.* **2**, (2017).
209. Yang, X., Long, M. & Shen, X. Effector–immunity pairs provide the T6SS nanomachine its offensive and defensive capabilities. *Molecules* **23**, (2018).
210. Wang, T. *et al.* Type VI secretion system transports Zn2+ to combat multiple stresses and host immunity. *PLoS Pathog.* **11**, (2015).
211. Whitney, J. C. *et al.* An interbacterial NAD(P)+ glycohydrolase toxin requires elongation factor Tu for delivery to target cells. *Cell* **163**, 607–619 (2015).
212. Russell, A. B. B. *et al.* A widespread bacterial type VI secretion effector superfamily identified using a heuristic approach. *Cell Host Microbe* **11**, 538–549 (2012).
213. Brooks, T. M., Unterweger, D., Bachmann, V., Kostiuk, B. & Pukatzki, S. Lytic activity of the *Vibrio cholerae* type VI secretion toxin VgrG-3 is inhibited by the antitoxin TsaB. *J. Biol. Chem.* **288**, 7618–7625 (2013).
214. Altindis, E., Dong, T., Catalano, C. & Mekalanos, J. Secretome analysis of Vibrio cholerae type VI secretion system reveals a new effector-immunity pair. *MBio* **6**, e00075 (2015).
215. Russell, A. B. *et al.* Diverse type VI secretion phospholipases are functionally plastic antibacterial effectors. *Nature* **496**, 508–512 (2013).
216. Jiang, F., Waterfield, N. R., Yang, J., Yang, G. & Jin, Q. A *Pseudomonas aeruginosa* type VI secretion phospholipase D effector targets both prokaryotic and eukaryotic cells. *Cell Host Microbe* **15**, 600–610 (2014).
217. Dong, T. G., Ho, B. T., Yoder-Himes, D. R. & Mekalanos, J. J. Identification of T6SS-dependent effector and immunity proteins by Tn-seq in *Vibrio cholerae*. *Proc. Natl. Acad. Sci. U. S. A.* **110**, 2623–2628 (2013).
218. Trunk, K. *et al.* The type VI secretion system deploys antifungal effectors against microbial competitors. *Nat. Microbiol.* **3**, 920–931 (2018).
219. Miyata, S., Unterweger, D., Rudko, S. & Pukatzki, S. Dual expression profile of yype VI secretion system immunity genes protects pandemic *Vibrio cholerae*. *PLoS Pathog.* **9**, e1003752 (2013).
220. Trunk, K., Coulthurst, S. J. & Quinn, J. A new front in microbial warfare-delivery of antifungal effectors by the

type VI secretion system. *J. Fungi* **5**, (2019).

221. Schwarz, S. *et al.* VgrG-5 is a *Burkholderia* type VI secretion system-exported protein required for multinucleated giant cell formation and virulence. *Infect. Immun.* **82**, 1445–1452 (2014).
222. Koskiniemi, S. *et al.* Rhs proteins from diverse bacteria mediate intercellular competition. *Proc. Natl. Acad. Sci. U. S. A.* **110**, 7032–7037 (2013).
223. Alcoforado Diniz, J. & Coulthurst, S. J. Intraspecies competition in *Serratia marcescens* is mediated by Type VI-Secreted Rhs effectors and a conserved effector-associated accessory protein. *J. Bacteriol.* **197**, 2350–60 (2015).
224. Jana, B., Fridman, C. M., Bosis, E. & Salomon, D. A modular effector with a DNase domain and a marker for T6SS substrates. *Nat. Commun.* **10**, (2019).
225. Lin, J. *et al.* A *Pseudomonas* T6SS effector recruits PQS-containing outer membrane vesicles for iron acquisition. *Nat. Commun.* **8**, (2017).
226. Lisher, J. P. & Giedroc, D. P. Manganese acquisition and homeostasis at the host-pathogen interface. *Frontiers in Cellular and Infection Microbiology* vol. 3 (2013).
227. Aguirre, J. D. & Culotta, V. C. Battles with iron: Manganese in oxidative stress protection. *Journal of Biological Chemistry* vol. 287 13541–13548 (2012).
228. Si, M. *et al.* Manganese scavenging and oxidative stress response mediated by type VI secretion system in *Burkholderia thailandensis*. *Proc. Natl. Acad. Sci.* **114**, E2233–E2242 (2017).
229. Si, M. *et al.* The type VI secretion system engages a redox-regulated dual-functional heme transporter for zinc acquisition. *Cell Rep.* **20**, 949–959 (2017).
230. Wettstadt, S. & Filloux, A. Manipulating the type VI secretion system spike to shuttle passenger proteins. *PLoS One* **15**, e0228941 (2020).
231. Lien, Y. W. & Lai, E. M. Type VI secretion effectors: Methodologies and biology. *Frontiers in Cellular and Infection Microbiology* vol. 7 254 (2017).
232. Ho, B., Fu, Y., Dong, T. & Mekalanos, J. *Vibrio cholerae* type 6 secretion system effector trafficking in target bacterial cells. *Proc. Natl. Acad. Sci. U. S. A.* **114**, 9427–9432 (2017).
233. Guidance for inspection of shellfish purification systems for local food authorities. *Local Auth. Food Law Enforc. Branch* (2009).
234. McLeod, C., Polo, D., Le Saux, J. C. & Le Guyader, F. S. Depuration and relaying: A review on potential removal of Norovirus from oysters. *Compr. Rev. Food Sci. Food Saf.* **16**, 692–706 (2017).
235. Shen, X., Su, Y. C., Liu, C., Oscar, T. & DePaola, A. Efficacy of *Vibrio parahaemolyticus* depuration in oysters (*Crassostrea gigas*). *Food Microbiol.* **79**, 35–40 (2019).
236. Whitesides, M. D. & Oliver, J. D. Resuscitation of *Vibrio vulnificus* from the viable but nonculturable state. *Appl. Environ. Microbiol.* **63**, 1002–1005 (1997).
237. Parvathi, A., Kumar, H. S., Karunasagar, I. I. & Karunasagar, I. I. Detection and enumeration of *Vibrio vulnificus* in oysters from two estuaries along the southwest coast of India, using molecular methods. *Appl. Environ. Microbiol.* **70**, 6909–13 (2004).
238. Lowry, P. W. *et al. Vibrio* gastroenteritis in Louisiana: a prospective study among attendees of a scientific

congress in New Orleans. *J. Infect. Dis.* **160**, 978–84 (1989).

239. Doherty, F. & Cherry, D. Tolerance of the Asiatic clam *Corbicula* spp. to lethal level of toxic stressors - a review. *Environ. Pollut.* **51**, 269–313 (1988).
240. McKeon, C. S., Tunberg, B. G., Johnston, C. A. & Barshis, D. J. Ecological drivers and habitat associations of estuarine bivalves. *PeerJ* **3**, e1348 (2015).
241. Kautsky, N. & Evans, S. Role of biodeposition by *Mytilus edulis* in the circulation of matter and nutrients in a Baltic coastal ecosystem. *Marine Ecology Progress Series* vol. 38 201–212.
242. Welladsen, H., Southgate, P., Heimann, K., Welladsen, H. M. & Southgate, P. C. The effects of exposure to near-future levels of ocean acidification on shell characteristics of Pinctada fucata (Bivalvia: Pteriidae). *Molluscan Res.* **30**, 125–130 (2010).
243. Kueh, C. S. W. & Chan, K. Bacteria in bivalve shellfish with special reference to the oyster. *J. Appl. Bacteriol.* **59**, 41–47 (1985).
244. Vasconcelos, G. & Lee, J. Microbial flora of Pacific oysters (*Crassostrea gigas*) subjected to ultraviolet-irradiated seawater. *Appl. Microbiol.* **23**, 11–16 (1972).
245. Kim, Y. W., Lee, S. H., Hwang, I. G. & Yoon, K. S. Effect of temperature on growth of *Vibrio parahaemolyticus* and *Vibrio vulnificus* in flounder, salmon sashimi and oyster meat. *Int. J. Environ. Res. Public Health* **9**, 4662–75 (2012).
246. Porsby, C. H. & Gram, L. *Phaeobacter inhibens* as biocontrol agent against *Vibrio vulnificus* in oyster models. *Food Microbiol.* **57**, 63–70 (2016).
247. Riisgdrd, H. U. Efficiency of particle retention and filtration rate in 6 species of Northeast American bivalves. *Mar. Ecol. Prog. Ser.* **45**, 217–223 (1988).
248. Evan Ward, J. & Shumway, S. E. Separating the grain from the chaff: particle selection in suspension- and deposit-feeding bivalves. *J. Exp. Mar. Bio. Ecol.* **300**, 83–130 (2004).
249. Froelich, B., Ayrapetyan, M. & Oliver, J. D. Integration of *Vibrio vulnificus* into marine aggregates and its subsequent uptake by *Crassostrea virginica* oysters. *Appl. Environ. Microbiol.* **79**, 1454–8 (2013).
250. Zhang, J., Fang, J. & Liang, X. Variations in retention efficiency of bivalves to different concentrations and organic content of suspended particles. *Chinese J. Oceanol. Limnol.* **28**, 10–17 (2010).
251. Barille, L., Prou, J., Heral, M. & Bougrier, S. Retention efficiency in oyster *Crassostrea gigas* exposed to variable food quantity and quality. *IFREMER* 1–32 (1992).
252. Srivastava, M., Tucker, M. S., Gulig, P. A. & Wright, A. C. Phase variation, capsular polysaccharide, pilus and flagella contribute to uptake of *Vibrio vulnificus* by the Eastern oyster (*Crassostrea virginica*). *Environ. Microbiol.* **11**, 1934–1944 (2009).
253. Froelich, B. & Oliver, J. Increases in the amounts of *Vibrio* spp. in oysters upon addition of exogenous bacteria. *Appl. Environ. Microbiol.* **79**, 5208–13 (2013).
254. Pu, M., Duriez, P., Arazi, M. & Rowe-Magnus, D. A. A conserved tad pilus promotes *Vibrio vulnificus* oyster colonization. *Environ. Microbiol.* **20**, 828–841 (2018).
255. Froelich, B., Ringwood, A., Sokolova, I. & Oliver, J. Uptake and depuration of the C- and E-genotypes of *Vibrio vulnificus* by the Eastern Oyster (*Crassostrea virginica*). *Environ. Microbiol. Rep.* **2**, 112–115 (2010).

256. Morrison, C. M. *et al.* Survival of *Salmonella* Newport in oysters. *Int. J. Food Microbiol.* **148**, 93–98 (2011).
257. Morrison, C. M., Dial, S. M., Day, W. A., Joens, L. A. & Joens, L. A. Investigations of *Salmonella enterica* serovar Newport infections of oysters by using immunohistochemistry and knockout mutagenesis. *Appl. Environ. Microbiol.* **78**, 2867–73 (2012).
258. Silver, M. Marine snow: A brief historical sketch. *Limnol. Oceanogr. Bull.* **24**, 5–10 (2015).
259. Kiørboe, T., Andersen, K. P. & Dam, H. G. Coagulation efficiency and aggregate formation in marine phytoplankton. *Mar. Biol.* **107**, 235–245 (1990).
260. Passow, U., Ziervogel, K., Asper, V. & Diercks, A. Marine snow formation in the aftermath of the Deepwater Horizon oil spill in the Gulf of Mexico. *Environ. Res. Lett.* **7**, 035301 (2012).
261. Grossart, H.-P., Kiørboe, T., Tang, K. & Ploug, H. Bacterial colonization of particles: growth and interactions. *Appl. Environ. Microbiol.* **69**, 3500–9 (2003).
262. Passow, U. Transparent exopolymer particles (TEP) in aquatic environments. *Prog. Oceanogr.* **55**, 287–333 (2002).
263. Nwodo, U. U., Green, E. & Okoh, A. I. Bacterial exopolysaccharides: functionality and prospects. *Int. J. Mol. Sci.* **13**, 14002–15 (2012).
264. Yurlova, N. A. & de Hoog, G. S. Exopolysaccharides and capsules in human pathogenic *Exophiala* species. *Mycoses* **45**, 443–8 (2002).
265. Bomfeti, C. A. *et al.* Exopolysaccharides produced by the symbiotic nitrogen-fixing bacteria of *Leguminosae*. *Rev. Bras. Ciência do Solo* **35**, 657–671 (2011).
266. Flemming, H.-C., Neu, T. R. & Wozniak, D. J. The EPS matrix: the 'house of biofilm cells'. *J. Bacteriol.* **189**, 7945–7 (2007).
267. Kiørboe, T. Small-scale turbulence, marine snow formation, and planktivorous feeding. *Sci. Mar.* **61**, 141–158 (1997).
268. Kiørboe, T., Tang, K., Grossart, H.-P. & Ploug, H. Dynamics of microbial communities on marine snow aggregates: colonization, growth, detachment, and grazing mortality of attached bacteria. *Appl. Environ. Microbiol.* **69**, 3036–47 (2003).
269. Biddanda, B. A. & Pomeroy, L. R. Microbial aggregation and degradation of phytoplankton-derived detritus in seawater. *Microb. Succession* **42**, 79–88 (1988).
270. Kiørboe, T., Ploug, H. & Thygesen, U. Fluid motion and solute distribution around sinking aggregates. I. Small-scale fluxes and heterogeneity of nutrients in the pelagic environment. *Mar. Ecol. Prog. Ser.* **211**, 1–13 (2001).
271. Gram, L., Grossart, H.-P., Schlingloff, A. & Kiørboe, T. Possible quorum sensing in marine snow bacteria: production of acylated homoserine lactones by *Roseobacter* strains isolated from marine snow. *Appl. Environ. Microbiol.* **68**, 4111–6 (2002).
272. Decho, A. W. & Gutierrez, T. Microbial extracellular polymeric substances (EPSs) in ocean systems. *Front. Microbiol.* **8**, 922 (2017).
273. Logan, B. E. & Hunt, J. R. Advantages to microbes of growth in permeable aggregates in marine systems. *Limnol. Oceanogr.* **32**, 1034–1048 (1987).
274. Durkin, C., Mock, T. & Armbrust, E. Chitin in diatoms and its association with the cell wall. *Eukaryot. Cell* **8**,

1038–50 (2009).
275. Li, Y. *et al.* Chitinase producing bacteria with direct algicidal activity on marine diatoms. *Sci. Rep.* **6**, 21984 (2016).
276. Williams, T., Ayrapetyan, M. & Oliver, J. Implications of chitin attachment for the environmental persistence and clinical nature of the human pathogen *Vibrio vulnificus*. *Appl. Environ. Microbiol.* **80**, 1580–7 (2014).
277. Frischkorn, K., Stojanovski, A. & Paranjpye, R. *Vibrio parahaemolyticus* type IV pili mediate interactions with diatom-derived chitin and point to an unexplored mechanism of environmental persistence. *Environ. Microbiol.* **15**, 1416–1427 (2013).
278. Williams, T. C., Ayrapetyan, M. & Oliver, J. D. Molecular and physical factors that influence attachment of Vibrio vulnificus to chitin. *Appl. Environ. Microbiol.* **81**, 6158–65 (2015).
279. Wong, E. *et al.* The *Vibrio cholerae* colonization factor GbpA possesses a modular structure that governs binding to different host surfaces. *PLoS Pathog.* **8**, e1002373 (2012).
280. Ward, J., Newell, R., Thompson, R. & Macdonald, B. In vivo studies of suspension-feeding processes in the eastern oyster, *Crassostrea virginica*. *Biol. Bull.* **186**, 22–240 (1994).
281. Cognie, B., Barillé, L., Rincé, Y., Barille, L. & Rince, Y. Selective feeding of the oyster *Crassostrea gigas* fed on a natural microphytobenthos assemblage. *Estuaries* **24**, 126 (2001).
282. Cabello, A. E., Espejo, R. T. & Romero, J. Tracing *Vibrio parahaemolyticus* in oysters (*Tiostrea chilensis*) using a Green Fluorescent Protein tag. *J. Exp. Mar. Bio. Ecol.* **327**, 157–166 (2005).
283. Laurence, M., Rose-Marie, L. & Phillippe, G. Alien species alert: *Crassostrea gigas* (Pacific oyster). *ICES Coop. Res. Rep.* **299**, (2009).
284. Fey, P., Dodson, R. J., Basu, S. & Chisholm, R. L. One stop shop for everything *Dictyostelium*: dictyBase and the Dicty stock center in 2012. in 59–92 (Humana Press, Totowa, NJ, 2013). doi:10.1007/978-1-62703-302-2_4.
285. Milton, D. L., O'toole, R., Horstedt, P., Horstedt, H. & Wolf-Watz, H. *Flagellin A is essential for the virulence of* Vibrio anguillarum*. Journal of Bacteriology* vol. 178 (1996).
286. Hansson, M. D., Rzeznicka, K., Rosenbäck, M., Hansson, M. & Sirijovski, N. PCR-mediated deletion of plasmid DNA. *Anal. Biochem.* **375**, 373–375 (2008).
287. Miles, A., Misra, S. & Irwin, J. The estimation of the bactericidal power of the blood. *J Hyg* **38**, 732–749 (1938).
288. Sussmann, M. Chapter 14. in *Biochemical and Genetic Methods in the Study of Cellular Slime Mold Development* 397–410 (1966).
289. Reyrat, J. M., Pelicic, V., Gicquel, B. & Rappuoli, R. Counterselectable markers: Untapped tools for bacterial genetics and pathogenesis. *Infection and Immunity* vol. 66 4011–4017 (1998).
290. Kaspar, C. & Tamplin, M. Effects of temperature and salinity on the survival of *Vibrio vulnificus* in seawater and shellfish. *Appl. Environ. Microbiol.* **59**, 2425–9 (1993).
291. Brands, D. A. *et al.* Prevalence of *Salmonella* spp. in oysters in the United States. *Appl. Environ. Microbiol.* **71**, 893–897 (2005).
292. Tagliavia, M., Salamone, M., Bennici, C., Quatrini, P. & Cuttitta, A. A modified culture medium for improved isolation of marine *Vibrios*. *Microbiol. Open* **8**, (2019).
293. Klevanskaa, K., Bier, N., Stingl, K., Strauch, E. & Hertwig, S. pVv3, a new shuttle vector for gene expression in

Vibrio vulnificus. *Appl. Environ. Microbiol.* **80**, 1477–81 (2014).

294. Geier, G. E. & Modrich, P. Recognition sequence of the dam methylase of *Escherichia coli* K12 and mode of cleavage of Dpn I endonuclease. *J. Biol. Chem.* **254**, 1408–13 (1979).
295. Hattman, S., Brooks, J. E. & Masurekar, M. Sequence specificity of the P1 modification methylase (M.Eco P1) and the DNA methylase (M.Eco dam) controlled by the *Escherichia coli dam* gene. *J. Mol. Biol.* **126**, 367–80 (1978).
296. Jajere, S. M. A review of *Salmonella enterica* with particular focus on the pathogenicity and virulence factors, host specificity and adaptation and antimicrobial resistance including multidrug resistance. *Veterinary World* vol. 12 504–521 (2019).
297. Cox, C. E., Wright, A. C., McClelland, M. & Teplitski, M. Influence of *Salmonella enterica* Serovar Typhimurium *ssrB* on colonization of Eastern oysters (*Crassostrea virginica*) as revealed by a promoter probe screen. *Appl. Environ. Microbiol.* **82**, 328 (2016).
298. Son, N. T. & Fleet, G. H. Behavior of pathogenic bacteria in the oyster, *Crassostrea commercialis*, during depuration, re-laying, and storage. *Appl. Environ. Microbiol.* **40**, 994–1002 (1980).
299. Basler, M., Ho, B. & Mekalanos, J. Tit-for-tat: type VI secretion system counterattack during bacterial cell-cell interactions. *Cell* **152**, 884–94 (2013).
300. Schaap, P. Evolutionary crossroads in developmental biology: *Dictyostelium discoideum*. *Development* **138**, 387–396 (2011).
301. Majerczyk, C., Schneider, E. & Greenberg, E. P. Quorum sensing control of type VI secretion factors restricts the proliferation of quorum-sensing mutants. *Elife* **5**, (2016).
302. Gallique, M., Bouteiller, M. & Merieau, A. The type VI secretion system: A dynamic system for bacterial communication? *Frontiers in Microbiology* vol. 8 (2017).
303. Tao, Z., Zhou, T., Zhou, S. & Wang, G. Temperature-regulated expression of type VI secretion systems in fish pathogen *Pseudomonas plecoglossicida* revealed by comparative secretome analysis. *FEMS Microbiol. Lett.* **363**, (2016).
304. Ishikawa, T. *et al.* Pathoadaptive conditional regulation of the type VI secretion system in *Vibrio cholerae* O1 strains. *Infect. Immun.* **80**, 575–584 (2012).
305. Yang, X. *et al.* The stringent response factor, RelA, positively regulates T6SS4 expression through the RovM/RovA pathway in *Yersinia pseudotuberculosis*. *Microbiol. Res.* **220**, 32–41 (2019).
306. Huang, Y. *et al.* Functional characterization and conditional regulation of the type VI secretion system in *Vibrio fluvialis*. *Front. Microbiol.* **8**, (2017).
307. Townsley, L., Sison Mangus, M. P., Mehic, S. & Yildiz, F. H. Response of *Vibrio cholerae* to low-temperature shifts: CspV regulation of type VI secretion, biofilm formation, and association with zooplankton. *Appl. Environ. Microbiol.* **82**, 4441–4452 (2016).
308. Salomon, D. *et al.* Type VI secretion system toxins horizontally shared between marine bacteria. *PLOS Pathog.* **11**, e1005128 (2015).
309. Unterweger, D. *et al.* The *Vibrio cholerae* type VI secretion system employs diverse effector modules for intraspecific competition. *Nat. Commun.* **5**, 3549 (2014).

310. Thomas, J., Watve, S. S., Ratcliff, W. C. & Hammer, B. K. Horizontal gene transfer of functional type VI killing genes by natural transformation. *MBio* **8**, (2017).
311. Kirchberger, P. C., Unterweger, D., Provenzano, D., Pukatzki, S. & Boucher, Y. Sequential displacement of Type VI Secretion System effector genes leads to evolution of diverse immunity gene arrays in *Vibrio cholerae*. *Sci. Rep.* **7**, (2017).
312. Schroll, C. *et al.* The SPI-19 encoded type-six secretion-systems (T6SS) of *Salmonella enterica* serovars Gallinarum and Dublin play different roles during infection. *Vet. Microbiol.* **230**, 23–31 (2019).
313. Blondel, C. J. *et al.* The type VI secretion system encoded in *Salmonella* pathogenicity island 19 is required for *Salmonella enterica* serotype Gallinarum survival within infected macrophages. *Infect. Immun.* **81**, 1207–20 (2013).
314. Blondel, C. J., Jiménez, J. C., Contreras, I. & Santiviago, C. A. Comparative genomic analysis uncovers 3 novel loci encoding type six secretion systems differentially distributed in *Salmonella* serotypes. *BMC Genomics* **10**, (2009).
315. Wang, M. *et al.* Molecular characterization of a functional type VI secretion system in *Salmonella enterica* serovar Typhi. *Curr. Microbiol.* **63**, 22–31 (2011).
316. Sana, T. G. *et al. Salmonella typhimurium* utilizes a T6SS-mediated antibacterial weapon to establish in the host gut. *Proc. Natl. Acad. Sci. U. S. A.* **113**, E5044-51 (2016).
317. Ma, A. T. & Mekalanos, J. J. *In vivo* actin cross-linking induced by *Vibrio cholerae* type VI secretion system is associated with intestinal inflammation. *Proc. Natl. Acad. Sci. U. S. A.* **107**, 4365–70 (2010).
318. Logan, S. L. *et al.* The *Vibrio cholerae* type VI secretion system can modulate host intestinal mechanics to displace gut bacterial symbionts. *Proc. Natl. Acad. Sci. U. S. A.* **115**, E3779–E3787 (2018).
319. Chinnadurai, S., Mohamed, K., Sharma, J., Venkatesan, V. & Kripa, V. Assessment of bio-accumulation of bacteria in oysters from shellfish growing waters in Ashtamudi Lake (Kerala, India): A RAMSAR wetland. *Reg. Stud. Mar. Sci.* **7**, 118–122 (2016).
320. Katz, B. Z. *Vibrio vulnificus* meningitis in a boy with thalassemia after eating raw oysters. *Pediatrics* **82**, 784–6 (1988).
321. Iwamoto, M., Ayers, T., Mahon, B. E. & Swerdlow, D. L. Epidemiology of seafood-associated infections in the United States. *Clin. Microbiol. Rev.* **23**, 399–411 (2010).
322. Ward, J. E. & Kach, D. J. Marine aggregates facilitate ingestion of nanoparticles by suspension-feeding bivalves. *Mar. Environ. Res.* **68**, 137–142 (2009).
323. Alldredge, A. The carbon, nitrogen and mass content of marine snow as a function of aggregate size. *Deep Sea Res. Part I Oceanogr. Res. Pap.* **45**, 529–541 (1998).
324. Shanks, A. L. & Edmondson, E. W. Laboratory-made artificial marine snow: a biological model of the real thing. *Mar. Biol.* **101**, 463–470 (1989).
325. Suckow, M., Weisbroth, S. & Franklin, C. *Seawater* - Its Composition, Properties and Behaviour. *Seawater* (Elsevier, 1995). doi:10.1016/b978-0-7506-3715-2.x5000-x.
326. Whitman, W. B., Coleman, D. C. & Wiebe, W. J. Prokaryotes: the unseen majority. *Proc. Natl. Acad. Sci. U. S. A.* **95**, 6578–83 (1998).

327. Bochdansky, A. B., Clouse, M. A. & Herndl, G. J. Eukaryotic microbes, principally fungi and labyrinthulomycetes, dominate biomass on bathypelagic marine snow. *ISME J.* **11**, 362–373 (2017).
328. Bradbury, J. Nature's nanotechnologists: unveiling the secrets of diatoms. *PLoS Biol.* **2**, e306 (2004).
329. Tiselius, P. & Kuylenstierna, M. Growth and decline of a diatom spring bloom: phytoplankton species composition, formation of marine snow and the role of heterotrophic dinoflagellates. *J. Plankton Res.* **18**, 133–155 (1996).
330. Pilskaln, C., Villareal, T., Dennett, M., Darkangelo-Wood, C. & Meadows, G. High concentrations of marine snow and diatom algal mats in the North Pacific Subtropical Gyre: Implications for carbon and nitrogen cycles in the oligotrophic ocean. *Deep Sea Res. Part I Oceanogr. Res. Pap.* **52**, 2315–2332 (2005).
331. Thornton, D. Diatom aggregation in the sea: mechanisms and ecological implications. *Eur. J. Phycol.* **37**, 149–161 (2002).
332. Schnetzer, A. *et al.* Marine snow formation by the toxin-producing diatom, *Pseudo-nitzschia australis*. *Harmful Algae* **61**, 23–30 (2017).
333. Behringer, G. *et al.* Bacterial communities of diatoms display strong conservation across strains and time. *Front. Microbiol.* **9**, 659 (2018).
334. Crenn, K., Duffieux, D. & Jeanthon, C. Bacterial epibiotic communities of ubiquitous and abundant marine diatoms are distinct in short- and long-term associations. *Front. Microbiol.* **9**, 2879 (2018).
335. Gooday, G. The ecology of chitin degradation. in *Advances in Microbial Ecology* vol. 11 387–430 (Springer, Boston, MA, 1990).
336. Aunkham, A. *et al.* Structural basis for chitin acquisition by marine *Vibrio* species. *Nat. Commun.* **9**, 1–13 (2018).
337. Meibom, K., Blokesch, M., Dolganov, N., Wu, C. & Schoolnik, G. Chitin induces natural competence in *Vibrio cholerae*. *Science (80-.).* **310**, 1824–1827 (2005).
338. Zobell, C. & Rittenberg, S. The occurrence and characteristics of chitinoclastic bacteria in the sea. *J. Bacteriol.* **35**, 275–87 (1938).
339. Brandl, M. *et al. Salmonella* biofilm formation on *Aspergillus niger* involves cellulose – chitin interactions. *PLoS One* **6**, e25553 (2011).
340. Frederiksen, R. *et al.* Bacterial chitinases and chitin-binding proteins as virulence factors. *Microbiology* **159**, 833–847 (2013).
341. Larsen, T. *et al.* Characterization of a novel *Salmonella* Typhimurium chitinase which hydrolyzes chitin, chitooligosaccharides and an N-acetyllactosamine conjugate. *Glycobiology* **21**, 426–36 (2011).
342. Holland, P., Abramson, R., Watson, R. & Gelfand, D. Detection of specific polymerase chain reaction product by utilizing the 5′ → 3′ exonuclease activity of *Thermus aquaticus* DNA polymerase. *Proc. Natl. Acad. Sci. U. S. A.* **88**, 7276–7280 (1991).
343. Wright, A. C., Morris, J. G., Maneval, D. R., Richardson, K. & Kaper, J. B. Cloning of the cytotoxin-hemolysin gene of *Vibrio vulnificus*. *Infect. Immun.* **50**, 922–4 (1985).
344. Wright, A. C. *et al.* Rapid identification of *Vibrio vulnificus* on nonselective media with an alkaline phosphatase-labeled oligonucleotide probe. *Appl. Environ. Microbiol.* **59**, 541–6 (1993).

345. Morris, J. G. *et al.* Identification of environmental *Vibrio vulnificus* isolates with a DNA probe for the cytotoxin-hemolysin gene. *Appl. Environ. Microbiol.* **53**, 193–5 (1987).
346. Ho, B., Dong, T. & Mekalanos, J. A view to a kill: the bacterial type VI secretion system. *Cell Host Microbe* **15**, 9–21 (2014).
347. Doran, J. *et al.* Diagnostic potential of *sefA* DNA probes to *Salmonella enteritidis* and certain other O-serogroup D1 *Salmonella* serovars. *Mol. Cell. Probes* **10**, 233–246 (1996).
348. SOFIA 2018 - State of Fisheries and Aquaculture in the world 2018.
349. Dubert, J. *et al.* Following the infection process of vibriosis in Manila clam (*Ruditapes philippinarum*) larvae through GFP-tagged pathogenic *Vibrio* species. *J. Invertebr. Pathol.* **133**, 27–33 (2016).
350. Bruto, M. *et al. Vibrio crassostreae*, a benign oyster colonizer turned into a pathogen after plasmid acquisition. *ISME J.* **11**, 1043–1052 (2017).
351. Lacoste, A. *et al.* A *Vibrio splendidus* strain is associated with summer mortality of juvenile oysters *Crassostrea gigas* in the Bay of Morlaix (North Brittany, France). *Dis. Aquat. Organ.* **46**, 139–145 (2001).
352. Herndl, G. J. & Peduzzi, P. The ecology of amorphous aggregations (marine snow) in the Northern Adriatic Sea. *Mar. Ecol.* **9**, 79–90 (1988).
353. Stevick, R. J. *et al.* Bacterial community dynamics in an oyster hatchery in response to probiotic treatment. *Front. Microbiol.* **10**, 1060 (2019).
354. Kang, C.-H., Gu, T. & So, J.-S. Possible probiotic lactic acid bacteria isolated from oysters (*Crassostrea gigas*). *Probiotics Antimicrob. Proteins* **10**, 728–739 (2018).
355. Corrêa, A. de A. *et al.* The depuration dynamics of oysters (*Crassostrea gigas*) artificially contaminated with hepatitis A virus and human adenovirus. *Mem. Inst. Oswaldo Cruz* **107**, 11–17 (2012).
356. Sana, T. G. *et al.* The second type VI secretion system of *Pseudomonas aeruginosa* strain PAO1 is regulated by quorum sensing and Fur and modulates internalization in epithelial cells. *J. Biol. Chem.* **287**, 27095–105 (2012).
357. Jones, M., Warner, E. & Oliver, J. Survival of and *in situ* gene expression by *Vibrio vulnificus* at varying salinities in estuarine environments. *Appl. Environ. Microbiol.* **74**, 182–187 (2008).

Publication

environmental microbiology

Environmental Microbiology (2020) **00**(00), 00–00 doi:10.1111/1462-2920.15123

Special Issue Article

A universal oyster infection model demonstrates that *Vibrio vulnificus* Type 6 secretion systems have antibacterial activity *in vivo*

Cameron L. Hubert* **and Stephen Ll. Michell*** *College of Life and Environmental Sciences, University of Exeter, Exeter, EX4 4QD, UK.*

Summary

With the rapid increase of aquaculture contributing to sustainable food security, comes the need to better understand seafood associated diseases. One of the major aquatic bacterial genera responsible for human infections from seafood is *Vibrio*, especially from oysters. Currently, *in vivo* study of bacterial interactions within oysters is limited by the inability to promote high-level uptake of bacteria by oysters. This study has therefore evolved current natural marine snow protocols to generate 'artificial' marine snow, into which bacteria can be incorporated to facilitate extensive uptake by oysters. This presents an adaptable model for bacterial study within filter-feeding shellfish. Using this model, we demonstrate for the first time the antibacterial activity of *Vibrio vulnificus* Type 6 secretion systems *in vivo*, revealing an important role for the T6SS in *V. vulnificus* ecology.

Introduction

The State of the World Fisheries and Aquaculture (SOFIA) report (2018) describes 80 million tonnes of aquaculture produced in 2016, of which molluscs totalled 17.1 million tonnes (SOFIA, 2018). Comprising 47% of global fish and mollusc production, fisheries and aquaculture are paramount food security concerns for ensuring continued and consistent seafood production. However, aquaculture practices are becoming increasingly intensive to meet this demand, resulting in proliferation of marine pathogens and food safety issues (Bondad-Reantaso *et al*., 2005; Rico *et al*., 2012). *Vibrio* species are a major hurdle in bivalve production, in particular oysters, due to their mortality in early developmental stages and their deleterious impact on adult shellfish (Dubert *et al*., 2016; Bruto *et al*., 2017). Seasonal losses to the oyster pathogen, *Vibrio splendidus*, have consistently reached up to 80% in oyster farms in the Bay of Morlaix over a 10-year span (Lacoste *et al*., 2001). Furthermore, the *Vibrionaceae* family harbours numerous human pathogens, including *Vibrio vulnificus*, *Vibrio cholerae* and *Vibrio parahaemolyticus*, which are responsible for around 80,000 vibriosis cases annually in the United States (CDC, n.d.). The investigation of *Vibrio* ecology is therefore essential for understanding how to best manage the threat they pose to aquaculture and human health.

Studies exploring bacterial behaviour within shellfish have previously utilized oysters inoculated through exposure to water supplemented with bacterial culture (Srivastava *et al*., 2009; Pu *et al*., 2018). However, this approach is limited by inefficient uptake of bacteria as oysters filter and ingest particles based primarily on size (Froelich *et al*., 2013). Planktonic *V. vulnificus* (2 μm) fall below the optimal size range for ingestion, therefore only achieving low levels of uptake in such experiments (Froelich and Noble, 2014). Incorporation of bacterial cultures into larger, naturally forming aggregates known as 'marine snow' has shown potential as a method for enhancing bacterial uptake by oysters (Froelich *et al*., 2013). Marine snow is composed of diatoms, faecal matter, microorganisms, protists and other miscellaneous elements brought together at random that present a unique environment for bacterial colonization and survival. However, this stochastic process generates inherent variability (Kiørboe *et al*., 1990; Grossart *et al*., 2003; Kiørboe *et al*., 2003; Passow *et al*., 2012).

Vibrio vulnificus is the leading cause of seafood-related disease in the United States and is increasing in prevalence globally, correlating with rising sea-surface temperatures (Jones and Oliver, 2009; Baker-

Received 30 April, 2020; revised 1 June, 2020; accepted 7 June, 2020. *For correspondence. E-mail ch524@exeter.ac.uk; s.l.michell@exeter.ac.uk, Tel. +44(0)1392725524

Austin *et al*., 2012; Vezzulli *et al*., 2015; Baker-Austin *et al*., 2017; Deeb *et al*., 2018). Ingestion can result in severe gastroenteritis which may develop into primary septicaemia, with symptoms including vomiting, haemorrhagic bullae, secondary lesions on extremities and severe hypotension (Beatty *et al*., 2017). Progression to primary septicaemia results in 50% patient fatality within 48 h of hospital admission (Chiang *et al*., 2003). Exposure of open wounds to contaminated water results in erythema, haemorrhagic bullae, cellulitis and intense pain (Oliver, 2005). Failing immediate treatment, infected lesions frequently turn necrotic. While visually more aggressive, wound infections carry a lower mortality rate of 25% compared with ingestion whose rates are >50% if treated within 24 h and 100% if untreated for over 72 h (Jones and Oliver, 2009; Kim *et al*., 2011). Particularly at risk are patients with compromised immune systems, liver disease and haematological disorders, with 80% of patients already presenting at least one pre-existing medical condition (Menon *et al*., 2014).

Studies comparing the genetic makeup of *V. vulnificus* strains identified two Type 6 secretion systems (T6SSs) labelled T6SS1 and T6SS2 (Church *et al*., 2016). A molecular syringe composed of 13 essential proteins, the T6SS functions to inject cytotoxic effectors into neighbouring cells (Ho *et al*., 2014). Shown to have a wide range of activity in other bacterial species, the T6SS has been implicated in both anti-prokaryotic and anti-eukaryotic activity (Salomon *et al*., 2013; Ray *et al*., 2017; Trunk *et al*., 2018; Berni *et al*., 2019). Interestingly, whilst the T6SS2 was identified in all *V. vulnificus* strains sequenced to date, only some strains possessed the T6SS1. *in vitro* competition assays showed that T6SS1-positive (T6SS1$^+$) strains were able to target and kill T6SS-negative (T6SS1$^-$) strains as well as other bacterial species. T6SS-mediated antibacterial activity has been demonstrated by a range of bacteria, such as *Klebsiella pneumoniae*, *V. cholerae* and *Vibrio fluvialis*, in various *in vivo* models including mice, rabbits and squid (Fu *et al*., 2018; Speare *et al*., 2018; Hsieh *et al*., 2019). It was thus hypothesised that the T6SS1 may play a significant role in competition between *Vibrios*, and on bacterial population dynamics *in vivo*.

Here we demonstrate that *V. vulnificus* T6SS1 and T6SS2 mediate antibacterial activity in an oyster *in vivo* model. Killing was shown to be thermoregulated with only T6SS1 active at 30°C, but both T6SS1 and T6SS2 active at 21°C. This is the first study to present a role for the T6SS2 of *V. vulnificus*. For *in vivo* studies, we have adapted current marine snow methodologies to develop a defined, highly controllable 'artificial marine snow' (AMS) based on aggregation of the diatom species, *Thalassiosira pseudonana*. Using inoculated AMS, we achieved higher uptake of *V. vulnificus* and *Salmonella enterica* serovar Enteritidis by oysters than any study to date. We believe this methodology may have much broader application within research and aquaculture. Co-culture of strains within oysters showed that T6SS1 and T6SS2 mediate intra- and inter-species competition *in vivo* and may play a pivotal role in the establishment of *V. vulnificus* strains within filter-feeding shellfish and subsequent prevalence of virulent strains.

Results

Vibrio vulnificus *T6SSs display no anti-eukaryotic activity against* Dictyostelium discoideum

The T6SS of *V. cholerae* demonstrates a range of anti-eukaryotic functionality, such as actin cross-linking to inhibit phagocytosis by macrophages (Pukatzki *et al*., 2007). We hypothesised that *V. vulnificus* T6SSs may also possess anti-eukaryotic activity. To explore this hypothesis, wild-type *V. vulnificus* 106-2A (T6SS1$^+$/T6SS2$^+$) and mutants of both T6SSs were employed in *Dictyostelium discoideum* plaque-forming assays. T6SS1 and T6SS2 mutants were generated through in-frame deletion of *hcp1* and *hcp2* genes encoding effector-transporting needle components of the T6SS (Fig. 1A) (Cascales and Cambillau, 2012). Mutants were labelled ΔT6SS1 (*hcp1*$^-$) and ΔT6SS2 (*hcp2*$^-$) respectively. Deletion of *hcp1* and *hcp2* was confirmed via PCR and expression of downstream genes verified by reverse-transcriptase-PCR (RT-PCR) (Fig. 1B and C). For *D. discoideum* plaque-forming assays, wild-type *V. vulnificus* 106-2A and T6SS deletion mutants were combined with predatory *D. discoideum* AX3 and plated as a lawn on SM agar for 3–5 days at 21°C. If the T6SSs possess anti-eukaryotic activity, larger plaques of predation should be observed relative to wild-type *V. vulnificus* 106-2A following their deletion. No plaques were observed on plates containing wild-type *V. cholerae* V52, a strain with previously characterized anti-eukaryotic activity (Fig. 1D) (Miyata *et al*., 2011). However, visible plaques were recorded on *V. vulnificus* 106-2A, ΔT6SS1 (*hcp1*$^-$) and ΔT6SS2 (*hcp2*$^-$) lawns, indicative of *V. vulnificus* predation by *D. discoideum* (Fig. 1E–G). Measurement of plaque diameter showed no significant difference in predation efficiency between *V. vulnificus* strains (Fig. 1H). These results indicate that the T6SSs of *V. vulnificus* are unable to target *D. discoideum* and have no observable anti-eukaryotic activity at 21°C in this model of infection. A similar lack of anti-eukaryotic activity has also been previously demonstrated in a *Galleria mellonella* model of virulence at 37°C (Church *et al*., 2016).

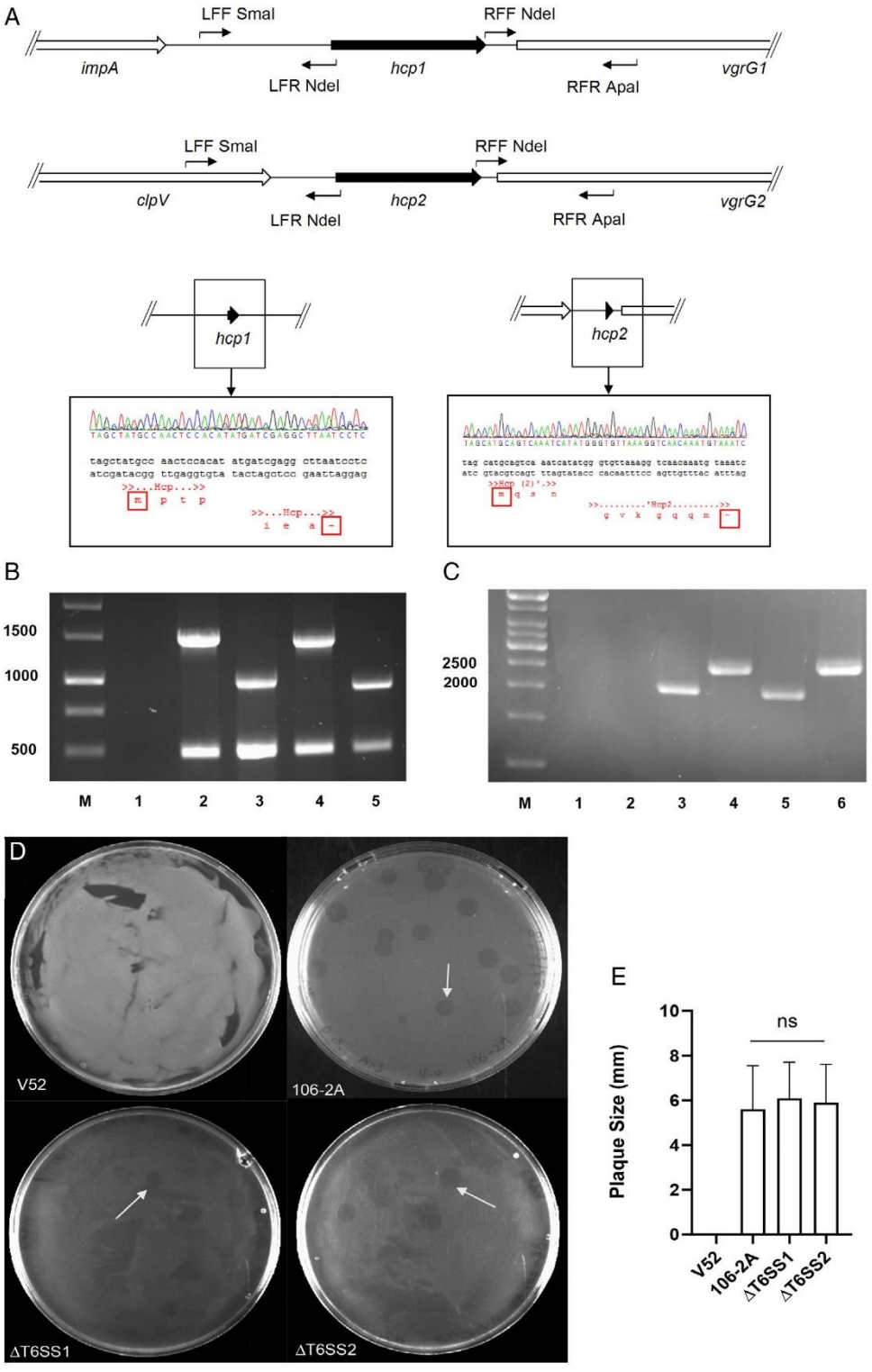

Both V. vulnificus *T6SS1 and T6SS2 demonstrate* in vitro *antibacterial activity at environmental temperatures*

Given the apparent lack of anti-eukaryotic phenotype from either of the T6SSs of *V. vulnificus* against *D. discoideum*, we sought to further investigate previous observations of *V. vulnificus* intra- and inter-species competition mediated by the T6SS (Church *et al*., 2016). As T6SS activation in *V. cholerae* has been identified at 23°C, we aimed to explore whether *V. vulnificus* also exhibits T6SS activity at environmental temperatures (Ishikawa *et al*., 2012). Competition assays were thus conducted at 21°C, an optimal temperature for *V. vulnificus* growth in sea water (Kaspar and Tamplin, 1993). To facilitate enumeration of strains in competition, attacker strains *V. vulnificus* 106-2A (wild-type), ΔT6SS1 (*hcp1*$^{-}$) and ΔT6SS2 (*hcp2*$^{-}$) were transformed with pVv3-Kan to confer kanamycin resistance (Klevanskaa *et al*., 2014). Likewise, an environmental 'prey' *V. vulnificus* strain, 99-743, (T6SS1^{-}, T6SS2^{+}), was transformed with pVv3-Tmp to confer trimethoprim resistance.

Competition between attacker and prey *V. vulnificus* confirms T6SS1 activity at 30°C, demonstrated by a clear and significant 1000-fold reduction of prey 99-743 following co-culture with 106-2A but no reduction when cultured with ΔT6SS1 (*hcp1*$^{-}$) (Fig. 2A). We therefore sought to see if a more environmentally representative temperature had an effect on T6SS activity. Competition assays were thus conducted at 21°C for both T6SS deletion strains (Fig. 2B). We observed a significant 10-fold reduction in 99-743 prey counts following individual co-culture with 106-2A and the ΔT6SS2 (*hcp2*$^{-}$) mutant at 21°C. In addition, at 21°C we also observed for the first time a T6SS2 antibacterial activity, manifested as a reduction in prey numbers comparable with that observed for the T6SS1 ($p < 0.05$) (Fig. 2B). To confirm that the observed reduction in prey numbers were indeed T6SS-dependent and not the result of alternative antibacterial mechanisms active at 21°C, a 106-2A Δ*hcp1*Δ*hcp2* double mutant was generated, named ΔT6SS1/2. No reduction in recovery of the prey strain 99-743 was observed following co-culture with ΔT6SS1/2 (*hcp1*$^{-}$, *hcp2*$^{-}$). These data confirm that killing by ΔT6SS1 (*hcp1*$^{-}$) and ΔT6SS2 (*hcp2*$^{-}$) was due to the T6SS2 and T6SS1, respectively, and that both systems are capable of intra-species targeting at 21°C *in vitro*. Given the broad nature of T6SS activity, we investigated whether the T6SS competent strains of *V. vulnificus* were able to demonstrate inter-species antibacterial activity. To address this question, we utilized *Salmonella* Enteritidis CC012 as a prey strain in competition with our panel of attacker *V. vulnificus* T6SS mutants. Similar to our intra-species data, we observed a T6SS1-driven 1000-fold reduction of prey CC012 at 30°C but no reduction with the ΔT6SS1 (*hcp1*$^{-}$) attacker strain (Fig. 2C). Of interest, the competition assays at 21°C demonstrated that CC012 was targeted by 106-2A, ΔT6SS1 (*hcp1*$^{-}$) and ΔT6SS2 (*hcp2*$^{-}$), resulting in significantly reduced prey recovery ($p < 0.01$) (Fig. 2D). This reduction was not observed when co-cultured with the double mutant, ΔT6SS1/2 (*hcp1*$^{-}$, *hcp2*$^{-}$), reinforcing the role of *V. vulnificus'* T6SS2 in bacterial killing at environmental temperatures.

Development of a delivery model to facilitate reproducible uptake of bacteria by oysters

Having demonstrated *V. vulnificus* T6SS activity *in vitro*, we sought to investigate whether such activity occurred *in vivo* by developing an oyster model for studying bacterial interactions. Previous *in vivo* models of bacterial uptake utilizing oysters have either employed directly inoculated sea water or 'natural marine snow' (NMS) (Srivastava *et al*., 2009; Froelich *et al*., 2013; Pu *et al*., 2018). Our attempt at incorporating *V. vulnificus* into NMS, formed by aggregating seawater particulate matter, showed some success but did not achieve incorporation $>3 \times 10^4$ CFU/g marine snow (Fig. 3A). This may be due to the competition from the naturally occurring bacteria that pre-colonize the particulate matter preventing *V. vulnificus* establishment. We showed that NMS contained diverse bacterial populations, including *Vibrio* species, as determined by growth on both LB and Thiosulfate-Citrate-Bile Salts-sucrose (TCBS) agar plates (Fig. 3A). Moreover, our NMS also varied by size and composition (Fig. S1). Given that the levels of

Fig. 1. Generation of *Vibrio vulnificus* 106-2A T6SS deletion mutants, ΔT6SS1 and ΔT6SS2, for *Dictyostelium discoideum* plaque-forming assays. A. Schematic view of *V. vulnificus* 106-2A Hcp1 and Hcp2 regions with marked primer-binding sites. Left and right flanking regions of *hcp1* and *hcp2* were ligated for construction of in-frame deletion cassettes. Deletion cassettes were introduced to *V. vulnificus* 106-2A using pDM4 to generate ΔT6SS1 (*hcp1*$^{-}$) and ΔT6SS2 (*hcp2*$^{-}$). Truncated *hcp1* and *hcp2* genes from *V. vulnificus* ΔT6SS1 and *V. vulnificus* ΔT6SS2 are shown below with confirmatory sequencing data. Start and stop codons for *hcp1* and *hcp2* are highlighted with red boxes.
B. PCR confirmation of *hcp1* and *hcp2* deletion. M – molecular marker (bp), 1 – no template control, 2 – *hcp1* positive control, 3 – ΔT6SS1 mutant, 4 – *hcp2* control, 5 – ΔT6SS2 mutant. Lanes 2–5 also exhibit a species-specific *vvhA* band at 500 bps to confirm mutants are *V. vulnificus*. C. Expression of genes downstream of *hcp1* and *hcp2* (*vgrG1* and *clpV* respectively) was confirmed using RT-PCR. M – molecular marker (bp), 1 – no template control, 2 – no reverse-transcriptase gDNA control, 3 – 106-2A wild-type positive *vgrG1* control, 4 – 106-2A wild-type positive *clpV* control, 5 – ΔT6SS1 *vgrG1*, 6 – ΔT6SS2 *clpV*. D. *Dictyostelium discoideum* cultures were combined with *Vibrio cholerae* V52, *V. vulnificus* 106-2A, *V. vulnificus* ΔT6SS1 and *V. vulnificus* ΔT6SS2. Example plaques are indicated with white arrows. E. Measurement of *D. discoideum* plaques ($n = 4$) following growth on *V. vulnificus* 106-2A, ΔT6SS1, ΔT6SS2 and *V. cholerae* V52. Ns – not significant.

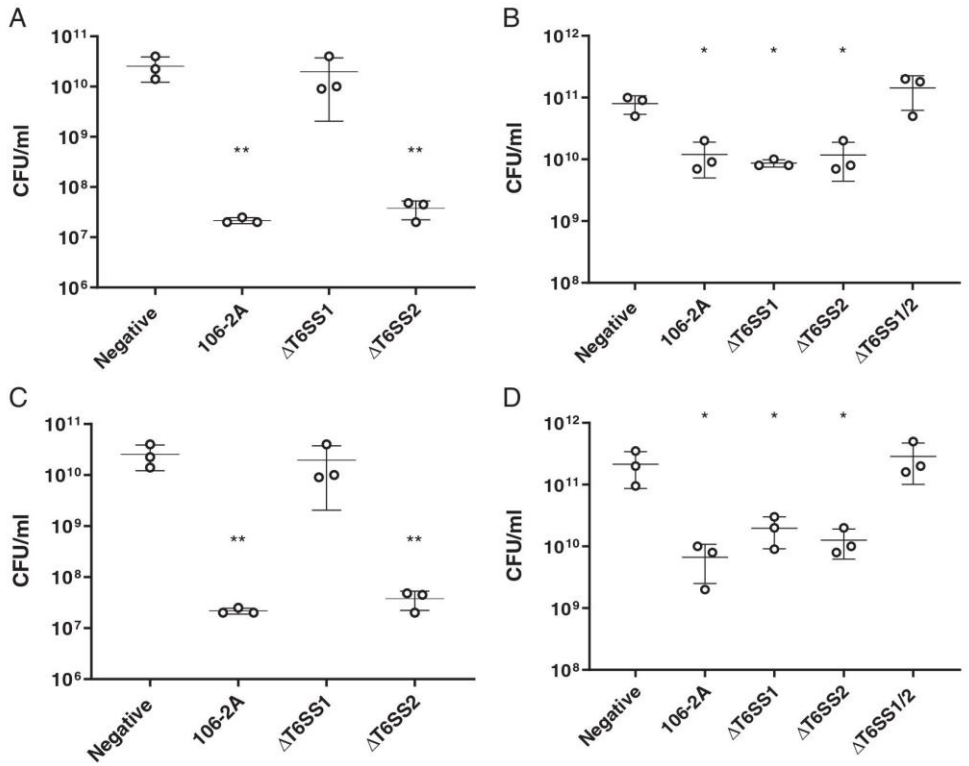

Fig. 2. Intra-/inter-species killing activity of *Vibrio vulnificus* 106-2A T6SS1 and T6SS2 at 21°C and 30°C *in vitro*. A. Viable cell counts of prey *V. vulnificus* 99-743 following co-culture with LB (negative control), *V. vulnificus* 106-2A, ΔT6SS1 or ΔT6SS2 at 30°C for 5 h. B. Viable cell counts of prey *V. vulnificus* 99-743 following co-culture with LB, *V. vulnificus* 106-2A, ΔT6SS1, ΔT6SS2 or ΔT6SS1/2 at 21°C for 24 h. C. Viable cell counts of prey *Salmonella* Enteritidis CC012 following co-culture with LB, *V. vulnificus* 106-2A, ΔT6SS1 or ΔT6SS2 at 30°C for 5 h. D. Viable cell counts of prey *S*. Enteritidis CC012 following co-culture with LB, *V. vulnificus* 106-2A, ΔT6SS1, ΔT6SS2 or ΔT6SS1/2 at 21°C for 24 h. Horizontal lines represent the mean, error bars represent the standard deviation. Assays were performed in triplicate ($n = 3$). Prey counts following co-culture with attacking strains were statistically compared with prey counts following co-culture with just LB using a one-way analysis of variance with Dunnett's corrections for multiple comparisons. * $p < 0.05$, ** $p < 0.01$.

incorporation into NMS were $<3 \times 10^4$ CFU/g marine snow and *Vibrio* levels in oysters can be up to 5×10^4 CFU/g tissue in areas where *V. vulnificus* infections are prevalent, it was clear that uptake material containing far higher numbers of *Vibrio* was required (Froelich *et al*., 2017).

To facilitate reproducible, high-level uptake of bacteria by oysters, we developed an AMS model, exploiting a natural food source for oysters. Commercial shellfish are often reared on microalgae concentrates and we therefore investigated whether bacteria could be rationally incorporated into this material. Essentially, our AMS model is the aggregation of the diatom species *T. pseudonana* CCMP 1335, with the subsequent incorporation of bacteria as detailed in the Experimental procedures section. This model reliably and reproducibly demonstrated levels of bacterial incorporation of $>10^7$ CFU/g AMS (Fig. 3B). These levels were observed for *V vulnificus* 106-2A, 99-743 and *S*. Enteritidis CC012. To control for the presence of contaminating bacteria in the *T. pseudonana*, AMS was plated on LB, *Vibrio*-selective TCBS and *Salmonella*-selective ChromoSelect agar. The remarkably high levels of bacterial incorporation into AMS, observed by plate count enumeration, contrasted starkly to the levels of incorporation into the NMS, the latter being of four orders of magnitude less than the $>10^7$ CFU/g AMS levels. Both *V. vulnificus* 99-743 and *S*. Enteritidis CC012 demonstrated significantly greater incorporation into AMS than *V. vulnificus* 106-2A ($p < 0.05$ and $p < 0.0001$ respectively). Given that we want to explore intra and inter-species competition, it was necessary to generate AMS with similar levels of bacterial strains. This was achieved simply by inoculating the starting material with appropriately higher numbers of bacterial cultures, resulting in AMS of consistent bacterial loads (Fig. 3C). Co-incorporation of attacker and prey bacteria into AMS confirmed that there was no significant killing of prey bacteria occurring in AMS that may impact

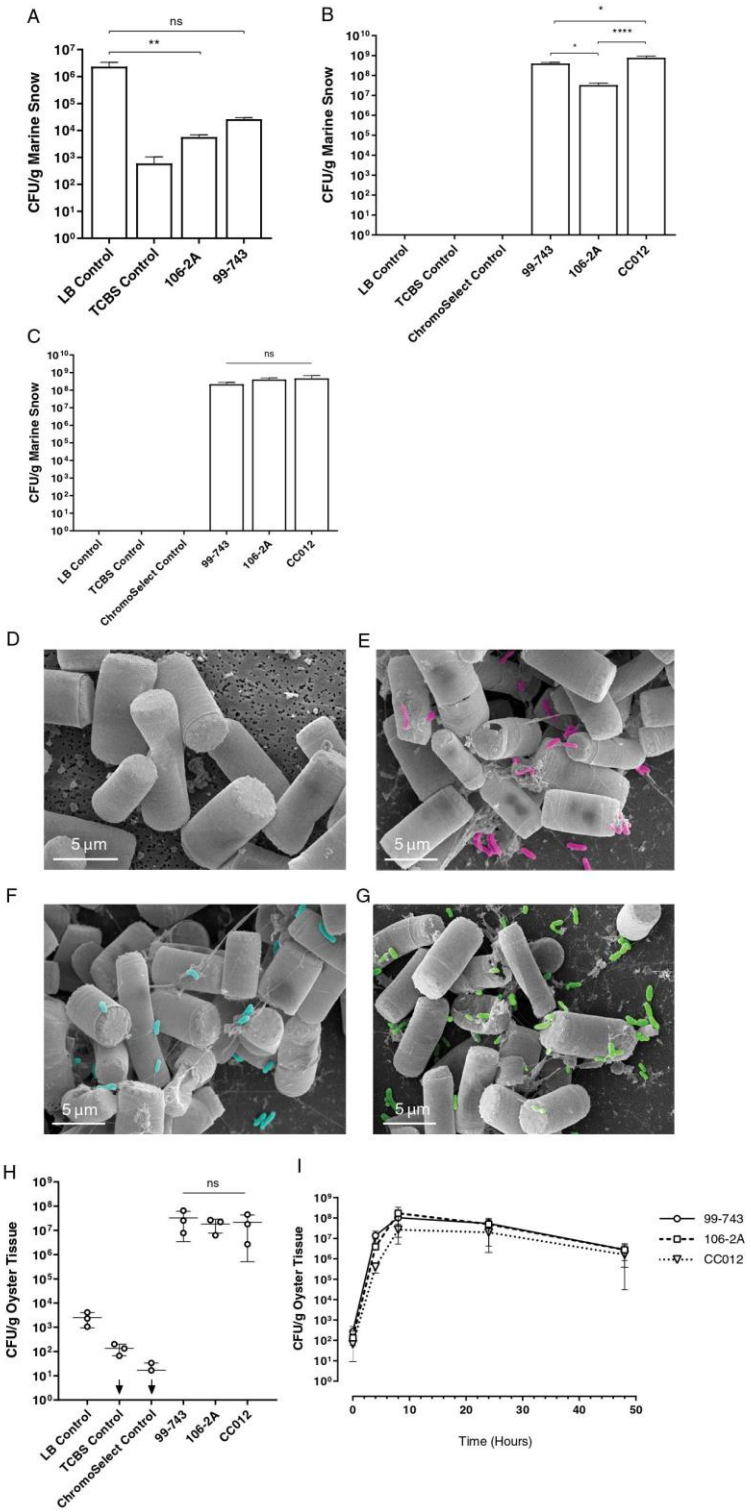

Fig. 3. Incorporation of *Vibrio vulnificus* 106-2A, 99-743 and *Salmonella* Enteritidis CC012 into AMS. A. Incorporation of *V. vulnificus* 106-2A and 99-743 into NMS generated using seawater as a substrate ($n = 3$). Bacteria-free controls were plated on LB and TCBS agar. B. Incorporation of *V. vulnificus* 106-2A, 99-743 and *S.* Enteritidis CC012 into AMS for 24 h at 21°C ($n = 3$). C. Enumeration of *V. vulnificus* 106-2A, 99-743 and *S.* Enteritidis CC012 from AMS following adjustment of starting culture concentrations to ensure equal incorporation of all strains ($n = 3$). D. Bacteria-free AMS control, magnification, ×5000. E. *Vibrio vulnificus* 106-2A (pink), magnification, ×4000. F. *Vibrio vulnificus* 99-743 (blue), magnification, ×4000. G. *Samonella* Enteritidis CC012 (green), magnification, ×4000. H. Oyster uptake of AMS inoculated *V. vulnificus* 106-2A, 99-743, or *S.* Enteritidis CC012. Each point represents the mean of six technical oyster replicates ($n = 3$), error bars show the standard deviation. Control oysters exposed to bacteria-free AMS were plated on LB, TCBS and ChromoSelect agar. Samples in which bacterial load fell below the limit of detection of 100 CFU/g oyster tissue are indicated by a downward arrow. I. Bacterial ingestion was measured over 48 h. Oysters were enumerated at T_0, T_4, T_8, T_{24} and T_{48} h ($n = 3$). Error bars represent the standard deviation. Statistics were performed using either a one-way analysis of variance (ANOVA) with Dunnett's corrections for multiple comparisons (Fig. 1A–C) or a nested one-way ANOVA with Dunnett's corrections for multiple comparisons (Fig. 1H). Ns – not significant, * $p < 0.05$, ** $p < 0.01$, **** $p < 0.0001$.

downstream assays (Fig. S2). AMS-incorporating bacteria were also imaged via scanning electron microscopy (SEM). *Vibrio vulnificus* 106-2A (blue), *V. vulnificus* 99-743 (pink) and *S.* Enteritidis CC012 (green) are clearly incorporated into *T. pseudonana* AMS (Fig. 3D–G).

Given the effectiveness of the developed AMS model, the next step was to investigate the suitability of this material for uptake by oysters. Oysters were exposed to inoculated AMS for 24 h at 21C. Following exposure, oyster stomachs were removed and homogenized for bacterial enumeration by plate counts. Figure 3H presents viable cell counts of *V. vulnificus* 99-743, 106-2A and *S.* Enteritidis CC012 in CFU/g tissue. To account for oyster variability, six oysters were utilized per replicate ($n = 3$). Control oysters were exposed to bacteria-free AMS and plated on LB, TCBS and ChromoSelect agar. Results showed low levels of naturally occurring microorganisms in all tested oysters (10^2–10^4 CFU/g tissue). Colony counts on TCBS and ChromoSelect agar determined that natural *Vibrio* and *Salmonella* levels were typically <1000 CFU/g and <100 CFU/g tissue respectively. Reassuringly, colony counts following exposure to inoculated AMS demonstrated highly successful uptake of both *V. vulnificus* and *S.* Enteritidis with levels of between 10^6 and 10^8 CFU/g tissue consistently recovered. Furthermore, no strain demonstrated significantly greater uptake than other strains being tested. Oyster uptake of AMS was assessed over 48 h (Fig. 3I). Rapid initial uptake was observed for all strains, with oysters showing 10^5–10^7 CFU/g tissue at T_4. Ingested concentrations rose to 10^7–10^8 CFU/g tissue at T_8; however, between T_8 and T_{48} there was no increase in bacterial uptake. While we observed $\sim 10^2$ CFU/g tissue at T_0 consisting of naturally occurring bacteria in the negative controls, this was not deemed a problem due to the significantly higher volumes resulting from exposure to inoculated aggregates.

Demonstration of controlled intra and inter-bacterial species killing in vivo *facilitated by AMS*

The aim of this study was to replicate *in vitro* competition assay data in an *in vivo* oyster model utilizing our AMS. Oysters were exposed to bacteria-free AMS and AMS containing individual attacker and prey bacterial cultures at 21°C for 24 h. These controls were enumerated by plating on LB and TCBS agar (Fig. 4A and B). Single culture controls demonstrated no significant difference in uptake between the attacker and prey strains. For the killing assays, oysters were exposed to separate AMS suspensions inoculated with either attacker or prey strains at final attacker to prey ratios of 5:1 and 10:1. Bacterial incorporation into AMS was adjusted to ensure oysters were exposed to the required attacker to prey ratios. *in vivo* co-culture of the prey strain 99-743 with either ΔT6SS1 or ΔT6SS2 resulted in significantly reduced recovery of 99-743 compared with the 99-743-only control oyster cohort ($p < 0.001$) (Fig. 4A). Typically, there was a reduction in viable counts from $>10^7$ to $<10^6$ CFU/g tissue. These reductions in numbers of prey are similar to those obtained with wild-type 106-2A as the attacker strain. To confirm that these *in vivo* levels of reduction of prey bacteria manifested by ΔT6SS1 and ΔT6SS2 were not attributable to alternative killing mechanisms, the assay was conducted using the double T6SS mutant, ΔT6SS1/2. Excitingly, we saw no significant impact on 99-743 viability when challenged with the ΔT6SS1/2 attacker strain compared with the wild-type 106-2A attacker strain. This striking observation demonstrates that the killing observed by attacker strains ΔT6SS1 and ΔT6SS2 is a consequence of the remaining T6SS. These data strongly support the hypothesis that both the T6SSs of *V. vulnificus* play a role in intra-species targeting *in vivo*. To further explore these results, we repeated the assay with an increased ratio of attacker to prey of 10:1 (Fig. 4B). This assay resulted in an even greater reduction of 99-743 when challenged with 106-2A, ΔT6SS1 and ΔT6SS2, typically a >1000-fold reduction from $>10^7$ to $<10^4$ CFU/g tissue ($p < 0.001$).

As we had previously observed that *V. vulnificus* is able to kill *S.* Enteritidis in addition to other species of *Vibrio* in a T6SS-dependent manner *in vitro*, we aimed to determine whether such a phenotype could be observed *in vivo* (Church *et al*., 2016). Thus, to test inter-species targeting of the *V. vulnificus* T6SSs, we conducted *in vivo* co-culture assays employing *S.* Enteritidis CC012 as the prey strain at an attacker to prey ratio of 5:1 (Fig. 4C). Similar to the killing of *V. vulnificus* 99-743 seen previously, the attacker strain *V. vulnificus* 106-2A was able to reduce *S.* Enteritidis levels from $>10^7$ to $<10^6$ CFU/g tissue following *in vivo* co-culture. Both attacking strains, ΔT6SS1 and ΔT6SS2, also killed *S.* Enteritidis to comparable levels as the wild-type attacker strain 106-2A. Fascinatingly, the ΔT6SS1/2 attacker strain had no observable killing phenotype towards the *S.* Enteritidis prey strain. As previously noted for 99-743, increasing the attacker to prey ratio from 5:1 to 10:1 resulted in a significant, dose-dependent reduction in *S.* Enteritidis within oyster stomach tissue, with levels being reduced from $>10^7$ to $<10^4$ CFU/g oyster tissue ($p < 0.05$) (Fig. 4D). In this study, we have demonstrated that *V. vulnificus* strains are capable of killing neighbouring bacterial species using both T6SS1 and T6SS2 at 21°C *in vivo* as demonstrated *in vitro*. Competition with a ΔT6SS1/2 mutant confirmed that this killing was T6SS-dependent.

Discussion

Relevant *in vivo* models are the idyll of studying host–bacteria interactions. While previous studies have

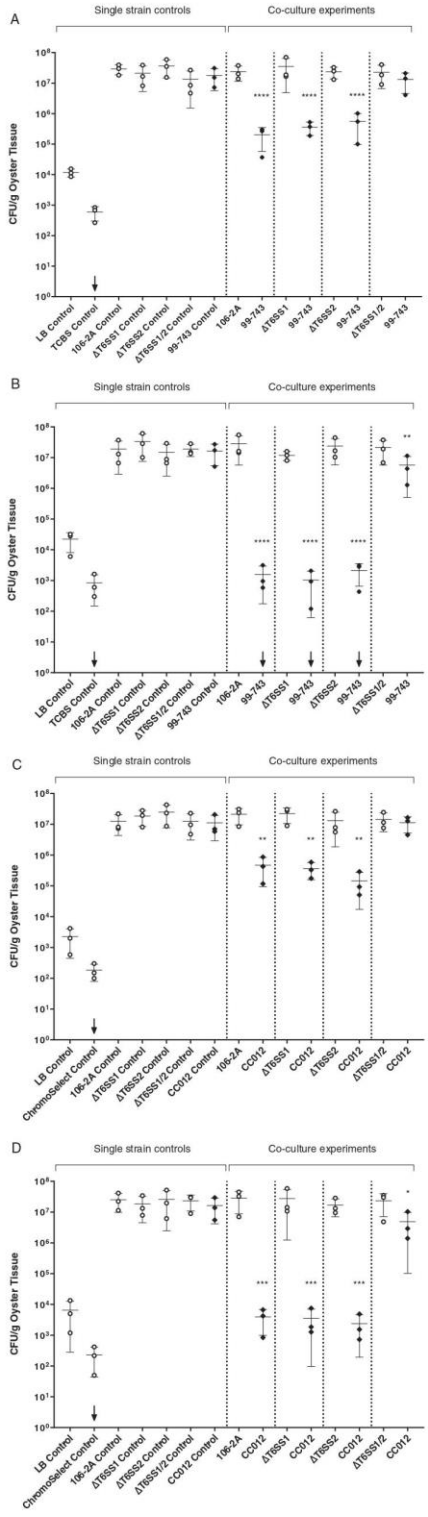

attempted to generate oyster models of bacteria uptake, these models have suffered from reproducibility issues, along with an inability to achieve sufficiently adequate levels of uptake (Morrison *et al*., 2011; Morrison *et al*., 2012; Froelich and Oliver, 2013). Our unique model of AMS, used here as a vector for delivery of bacteria to oysters, provides a robust and relevant model for studies requiring bacteria–oyster interaction. We utilized this model to demonstrate its suitability for investigating intra and inter-species bacterial killing, reporting for the first time an *in vivo* phenotype for the T6SSs of *V. vulnificus*.

The roles of T6SSs of bacteria are multifaceted, providing a selective advantage to bacteria possessing these systems over those without, through the secretion of 'effector' proteins involved in disabling target cells. Several bacterial pathogens, such as *V. cholerae*, also secrete effectors that are involved in virulence, although no one factor is uniquely correlated with virulence (Pukatzki *et al*., 2006; Burtnick *et al*., 2011; Baker-Austin and Oliver, 2018). Given that the T6SS2 is present in all sequenced strains of *V. vulnificus* to date, we assessed the potential role of this T6SS in virulence in a *D. discoideum* eukaryotic model at 21°C (Solomon *et al*., 2000). As shellfish digestive glands are highly polymicrobial, we hypothesised that T6SS1 and T6SS2 may target eukaryotic microorganisms at this lower temperature. Anti-eukaryotic T6SS activity has been observed in a number of microorganisms, such as the antifungal T6SS effectors, Tfe1 and Tfe2, of *Serratia marcescens* (Trunk *et al*., 2018). However, our data demonstrated that unlike *V. cholerae*, neither the wild-type nor the T6SS mutants of *V. vulnificus* exhibited any anti-eukaryotic

Fig. 4. *Vibrio vulnificus* 106-2A has intra-/inter-species killing activity at 21°C *in vivo*. Attacker *V. vulnificus* strains (106-2A, ΔT6SS1, ΔT6SS2, ΔT6SS1/2) were individually co-cultured in oysters with either prey *V. vulnificus* 99-743 or prey *Salmonella* Enteritidis CC012 for 24 h at 21°C at attacker to prey ratios of 5:1 and 10:1. In parallel to co-culture oysters, single strain uptake and bacteria-free controls were assessed to ensure bacteria were being ingested as expected. Each point represents the mean of six technical oyster replicates ($n = 3$). Horizontal bars represent the mean, error bars represent the standard deviation. Attacking strains are represented with circles, prey strains with diamonds. Vertical dotted lines separate attacker, prey and control values into their respective groups. Downward arrows indicate that some oysters were below the 100 CFU/g tissue limit of detection. A. *Vibrio vulnificus* 106-2A, ΔT6SS1, ΔT6SS2 and ΔT6SS1/2 co-culture with *V. vulnificus* 99-743 at a 5:1 ratio. B. *Vibrio vulnificus* 106-2A, ΔT6SS1, ΔT6SS2 and ΔT6SS1/2 co-culture with *V. vulnificus* 99-743 at a 10:1 ratio. C. *Vibrio vulnificus* 106-2A, ΔT6SS1, ΔT6SS2 and ΔT6SS1/2 co-culture with *S.* Enteritidis CC012 at a 5:1 ratio. D. *Vibrio vulnificus* 106-2A, ΔT6SS1, ΔT6SS2 and ΔT6SS1/2 co-culture with *S.* Enteritidis CC012 at a 10:1 ratio. Statistical significant reduction in prey strain CFU/g tissue was determined through comparing prey counts from co-culture oysters to prey counts from the single-strain prey cohort using a nested one-way analysis of variance with Dunnett's multiple comparisons test. * $p < 0.05$, ** $p < 0.01$, *** $p < 0.001$, **** $p < 0.0001$.

properties in this model, reinforcing the hypothesis that these T6SSs are predominantly antibacterial.

Examination of *V. vulnificus* genomes has identified two T6SSs, termed T6SS1 and T6SS2 (Church *et al*., 2016). While all sequenced *V. vulnificus* strains possess a T6SS2, only a subset possesses a T6SS1. *in vitro* competition assays have previously demonstrated that T6SS1$^+$ strains exhibit antibacterial activity against T6SS1$^-$ strains, suggesting a role for the T6SS1 in bacterial competition (Church *et al*., 2016). In this paper, we demonstrate that both the T6SS1 and T6SS2 are active at environmental temperatures and that both facilitate intra- and inter-species killing. Interestingly, our data show that *V. vulnificus* 106-2A is able to target and kill *V. vulnificus* 99-743 in a T6SS2-dependent manner, despite 99-743 also being T6SS2$^+$. This may be due to 106-2A encoding T6SS2 effectors not found in 99-743, against which it does not express cognate immunity proteins. This has been demonstrated previously in *V. cholerae* where genomic analysis of a panel of *V. cholerae* strains revealed that strains possessed a variety of effectors not always identical to one another (Unterweger *et al*., 2014). Strains with dissimilar effector panels were labelled 'incompatible' and shown to compete with one another. Similarly, *V. alginolyticus* contains an array of 'orphan' effectors neighbouring mobile elements obtained from other marine bacteria through horizontal gene transfer (Salomon *et al*., 2015). It is thus possible that *V. vulnificus* 106-2A has horizontally acquired T6SS2 effector proteins to which *V. vulnificus* 99-743 does not possess the cognate immunity protein, rendering 99-743 vulnerable to T6SS2-mediated killing. Future work will be required to confirm this is the case in *V. vulnificus*.

Although the large majority of seafood-related deaths in the United States are attributed to *V. vulnificus* with several reported cases having a fatality rate exceeding 50%, the clinical incidence is low given the prevalence of *V. vulnificus* in shellfish coupled with the quantity consumed. Of between 18.5 and 26.5 million Americans at risk, fewer than 100 cases are reported annually (Warner and Oliver, 2008). Historical reports demonstrate a varied population structure of *V. vulnificus* within oysters, and it may well be that the T6SS1 and T6SS2 systems contribute to a reduction in numbers of strains that are clinically isolated. We further demonstrated *in vitro* inter-species killing potential of both T6SSs by co-culture assays utilizing *S.* Enteritidis CC012 as prey. *Salmonella* species have been identified in up to 8.6% of domestic oysters within the United States, although there are few *Salmonella* outbreaks associated with fish or shellfish documented in the literature (Morrison *et al*., 2012). Whether this is a reflection on detection techniques or in part due to inter-species bacterial competition, or both, remains to be resolved.

While the *in vitro* data presented in this paper empirically demonstrate the competitive ability of *V. vulnificus*, the experimental approach of using AMS to replicate an *in vivo* scenario supports this competitive behaviour *in vivo*. The AMS model provides a means for reproducible and efficient uptake of high numbers of bacteria by oysters. Previous studies into the uptake of *V. vulnificus* or *S.* Enteritidis by oysters have relied on the filtration of planktonic bacteria added to oyster tank water. Such research resulted in levels no higher than 10^5 CFU/g tissue (Srivastava *et al*., 2009; Froelich *et al*., 2010; Morrison *et al*., 2011; Morrison *et al*., 2012; Froelich and Oliver, 2013; Pu *et al*., 2018). NMS as a vehicle to promote *V. vulnificus* uptake by oysters was first documented by Froelich *et al*. (2013), where bacteria were incorporated into NMS generated from seawater. Despite successful incorporation of bacteria into NMS, a number of factors limiting incorporation and subsequent oyster uptake levels were proposed. To resolve these issues, we developed an AMS model using the diatom, *T. pseudonana* CCMP 1335, as a substrate for aggregate formation as it had previously been shown that marine snow can be generated using a range of diatom species (Grossart and Ploug, 2001; Flintrop *et al*., 2018). Utilizing *T. pseudonana* in AMS at specific concentrations led to consistent aggregate formation, with reproducible incorporation levels of *V. vulnificus* and *S.* Enteritidis, 10,000-fold greater than those observed with NMS. Exposure of oysters to AMS resulted in extremely rapid ingestion of bacterial cultures to levels of 10^6–10^8 CFU/g tissue, >1000-fold higher than other oyster uptake experiments published to date (Froelich and Oliver, 2013). This study has demonstrated that AMS is a versatile and highly reproducible model for facilitating rapid and high-level uptake of bacteria into oysters compared with NMS or simple tank-inoculation practices.

We employed our AMS model to prove that *V. vulnificus* T6SS1 and T6SS2 have intra- and inter-species antibacterial activity in an oyster *in vivo* model. This is the first study to demonstrate T6SS *in vivo* activity in oysters facilitated by AMS. Our work suggests that both T6SS1 and T6SS2 are responsible for killing at environmental temperatures around 21°C. It will be of interest to determine the effective environmental ranges of the T6SS *in vivo* through further studies and the control that other regulators such as salinity have over the activity of the two systems. Interestingly, we observed more effective killing of prey bacteria *in vivo* compared with the *in vitro* plate-based assays. While this may be simply explained by the greater ratio of attacker to prey, another reason for this may lie in the regulation of the T6SSs, of which little is still fully understood. As T6SSs are involved in microbial competition, it is possible that they are upregulated under conditions where increased competition is required, such as

nutrient-limiting environments. Specifically, recently identified roles for bacterial T6SSs have been in the acquisition of essential micronutrients. *Burkholderia thailandensis*, *Pseudomonas aeruginosa* and *Yersinia pseudotuberculosis* T6SSs have all demonstrated secretion of effectors involved in nutrient acquisition, including manganese scavengers, zinc-binding proteins and iron-chelators (Liu *et al*., 2015; Si *et al*., 2017a; Si *et al*., 2017b).

In conclusion, this study has further characterized the activity of the T6SSs of *V. vulnificus* and has identified thermoregulatory conditions under which these are active. These are the first published findings confirming T6SS2 antibacterial activity of *V. vulnificus*. This study has also developed a widely applicable AMS model which facilitates incorporation of high numbers of bacterial that can subsequently be ingested by oysters for *in vivo* studies. Such studies demonstrated that both the T6SS1 and T6SS2 of *V. vulnificus* are active *in vivo* and capable of intra- and inter-species killing. Future work will look at expanding these competition assays to further understand T6SS regulation, activity and mode of action both *in vitro* and *in vivo*.

Experimental procedures

Culture conditions

Vibrio vulnificus and *S*. Enteritidis, were routinely cultured at 37°C in Luria-Bertani (LB) broth (Oxoid). *Vibrio vulnificus* plate cultures were maintained on TCBS agar (Oxoid) at room temperature. *Salmonella* Enteritidis plate cultures were maintained on ChromoSelect *Salmonella* chromogenic media (Merck). Where necessary, antibiotics were added at the following concentrations: ampicillin (50 μg/ml), kanamycin (100 μg/ml), trimethoprim (100 μg/ml) and chloramphenicol (35 μg/ml for *Escherichia coli*, 10 μg/ml for *V. vulnificus*). All utilized strains, plasmids and primers are listed in Tables S1–S3.

Dictyostelium discoideum (accession number: DBS0235542) was ordered via DictyBase (Fey *et al*., 2013) and received growing on a lawn of *E. coli* B/r. Axenic cultures were generated by inoculating 30 ml HL5 media (Formedium™) supplemented with ampicillin (100 μg/ml) and streptomycin (300 μg/ml) with an inoculating loop of *D. discoideum* fruiting bodies. Cultures were incubated at 21°C, 180 rpm for 2–3 days. Before cultures exceeded 10^6 cells/ml, 1 ml of culture was used to inoculate 30 ml of antibiotic-free HL5. Cultures were incubated at 21°C, 180 rpm for 2–3 days and routinely checked for contamination.

Generation of T6SS in-frame deletion mutants

V. vulnificus ΔT6SS1, ΔT6SS2 and ΔT6SS1/2 were generated through in-frame deletion of *hcp1* and *hcp2*. Upstream and downstream flanking regions for both genes were PCR-amplified and cloned into pGEM-T Easy for sequencing (Eurofins). Once confirmed, regions were enzymatically excised, purified and ligated into allelic exchange vector, pDM4 (Milton *et al*., 1996). Constructs pDM4-Δ*hcp1* and pDM4-Δ*hcp2* were transformed into *E. coli* S17-1 λ *pir* and triparentally conjugated into *V. vulnificus* 106-2A using conjugal donor, *E. coli* HB101 pRK2013. First crossover integrants were selected for on TCBS agar supplemented with chloramphenicol. To promote a second crossover event, first crossovers were plated on LB agar supplemented with 10% sucrose and incubated at 37°C for 24 h. Second crossover mutants were confirmed through PCR and sequenced to confirm the insertion was in-frame. Expression of downstream genes was confirmed using RT-PCR.

RNA extraction and RT-PCR

RNA was extracted from bacterial cultures using the RiboPure™-Bacteria kit (ThermoFisher) according to the manufacturer's instructions. 50 ng random hexamers were mixed with 1 μg total RNA, 1 μl 10 mM dNTPs and MiliQ H_2O to 13 μl. This solution was incubated at 65°C for 5 min and incubated on ice for a further 5 min. Following incubation, the following reagents were added to the microcentrifuge tube: 4 μl 5× First-Strand Buffer, 1 μl 0.1 M DTT, 1 μl RNaseOUT™, 1 μl SuperScript™ III RT (all reagents Invitrogen). The solution was incubated at 25°C for 5 min before being incubated for a further 60 min at 50°C for cDNA generation.

Generation of antibiotic-resistant V. vulnificus *strains*

To enable antibiotic selection of *V. vulnificus* attacker and prey strains following co-culture, plasmids conferring antibiotic resistance were electroporated into *V. vulnificus* and selected for on LB supplemented with either kanamycin or trimethoprim. pVv3-Kan was utilized to confer kanamycin resistance to attacker strains (Klevanskaa *et al*., 2014), and pVv3-Tmp was employed to confer resistance to trimethoprim for prey strains. Electroporation was performed according to the protocol presented in Klevanskaa *et al*. (2014). As selective chromogenic media was utilized for *Salmonella* selection, there was no need to generate antibiotic-resistant *Salmonella* strains.

In vitro *co-culture competition assays*

Attacker and prey strain cultures were subcultured in 30 ml fresh selective LB to an OD_{590nm} of 0.03 and grown to an OD_{590nm} of 1 before being adjusted to an OD_{590nm} of 0.8. Cultures were pelleted, washed twice with phosphate-buffered saline (PBS) to remove any antibiotics before

being resuspended in PBS at an OD_{590nm} of 0.8. Attacker and prey strains were combined at a ratio of 3:1 and 25 μl spotted onto LB agar. Following incubation, bacterial spots were excised using a scalpel and resuspended in 1 ml PBS. Tenfold serial dilutions were performed and triplicate 10 μl spots for each dilution were plated on the required selective media. Plates were incubated at 37°C and the average CFU/ml was calculated the following day.

Dictyostelium discoideum *plaque-forming assays*

Overnight bacterial cultures were pelleted by centrifugation and resuspended to an OD_{590nm} of 5.5 in KK2 buffer. Of note, 1 ml *D. discoideum* culture was pelleted by centrifugation at 2500 rpm for 5 min. Pelleted cells were washed once with KK2 buffer, centrifuged for a further 5 min and resuspended in 1 ml KK2 buffer. Resuspended *D. discoideum* AX3 were added to 1 ml of bacterial culture at a final concentration of 10^2 cells/ml. Of note, 200 μl of the resulting suspension was spread on SM agar and incubated at 21°C for 3–5 days to allow plaque formation (Pukatzki *et al*., 2006).

Generating natural and AMS

NMS was generated by combining 1 l collected seawater (Dawlish Warren) with 1 ml bacterial culture adjusted to an OD_{590nm} of 0.8 and 1 μg/L hyaluronic acid (Fisher). Tubes were rolled for 24 h at 8 rpm and 21°C. AMS was generated by combining 1 l artificial seawater (20 ppt salinity), with 1 ml TP 1800 (10^9 cells) (Reed Mariculture), 1 ml bacterial culture adjusted to an OD_{590nm} of 0.8 and 1 μg/L hyaluronic acid (Fisher). Tubes were rolled for 24 h at 8 rpm and 21°C.

Enumerating bacterial incorporation into marine snow

Marine snow was vacuum-filtered through qualitative filter paper No. 6 (Whatman) with a pore size of 3 μm. Non-aggregated bacteria are too small to be retained by the filter paper. Any cells incorporated into larger marine snow aggregates were retained on the filter paper. Filtered aggregates were resuspended in 50 ml PBS and vortexed vigorously to disrupt the aggregates. Samples were centrifuged to pellet the material, resuspended in 10 ml PBS and serially diluted 10-fold for spread-plate enumeration on LB, TCBS or ChromoSelect agar. Plates were incubated at 37°C overnight and CFU/g marine snow calculated the following day.

Scanning electron microscopy

Marine snow samples were fixed in 2% glutaraldehyde and 2% paraformaldehyde in 0.1 M Pipes buffer pH 7. Fixed samples were transferred onto a 0.1 μm polycarbonate filter and washed for 5 min in Pipes buffer for a total of three times. Aggregates attached to the filter were dehydrated using an ethanol gradient. The filter was incubated for 3 min in hexamethyldisilazane before air-drying. Dried filters were mounted onto an aluminium sample pin using carbon conductive tabs. Samples were then sputter-coated with 10 nm gold/palladium (80/20) and imaged using a JEOL JSM 6390 LV scanning electron microscope operated at 5 kV. Images were contrast-adjusted and false-coloured using Adobe Photoshop CC 2019 V20.0. Raw images can be seen in Figure S3A–D.

Oyster husbandry

Pacific oysters (*Crassostrea gigas*) were obtained from Lindisfarne oyster farm (Lindisfarne oysters, Northumberland). Upon arrival, oysters were scrubbed and placed in static holding tanks containing 20 ppt salinity artificial seawater at 21°C. Oysters were maintained at the University of Exeter in the Aquatic Resources Centre under their prescribed oyster husbandry protocols. Oysters were allowed to acclimatize for 5 days. Water was changed daily, and oysters were fed with 250 μl TP 1800® (Reed Mariculture) every other day.

In vivo *oyster exposure assays*

Oysters were maintained in individual 5 l holding aquaria at 21°C. AMS was added to the holding tanks taking care to not disrupt the aggregates. Six oysters were utilized for each exposure. Oysters were left to filter and ingest the inoculated marine snow for 24 h. A circulatory current was generated by the presence of an air stone to prevent aggregate settling. Following exposure, oysters were removed from their tanks and briefly cleaned with 70% ethanol to remove non-ingested microorganisms. Using a flame-sterilized knife, oysters were shucked and the stomachs excised. Samples were weighed before being suspended in 10 ml PBS and homogenized for 3 min in a Stomacher 400 (Seward). The resulting homogenate was filtered through a 40-μm cell strainer (Merck) into a clean 50-ml falcon tube to remove tissue debris. The resulting filtrate was serially diluted 10-fold in PBS. Of note, 100 μl of each dilution was spread on LB agar and incubated overnight at 37°C. The following day, all colonies were replica plated onto *Vibrio* selective TCBS and incubated overnight at 37°C. Colonies were then enumerated based off colour and recorded for CFU/g tissue calculations. Assays involving *Salmonella* were not plated onto LB but instead straight onto *Salmonella*-selective ChromoSelect agar.

Acknowledgements

The authors would like to thank Dr Stefan Hertwig for the donation of the pVv3-Kan and pVv3-Kan-Tmp plasmids and Dr Christian Hacker for his technical assistance obtaining the SEM images. This research was funded by The Natural Environment Research Council, grant number NE/L002434/1.

Author contributions

C.L.H. and S.L.M. designed the experiments. Both authors contributed to the preparation of the manuscript. S.L.M. conceived the study and obtained the funding.

References

Baker-Austin, C., and Oliver, J.D. (2018) *Vibrio vulnificus*: new insights into a deadly opportunistic pathogen. *Environ Microbiol* **20**: 423–430.

Baker-Austin, C., Trinanes, J.A., Taylor, N.G.H., Hartnell, R., Siitonen, A., Martinez-Urtaza, J. (2012) Emerging *Vibrio* risk at high latitudes in response to ocean warming. *Nat Clim Chang* **3**: 73–77.

Baker-Austin, C., Trinanes, J., Gonzalez-Escalona, N., and Martinez-Urtaza, J. (2017) Non-cholera *Vibrios*: the microbial barometer of climate change. *Trends Microbiol* **25**: 76–84.

Beatty, N.L., Marquez, J., and Al Mohajer, M. (2017) Skin manifestations of primary *Vibrio vulnificus* septicemia. *Am J Trop Med Hyg* **97**: 1–2.

Berni, B., Soscia, C., Djermoun, S., Ize, B., and Bleves, S. (2019) A type VI secretion system trans-kingdom effector is required for the delivery of a novel antibacterial toxin in *Pseudomonas aeruginosa*. *Front Microbiol* **10**: 1218.

Bondad-Reantaso, M.G., Subasinghe, R.P., Arthur, J.R., Ogawa, K., Chinabut, S., Adlard, R., *et al*. (2005) Disease and health management in Asian aquaculture. *Vet Parasitol* **132**: 249–272.

Bruto, M., James, A., Petton, B., Labreuche, Y., Chenivesse, S., Alunno-Bruscia, M., *et al*. (2017) *Vibrio crassostreae*, a benign oyster colonizer turned into a pathogen after plasmid acquisition. *ISME J* **11**: 1043–1052.

Burtnick, M.N., Brett, P.J., Harding, S.V., Ngugi, S.A., Ribot, W.J., Chantratita, N., *et al*. (2011) The cluster 1 type VI secretion system is a major virulence determinant in *Burkholderia pseudomallei*. *Infect Immun* **79**: 1512–1525.

Cascales, E., and Cambillau, C. (2012) Structural biology of type VI secretion systems. *Philos Trans R Soc Lond B Biol Sci* **367**: 1102–1111.

CDC n.d. Oysters and vibriosis | features | CDC.

Chiang, C., Chiang, S.-R., and Chuang, Y.-C. (2003) *Vibrio vulnificus* infection: clinical manifestations, pathogenesis, and antimicrobial therapy. *J Microbiol Immunol Infect* **36**: 81–88.

Church, S.R., Lux, T., Baker-Austin, C., Buddington, S.P., and Michell, S.L. (2016) *Vibrio vulnificus* type 6 secretion system 1 contains anti-bacterial properties. *PLoS One* **11**: e0165500.

Deeb, R., Tufford, D., Scott, G., Gooch Moore, J., and Dow, K. (2018) Impact of climate change on *Vibrio vulnificus* abundance and exposure risk. *Estuar Coasts* **41**: 2289–2303.

Dubert, J., Nelson, D.R., Spinard, E.J., Kessner, L., Gomez-Chiarri, M., Costa, F.., *et al*. (2016) Following the infection process of vibriosis in Manila clam (*Ruditapes philippinarum*) larvae through GFP-tagged pathogenic *Vibrio* species. *J Invertebr Pathol* **133**: 27–33.

Fey, P., Dodson, R.J., Basu, S., and Chisholm, R.L. (2013) *One Stop Shop for Everything* Dictyostelium*: dictyBase and the Dicty Stock Center in 2012*. Totowa, NJ: Humana Press, pp. 59–92.

Flintrop, C.M., *et al*. (2018) Embedding and slicing of intact *in situ* collected marine snow. *Limnol Oceanogr Methods* **16**: 339–355.

Froelich, B.A., and Noble, R.T. (2014) Factors affecting the uptake and retention of *Vibrio vulnificus* in oysters. *Appl Environ Microbiol* **80**: 7454–7459.

Froelich, B., and Oliver, J. (2013) Increases in the amounts of *Vibrio* spp. in oysters upon addition of exogenous bacteria. *Appl Environ Microbiol* **79**: 5208–5213.

Froelich, B., Ringwood, A., Sokolova, I., and Oliver, J. (2010) Uptake and depuration of the C- and E-genotypes of *Vibrio vulnificus* by the eastern oyster (*Crassostrea virginica*). *Environ Microbiol Rep* **2**: 112–115.

Froelich, B., Ayrapetyan, M., and Oliver, J.D. (2013) Integration of *Vibrio vulnificus* into marine aggregates and its subsequent uptake by *Crassostrea virginica* oysters. *Appl Environ Microbiol* **79**: 1454–1458.

Froelich, B.A., Phippen, B., Fowler, P., Noble, R.T., and Oliver, J.D. (2017) Differences in abundances of total *Vibrio* spp., *V. vulnificus*, and *V. parahaemolyticus* in clams and oysters in North Carolina. *Appl Environ Microbiol* **83**: e02265-16.

Fu, Y., Ho, B.T., and Mekalanos, J.J. (2018) Tracking *Vibrio cholerae* cell-cell interactions during infection reveals bacterial population dynamics within intestinal microenvironments. *Cell Host Microbe* **23**: 274–281.e2.

Grossart, H.-P., and Ploug, H. (2001) Microbial degradation of organic carbon and nitrogen on diatom aggregates. *Limnol Oceanogr* **46**: 267–277.

Grossart, H.-P., Kiørboe, T., Tang, K., and Ploug, H. (2003) Bacterial colonization of particles: growth and interactions. *Appl Environ Microbiol* **69**: 3500–3509.

Ho, B., Dong, T., and Mekalanos, J. (2014) A view to a kill: the bacterial type VI secretion system. *Cell Host Microbe* **15**: 9–21.

Hsieh, P.-F., Lu, Y.-R., Lin, T.-L., Lai, L.-Y., and Wang, J.-T. (2019) *Klebsiella pneumoniae* type VI secretion system contributes to bacterial competition, cell invasion, type-1 fimbriae expression, and in vivo colonization. *J Infect Dis* **219**: 637–647.

Ishikawa, T., Sabharwal, D., Bröms, J., Milton, D.L., Sjöstedt, A., Uhlin, B.E., and Wai, S.N. (2012) Pathoadaptive conditional regulation of the type VI secretion system in *Vibrio cholerae* O1 strains. *Infect Immun* **80**: 575–584.

Jones, M., and Oliver, J. (2009) *Vibrio vulnificus*: disease and pathogenesis. *Infect Immun* **77**: 1723–1733.

Kaspar, C., and Tamplin, M. (1993) Effects of temperature and salinity on the survival of *Vibrio vulnificus* in seawater and shellfish. *Appl Environ Microbiol* **59**: 2425–2429.

Kim, D.M., Jung, S.I., Jang, H.C., Lee, C.S., Lee, S.H., Yun, N.R., *et al*. (2011) *Vibrio vulnificus* DNA load and mortality. *J Clin Microbiol* **49**: 413–415.

Kiørboe, T., Andersen, K.P., and Dam, H.G. (1990) Coagulation efficiency and aggregate formation in marine phytoplankton. *Mar Biol* **107**: 235–245.

Kiørboe, T., Tang, K., Grossart, H.-P., and Ploug, H. (2003) Dynamics of microbial communities on marine snow aggregates: colonization, growth, detachment, and grazing mortality of attached bacteria. *Appl Environ Microbiol* **69**: 3036–3047.

Klevanskaa, K., Bier, N., Stingl, K., Strauch, E., and Hertwig, S. (2014) pVv3, a new shuttle vector for gene expression in *Vibrio vulnificus*. *Appl Environ Microbiol* **80**: 1477–1481.

Lacoste, A., Jalabert, F., Malham, S., Cueff, A., Gélébart, F., Cordevant, C., *et al*. (2001) A *Vibrio splendidus* strain is associated with summer mortality of juvenile oysters *Crassostrea gigas* in the bay of Morlaix (North Brittany, France). *Dis Aquat Org* **46**: 139–145.

Liu, L., Hao, S., Lan, R., Wang, G., Xiao, D., Sun, H., and Xu, J. (2015) The type VI secretion system modulates flagellar gene expression and secretion in *Citrobacter freundii* and contributes to adhesion and cytotoxicity to host cells. *Infect Immun* **83**: 2596–2604.

Menon, M., Yu, P., Iwamoto, M., and Painter, J. (2014) Pre-existing medical conditions associated with *Vibrio vulnificus* septicaemia. *Epidemiol Infect* **142**: 878–881.

Milton, D.L., O'toole, R., Horstedt, P., Horstedt, H., and Wolf-Watz, H. (1996) Flagellin A is essential for the virulence of *Vibrio anguillarum*. *J Bacteriol* **178**: 1310–1319.

Miyata, S.T., Kitaoka, M., Brooks, T.M., McAuley, S.B., and Pukatzki, S. (2011) *Vibrio cholerae* requires the type VI secretion system virulence factor VasX to kill *Dictyostelium discoideum*. *Infect Immun* **79**: 2941–2949.

Morrison, C.M., Armstrong, A.E., Evans, S., Mild, R.M., Langdon, C.J., and Joens, L.A. (2011) Survival of *Salmonella* Newport in oysters. *Int J Food Microbiol* **148**: 93–98.

Morrison, C.M., Dial, S.M., Day, W.A., Joens, L.A., and Joens, L.A. (2012) Investigations of *Salmonella enterica* serovar Newport infections of oysters by using immunohistochemistry and knockout mutagenesis. *Appl Environ Microbiol* **78**: 2867–2873.

Oliver, J. (2005) Wound infections caused by *Vibrio vulnificus* and other marine bacteria. *Epidemiol Infect* **133**: 383–391.

Passow, U., Ziervogel, K., Asper, V., and Diercks, A. (2012) Marine snow formation in the aftermath of the Deepwater horizon oil spill in the Gulf of Mexico. *Environ Res Lett* **7**: 035301.

Pu, M., Duriez, P., Arazi, M., and Rowe-Magnus, D.A. (2018) A conserved tad pilus promotes *Vibrio vulnificus* oyster colonization. *Environ Microbiol* **20**: 828–841.

Pukatzki, S., Ma, A.T., Sturtevant, D., Krastins, B., Sarracino, D., Nelson, W.C., *et al*. (2006) Identification of a conserved bacterial protein secretion system in *Vibrio cholerae* using the *Dictyostelium* host model system. *Proc Natl Acad Sci U S A* **103**: 1528–1533.

Pukatzki, S., Ma, A.T., Revel, A.T., Sturtevant, D., and Mekalanos, J.J. (2007) Type VI secretion system translocates a phage tail spike-like protein into target cells where it cross-links Actin. *Proc Natl Acad Sci U S A* **104**: 15508–15513.

Ray, A., Schwartz, N., Souza Santos, M., Zhang, J., Orth, K., and Salomon, D. (2017) Type VI secretion system MIX-effectors carry both antibacterial and anti-eukaryotic activities. *EMBO Rep* **18**: 1978–1990.

Rico, A., Satapornvanit, K., Haque, M.M., Min, J., Nguyen, P.T., Telfer, T.C., and van den Brink, P.J. (2012) Use of chemicals and biological products in Asian aquaculture and their potential environmental risks: a critical review. *Rev Aquac* **4**: 75–93.

Salomon, D., Gonzalez, H., Updegraff, B.L., and Orth, K. (2013) *Vibrio parahaemolyticus* type VI secretion system 1 is activated in marine conditions to target bacteria, and is differentially regulated from system 2. *PLoS One* **8**: e61086.

Salomon, D., Klimko, J.A., Trudgian, D.C., Kinch, L.N., Grishin, N.V., Mirzaei, H., and Orth, K. (2015) Type VI secretion system toxins horizontally shared between marine bacteria. *PLoS Pathog* **11**: e1005128.

Si, M., Wang, Y., Zhang, B., Zhao, C., Kang, Y., Bai, H., *et al*. (2017a) The type VI secretion system engages a redox-regulated dual-functional heme transporter for zinc acquisition. *Cell Rep* **20**: 949–959.

Si, M., Zhao, C., Burkinshaw, B., Zhang, B., Wei, D., Wang, Y., *et al*. (2017b) Manganese scavenging and oxidative stress response mediated by type VI secretion system in *Burkholderia thailandensis*. *Proc Natl Acad Sci* **114**: E2233–E2242.

SOFIA State of fisheries and aquaculture in the world 2018.

Solomon, J.M., Rupper, A., Cardelli, J.A., and Isberg, R.R. (2000) Intracellular growth of *Legionella pneumophila* in *Dictyostelium discoideum*, a system for genetic analysis of host-pathogen interactions. *Infect Immun* **68**: 2939–2947.

Speare, L., Cecere, A.G., Guckes, K.R., Smith, S., Wollenberg, M.S., Mandel, M.J., *et al*. (2018) Bacterial symbionts use a type VI secretion system to eliminate competitors in their natural host. *Proc Natl Acad Sci* **115**: E8528–E8537.

Srivastava, M., Tucker, M.S., Gulig, P.A., and Wright, A.C. (2009) Phase variation, capsular polysaccharide, pilus and flagella contribute to uptake of *Vibrio vulnificus* by the eastern oyster (*Crassostrea virginica*). *Environ Microbiol* **11**: 1934–1944.

Trunk, K., Peltier, J., Liu, Y.C., Dill, B.D., Walker, L., Gow, N. A.R., *et al*. (2018) The type VI secretion system deploys antifungal effectors against microbial competitors. *Nat Microbiol* **3**: 920–931.

Unterweger, D., Miyata, S.T., Bachmann, V., Brooks, T. M., Mullins, T., Kostiuk, B., *et al*. (2014) The *Vibrio cholerae* type VI secretion system employs diverse effector modules for intraspecific competition. *Nat Commun* **5**: 3549.

Vezzulli, L., Höfle, M., Pruzzo, C., Pezzati, E., and Brettar, I. (2015) Effects of global warming on *Vibrio* ecology. *Microbiol Spectr* **3**(VE-0004-2014), 1–9.

Warner, E., and Oliver, J. (2008) Population structures of two genotypes of *Vibrio vulnificus* in oysters (*Crassostrea virginica*) and seawater. *Appl Environ Microbiol* **74**: 80–85.

Supporting Information

Additional Supporting Information may be found in the online version of this article at the publisher's web-site:

Appendix S1: Supporting Information